A Multiscale Framework for Predicting Distributed Renewable Thermal Energy Integration

Pilar Monsalvete Álvarez de Uribarri

Supervised by:

Prof Darren Robinson
Dr Gavin Long
Prof Ursula Eicker

A thesis submitted to the University of Nottingham for the degree of Doctor of Philosophy in the

Laboratory of Urban Complexity And Sustainability
Faculty of Engineering

April 14, 2020

A mis padres.
Gracias por ayudarme a llegar hasta aquí.

Abstract

With the increase in energy demand in cities and the growing need to mitigate the anthropogenic impact on climate, the interest in understanding the energy flows in cities has risen in recent decades. This thesis aims to contribute towards the development of useful and flexible tools which help to understand the energy flows in cities. It is specifically focused on the building sector, with emphasis on thermal energy performance and the potential of renewable energy integrated into district heating systems.
The participation on the development of an adaptive urban energy modelling tool that, on the one side tackles different levels of complexity of the energy system according to the scope of analysis and on the other side, can adjust the models to the data available is presented.

This thesis describes a dynamic building demand model that can be used for urban energy modelling thanks to the automation of input data setting and its flexibility to adapt to different levels of data resolution. Likewise, the thesis contributes to the improvement of a District Heating Network model by developing a methodology to avoid artificial diffusion and wave delay in network pipes. In this way, the dynamics of the fluid inside pipes can be reproduced, which is crucial when introducing very intermittent elements to the system, such as thermal solar panels or the buildings themselves.
The workflow followed by the tools where the models have been integrated is also explained, paying attention to its modular structure and the input data preprocessing.

Finally, the thesis presents two case studies that show the performance and the potential of the developed models and the tools where they are embedded. In the first case study, the capacity of the building model to adapt to two different levels of detail of the input data is shown. In contrast, the second case study focuses on the DHN model and how it can be used to study the impact of connecting distributed supply sources, which are very common in renewable applications.

Acknowledgements

First of all I would like to express my gratitude to my supervisors. Thank you Ursula Eicker and Darren Robinson for giving me the opportunity to enrol in this journey five years ago. Thanks Ursula for the great welcome at HfT-Stuttgart, for the invaluable help and for trusting me and my work. Thanks Darren for the guidance, the great supervision and support and the patience (and the English corrections).

I would also like to thank my co-workers, specially Preston for all the hours invested in bringing my thesis to the end, and Jürgen for sharing tools, knowledge and time. My gratitude to Jacopo, too. I think we really did a good job together, during the team work and in the results.

Finally, I would like to thank those that made my live easier during the harder days. Thanks Dani for the great time together in the office and out of it, for making me feel almost at home. Also Ruben, for the long discussion inside and outside the office, for taking care of Calvin so many times and for the pieces of fruit, chocolate and other energy bits during those long working days. Muchas gracias Patri por cuidarme, alimentarme y encargarte de Calv cuando mi vida no daba para más.

Contents

List of Figures

List of Tables

Acronyms

4GDH: 4^{th} Generation District Heating systems.

ACH: Air Changes per Hour.

ADE: Application Domain Extension.

BAU: Business As Usual.

BESTEST: Building Energy Simulation Test.

CAD: Computer-aided design.

CFL: Courant-Friedrichs-Lewy.

DBM: Dynamic Building Model.

DHCS: District Heating and Cooling Systems.

DHN: District Heating Network.

DHS: District Heating Systems.

DHW: Domestic Hot Water.

ECS: Environmental Control System.

EU: European Union.

FDM: Finite Difference Method.

FMI: Functional Mock-up Interface.

FMU: Functional Mock-up Units.

GDI NRW: Geodata Infrastructure North-Rhine Westphalia.

GIS: Geographic Information System.

HVAC: Heating, ventilation, and air conditioning.

HP: Heat Pump.

IEA: International Energy Agency.

LiDAR: Laser Imaging Detection and Ranging.

LoD: Level of Detail.

MFH: Multi Family House.

MIT: Massachusetts Institute of Technology.

nRMSE: normalised Root Mean Square Error.

NSF: National Science Foundation.

OECD: Organisation for Economic Co-operation and Development.

PLF: Partial Load Factor.

SFH: Single Family House.

SIG 3D: Special Interest Group 3D.

SOA: Service-Oriented Architecture.

SOAP: Simple Object Access Protocol.

SRA: Simplified Radiosity Algorithm.

TMY: Typical Meteorological Year.

UBEM: Urban Building Energy Modelling.

UDDI: Universal Discovery, Description and Integration.

UESM: Urban Energy System Model.

UHI: Urban Heat Island.

YoC: Year of Construction.

WEO: World Energy Outlook.

WSDL: Web Service Description Language.

Chapter 1

Introduction

1.1 Background and problem statement

The world population has increased exponentially since the Industrial Revolution, and it has moved from rural to urban areas, most probably thanks to the easy access to energy and other resources that the revolution brought with it. This increase will continue according to the UN's report on *World Urbanization Prospects* in 2014 [148]. It is projected to add 2500 million people to the world population by 2050, reaching the population living in urban areas the 66% by the same year. The increase of population, inevitably leads to a rise of environmental impact (I). Ehrlich and Holdren [68] considered the environmental impact to be proportional to population (P), economic activity (A) and the technology to support technological activity (T): $I \propto P.A.T.$ The growth of population mainly occurs in the so-called 'developing' countries, only three countries –India, China and Nigeria– are expected to add together more than half of the urban population growth, 37%. In such countries, the technology used has a bigger impact, and the urban population is more economically active than in 'developed' countries, increasing even faster the stress on the environment under business as usual conditions.
Corroborating this relationship, the *World Energy Outlook (WEO) 2008* [211], with a chapter focused on energy use in cities, forecasts continued increase of energy use per capita for the next years (Figure 1.2), after a breakneck growth since the beginning of last century (Figure 1.1). The primary energy use in cities was in 2006 already 67% of the total, and it is projected to grow up to 73% by 2030. Non-OECD countries account for 81% of this growth.

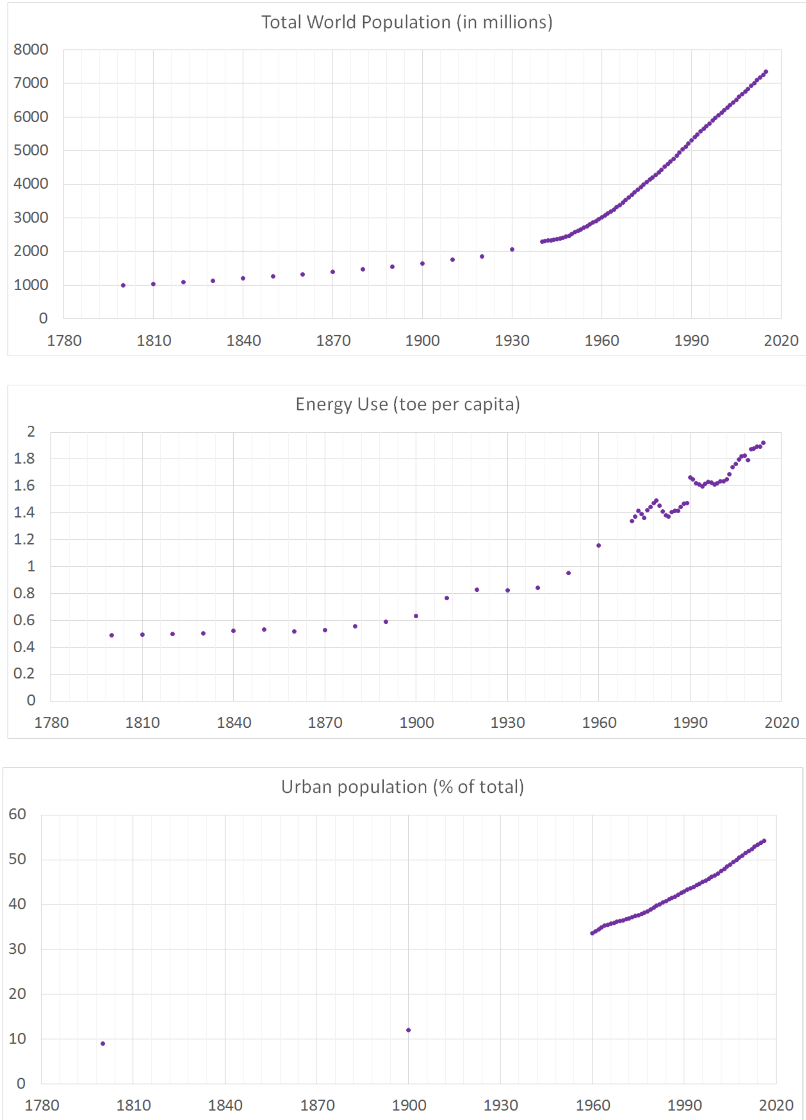

Figure 1.1: Growth on population and energy use (Sources: World Bank Database [7] and Roser's work for the *Our World in Data* website [8]).

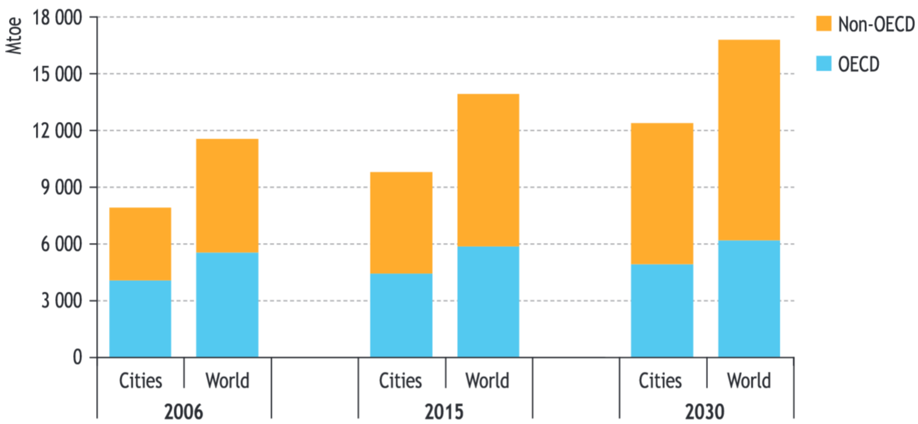

Figure 1.2: World and city primary energy use (Source: [211]).

If zooming in the global energy system [212], three groups are the more significant energy users: Industry, Transport and Building sectors, being the last one the biggest (Figure 1.3). This proportion fits with the previous statement since energy use in cities include almost the entire Building sector and part of the Industry and Transport [211].

This whole scenario raises the exciting challenge for the society of creating more efficient cities. Moreover, it explains the global interest in urban climate and energy issues as it was reflected in two relevant reports. First, the *Millennium Development Goals Report, 2008* [152], which alerts about the growth of the population in cities and the importance of managing it in such a way that the access to all resources can be ensured. Second, the *WEO, 2008*, which focuses specifically on urban energy use. Furthermore, many activities of organizations[a] as well as the continuously increasing investments, according to the International Energy Agency (IEA) [213] (Figure 1.4), also reflect a "growing recognition that energy use in cities is a key element in the fight against global climate change" [38].

Following the same path as the international community, the European Union (EU) has focused its energy policy in the reduction of CO_2 emissions related to energy use in urban areas. Its main target is to decrease the energy use and promoting renewable energy, as the objectives of the *Strategy Europe 2020* reflect [55].

[a]i.e. the Global Carbon Project's Urban and Regional Carbon Management theme, the International Council for Local Environmental Initiatives Cities for Climate Protection, the C40 Climate Leadership Group, Energie-Cités, Columbia University's Urban Climate Change Research Network, among others.

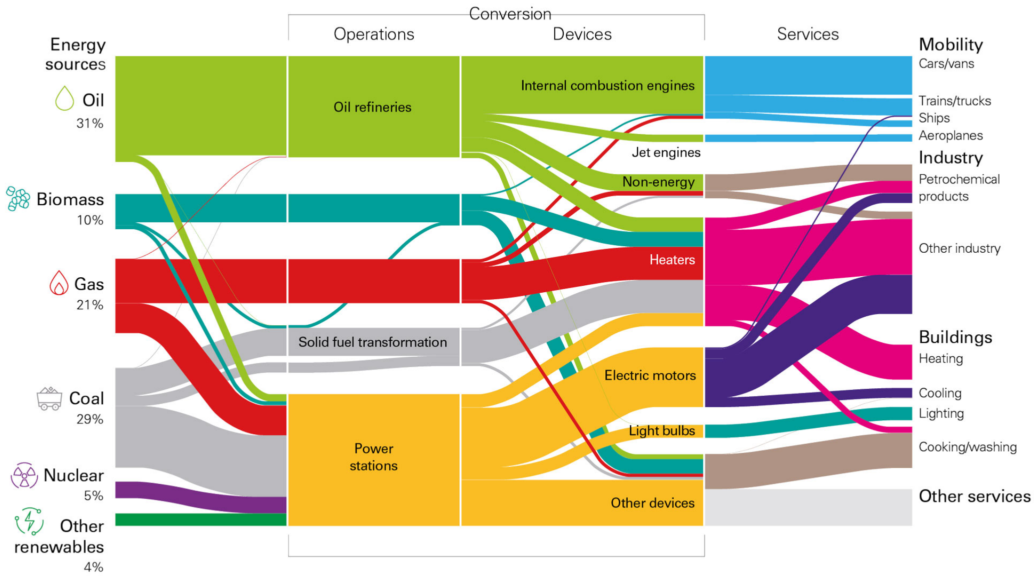

Figure 1.3: The global energy system, 2013 (From [40], based on IEA data from the World Energy Statistics and Balance, OECD/IEA 2013).

	Average annual investments					Cumulative investments	
	Historical	New Policies Scenario				NPS	450
	2000-13	2014-20	2021-25	2026-30	2031-35	2014-35	2014-35
Energy Efficiency *(billion, year-2012 US dollars)*							
Total	212	334	436	533		8 002	13 531
Industry	21	31	40	48		739	1 371
Energy intensive	8	11	15	19		284	529
Non-energy intensive	13	19	25	29		455	842
Transport	115	193	276	356		4 928	8 120
Road	109	179	250	317		4 496	7 267
Aviation, navigation and rail	6	14	26	39		432	854
Buildings	77	110	120	129		2 334	4 040

Figure 1.4: Average global annual investment according to the IEA. Especial emphasis on the Building sector (Source: [213]).

The third target for the EU in 2020, *Climate change and energy sustainability*, establishes three objectives that were upwardly revised in 2018:

1. The reduction of greenhouse gas emissions 40% lower than in 1990.
2. The promotion of energy from renewable sources until 32% of the total.
3. The increase of 32% in energy efficiency.

In this third objective, the main focus is on the use of energy in buildings because it is in that sector where lies the most significant energy-saving potential, as it is explicitly expressed in the *Communication from the Commission to the European Parliament* in 2011 [54].

Furthermore, the *Directive 2012/27/EU* [159] emphasizes the importance of working towards efficient district heating and cooling[b], and encourages the Member States to develop those solutions in the framework of low energy cities in its *Chapter III – Article 14: 'Promotion of efficiency in heating and cooling'*.

It is not surprising, then, that the trend nowadays is to go away from energy supply systems for single buildings and consider District Heating and Cooling Systems (DHCS) with semi-centralized (renewable or waste heat complemented with centralized conventional) energy supply systems for urban blocks as a better solution [100]. It has been proved that they can have a significant effect on the reduction of CO_2 emissions for several reasons. First, the aggregated heat load curve (the sum of all singular demands) is smoother than the individual load curves. Therefore, there is less need of total generating capacity and the supply systems work more efficiently (better when more industries are included in the network) [64], taking advantage of the economies of scale, too. Furthermore, the total supply energy is reduced by the use of industrial waste heat [136, 70], co-generated heat [151], waste incineration [98] or renewable energy such as solar [134], biomass [73] or geothermal [34, 95]. These advantages become even more evident when moving towards 4^{th} Generation District Heating systems (4GDH). By decreasing the working temperatures of the network, the potential of integrating new resources increases exponentially [135].

DHCS are traditionally divided into three components [214, 186, 171]:

- *The demand* ('consumers'): space conditioning and Domestic Hot Water (DHW) preparation. The ultimate purpose of the system is to

[b][159] defines efficient district heating and cooling as "a district heating or cooling system using at least 50 % renewable energy, 50 % waste heat, 75 % co-generated heat or 50 % of a combination of such energy and heat".

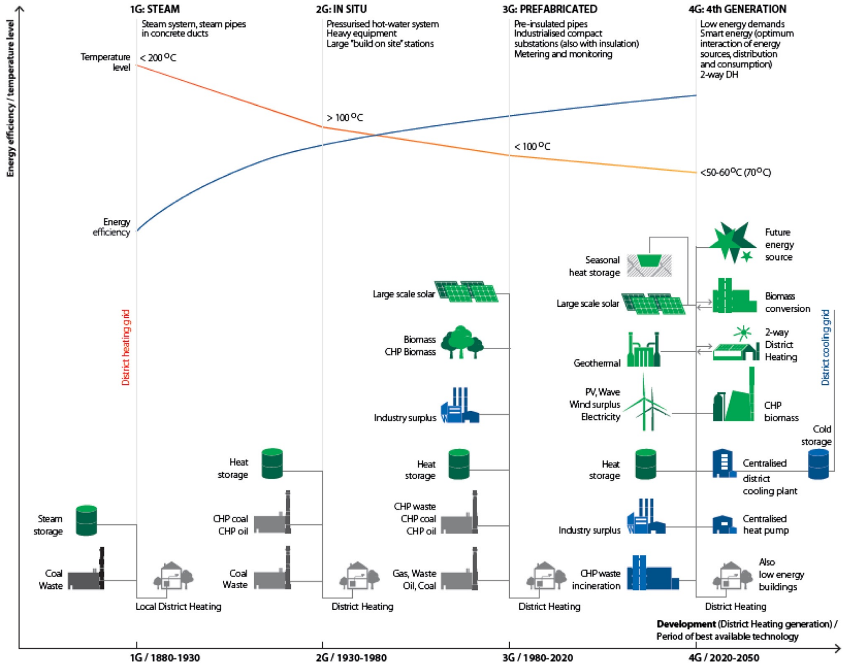

Figure 1.5: Illustration of the concept of 4GDH in comparison to the previous three generations (Source: [135]).

cover the energy demand of all consumers: single-family or multi-family houses, commercial buildings, institutional buildings, offices, industries, hospitals, etc.

- *The distribution network*: heat is distributed from thermal plants to the consumers (or in the other way around when talking about cooling systems) though a heat-carrying fluid (normally hot water or steam) in supply pipes. Heat and pressure losses are the critical elements in designing the network. *Storage* is usually considered at this level [137, 205].
- *The supply* (thermal energy plants): They 'generate' the thermal energy to satisfy the demand. They can be conventional thermal plants, heat pumps, co-generation plants, renewable plants, etc. *Storage* can also be considered here, mostly when the supply comes from renewable energy.

However, when moving towards 4GDH, the system becomes more complex by, for example, mixing different centralized supply systems or with the emergence of prosumers as Figure 1.5 shows. The term 'prosumer', already used in the power sector [83, 182], started to be also used in the thermal energy sector in recent years [162, 206, 42, 43, 41, 154]. It refers to those buildings that can 'consume' energy from the net as well as 'produce' energy (typically through renewable sources) for self-consumption or feeding into the net[c]. Due to this increase in complexity, a fourth component is becoming more and more important: *the control systems* [171, 186].

In order to understand these systems and tackle the problems of the high non-renewable proportion of thermal energy use in cities and the CO_2 emissions related to it, simulation becomes essential. Simulation enables to create a virtual model using the computer as a laboratory when doing it in real life is too costly or impossible. Thanks to simulation, different technical options can be easily and cheaply tested, leading to a conscious and sound decision-making in the urban planning and development.
Two critical issues have to be considered at this point. On the one hand, all components of the system can be considered from different points of view, depending on the question to be solved with the model. For example, if defining energy-saving policies, the level of complexity of the system's definition must be much lower than if performing technology design or creating operational control strategies. The intended audiences vary, then, from policymakers to engineers, and from urban planners to researchers. On the other hand, no model has sense without the corresponding input data. Feeding a simplified model with very good input data, or in the other way around, taking low-quality data and feeding it into a very detailed model, could produce unreliable results [161].

Therefore, models must adapt to the different levels of complexity required by the question to be solved, as well as to the different levels of detail of the data available.

1.2 Aim and objectives

This thesis aims to produce a useful and flexible tool by coherently connecting data and system models to help in decision-making processes regarding the urban energy system with a particular focus on thermal energy performance and renewable energy potential in heating and cooling systems.

In order to achieve this aim, several of specific objectives have been set:

[c]Although the terms 'consume' and 'produce' energy, are not thermodynamically accurate, they are widely used in the urban energy field. Hence, the author will adopt them for this thesis, too.

Technique	Method	Validation datasets
Code checking	Computer code is checked line by line.	–
Analytical tests	Predictions for a simple simulation are compared with expected results which can be calculated analytically.	EMC analytical tests
Interprogram comparison	Predictions are compared with those other simulation programs supplied with equivalent input data.	IEA annex 21, task 12: BESTEST / VDI6020 (German standard)
Empirical validation	Predictions compared with real building measurements. Predictions should be made without knowledge of actual measured performance (i.e. blind)	IEA annex 21, task 12: empirical validation test / IEA Annex 58 subtask 4: Twin houses

Table 1.1: Validation techniques with examples of validation datasets for single building models (Source: [28]).

1. To develop a flexible building model able to represent the variety of the city's building stock.
2. To produce a District Heating Network (DHN) model able to capture the dynamic thermal behaviour of the networks.
3. To validate models using different available methodologies (Table 1.1).
4. To integrate the models in a modular Urban Energy System simulation environment that facilitates input data and incorporates building-urban and building-supply system[d] interactions.
5. To demonstrate the usefulness of the modular urban simulation tool for decision-making processes by accomplishing diverse tasks with the same software.

1.3 Originality and contribution to knowledge

By achieving the objectives previously defined, this research has contributed to the urban energy modelling sector in the following ways:

1. A dynamic building model has been produced. This model has, among others, the following characteristics that are not found all together in any other model:
   - Flexibility to adapt to any type of building of a city stock.
   - The internal long-wave radiation is explicitly presented in the model.

[d] The supply system also includes the supply network.

  - The consideration of the thermal bridges.
  - Modularity to allow integration of smaller modules that perform specific functions, such as stochastic models that produce use profiles or more sophisticated and up-to-date construction alternatives.

2. A pseudo-dynamic DHN model is provided. It can represent the dynamic thermal behaviour of the net, which is crucial when evaluating the impact of very intermittent elements in the system, such as individual building demands or renewable energy supply.
3. A novel prototype of an urban energy simulation tool has been developed. This tool integrates both models, together with traditional and renewable supply system models. The tool has three main characteristics that can be considered substantive contributions:
   - It is very modular, allowing different studies with the same tool and being able to adjust the models to the level of detail of the input data available.
   - It includes the automation of data setting for dynamic simulation, which facilitates the simulation of large areas.
   - It considers the interaction building-urban context as well as building-network. No other tool in urban energy simulation has been found in literature able to do that at such level of resolution.

1.4 Organization of the thesis

The flowchart 1.6, presents the workflow followed within this thesis. The purple path was the one taken. The first step in this workflow is the literature review on Urban Energy System Model (UESM), presented in chapter 2. The system has been divided into the three main components (demand, network and supply) and a review on each of them was made. First, the building energy models, considering the urban context. Second, a review of network models and, finally, a search on supply systems for DHN were also done.
Considering the output of the models' reviews, research on simulation tools that use the desired models and fit the requirements defined in section 1.2 was performed. Two paths were followed in this research:

1. **No co-simulation**: A catalogue of software for UESM was produced. The catalogue divided the tools into two groups, comprehensive software and platforms. From those, a selection of the preferred tools was made, and a more in-depth explanation on the final selection (a platform called `SimStadt`) is given.

According to the platform selected, a final review on simulation tools to be plugged into the platform was performed. These tools were catalogued, depending on how well their models fit the requirements previously defined in section 1.2. `INSEL` was finally preferred as simulation engine.

2. **Co-simulation**: A brief introduction to this approach is presented in section 2.2. An on-line co-simulation platform called `Ci-NERGY` was selected together with the `SimStadt` platform. They are very similar in their concept, but, in addition to the benefits of being a web-service oriented tool, `Ci-NERGY` allows two-way data exchange between tools (enabling co-simulation) while `SimStadt` allows only one way.

Chapters 3, 4 and 5 dig dipper into the workflow structure and the models' development. The models of the building components together with the building model itself, are first explained in chapter 4. Its validation following the Building Energy Simulation Test (BESTEST) is presented at the end of this chapter. In chapter 5, the adjustments done for the network model is discussed, and the verification and calibration of the modified model is presented.

In order to give an idea of the potential of the developed tool, two application cases with different objectives have been carried out. The first one is also used to go over the structure of the workflow, reviewing each step and clarifying their single targets inside the complete workflow. Furthermore, with the applications, the innovations provided by the tool are pointed out, using each application to highlight a subset of them. The first application, in chapter 6, calculates heat demand at block-scale in a neighbourhood in Stuttgart. A dynamic simulation of every building has been carried out, taking into account the building-to-building interactions in terms of irradiation. Different types of buildings with different uses compose the neighbourhood. The simulation has been carried out for two different levels of detail of the 3D input data, allowing a comparison in the outputs of both cases. Furthermore, the potential of a decentralized heat pumps system powered by distributed solar electricity from PV and supported by the grid when needed was analysed for the most detailed case: the one with LoD2 input data.
The second application, presented in chapter 7, is focused on the behaviour of a DHN. The impact to the DHN of a distributed solar thermal system has been analysed, together with the potential of such a system on a real network in the city of Vienna. The heat demand is given as an input to the study (it has not been calculated). Finally, the conclusions of the thesis and future work are tackled in chapter 8.

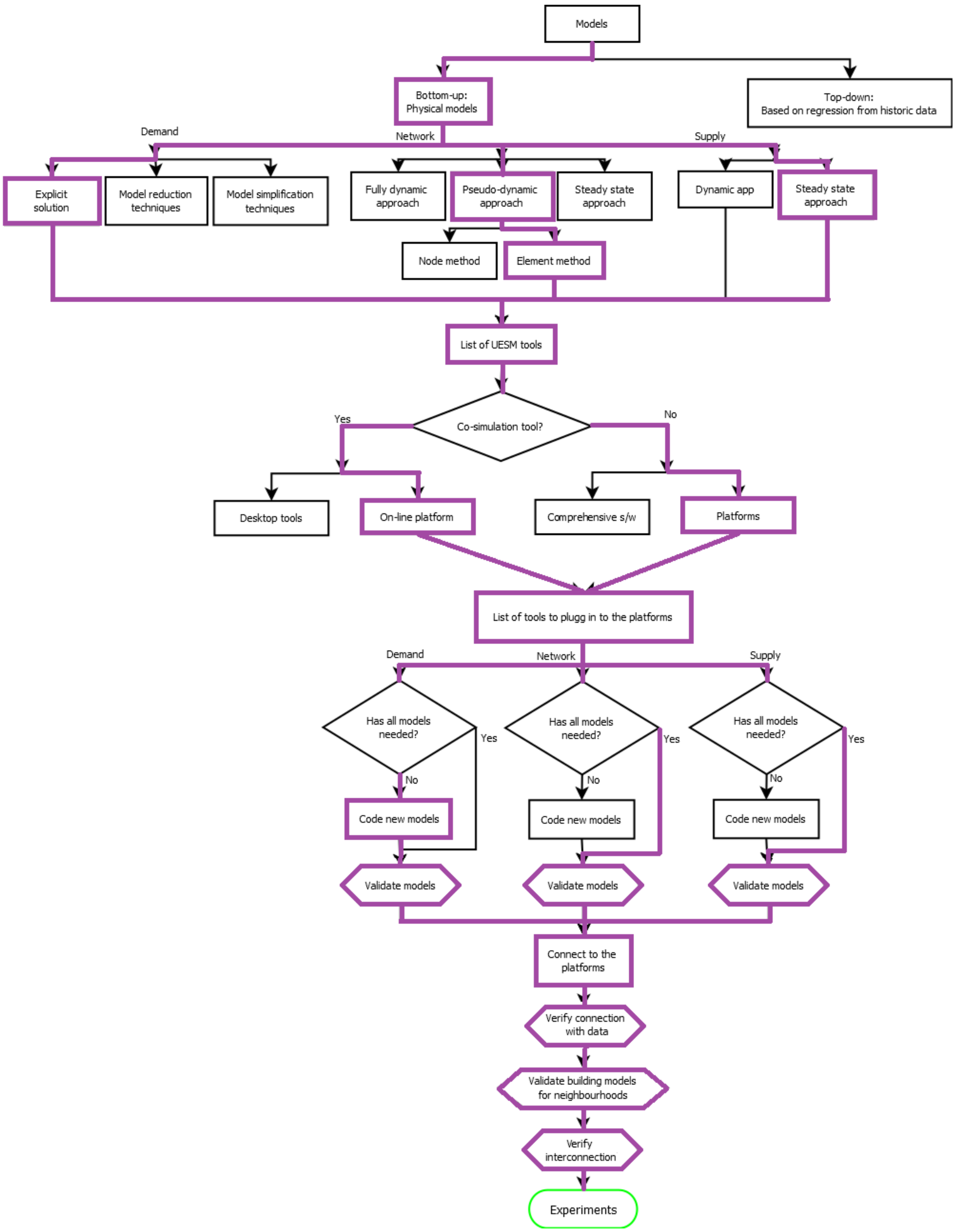

Figure 1.6: Workflow of thesis.

Chapter 2

Review on Urban Energy System Models and Software

The term Urban System Model gathers up a large number of conceptually different model topics, from traffic to building location or resources flows (energy, water, food, waste, etc.). The urban system model may then consider only one of those topics, some or all of them together, as they interrelate in real life. This thesis focuses specifically on energy system models, but being aware of the real complexity of the urban systems.
Also, analysing the energy system in the urban context is a complex issue, and some boundaries must be defined to delimit the target such as the urban area size or the type of energy use from all possibilities: thermal, electric, energy for transport, etc.
As the subject of this thesis is DHCS, the size of the area of study is closer to a neighbourhood than to a complete city. Robert E Best [32] defined a 'district or community scale' as 10^2 to 10^3 neighbouring buildings with peak power consumption between 10 and 100 MW. That is consistent with the size extracted from the review in district heating and cooling technology done by Rezaie, B. and Rosen, M.A. [171]. In order to include also small-scale DHCS [162, 101], the considered size in this thesis ranges between a few buildings to a thousand. As well, the focus is on the thermal building demand and supply.

This chapter gives an overview of the different UESMs found in the literature, focusing on those that consider the defined size and that include thermal energy flows. Models are usually embodied in computer programs [17] that enable the results to be tested against data (if available), and the user to

easier analyse the target scenarios. These tools are also discussed in this chapter.
Regarding the tools, there is considerable ambiguity in the literature concerning the meaning of certain technical terms. To ensure that the reader understands the intended meanings of key terms used in this thesis, please refer to the glossary in Appendix A.

2.1 Urban energy system models

Huber and Nytsch-Geusen [100], defined four levels of resolution in urban energy simulation:

1. Spreadsheet analysis.
2. Non-integrated building and supply system simulation.
3. Coupled building and supply system simulation.
4. Computational Fluid Dynamics (CFD) simulation.

With level one, only basic estimations of demands can be performed as it is mainly based on monthly average values. This level is too simple for the thesis' target.
Both the second and third levels consider dynamic simulation. They consist of different resolution approaches to the same problem. In the non-integrated case, the simulation is done sequentially in different steps, and the data exchange between simulations take place only in one direction. First, loads are calculated, considering zone temperatures equal to set zone temperatures. Then, the network and the supply systems are simulated with the input of those 'ideal loads'. This approach ignores, for example, the impact of the thermal capacity of the building and the control strategies of the supply systems. In the case of coupled simulation, the data exchange goes in both directions. Therefore, all components can interact with each other during the simulation. Both of these two levels fit the objective of this thesis. Finally, the fourth level can answer detailed questions such as thermal comfort conditions or the wind flow patterns. This level is too detailed, and it is out of the scope of this work.

It is hard to find a model that considers demand and supply together at the second and third levels of resolution. Rezaie et al. [171] showed that those that consider them together mainly use qualitative decision-making techniques rather than quantitative evaluations of environmental benefits, remaining at the first level: spreadsheet analysis. The review is, therefore, divided in three parts to classify the models depending on their target separately: first the Urban Building Energy Modelling (UBEM), then the network models and finally the supply systems ones.

2.1.1 Urban building energy models

Buildings are the main components of the UESM because they provide the starting point for other analysis such as refurbishment purposes, system dimensioning or optimization. Two different analytical strategies are generally differentiated [199, 194, 76], including Top-Down and Bottom-Up.

a. Top-Down strategy

This strategy is associated with the economical paradigm. The technology is treated as black boxes being difficult to analyse detailed technical proposals. Still, they are suitable for energy policy questions related to macroeconomic aspects thanks to the explicit inclusion of inter-linkages between the energy and economy sectors. This strategy usually is highly endogenized, i.e. many parameters are defined within the equations of the model, and uses aggregated data. The models are derived based on regression from historical data so they are intrinsically limited to the cases from which they were derived, losing generality.

b. Bottom-Up strategy

Swan L. G. and Ugursal, V. I. [194] pointed out that there are essentially two bottom-up approaches: statistical and physical. Statistical methods generally apply some form of regression with common regression factors. Such models can include macroeconomic and socioeconomic effects, but they rely on historical consumption data. Therefore they are restricted to the cases from which they were derived and to a relatively short term as far as heat demand is concerned [116]. However, they are of great use when performing typological sampling for stock modelling (e.g. Project TABULA [5]).

On the other hand, the physical approach is associated with the engineering paradigm. It is used to make engineering studies separated from the market behaviour since they describe energy end-use and technological options in detail. To do so, it needs high disaggregated but measurable data. This approach is then the most powerful one since detailed scenarios for refurbishment or renewable energy systems can be tested, but the volume of required data makes it difficult to use in large areas. This can be overcome by using as inputs building archetypes or human behavioural patterns obtained through statistical models, which is, in fact, a common practice [188]. Nonetheless, the fact that it is independent of the market makes an over-estimation of the potential for efficiency improvements.

Nowadays, the line that separates these two strategies is getting more and more diffuse as the number of hybrid models available increases [36]. It can be concluded that the right approach to use in this thesis is the **bottom-up physical** approach. Statistical models of human behaviour or building archetypes should be employed. This approach allows accounting for the energetic coupling between buildings and with the urban context, or the effect of prosumers on the district network. Kämpf, J. H. and Robinson, D. [114] defined three physical modelling strategies:

1. Explicit solution of the heat diffusion equation.
2. Model reduction techniques.
3. Model simplification techniques.

From these, the reduction techniques are restricted to the cases used for developing the model, losing general applicability. The other two techniques are more general and, depending on the degree of simplification, also modular. But, this thesis intends to cover a big range of data availability cases. Thus, a more detailed simulation model seems to be a better option since it can be used for high or low level of detail of the data model. As a summary, the most appropriated modelling strategy for the target of this thesis has been considered to be the **explicit solution of the heat diffusion equation** using **physical nodal building models**. The thermal building model is explained in detail in chapter 4.

Every target building in an UBEM must have information related to four input datasets [169] to feed in the thermal model:

D1. **Weather data** can be found for many places around the world either from local meteorological surveys [1] or as mean values of previous years in standard formats such as Typical Meteorological Year (TMY) [112]. TMY format was considered by Crawley the best for building performance simulation [57]. These values are normally taken from meteo-stations out of the urban area; therefore, some studies have lastly been carried out in order to characterise the local micro-climate [44, 155, 164]. Effects like the heat island, the long-wave reflection or street canyon effect can have a big influence in the building demand simulation [141].

D2. Building geometry includes the external geometry, with windows, doors, elements on the façades or the roof, among others. But also internal geometry and even furniture. Geographic Information System (GIS) combined with Laser Imaging Detection and Ranging (LiDAR) [167] can be used to generate 2.5D or 3D external geometry automatically. However, up to now, there is no method to generate internal geometries automatically. Finally, some techniques like Mobile Mapping together with Automatic Object Extraction [139] can be used to generate the window areas information, but it is rarely used. Another option is creating the data from scratch, but it is very time consuming and a source of errors. In the building geometry databases exist very few buildings with detailed information, typically only the footprint and high or number of storeys can be found.

D3. Construction data. Some countries developed databases with information related to the construction, thermal and optical properties of buildings for different archetypes, usually clustered by type of building and year of construction. In Europe, under the projects TABULA (2009-2012) and EPISCOPE (2013-2016), 20 countries developed building archetypes with construction information, among others. This values are accessible from the TABULA WebTool [4]. Again, this information can be generated from scratch with the same problems as mentioned before.

D4. User schedules are the last related data family. Two types of schedule models can be used, either deterministic or stochastic. The occupants should be treated as individual agents rather than identical robots. However, the majority of the building models use deterministic schedules, losing information about the erratic behaviour of occupants. But, when simulating a large number of buildings connected to the same distribution system, the demand curves overlap, producing overshoots at specific moments due to the repetition of the schedules. In these cases, the importance of stochasticity increases. The idea of considering stochastic schedules at the urban level was already proposed by CitySIM [176].

2.1.2 Network models

Two significances can be found in network modelling, including the model of a specific component, e.g. substations, pipes, pumps, heat generators; or the model of the complete district heating system. In this chapter, the

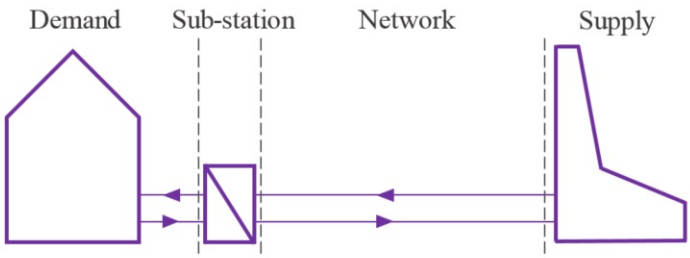

Figure 2.1: Schema of a District Heating System.

discussion goes around a meaning that is closer to the second option, in which the network and sub-stations are modelled together (see Figure 2.1). This meaning is also the most common one in the field.
The network system includes here pipes and all pipe connectors, pumps and substations (both, for the 'consuming' and the 'producing' sides), considering as thermal carrier only liquid water. Steam was commonly used in first-generation DHN, but nowadays, very few networks (e.g. New York and Paris) still use it due to its thermal and economic inefficiency [215]. Steam is a high exergy carrier, with correspondingly high potential for energy dissipation.

As in the previous case, there are two strategies to model the network, the top-down and the bottom-up. Following the same conclusions extracted for the building models, the top-down (e.g. [126]) strategy was rejected. Only the approaches for the bottom-up are considered, including steady-state and dynamic approaches [35].

a. Steady-state approach

The steady-state approach is commonly used in DHCS for network dimensioning and optimization of the layout [80], together with optimization of the performance [58, 209, 35] or simulation analysis [132]. Both parts of the model, the hydraulic and the thermal ones are uncoupled. Thus, the modelling is done in two steps: first, the flow rates through every pipe and pressures at each node are calculated with constant water properties (density, viscosity, heat capacity and thermal conductivity). Then, the temperatures field is obtained by doing a heat balance equation in every pipe. The heat transfer is considered to be radial only, and the water and surroundings' temperatures are assumed to be constant along the pipe.

b. Dynamic approach

Many temperature and velocity fluctuations appear when connecting unstable sources to the network, i.e. waste or solar heat. Furthermore, in District Heating Systems (DHS), a temperature wave is deliberately produced to reduce the flow during peak consumption periods [79]. A correct control of the dynamics of the network has been proved to lower the total fuel consumption in, at least, 2% ([115] cited in [191]). This behaviour is not possible to capture with a steady-state approach, and a dynamic one must be used [78].

Velocity fluctuations increase the probability of turbulence and turbulent diffusion leads to higher heat exchange. This means that the higher the velocity, the bigger the heat flows. Furthermore, the temperatures field affects the fluid physical properties involved in both heat transfer and fluid flow. Hence, a **fully dynamic approach** must also couple both parts of the model: hydraulic and thermal.

Nonetheless, the dynamics of the hydraulic part are much faster than those of the thermal part [191]. Pressure waves travel at the speed of sound. In contrast, temperature waves do it with the water flow (the typical time-steps for velocity and pressure calculations are between 0.5 and 2 seconds, while the time-step of temperature waves can be minutes or even hours). Hence, the dynamics of the flow are less important from the operational point of view than the thermal dynamics. A **pseudo-dynamic approach**, with a large time-step of calculation (some minutes), leads to an uncoupled approach where the velocities are steady-state calculated. Still, the thermal transients are captured, including the time delay of the temperature propagation, the thermal capacity of the network and the heat losses [35]. Gabrielaitiene, I. et al. [81] compared with numerical experiments a coupled and uncoupled models and proved that not considering the coupling between thermal and hydraulic models leads to insignificant errors in temperature predictions. The pseudo-dynamic is the approach that is most frequently used in engineering for network simulation [157] and is the one selected for this work.

Two methods are used to model the dynamics of the thermal behaviour based on the pseudo-dynamic approach, including the element and the node methods [157]. Each of them uses a different approach to solve the 1-D fluid's energy conservation equation.

The node method was described in 1997 by Benonysson [219]. It integrates energy conservation equation along a fluid's particle path line using the method of characteristics described by Wylie et al. in 1978 [220]. Through this method, the outlet temperature of a pipe can be inferred from a past inlet value, taking into account the heat capacity of the pipe and the thermal losses in a second step. (For more details, refer to [86]).

Alternatively, the energy conservation equation can be solved using **the element method** [200, 93]. It solves the energy balance in a defined control volume where the temperature is assumed to be uniform. The energy conservation equation can be solved with an implicit or an explicit formulation, but in both cases normally under the following assumption:

- The heat losses in the radial direction are calculated considering a single uniform temperature in water and pipe, and also uniform temperatures in insulation and surrounding ground for every control volume at each time-step. The axial conduction in the fluid and pipe wall is negligible.
- The thermal conductivity is assumed constant for every component. The jacket pipe thickness is ignored for the heat transfer calculation.
- Compressibility of the fluid is neglected.
- Fluid physical properties (density, viscosity, heat capacity and heat conductivity) are constant at each time-step.
- Leakage is obviated.
- Temperature rises due to friction losses is neglected.
- The effect of the heat losses to the ground is neglected, considering that the ground temperature is not affected by the network. This assumption is not as common as the others, and it can be overcome in the future by developing a more detailed model of the ground-network interconnection.

Several studies proved that both methods provide similar results. In 1997, Pálsson, H. [156] made a theoretical comparison between both models concluding that none of the methods could be considered better concerning accuracy. Both models have problems with artificial diffusion, which results in abnormal smoothing of sharp temperature profiles. In both cases, it was proved that the problem could be overcome by improving the model through a better understanding of how the relationship between the velocity through the pipes and the velocity of calculation (length of pipe segments divided by the simulation time-step) affects each method. This relationship is normally studied through the Courant-Friedrichs-Lewy (CFL) number, presented in section 5.3 and affects each method in opposite ways. At the same time, the nodal one behaves better in general at low CFL, the element method solves the artificial diffusion at high CFL but could provoke small overshoots in sharp temperature gradients.

Other comparisons were performed using measured data. Gabrielaitiene, I. et al. [79] used both models to simulate the propagation of a temperature front and then contrasted their results against measured data. They concluded that with a correct selection of floating points in the element method, there were similar results in terms of accuracy between the node and the element methods. Furthermore, the element method predicted better the peak of the temperature wave. The node methods seemed to predict better the delay on its appearance. More recently, Wang, Y. et al. [209] carried out another experiment using measured data from an existing DHN in Shijiazhuang, coming to the same conclusion: both methods could keep the errors within $\pm 0.5°C$. Besides that, the node method requires much lower computational time [31]. However, the higher computational time of the element method can be overcome by the parallelization of the computations.
In any case, this method is not suitable to be used in meshed networks or networks with multiple heat sources (e.g. prosumers). That is because the node method only calculates temperatures in nodes, but not their distribution along the pipes. Therefore, it can not capture the changes in the direction of the water flow rates due to the hydraulic variations [209]. Therefore, the node method is not suitable for the scope of this thesis. Those software based on the element method or that allow users to code their models, are discussed in section 2.3.

2.1.3 Systems models

In the same way as for the networks, two approaches can be found for modelling the supply systems:

a. Steady-state approach

The steady-state is the most commonly used approach in supply systems for DHS simulation [197]. Depending on the objective of the study, either the performance of the equipments are modelled with seasonal or annual constants values of efficiency and heat generation output, or these parameters can also be dependent on variables such as temperatures, the Partial Load Factor (PLF) or solar radiation, through performance curves. Delangle, A.[61] studied the optimization of the marginal expansion of an existing DHS and defined annual constant efficiencies for all possible supply systems considered in the study. Also, Wang, D. et al.[208] used a constant efficiency of solar panels for early-stage designs of DHS with distributed solar thermal energy supply. Pavičević, M.[160] used a model in which generated heat and efficiencies of systems depended on temperatures or PLF at every time-step of one hour to optimize and size a district heating systems considering building refurbishment. Afjei, T. et al.[12] used a steady-state approach to “provide a fast but sufficiently precise calculation of heat pump system performance” to compare different equipment for the same network.

b. Dynamic approach

The dynamic approach is, however, needed in some cases due to the high dynamical behaviour of some equipments in unstable periods, like during starting and shutdown regimes. Giraud, L. et al.[85] built a complete dynamic simulation of network and supply systems to evaluate control strategies.

None of the approaches have been excluded from the review of simulation tools.

2.2 Urban simulation tools

Many tools have been developed in the last years trying to simplify the use and access to urban energy models, but covering only partially the complexity of the energy system in cities [120]. Allegrini et al. [17] concluded in their review on urban models and tools that the building-to-building thermal and solar interactions, Urban Heat Island (UHI) or vegetation might actively modify the results of urban energy system simulations. This building-urban interactions were in 2005 for the first time considered in the Sustainable Urban Neighbourhood modelling tool, `SUNtool` [175]. This software has a thermal model, coupled with Heating, Ventilation, and Air Conditioning (HVAC) and Environmental Control System (ECS) models, with an urban-sensitive radiation model, the Simplified Radiosity Algorithm (SRA) [177]. Heavily inspired by `SUNtool`, but further refined with more rigorous thermal and behavioural models is the comprehensive software `CitySim` (see Table 2.1). Since then, many other tools emerged, either as simulation platforms or comprehensive software as the previous ones. In recent years, the first option has more and more followers, thanks to its flexibility and the possibility of interconnecting tools highly valued by the scientific community. Following this idea of flexibility and interconnections, the co-simulation is gaining the interest of the urban simulation community. Co-simulation stands for coupled simulation; the coupled models share common variables, but are implemented in two or more different software. The use of standards to share the information is, therefore, a common practice in this relatively new field. An example of this is the Functional Mock-up Interface (FMI) standard [24]. FMI is a "tool independent standard to support both model exchange and co-simulation of dynamic models" [23]. The simulation models must be encapsulated in zip files called Functional Mock-up Units (FMU). Some well-established energy simulation tools have already FMU export utilities that allow the encapsulation of models developed in the mentioned tool. That is the case of `TRNSYS FMU` export utility [9] or the `EnergyPlusToFMU` tool [124]. Other tools like `Dymola` are already based on the FMI standard [196] or have been extended to use it like `CitySIM` [198]. Moreover, there are some attempts of joining the capabilities of FMI and building modelling standards like the *IBPSA Project 1* started in 2017 [102], or the tools developed by Wetter, M. et al. [216]. Nevertheless, to the best of the author's knowledge, there are not urban simulation tools already available that use this approach. A second example of the use of standards for co-simulation is the work presented by Wate, P. et al. [210]. They make use of the Service-Oriented Architecture (SOA) computing paradigm. SOA acts as an enabler to expose software functionalities/applications as web services using three key standards: Simple Object Access Protocol (SOAP), Web Service Description Language (WSDL) and Universal Discovery, Description and Integration (UDDI). This second approach, together with the concept of co-simulation, has the advantage of being web service-oriented. The advantages of a web service are clear; installations or configurations are not needed, updates are made automatically, any computer system can be used regardless where it is placed, and the consumption of resources corresponds to third parties. This last advantage gets even clearer when simulating complex models because they have huge computational costs. With an online solution, these costs can be divided into many computers, calling multiple instances of the solver installed in different servers and, by doing so, diminishing the computational load per unit. This tool was later presented by Agugiaro, G. under the name of `Ci-NERGY` platform [13].

Not only the models' interaction, but also the interfaces of models with data and the user are recurrent topics in the software development field. Many authors [17, 116, 120, 185] deep into the relevance of data input automation. It reduces the chance of input errors, and also human costs as the data is, in most cases, one of the highest time consumers [100], making it more feasible to simulate large models. Also, a clear communication of results has long been an issue in the use of urban simulation tools [17]. In urban simulation tools field, the GIS thematic mapping becomes a very intuitive tool for final users to access and understand results [37, 150, 222].

To combine these three aspects, models, input management and results communication, many authors agree on the crucial role of modularity [146, 147, 189]. Baldwin and Clark [26] recognize the use of modularity in a large number of fields to deal with complex systems. The idea behind is the division of a complex system into simpler and more manageable modules. They define a module as "a unit whose structural elements are strongly connected among each other and relatively weakly connected to elements in other units". The modules can then be independently created and used in different systems or for different purposes. Furthermore, they can be improved, updated or modified in parallel, and allows the developer to easily add new capabilities to the software [27], like adding UHI effect, electricity networks or improve the actual models for; for example, including DHW, electrical demand or even internal zoning. These characteristics help to prolong the life of the tool by allowing accommodation to future uncertainties, like behavioural changes and innovative designs. In sum, modularity makes complexity manageable and adds flexibility and adaptability to the tools [189]. Allegrini et al. [17] also highlighted the challenges that the urban energy modelling community must face regarding the development of tools that can support decision-makers at an early design process, as well as develop others with more detailed models for specific case studies. They proposed the development of tools that could bridge the different levels of detail and model types. A modular structure is an excellent strategy to adapt to various configurations.

To summarise, a list of requirements for urban energy tools can be listed. They should:

- R1. Take into account the urban context.
- R2. Allow automatic data mapping.
- R3. Have the ability to call multiple instances of the solver to simulate multiple buildings.
- R4. Display results via GIS thematic mapping.

And, by being modular tools, they may:

- R5. Have the ability to accommodate to different levels of detail to solve distinct tasks.
- R6. Be open to modifications, updates or improvements in every step of the workflow, to avoid fast obsolescence and allow further developments from the UESM community.

Finally, the models implemented in such a tool should:

R7. Cover DHS up to the 4^{th} generation (see Figure 1.5), including demand, high and low temperature networks and conventional and renewable energy supply systems. The models should follow the Parsimonious strategy: be as simple as the most complex case to be analysed allows, but not simpler.

R8. Account with stochasticity of human behaviour and DHW consumption.

R9. Have the ability to perform not only static but also dynamic simulations so it can catch the inertias of the system. That is essential to analyse unstable behaviours very common in the 4GDH systems (e.g. the potential of prosumers or the analysis of bi-directional networks with pronounced transient regimes).

Table 2.1 presents an overview of bottom-up strategy based tools. The tools that model only the electrical part of the energy flows (like only electrical demands and grids) such as `HOMER` [143] have not been considered. Neither have been those whose models for building demand uses a steady-state approach. Examples of these tools are the one used by Quan et al.[165] for simulating Manhattan that performed hourly balance formulations, or `MODEST` [94] using a monthly energy balance approach. Only tools that are already capable of running dynamic simulations of thermal flows or give the option to plug in some other tools are presented. The table shows some characteristics of the tools together with how they fit each requirement previously listed.
In column “Type” of Table 2.1, it is written whether the tool is a Comprehensive Software (CS) or a Platform (P). Column ‘Models’ shows if the tool has models (at any detail) of any of the three parts of the system, Demand (D), Supply (S) and Network (N), or if all three are represented (All). In R1 the detail in which the urban context is considered within four possibilities is presented: Building-to-building thermal interaction (TI), building-to-building solar interaction (SI), Urban Heat Island (UHI) or vegetation (V). Columns R2 to R9 (except R5) say whether the tool fits the corresponding requirement or not. Column R5 shows whether the software uses an external simulation engine or this is already incorporated; in this case, the word ‘Same’ is written. Finally, the last two columns give some references of urban projects using each tool and the website where to find the tool, when it is available.

As can be extracted from Table 2.1, current tools only partially address the key features previously defined:

1. Often focus on specific building type like `BEDEM`.
2. Often focus on specific places like `BEDEM` or `EEP`.

Name	Type	Models	R1[a]	R2	R3	R4	R5	R6[b]	R7	R8	R9	Ref.	Website
Building Controls Virtual Test Bed (BCVTB)	P	D & S	✗	✗	✓	✗	✓	✗	✗	✗	EnergyPlus & Simulink	[100, 158]	https://simulationresearch.lbl.gov/bcvtb,http://www.geedindia.org/Research.html
BEDEM	CS	All[c]	?	✗	✓	✗	✗	✗	✓	✗	TRNSYS	[117, 118]	-
Ci-NERGY	P	-	-	✓	✓	✓	-	✓	✗	-	-	[13, 210]	http://dmz02.rz.hft-stuttgart.de:8080/CINERGY/
CitySIM	CS	D & S	TI, SI	✓	✓	✓	✗	✓[d]	✗	✓	Same	[176, 122, 130]	http://citysim.epfl.ch/
EEP	P	D[e]	?	✗	✓	✓	✗	✓	✗	✗	HTB2	[109, 108]	http://www.cardiff.ac.uk/archi/research/cost8/case/assessment/eep.html
SimStadt	P	D & N[f]	SI	✓	✓	✓	✓	✓	✗	✗	✗	[150, 192]	http://www.simstadt.eu/en/index.html
SOLENE	CS	D	TI, SI, UHI	✗	✓	✓	✗	✓	✗	✗	Same	[145, 39]	https://groupes.renater.fr/wiki/solenetb/
UMI	P	D	SI, UHI	✗	✗	✓	✗	✓	✗	✗	EnergyPlus	[168]	http://urbanmodellinginterface.ning.com/

Table 2.1: Software summary: Urban simulation tools.

The requirements are:
R1. Take into account the urban context.
R2. Automatic data mapping.
R3. Ability to call multiple instances of the solver.
R4. Display results via GIS thematic mapping.
R5. Ability to accommodate to different levels of detail.
R6. Be open to modifications, updates or improvements.
R7. Model up to 4GDH system.
R8. Account with stochasticity.
R9. Ability to perform dynamic simulations.

[a] This requirement was not clear in the literature review for some tools. They are labelled with a question mark.

[b] This requirement is difficult to analyse from the literature review. It is normally not explicitly stated, thus this column is only indicative.

[c] But only for a specific area and building type; Belgrade Housing.

[d] Under restrictions.

[e] Only for UK. Results showed per post-code: 10 to 15 houses or 1 individual non-domestic building.

[f] Only design and dimensioning, no simulation.

3. They may need manual data input like `EEP` or `UMI`.
4. Almost no one can simulate DHS with renewable sources.

The `Ci-NERGY` platform is an exceptional case. As already mentioned, it is a co-simulation web service-oriented tool. It has the advantage that handles CityGML standard and that it is thought to interconnect any energy simulation tool, so there are in principle no limits to its simulation capabilities. On the flip side, it is still on a very early stage of development.

From the rest of the tools, only `SimStadt` had already solved the automation of the input data. In fact, its main specialization is the data management using virtual 3D city data models, as realistic inputs for simulation. It is also the only one that explicitly states that it considers the extension of the capabilities. It is intended to be sufficiently open on its structure to allow for the integration of any number of simulation plug-ins, which could solve the lack of dynamic models [149]. It is also the only one that was developed, allowing different levels of detail of the input data. Also, the visualisation and communication support is its second big virtue. The results are presented in different formats, including files with time series results, tables and 2D or 3D GIS maps.
`SimStadt` manages CityGML databases, in which the building data model is defined in different levels of abstraction. That makes it easy, from the data side, to adjust it to the different levels of complexity required. That is a compelling advantage that enables automatic creation of the input file for building energy simulation and therefore, saves a significant amount of time and effort. Moreover, automation reduces errors and mismatches in the building energy simulation process.
Not only the 3D model, but also some other characteristics of the urban area crucial for thermal simulation are described in the database thanks to the so-called CityGML Application Domain Extension (ADE) [6]. Especially interesting for this project are:

- UtilityNetwork ADE, which defines a topological network model.
- Solar ADE, which manages information of use to local authorities for encouraging the adoption of solar energy.
- Energy ADE, which extends the CityGML standard with the necessary features and properties to perform energy simulations.

Therefore, this tool fits at different levels four of the requirements listed in section 1.2; it allows automatic data mapping, it is also thought to be modified and extended and finally, it handles GIS thematic mapping results.

On top, R6 is covered partially in the data side thanks to the definition of different Level of Detail (LoD) of the data models in CityGML.

Both SimStadt and the Ci-NERGY platform have been considered interesting tools for the development of this thesis. Moreover, any model developed for the platform SimStadt is susceptible to be also connected to Ci-NERGY as a separated plug-in or as part of SimStadt itself as it was already done by Wate, P. et al. [210].

2.3 Specific simulation tools

The literature showed two different feasible types of tools for modelling the elements of the system. On the one hand, the energy simulation tools that provide general energy models and allow the user to code new ones if necessary. On the other hand, specific tools to simulate one or more of the components of the system.
In the first group, three software must be mentioned, including INSEL, Dymola and TRNSYS. These tools are object-oriented, multi-domain modelling tools for component-oriented modelling of complex systems. They are modular and are prepared to exchange data with other tools. Furthermore, they have some detailed dynamic models already implemented.
The second option –the specific tools (presented in Table 2.2) for buildings, networks or supply systems– do not always offer the advantage of modularity, neither they allow interconnectivity. For example, almost none of them use non-standardized input-output formats, requiring specific interfaces. Only EnergyPlus offers a tool called EnergyPlusToFMU (see section 2.2) to translate its outputs to a standard. But, EnergyPlus in stand-alone mode, models single buildings, not taking into account the building-urban or building-network interactions. Furthermore, some tools are very specific, like SUNREL, that simulates only dwellings. Table shows what parts of the system are modelled within the tool together with some references of use and the tool website.

General energy models tools: Dymola, TRNSYS and INSEL

Dymola [69] is a modelling tool based on MODELICA [77] modelling language. It was initially oriented to model the dynamics of vehicles, but later on, increased the scope and at the moment it has multi-engineering capa-

Name	Dem.	Netw.	Supp.	Ref.	Website
Bsim	✓	✗	✗[d]	[125, 131]	http://sbi.dk/en/bsim
DOE2.1E	✓	✗	✗	[14, 15, 89]	http://doe2.com/DOE2/index.html
EDSL-TAS	✓	✗	✗	[181, 19, 82]	http://www.edsl.net/main/Software/Designer.aspx
EnergyPlus	✓	✗	✗	[99, 201, 138]	http://apps1.eere.energy.gov/buildings/energyplus/
EnergyPro	✗	✓[a]	✓	[207]	http://www.emd.dk/energypro/
eQuest	✓	✗	✗	[187, 119, 221]	http://www.doe2.com/equest/
ESP-r	✓	✗	✓	[50, 217]	http://www.esru.strath.ac.uk/Programs/ESP-r.htm
HTB2	✓	✗	✗	[53, 121, 129]	http://sites.cardiff.ac.uk/architecture/about-us/facilities/environmental-lab/computer-modelling/
IDA-ICE	✓	✗[c]	✓	[97, 173, 144]	http://www.equa.se/en/ida-ice
IES-VE	✓	✗	✗	[18, 16, 107]	http://www.iesve.com/software/ve-for-engineers
Neplan	✗	✓[a b]	✓	[127, 223, 48]	http://www.neplan.ch/
NetSim	✗	✓[a b]	✗	[41, 42, 123]	https://www.vitecsoftware.com/en/product-areas/energy/products/netsim-grid-simulation/
OpenStudio	✓	✗	✗	[67, 179, 52]	https://openstudio.nrel.gov/
Polysun	✗	✗	✓	[87]	http://www.velasolaris.com/english/home.html
Riuska	✓	✗	✗	[113]	http://www.granlund.fi/en/software/riuska/
STANET	✗	✓[a b]	✗	[3, 74, 172]	http://www.stafu.de/en
SUNREL	✓	✗	✗	[62, 184, 30]	https://www.nrel.gov/buildings/sunrel.html
Termis	✗	✓[a b]	✗	[29, 20]	https://sw.aveva.com/webinars/discover-termis

Table 2.2: Software summary: Specific simulation tools.

[a]Steady-state approach.
[b]Dynamic approach.
[c]Under development.
[d]Only PV.

bilities, i.e. the models can consist of components from many engineering domains. As it is based on MODELICA modelling language, there is a big community working with it and developing new models, which are very easy and fast to implement. On the other hand, it is slow for big models, and it has many components still under development, like the connection with external databases, or the DHN library [86]. Therefore, although the tool has a significant potential, the solver is still on an early stage for exploiting all its advantages.

`INSEL` [183] is a modular simulation tool to understand, plan, monitor, and visualize energy systems. As guaranteed in its web, `INSEL` offers users ready-made simulation models organized in blocks for a quick start, but users can design entirely new blocks for many system applications. These blocks can be interconnected to a detailed model of a specific simulation problem.
`TRNSYS` [153] and `INSEL` are very similar in their concept, having as the most significant difference the way that they solve the equations. In `INSEL`, the physical models of each component are solved within each single block. Therefore, there is no need for a common equations solver, which is the case of `TRNSYS`. That has the potential to make the simulations of complex models faster in `INSEL`. Furthermore, both tools have similar packages of models of solar systems already implemented, but they do not have special packages for DHN models. In fact, the initial scope of `TRNSYS` excluded hydraulics, so extending the code to account on new physical phenomena needed for the DHS could be very arduous [84]. Finally, `TRNSYS` have a dynamic model for buildings. Still, it is an all-in-one not-modular block, so it would force to prepare different templates for different building geometries and levels of detail of them, losing the concept of modularity. On top of that, the coding and implementation of new blocks in `INSEL` is more straightforward than new types in `TRNSYS`.

2.4 Conclusions of Literature Review

This chapter has presented a review on simulation models of urban energy systems dividing them into the three main components, including building and its interactions with the urban context, the DHN and the systems that supply them. Some conclusions have been extracted from the review. Regarding the building models, a physical bottom-up approach was found to be the most adequate to the purpose of this thesis. Inside those, the models that explicitly present the heat transfer equations are better to ensure flexibility and adaptability. Also, it was found to be necessary to model DHN with, at least, a pseudo-dynamic approach to cover the needs of the system to be modelled. Finally, the model of the supply systems do not impact so much in the behaviour of the complete system. Therefore, both approaches have been considered suitable, including steady-state and dynamic approaches.

After this review, research on tools where those models are embedded has also been done. The characteristics of the models extracted from the previous section were the focus of that research. After the extensive review, a list of nine requirements for urban energy modelling tools have been defined and a set of tools have been selected to develop the work of this thesis: `Ci-NERGY` and `SimStadt` platforms and `INSEL` engine.

Chapter 3

Methodological approach and Model structure

The developed simulation methodology articulates in a linear workflow (Figure 3.1). Starting with the data acquisition and preprocessing, then the model definition, the simulation step and finally, the presentation of results. This linear process does not imply the absence of loops or tree-paths inside each workflow step.

The workflow based on the developed methodology has been implemented in two different platforms called `SimStadt` and `Ci-NERGY`. `SimStadt` is a desktop platform under development since 2013 within the project of the same name. The second one, `Ci-NERGY` [13], is being developed as an orchestration of web services in parallel to this thesis by the Dept. Geomatics, Computer

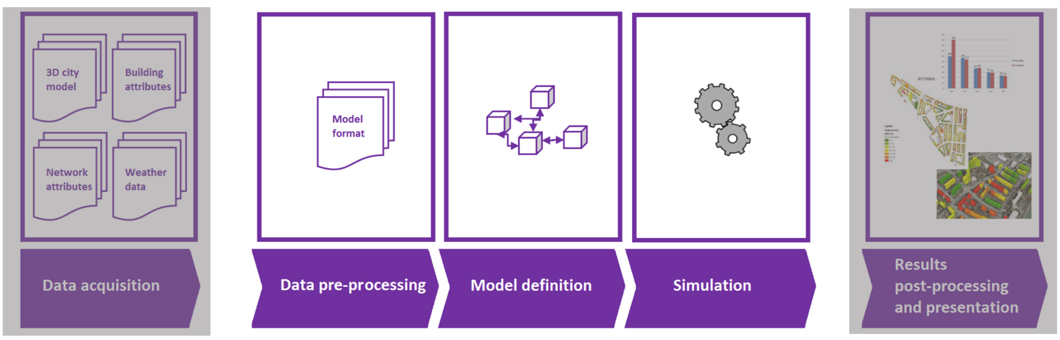

Figure 3.1: Software workflow.

Science and Mathematics at the University of Applied Sciences, Stuttgart (see section 2.2).

The five steps that make up the workflow are addressed in this chapter to give a better overview, but the work developed within this thesis concerns only steps 2 to 4. While steps 1 and 5 have been implemented by the platforms' developers. All steps can be treated, modified or updated independently, and they are similar in both platforms with some small differences, which are tackled within this chapter.

Figure 3.2 presents as an example of workflow, the demand simulation integrated into the `SimStadt` platform. It can be seen how the resolution algorithm, implemented in `INSEL` (blue box), is clearly separated from the modelling part done in `SimStadt` (yellow box). Once the data is preprocessed and the model defined in `SimStadt`, `INSEL` is called as a simulation engine to calculate the demand of one single building. `INSEL` is called as many times as buildings to be calculated are. Finally, the results are sent back to `SimStadt` to be post-processed and presented in the different formats.

3.1 Step 1. Data acquisition

Except for the weather information, the data sources are formatted according to the CityGML standard. CityGML is a common semantic information model for the representation of 3D urban objects that can be shared over different applications. It is designed as an open standard that helps to support data aggregation, usability and exchange. As said in its website, CityGML is thought to admit not only individual buildings but larger scale such as cities or even whole countries. This characteristic makes it ideal for the urban size target of the tool, the district. CityGML provides a place to hold geometrical, topological, semantical and appearance properties of city models [90]. It is structured in five well-defined consecutive LoD of the building model. The definition of those LoD as well as the suggested use for each of them can be found in the CityGML wiki[a] and are reproduced hereunder (Figure 3.3):

- LoD0 – *regional, landscape*. The building is represented by horizontal surfaces describing the footprint and the roof edge.
- LoD1 – *city, region*. The different structural entities of a building are aggregated to a simple block and not differentiated in detail.

[a] `http://www.citygmlwiki.org/index.php?title=Citygml_Wiki`

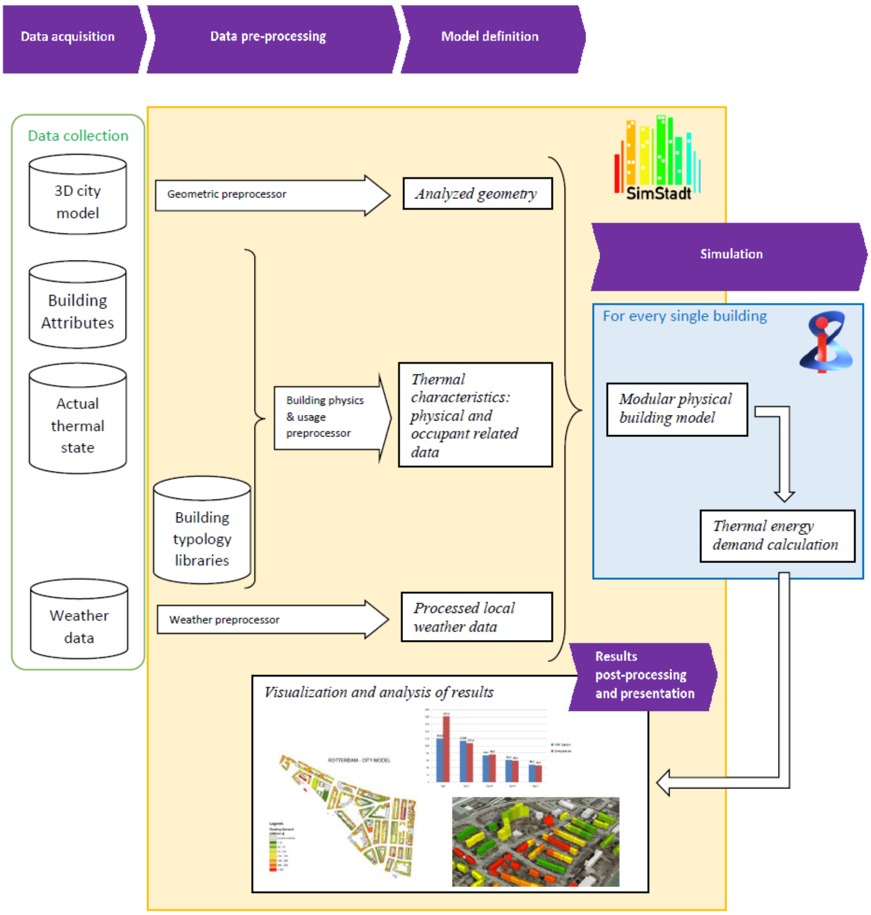

Figure 3.2: SimStadt workflow.

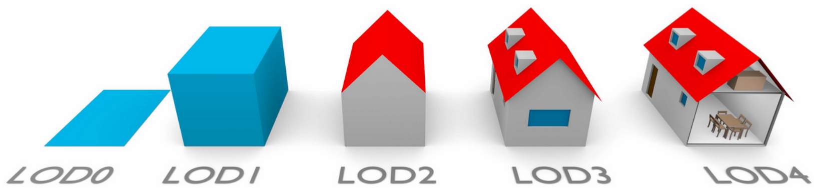

Figure 3.3: Building model from LoD0 to LoD4 of CityGML (Source: [33]).

- LoD2 – *city districts, projects*. In LoD2 there is a differentiation between wall, roof and ground surfaces. Also, smaller features of the building ('outer building installations') can be included if their extents exceed the proposed minimum dimensions (for more information, visit [6]). Typical candidates for this class are chimneys, dormers, balconies, outer stairs, or antennas.
- LoD3 – *architectural models (outside), landmarks*. It includes the openings in a building corresponding with windows or doors.
- LoD4 – *architectural models (interior)*. Concerning the exterior building shell, the LoD4 data model is identical to that of LoD3, but LoD4 provides the possibility to model the interior structure of a building.

Not only the geometry, but also other related information regarding the energy systems can be stored by using the extensions provided by this standard, the so-called ADEs:

- *Utility Network ADE:* CityGML ADE for the modelling of utility networks in 3D city models. The UtilityNetworkADE defines topological network models, either thermal or electrical.
- *Solar ADE*: "The Solar ADE manages information of use to local authorities for encouraging the adoption of solar energy".
- *Energy ADE*: The CityGML Energy ADE extends the CityGML standard with the required information to perform energy simulations and to store the corresponding results.

Considering the four data families presented in section 2.1, the data is currently obtained from:

D1. Weather data. `SimStadt` can call `INSEL` to obtain ambient temperature and global radiation values of any country around the world. The database that `INSEL` uses provides only monthly values. The hourly ones are then calculated also with `INSEL`, the radiations by following the Gordon-Reddy model [88] and the external temperature with the

Erbs-Klein-Beckman correlation [72].
`SimStadt` can also handle TMY data, but the user must provide it. The `Ci-NERGY` platform, on the contrary, is able not only to read TMY files[b] (which are already available on the server), but also extract the data from weather platforms depending on the location defined in the CityGML file. This databases contain at least hourly external temperature and horizontal global and diffuse radiation. So far, only Switzerland, through the *MeteoSwiss platform*, is connected. The *Weather preprocessor* is intended to be gradually extended by extracting the information from other national weather platforms.

D2. Geometry and location. Both platforms handle CityGML[c] data models. For the building model, the Level of Detail must be LoD2 or higher. The geometry of the DHN and the solar systems are not yet automatized because the corresponding ADEs are still on an early stage of development (the first release is planned for December 2019). Nevertheless, the author participates actively in the development of the *Utility Network ADE*, and it is planned to be incorporated to the platforms in the future.

D3. Construction data. Both platforms can extract the data either from the CityGML *Energy ADE* file or from a predefined *Construction library*. A Library Editor is also available to create new *Construction libraries* for `SimStadt`, and the `Ci-Nergy` platform has already the libraries available on the server. The *Construction library* is accessed by the type of building and the period of construction, following the concept of descriptors and IDefaults already defined by Robinson et al. in [174]. From the two descriptors, the period (or year) of construction, must be provided within the CityGML data model. At the same time, the type of building is internally defined depending on the building geometry, producing one of the five categories: Single Family House, Multi-Family House, Big Multi-Family House, Row House and High Tower during the geometrical preprocessing. They are then used to access default values (iDefaults) from the corresponding library. The available *Construction library* up to now is based on the German standard *Deutsche Gebaeudetypologie, Institut Wohnen und Umwelt*[d] (2003 [104] and 2011 [105]) including the *EnEV2014* [71] standards. It has relevant information on construction composites, such as the number

[b]`Meteonorm`[170] is a combination of data sources and calculation tools that provides access to typical years and historical time series in the format of TMY files.

[c]By 'CityGML' it must be understood not only the Base 3D model but also the corresponding ADEs.

[d]German Building Typologies, Institute for Housing and Environment

of layers per wall, differentiating if it is external or internal wall, roof or ground. It also contains thermophysical and radiometric properties of the layers, including thickness, density, heat transfer coefficient, specific heat capacity or short-wave reflectance. Also, the windows' construction and window ratio, together with infiltration ratio or global thermal bridges transmittance.

D4. Human behaviour and internal loads data. In the same way, the user-related parameters can be obtained either from the *Energy ADE* model or from the corresponding library, the *Usage library*. A Usage Library Editor is also available for `SimStadt`. This library is accessed by building usage (descriptor provided within the CityGML file) and stores two different levels of detail of deterministic iDefaults. In essence, fixed annual values or hourly values organized in five typical days. The data that can be found is related to occupancy, including convective and radiative internal gains due to presence, electrical appliances and lighting and DHW consumption, together with setpoints and ventilation ratio. Two *Usage libraries* are already incorporated into the platforms for two different countries. The first for Switzerland, based on the Swiss norm *SIA380* [193], and the second one from the German standards *DIN 18599-10* [65], *VDI 3807-2* [203] and *VDI 2089-1* [202].

3.2 Step 2. Data preprocessing

Some information is mandatory and should directly come from the different databases. This unavoidable data is, depending on the model:

- **Common data:**
  - *Location:* The location allows access to the weather data and provides ambient temperature and global (or beam) and diffuse radiation.
  - *Geometry:* The buildings' geometry at any LoD must be provided. The DHN geometry is needed depending on the target. If the installation of a new DHN is studied, then the geometry of the streets and roads are required; if, on the contrary, an existing network wants to be analysed, then its layout must be provided. The same applies to the solar systems.
- **Specific for Building model:**
  - *Period of construction:* The type of construction of a building profoundly influences its thermal energy demand. The year or

period of construction of the building is essential to access the data related to the type of construction; e.g., the layers that make up the walls, the windows characteristics, or the air infiltration rate.

- *Building usage:* The internal gains of a building also influences the demand, being its impact higher when the building is better isolated. These internal gains depend on the building usage, not only the total amount, but also how this amount is distributed along the day or week.

With this minimum data, all other parameters required by the different models can be either calculated or assumed. The process integrates systematic and automatic data preprocessing for different LoD and data availabilities, but up to now, only the preprocessing related to the building model has been developed. Other procedures will be integrated when the *Utility Network* and *Solar ADEs* are available.
The *Weather preprocessor* has several functions; it calculates the beam and diffuse radiations on the external surfaces (walls and roofs) using SRA (see section 2.2). Also, it calculates the sky temperature as a function of the ambient temperature following, the Swinbank correlation for clear skies [195] (equation 3.1).

$$T_{sky} = 0.0552\, T_{amb}^{1.5} - 273.15 \tag{3.1}$$

Where the ambient temperature T_{amb} is expressed in Kelvin and the sky temperature T_{sky} in Celsius. And finally, calculates two ground temperatures. The virtual ground temperature is calculated as a function of the external temperature, following the ISO 13370:2007 [103] (see section 4.4), used for the building demand simulation. And, the undisturbed ground temperature for the DHN losses calculation, is calculated as the mean ambient temperature of the year.
The *Geometrical preprocessor* defines the building's internal zoning (see section 3.3) and its type in case that it is not explicitly described in the CityGML model. The type is defined according to the IWU building typology library [105] –further developed in the TABULA [133] project– which defined the following logic:

1. If the total height is over 20m, the building is defined as High Tower (HH).

2. Else, if the total height is over 16m, the building is defined as Big Multi-Family House (GMF).
3. Else, if the total height is over 11m, the building is defined as Multi-Family House (MFH).
4. Else, if any of these conditions are met, the building is defined as Row House (RH): the footprint area is over 200m^2, the number of dwellings is larger than 2, or the ratio between shared wall area and total external wall area is greater than 0.2.
5. Else, the building is defined as Single-Family House (EMF).

This preprocessor also calculates:

- The windows ratio (for LoD2) is extracted from the Construction library depending on the Year of Construction (YoC). With this value, virtual windows are created for the corresponding external walls or roofs.
- Geometrical parameters of the internal rooms, including the view factors for the long-wave radiation exchange and the internal solar fractions for the transmitted solar radiation distribution. The view factor is the proportion of the radiation, which leaves surface i that strikes surface j, and it is defined as in equation 3.2. They are calculated using Monte Carlo Ray Tracing.

  $$F_{i,j} = \frac{1}{A_i} \int_{A_i} \int_{A_j} \frac{\cos\theta_i \cos\theta_j}{\pi S^2} dA_j \, dA_i \tag{3.2}$$

  Where the areas A_i and A_j are measured in m^2 and the distance that separates them S in m. The description of the different parameters is presented in Figure 3.4.
- The thermal bridges (this calculation is explained in detail in chapter 4).
- The virtual layer of the surfaces touching the ground (see section 4.4) using the definition of the construction of every surface and the ground characteristics if known. If there is no information about the basement (LoD2) and/or about the ground, these hypotheses are taken:
  - Groundwater has a negligible effect on the heat transfer.
  - The floor consists of a slab in contact with the ground over its whole area. This corresponds to the construction option (a) ‘slab-on-ground floor’ presented in Figure 3.5.

  If more information about the basement is provided, then the applicable case is selected from the ISO 13370-2007 norm:

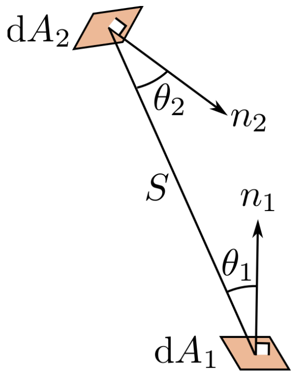

Figure 3.4: View factor between two differential areas in arbitrary configuration (Source: Dov Grobgeld under creative commons.)

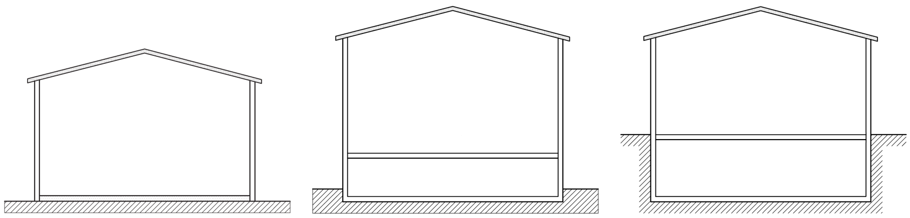

(a) Slab-on-ground floor. (b) Suspended floor. (c) Basement.

Figure 3.5: Basement construction options (Source: [103]).

- Slab-on-ground floor (Figure 3.5(a)).
- Suspended floor (Figure 3.5(b)).
- Heated basement (Figure 3.5(c)).
- Unheated basement (Figure 3.5(c)).
- Partly heated basement (Figure 3.5(c)).

Finally, the *Usage preprocessor* generates, on one side, one-year time series with a time-step of one hour for human behaviour and internal loads. It provides convective and radiative internal loads as well as heating and cooling set temperatures and air renovations due to ventilation. The data is extracted from the *Usage library* by building usage to create an entire year either from annual values or from typical days if available. Therefore, no external or internal dependencies (e.g. weather conditions or internal comfort) are considered yet. These dependencies would provoke steps backwards and loops in the software workflow, thus only the `Ci-Nergy` platform could in the future be able to manage them. On the other side, the *Usage preprocessor* generates the input file required by `DHWCalc`. `DHWCalc` is a tool that gen-

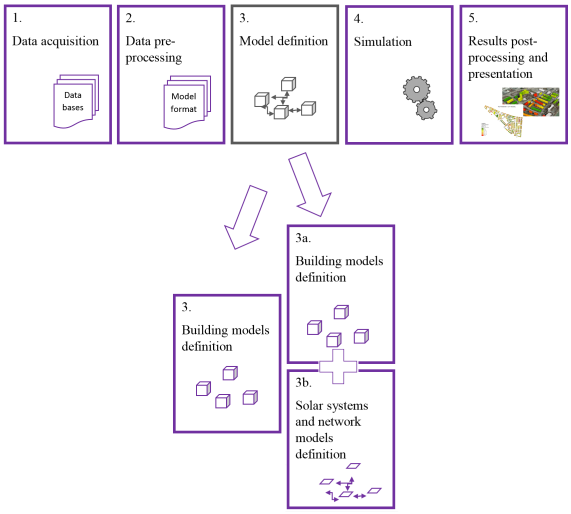

Figure 3.6: Simulation workflow.

erates DHW profiles on a statistical basis depending among others, on the number of occupants and the total mean daily volume of DHW used in the building. This tool has been integrated into the workflow to complete the thermal demand of the buildings. This tool was developed within the scope of the Solar Heating and Cooling Program of the International Energy Agency (IEA-SHC), Task 26: Solar Combisystems by Kassel University [110].
Other urban characteristics could be added in the future to the workflow at this step, for example, UHI, street canyon effects or vegetation shadowing. Also, some building parameters like stochasticity in human behaviour could be included by, for example, plugging a software like `NO-MASS` [10].

3.3 Step 3. Model definition

The model definition depends on the simulation target. Thus, it can be defined either the whole system or only the buildings (Figure 3.6). When only the building demands are required, the thermal models of every building in the region selected are defined and sent to be simulated independently one from each other. If the target is the complete system, then two options can be considered:

1. If the purpose is to simulate the system as it is to perform predictive analyses, then all the parameters of the network and systems must be extracted from the databases. Then, this information together with

the data to define the buildings would be used to define the complete model and sent to the simulation step. This option is not yet available due to the status of the *Utility Networks ADE*.

2. If, on the contrary, the purpose is to perform what-if analyses, then a DHN is automatically generated (this capability is provided already by the `SimStadt` platform). A what-if analysis is done by running pre-set scenarios to answer the question 'What if we do this?'. In the case we are concerned, the question is 'What if we install a DHN to supply heat to a defined area?'. The automatic generation of DHNs is based on the buildings demands and the location of those buildings as well as the roads and other city's infrastructure defined in the input data. The solar system is also automatically dimensioned based on a few user inputs. This dimensioning is addressed below. The just generated parameters, together with the required input to the buildings simulation, are sent to the next step.

At this point, depending on the information available, all or some of the following hypotheses are taken. Related to the input data:

D1. Weather data: Some needed inputs like the ground or sky temperatures, which usually are not included in the databases, are calculated during the weather preprocessing (section 3.2).

D2. Building geometry and location: The model can simulate buildings with internal zone divisions, which allows assuming some internal zoning. For LoD2 or LoD3, where no internal structure is provided, it is assumed that the building is divided vertically, assigning one thermal zone to each storey. Internal ceilings are added to the model, and the air volume is reduced by the volume occupied by these surfaces. This assumption implies that only buildings with the same footprint at all storeys can be handled (Figure 3.7). Information related to cellar can be externally provided, clarifying if the cellar exist and, in that case, if it is conditioned or not. If this information is not furnished, it is assumed that there is no cellar and, therefore, the floor is in contact with the ground. The attic is assumed to be ventilated, but not heated. Finally, if the model does not include windows (LoD2), the window ratio extracted from the database is assigned to all external walls, except for shared walls, and these last ones are treated as adiabatic[e]. If the

[e]If in the data models there are two walls closer than 0.25 meters, then they are considered adjacent and are treated in the simulation model as shared walls for both buildings

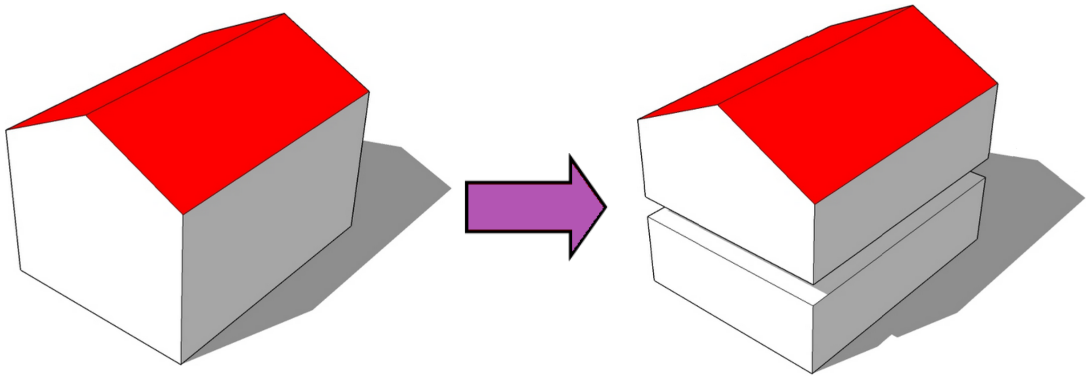

Figure 3.7: Division of LoD2 and LoD3 building models by number of storeys.

data model is LoD4, the thermal model is built with the information of the internal structure. The location is a mandatory parameter.

D4. Human behaviour and internal loads data: The time series values prepared in the previous step are assigned to each thermal zone depending on its usage that must be specified in the CityGML file. If the LoD is lower than 4, it is assumed that the whole building has the same usage, unless there is a mix-usage of the building ('sales + apartment building' or 'sales + office') and it has more than one storey. In this case, the usage 'sales' is assigned to the base storey, and all the rest have the other usage ('office' or 'apartment building').

Related to the models' definition:

1. **Network**. It is a two-pipes network without storage and with a conventional supply system.
2. **Solar system**. One solar system is placed at each building roof, converting it in a 'prosumer'. The storage tanks belong to the solar systems.

Solar System dimensioning.

The hypothesis followed in the dimensioning process is that the systems should be thought to cover each single-building demand up to the maximum size that the roofs allow. Meaning that the total solar area of one collector field may be smaller than the maximum area that could fit on the corresponding roofs.

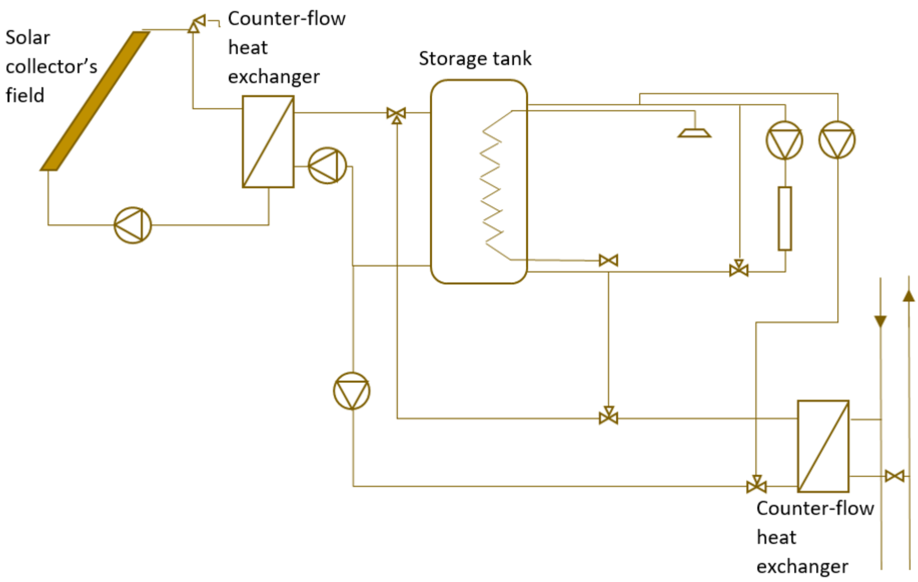

Figure 3.8: Solar system schema.

The predefined solar system schema is presented in Figure 3.8. Its main components are the solar collector field, a storage tank and two heat exchangers, one that separates the collector field from the rest of the system and a second one that connects the 'prosumer' with the district heating network.
Therefore, the values to be dimensioned are:

- Total area of solar collectors filed.
- Azimuth and tilt of collector field.
- Heat exchangers' overall heat transfer coefficients.
- Tank volume.

The total area of the solar collector field depends not only on the available roof area but also on the demand as previously commented. To take into account the building demand before the simulation is performed, a reduction factor based on the German Standards "KfW-Effizienthaus" [2] was defined. The "KfW-Effizienthaus" standards define the construction requirements that a building must satisfy to obtain a specific label: 55, 70, 85, 100 and 115. Those numbers refer to the percentage of a standard heating demand (also defined in the norm) that the building constructed following the specifications may have.
The reduction factor due to a low demand is then defined as:

$$Rf_{dem} = \frac{KfW value}{100} \tag{3.3}$$

This reduction factor is a suggestion of the workflow but can be modified by the user.

Romero, L. et al. [178] defined a systematic process to evaluate the usable roof area for both PV and solar thermal, depending on the available geometrical data of the building is defined. According to them, the maximum collector area depends on a list of restrictions that diminish the total available roof area. This restriction leads to a set reduction coefficients:

- *Construction restrictions*: space already occupied by elements located on the roof, such as elevators, air extractors, chimneys, stairwells, water tanks, HVAC installations or windows.
- *Protected buildings*: applied when, for some reason, no facility can be built on, due to historical considerations, for example.
- *Separation of panels*: it considers the distance between the panels to avoid reciprocal shadowing.
- *Service area*: the necessary space for maintenance and access.

They also propose some values for the coefficients either individually as is the case of the Construction restrictions or together, like the service area and separation of panels:

- *Construction restrictions*: $C_{CON} = 0.8$ for flat roofs, $C_{CON} = 0.9$ for pitched.
- *Protected buildings*: If the building is protected, then $C_{PROT} = 0$, otherwise $C_{PROT} = 1$. If no information is provided, it is assumed that the building is not protected.
- *Separation of panels*: $C_{GCR} = 0.46$ for flat roofs, $C_{GCR} = 0.9$ for pitched.
- *Service area*: This factor is already included in C_{GCR}.

Thus, the total collector field area [m^2] is calculated as:

$$A_{coll} = A_{roof} R f_{dem} C_{CON} C_{PROT} C_{GCR} \tag{3.4}$$

where A_{roof} is the total available roof area [m^2].

The azimuth and tilt of the collector field correspond to those of the roof in case of tilted roofs. If they are flat, then the orientation is south, and the tilt corresponds to the latitude of the location (with a minimum of 15°to assist thermosyphon effect), which give the optimum collector tilt from September to March according to the AEE-Institute for Sustainable Technologies [75].

Heat exchangers' overall heat transfer coefficients. The heat exchanger connected to the solar field (HX1) depends on the collector field area and the one connected to the network (HX2) on the demand and the temperatures on the net. The minimum overall heat transfer coefficients are defined as:

$$UA_{HX1} = \frac{1000[W/m^2]\,A_{coll}}{5[K]} \tag{3.5}$$

where $1000[W/m^2]$ is the design irradiance in W/m^2 of solar collector area, and $5[K]$ is the minimum difference between the temperatures of the one and the other circuit.

And:

$$UA_{HX2} = \frac{\dot{Q}_{max}}{5[K]} \tag{3.6}$$

where $\dot{Q}_{max}$ [W] is the building's maximum demand.

Tank volume. For the dimensioning of the tank, the conclusions extracted from [142] were followed, leading to a range of possibilities that go from a ratio of tank volume to solar area of 0.05 m^3/m^2 to 0.2 m^3/m^2 (the typical ratio in systems to cover only DHW is from 0.05 to 0.08 m^3/m^2 [218, 166]). The proposed value to the user is 0.15 m^3/m^2, but this value can be modified.

Heat Pump plus PV systems dimensioning.

In this case, the hypothesis taken is that all extra electricity generated and not used by the Heat Pump (HP) can be fed into the grid and, therefore, the PV collector field can be sized to the maximum allowed by the roofs.

The electricity hourly generated by the PV panels at each roof is calculated as:

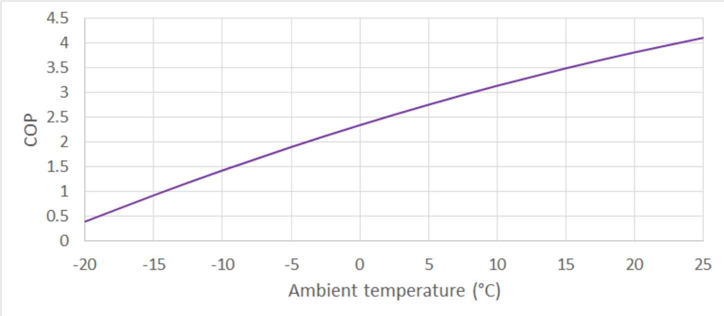

Figure 3.9: COP of air-water heat pumps.

$$P_{PV} = \sum_{i=1}^{roofs} (I_i\, A_i)\, C_{CON}\, C_{PROT}\, C_{GCR}\, \eta_{PV} \tag{3.7}$$

where I_i [W/m^2] is the hourly irradiance on roof i, A_i [m^2] is the area of the corresponding roof, and η_{PV} [-] is the efficiency of the PV system that includes the modules efficiency and the system performance ratio. Finally, the reduction coefficients are the same ones previously described for the thermal solar panels.

The assumptions taken for the heat pumps dimensioning are:

1. The nominal power (P_{HPnom} [kW]) of the heat pumps is calculated as:

$$P_{HPnom} = 0.85\, P_{max} \tag{3.8}$$

   where P_{max} [kW] is the maximal demand of the building over the year.
2. An electrical back-up heater is added to cover the peaks, which is the Business As Usual (BAU) [140].
3. No electrical storage is considered.
4. The PV panels serve each corresponding heat pump when possible. If there is not enough electricity from PV available, the heat pumps use the grid.
5. If there is excess of PV electricity production (after covering heat pump needs), it is sent to the grid.

Finally, the COP [-] (Figure 3.9) at every hour is calculated as:

$$COP = -0.0006\, T_{amb}^2 + 0.0856\, T_{amb} + 2.3471 \tag{3.9}$$

where T_{amb} is the ambient temperature in °C. This equation has been derived from the analysis of heat pump efficiency in real-live conditions carried out by the Fraunhofer ISE Institute between 2005 and 2010 [140].

3.4 Step 4. Simulation

Not only the workflow, but also the simulation models are very modular. Hence, the three main models, including buildings, district energy network and solar supply systems, are separated and can be simulated together in two different ways depending on the platform used. If `SimStadt` is used, the data exchange goes only one way. Thus, the buildings demand is firstly simulated. In a second step, the solar system models are simulated together with the network using the results of the building simulation as input. If the `Ci-NERGY` platform is used, either the same workflow is followed (first demand calculation and then network and solar systems together), or all three models can be co-simulated [f]. Furthermore, using `INSEL` each component of the building and supply system models is written in a different block to be later interconnected according to the system definition and simulated.

The hypotheses taken at this point can be divided into two groups: those common to all models and those specific for one model or a part of it. The specific hypotheses are explained for every model in the corresponding chapters 4 and 5. The common hypotheses are:

- The reflection of the solar radiation in the urban context is diffuse.
- No stochasticity is yet considered except for the DHW calculation.
- The long-wave radiation couplings between buildings are not handled.

Moreover, both models use explicit methods for solving the equations system. The advantages of choosing an explicit method are mainly its simplicity and the computational effort. But, if the problem to be solved is stiff, i.e. it can be numerically unstable, then the explicit methods require very small time-steps to ensure stability. That means that much more computational time is required, increasing the worth of implicit methods. Nevertheless, both models include stability conditions that ensure the obtention of results at calculation periods of no less than 2 minutes. And, even though this small time-step requires much larger computational time, this drawback is solved

[f] When writing these words, this second option is not yet available, but still work in progress.

by splitting the model into many machines thanks to its modularity. These methods are explained in more detail in chapters 4 and 5.

3.5 Step 5. Results postprocessing and presentation

The simulation results provided by the tools are, at every hour:

1. Related to the 'prosumer' model, which include the solar system and the building:
    - Internal temperatures of each room.
    - Heat demand (heating or cooling) of each room.
    - Solar energy absorbed by the panels.
    - Temperatures and volume flows in the pipes and into the storage tank.
    - Storage tank heat losses.
2. Related to the network model:
    - Critical pressure.
    - Heat loses to the ground.
    - Water flows through every pipe.
    - Temperature and pressure at each node.
3. Related to the DHW from the tool `DHWCalc`:
    - Heat demand for water preparation.

All hourly values can be downloaded as a .csv file. And, the monthly energy values can also be visualized in bar-charts. Finally, the annual heat demand can be visualized in 2D or 3D GIS maps.

3.6 Conclusions of Methodological approach and Model structure

In this chapter, the workflow followed by the two Urban Energy System simulation environments has been introduced, and the role of each independent step that conform the workflow has been clarified. Also, it has been defined the limits of the contribution of this thesis, which is focused on steps 2 to

4. Each step was presented in detail, explaining their inputs and outputs, as well as their purposes and internal processes, except for the definition of the models embedded in the tool. These are tackled in the following chapters.

Chapter 4

The Building model

This chapter presents the developed building model. First, its physical description is explained, focusing on the set of heat transfer equations that make up the complete model. After that, the clustering of those equations in separated blocks, as well as their resolution processes, are discussed. The last section presents the verification of the model using BESTEST, and its results are also compared to those obtained by `EnergyPlus`.

4.1 Physical description of the building model

The dynamic building model aims to calculate the thermal energy demand for air conditioning of one building based on the physical nodal method. This method is widely used for building simulation.

According to Foucquier et al. [76], the principal assumptions taken by this method are:

- Each building zone is a homogeneous volume characterised by uniform state variables.
- A node represents the air inside a room, a wall, a window or the exterior of the building.
- The thermal transfer equations are solved for each node of the system.
- The nodal method can be considered as a one-dimensional approach.

Figure 4.1 illustrates the energy flow paths considered for the building model. The traditional energy flow paths in buildings [51] also consider furniture

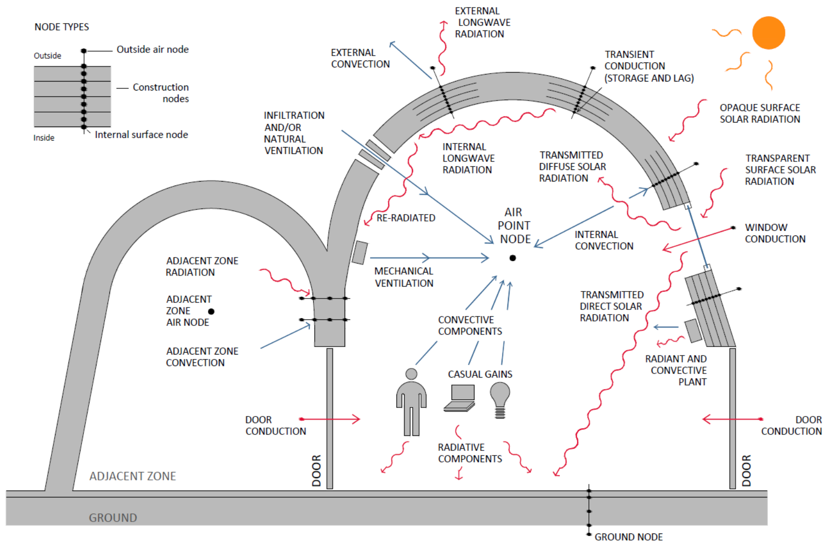

Figure 4.1: Energy Flow Paths (Source: adapted for this thesis by Alfonso García-Leyaristy from [51]).

and latent flows, which are not included here. However, the ground surface is explicitly studied, which is not done in the traditional model. Also, the heat transfer due to thermal bridges is taken into account using a semi-empirical solution. The thermal performance of the building envelope can be greatly affected by thermal bridges [96, 45], and yet they are rarely included in building models [25]. Finally, note that natural airflow between different zones is not included. The nodal model is a thermal model, and therefore it is not able to represent the difference in pressure between zones, which is the driving force of the natural airflow.

Starting from the energy balance in the air point node of every thermal zone, the energy flows are broken down step by step to explain the building model. The demand is calculated as the heat needed to reach and maintain the temperature setpoint at the air point node.

$$\frac{dU}{dt} = \dot{Q}_{conv} + \dot{Q}_{TB} + \dot{Q}_{vent} + \dot{Q}_{inf} + \dot{Q}_{IGconv} + \dot{Q}_{sys\_conv} + \dot{Q}_{dem} \tag{4.1}$$

where the internal energy variation over time of the room's air ($\frac{dU}{dt}$) is a function of its temperature (T_{room}):

$$\frac{dU}{dt} = m\, c_p \frac{dT_{room}}{dt} \tag{4.2}$$

Figure 4.2: Ventilation and infiltration (By R. Monsalvete[a]).

where m [kg] is the mass of the air inside the room and c_p [J/kgK] its heat capacity. $\frac{dT_{room}}{dt}$ is the variations over time t [s] of the air temperature, T_{room} [°C]. $\dot{Q}_{vent}$ [W] and $\dot{Q}_{inf}$ [W] are the mechanical ventilation (external air mass flow, $\dot{m}_{vent}$ [kg/s], voluntary introduced at a temperature T_{vent} [°C] to maintain good air quality) and infiltration (involuntary external air mass flow, $\dot{m}_{inf}$ [kg/s], at ambient temperature T_a [°C] into the volume) heat inputs respectively (Figure 4.2):

$$\dot{Q}_{vent} = \dot{m}_{vent} c_p (T_{vent} - T_{room}) \tag{4.3}$$

$$\dot{Q}_{inf} = \dot{m}_{inf} c_p (T_a - T_{room}) \tag{4.4}$$

All parameters of both equations (except T_{room} [°C]) are inputs to the model. $\dot{Q}_{IGconv}$ [W] and $\dot{Q}_{sys\_conv}$ [W] (Figure 4.3), which are the convective heat inputs due to casual gains (or internal gains) and convective fraction of the heat emitted by the thermal systems (plants), are also inputs to the model. Therefore, these parameters do not need to be internally calculated.

The term $\dot{Q}_{TB}$ [W] appears due to the one-dimensional heat transfer model of the nodal method approach. The points (e.g. corners) and linear details (e.g. two walls intersection, window-wall junction) must be treated separately.

$$\dot{Q}_{TB} = H_{TB}(T_a - T_{room}) \tag{4.5}$$

where T_a [°C] is the ambient temperature, and H_{TB} [W/K] is the total heat transmittance due to thermal bridges at each thermal zone. The last one

[a]Rocío Monsalvete Álvarez-Uríbarri. Arquitectura e Interiorismo (rociomonsalvete.com).

Figure 4.3: Convective loads (By R. Monsalvete).

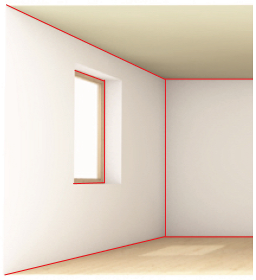

Figure 4.4: Thermal bridges (By R. Monsalvete).

may come as a fixed value for the complete building from the *Construction library* or be calculated during the *Geometrical preprocessing*.
If the first option is chosen, the value from the *construction library* is divided by volume between all building thermal zones. If the needed data for a more detailed calculation is available, then the heat transmittance is calculated as:

$$H_{TB} = \sum(\Psi_i \cdot L_i) + \sum \chi_j \quad (4.6)$$

where Ψ_i [W/mK] is the linear heat transmittance value of detail i, L_i [m] is the total length of the linear detail i in the analysis zone, and χ_j [W/K] is the point heat transmittance value of detail j.

Note that in equation 4.1, two terms of convective supply systems appear: $\dot{Q}_{sys\_conv}$ [W] and $\dot{Q}_{dem}$ [W]. The first term, $\dot{Q}_{sys\_conv}$, is an input to the model when the convective part of the heat delivered by supply systems is known. The radiative part of the heat delivered by the supply systems is also an input to the model, but it is associated with the surfaces surrounding the zone (equation 4.8). The second term, $\dot{Q}_{dem}$, is an output and represents the needed convective heat flow to achieve the required set temperature, T_{room} [°C]. Equation 4.1 can also be used to calculate the temperature of the node if ($\dot{Q}_{dem} = 0$).

$\dot{Q}_{conv}$ [W] is a function of T_{room} [°C], and its calculation is developed hereunder. It is the sum of all internal convective flows. The internal convection is caused by the difference between the temperatures of the different enclosures (walls, windows, doors and ground) and the air node. It is obtained from 4.7 using inputs from 4.8) for every enclosing surface:

$$\dot{Q}_{conv} = -\sum_{i}(\dot{q}_{conv\_i} A_{surf\_i}) \tag{4.7}$$

$$\forall i, \quad \frac{du}{dt} = \dot{q}_{conv} + \dot{q}_{cond} + \dot{q}_{rad\_lw} + \dot{q}_{rad\_sw} + \dot{q}_{IGrad} + \dot{q}_{sys\_rad} \tag{4.8}$$

where $\dot{q}_{IGrad}$ [W/m^2] and $\dot{q}_{sys\_rad}$ [W/m^2] are the radiative component of casual gains and radiant plants respectively and are inputs to the model (Figure 4.5). In both cases, the radiation is assumed to be equally distributed between the surrounded surfaces according to their areas. $\dot{q}_{cond}$ [W/m^2] is the conduction through room enclosures and is calculated using the one-dimensional heat transfer equation of the Finite Difference Method (FDM) (see section 4.4). $\dot{q}_{rad\_sw}$ [W/m^2] is the incident short-wave radiation (equation 4.12). This is the fraction of the transmitted solar radiation that enters the room through the transparent enclosures (windows) which is absorbed by the room enclosure. It can be divided between direct ($\dot{q}_{sw\_b}$ [W/m^2]) and diffuse ($\dot{q}_{sw\_d}$ [W/m^2]) radiation (see Figures 4.6 and 4.7). And:

$$\frac{du}{dt} = m\, c_p \frac{dT_i}{dt} = \rho\, x\, c_p \frac{dT_i}{dt} \tag{4.9}$$

$$\dot{q}_{conv} = h_{ci}(T_i - T_{room}) \tag{4.10}$$

where x [m] is the virtual thickness of the surface where dT occurs and is defined as half of a sublayer. A sublayer is each division of every layer that make up a wall, and it must accomplish the stability condition $Fo < 0.5$ (refer to section 4.4).

Figure 4.6 shows how the direct radiation enters the room through the window and hits a small part of the floor. This solar spot moves along the day

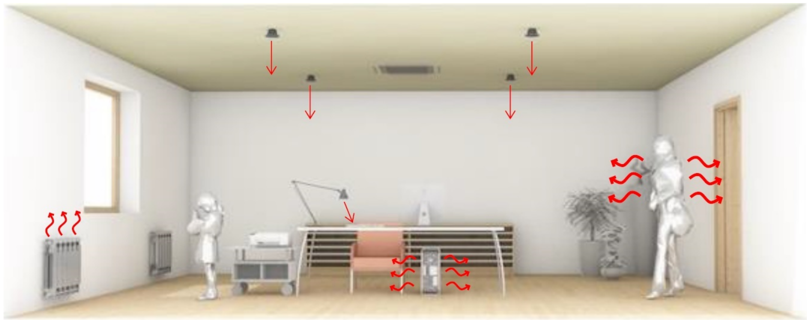

Figure 4.5: Radiative components of casual gains and radiant plants (By R. Monsalvete).

Figure 4.6: Transmitted direct solar radiation (By R. Monsalvete).

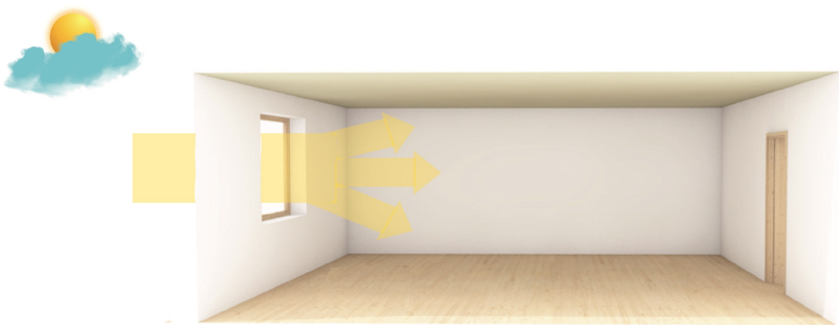

Figure 4.7: Transmitted diffuse solar radiation (By R. Monsalvete).

with the sun changing the temperature of the surfaces. Following this process has high computational costs, so three approaches are usually used to solve this problem [60].

- Predefined distribution (60% to the floor and the rest is divided per area between the rest of surfaces).
- Approximated distribution (using correlations).
- Backwards-ray-tracing method[a].

That is calculated during the *Geometrical Preprocessing* accounting with the walls' absorptivity. As a result, the simulation model receives the direct and diffuse solar fractions (SF_{sw} [-]) on every enclosing surface. Up to now, the method used for this calculation is the *predefined distribution*.

$$\dot{q}_{rad\_sw} = \dot{q}_{sw\_b} + \dot{q}_{sw\_d} \tag{4.11}$$

$$\dot{q}_{sw\_b} = SF^b_{sw} \frac{\sum_{wi} g_{wi} I_{bi} A_{wi} f_{wi} (1 - f_{bi})}{A_j} \tag{4.12}$$

$$\dot{q}_{sw\_d} = SF^d_{sw} \frac{\sum_{wi} g_{wi} I_{di} A_{wi} f_{wi} (1 - f_{bi})}{A_j} \tag{4.13}$$

where I_{bi} [W/m^2] and I_{di} [W/m^2] are the direct and diffuse solar radiation at the window's tilt, respectively, and include the effect of external shadows and reflections. These values are inputs to the building model. A_{wi} [m^2] is the area of each window, f_{wi} [-] their glass-frame ratio ($f_{wi} = 1$ would mean only glass), g_{wi} [-] their direct-beam transmittance at normal incidence and f_{bi} [-] the darkness factor due to blind devices ($f_{bi} = 1$ is completely dark).

Back to equation 4.8, the last term to be defined, $\dot{q}_{rad\_lw}$ [W/m^2], refers to the internal long-wave radiation. This radiation is calculated as (i refers to the cited surface and j to the rest of them in a given enclosed volume):

$$\dot{q}_{rad\_lw} = E_i - \epsilon_i \frac{\sum_{j=1}^{n} \left(A_j F_{ij} (E_j + (1 - \epsilon_j) \overline{q_{rad}}) \right)}{A_i} \tag{4.14}$$

where:

$$E_i = \sigma \epsilon_i T_i^4 \tag{4.15}$$

$$\overline{q_{rad}} = \frac{\sum_{i=1}^{n} E_i A_i}{\sum_{i=1}^{n} \epsilon_i A_i} \tag{4.16}$$

[a]For a better understanding see [22].

where $\sigma = 5.67x10^{-8}$ [W/m^{2}K^4] is the Stefan-Boltzmann's constant, ϵ_i [-] is the emissivity of surface i, and E_i [W/m^2] refers to the radiant energy emitted by surface i due to its temperature T_i [°C]. The view factor F_{ij} [-] is the proportion of the radiation, which leaves surface i that strikes surface j. The view factors can profoundly impact the thermal demand calculation (errors can rise to 20% of yearly thermal demand), being more acute in colder climates. [59]. They are also calculated during the *Geometrical Preprocessing* (step 2 of the workflow, section 3.2).

It is also contemplated the particular case of enclosures with a low time constant, such as very thin walls or, most commonly, windows (the windows time constant is usually around one-two minutes. Therefore the environmental conditions can thus be considered constant over the time response [180]). In that case, the enclosure can be simulated in steady-state conditions and, therefore equation 4.8 gets simplified, and the conductive heat transfer through the enclosure is calculated with the Fourier equation for steady-state:

$$\frac{du}{dt} = 0 \tag{4.17}$$

$$\dot{q}_{cond} = U_{tot}(T_i - T_o) \tag{4.18}$$

where U_{tot} [W/m^{2}K] is the overall heat transfer coefficient of the enclosure, and T_i [°C] and T_o [°C] are the temperatures of the internal and external surfaces (either outside or an adjacent zone).

Therefore:

$$0 = \dot{q}_{conv} + U_{tot}(T_i - T_o) + \dot{q}_{rad\_lw} + \dot{q}_{rad\_sw} + \dot{q}_{IGrad} \tag{4.19}$$

4.2 Structure of the building model in INSEL

According to the idea of creating a very modular building model, this has been divided into different parts (called blocks) to be connected within the simulation engine to create the desired building model. All blocks are defined by parameters (constant values externally defined: by the user or from a library), containing a subset of the equations described in 4.1 and the solving process, and are interconnected through sets of inputs and outputs. The inputs, in contrast to the parameters, are time-varying values that come either externally (for example the weather values that are provided via text files) or from other blocks (the outputs of those).

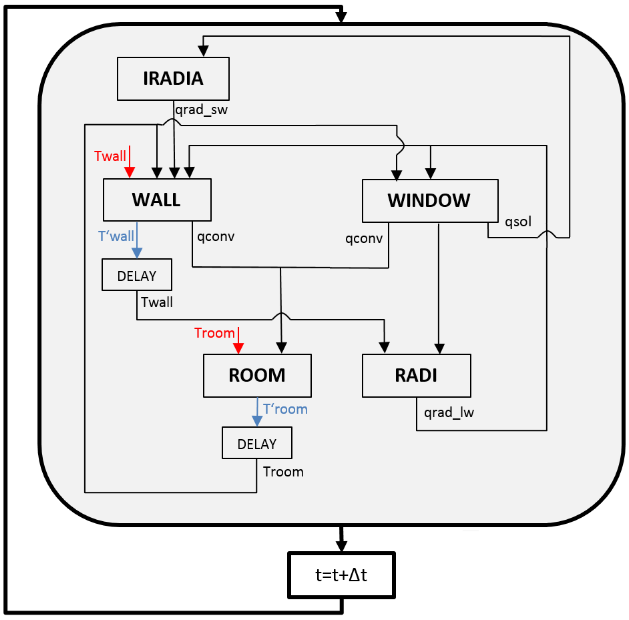

Figure 4.8: Schema of the block connection.

Figure 4.8 shows a simple schema of the connection between the blocks. In blue, the outputs for a defined time-step. They are inputs to the next one (in red). As presented in the schema, the building model has been divided into five main blocks. In a given building, every thermal zone is modelled independently through a set of three blocks ROOM, RADI and IRADIA. The boundaries of a thermal building are modelled using either WALL blocks (if opaque) or WINDOW blocks (if transparent). The WALL blocks model internal or external walls as well as ground surfaces (floor touching the ground), ceilings (internal horizontal surfaces) and roofs. The internal walls and ceilings interconnect thermally two adjacent thermal zones. The following sections describe the five blocks.

4.3 ROOM block

4.3.1 Model scope and objectives

The ROOM block calculates the air node temperatures under free-floating condition or the energy load for a set node temperature when system ON. In both cases, the calculation is based on the differential energy balance in the air node.

4.3.2 Physical model description

All heat flows are considered constant during the time-step of calculation. That means that the differential equation can be solved using the Euler method. The enclosures' temperatures to calculate the internal convection, as well as the temperature of the air node used to calculate the heat input from ventilation, infiltration and thermal bridges, are constants and equal to the result of the previous time-step.

$$\frac{\Delta U}{\Delta t} = \dot{Q}_{conv} + \dot{Q}_{TB} + \dot{Q}_{vent} + \dot{Q}_{inf} + \dot{Q}_{IGconv} + \dot{Q}_{sys\_conv} + \dot{Q}_{dem} \quad (4.20)$$

where:

$$\frac{\Delta U}{\Delta t} = V_{room}\rho_{air}c_{p\,air}\frac{T_{room}(t+\Delta t) - T_{room}(t)}{\Delta t} \quad (4.21)$$

$$\begin{aligned} \dot{Q}_{cool} &= \dot{Q}_{dem}, \quad if \quad \dot{Q}_{dem} < 0 \\ \dot{Q}_{heat} &= \dot{Q}_{dem}, \quad if \quad \dot{Q}_{dem} > 0 \end{aligned}$$

$\dot{Q}_{inf}$ and $\dot{Q}_{vent}$ are calculated as:

$$\dot{Q}_{inf} = V_{room}n_{inf}\rho_{air}c_{p\,air}(T_a - T_{room}(t)) \quad (4.22)$$

$$\dot{Q}_{vent} = V_{room}n_{vent}\rho_{air}c_{p\,air}(T_{vent} - T_{room}(t)) \quad (4.23)$$

So:

$$\begin{aligned} T_{room}(t+\Delta t) &= T_{room}(t) + \frac{\Delta t}{V_{room}\rho_{air}c_{p\,air}} \\ &\cdot [\dot{Q}_{heat} + \dot{Q}_{cool} + \dot{Q}_{IGconv} + \dot{Q}_{conv} + \dot{Q}_{sys\_conv} \\ &+ V_{room}n_{vent}\rho_{air}c_{p\,air}(T_{vent} - T_{room}(t)) \\ &+ V_{room}n_{inf}\rho_{air}c_{p\,air}(T_a - T_{room}(t)) \\ &+ H_{TB}(T_a - T_{room}(t))] \end{aligned} \quad (4.24)$$

The first time this block is called by the simulation engine, it is calculated under free-floating conditions for initialization, so $\dot{Q}_{heat} = \dot{Q}_{cool} = 0$. For all other calls, the calculation process is as follows: T_{room} is calculated with equation 4.24, considering $\dot{Q}_{heat} = \dot{Q}_{cool}$ is 0. If the heating system is ON and the temperature calculated results lower than T_{min}, then $T_{room}(t+\Delta t) = T_{min}$, $\dot{Q}_{cool} = 0$ and eq. 4.24 is used again to calculate $\dot{Q}_{heat}$. This result is obtained considering ideal unlimited capacity systems, and it is used to calculate demand. If the model has a system with limited capacity, then a second check must be done: if $\dot{Q}_{heat} > P_h$, then $\dot{Q}_{heat} = P_h$ and $T_{room}((t+\Delta t)$ is calculated again as a final result.

The same process is followed if the cooling system is ON. The temperature is first calculated, if it is higher than T_{max}, then $T_{room}(t + \Delta t) = T_{max}$, $\dot{Q}_{heat} = 0$ and $\dot{Q}_{cool}$ is the result of equation 4.24. Again, if the cooling system has limited capacity, then if $\dot{Q}_{cool} < -P_c$, then $\dot{Q}_{cool} = -P_c$ and $T_{room}((t + \Delta t)$ is finally obtained.

4.4 WALL blocks

4.4.1 Model scope and objectives

The WALL block describes the conducting heat transfer through an opaque envelope element. There are three types of walls[b] modelled in the same block: internal wall (WALL block), external wall (WALLX block) and wall touching the ground (WALLG block).

The block solves the one-dimensional heat transfer equation of a wall consisting of several layers, varying thickness and material properties (density, heat conductivity and heat capacity). Short-wave and long-wave radiation on the wall together with the air and/or ground temperatures are given as boundary conditions.

4.4.2 Physical model description

The forward FDM [106] is used to solve the one-dimensional heat transfer problem.

1. Resolution process:

[b]The word *wall* is used in this section for walls but also floors, ceilings and roofs.

If the wall consists of only one layer and its time constant (calculated as $\tau = \frac{e^2 \rho c_p}{\lambda}$) is shorter than the simulation time-step, the wall is considered to be in steady-state and is solved as follows[c]:

The internal surface of each wall is modelled with the same equation:

$$\dot{q}_{radi} + h_{ci}(T_{roomi} - T_i) = \frac{\lambda}{e}(T_i - T_o) \tag{4.25}$$

But, the other surface depends on the type of wall, in case of internal walls (WALL block):

$$\dot{q}_{rado} + h_{co}(T_{roomo} - T_o) = \frac{\lambda}{e}(T_o - T_i) \tag{4.26}$$

And, in case of external walls (WALLX):

$$\dot{q}_{sol} + h_{eq}(T_{eq} - T_o) = \frac{\lambda}{e}(T_o - T_i) \tag{4.27}$$

$$h_{eq}(T_{eq} - T_o) = h_{co}(T_a - T_o) + F_{wall-sky}\, h_{ro}(T_{sky} - T_o) \tag{4.28}$$

where [92]:

$$h_{co} = h_{co1} + h_{co2}\, ws \tag{4.29}$$

Finally, the ground walls (WALLG) do not need to be model at the external surface as the temperature at that point is provided.

If the wall has more than one layer, then from layer 1 to n, the time constant of every layer is compared to the simulation time-step. If the time constant is shorter than the time-step, this layer is added to the previous one and its parameters are recalculated as (Figure 4.9):

$$e' = e_1 + e_2 \tag{4.30}$$

$$\lambda' = \frac{e'}{\frac{e_2}{\lambda_2} + \frac{e_1}{\lambda_1}} \tag{4.31}$$

$$\rho' = \frac{e_1\rho_1 + e_2\rho_2}{e'} \tag{4.32}$$

$$c_p' = c_{p1}\left(\frac{\rho_1 e_1}{\rho' e'}\right) + c_{p2}\left(1 - \frac{\rho_1 e_1}{\rho' e'}\right) \tag{4.33}$$

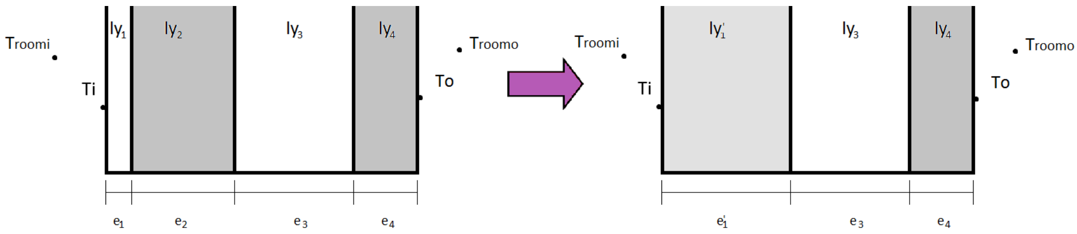

Figure 4.9: Layers aggregation in a wall.

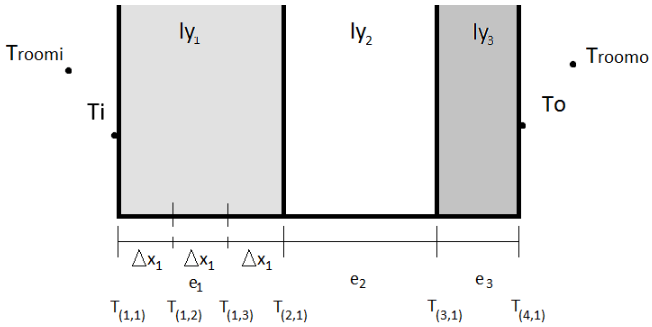

Figure 4.10: Sublayers' temperatures.

Once all layers are analysed, if the result of this aggregation is a one-layer wall still in steady-state, then it is again solved with equations from 4.25 to 4.29. Otherwise, the wall is dynamically simulated following the FDM to solve the one-dimensional heat transfer problem. All layers from 1 to n' (the result of the aggregation process) are divided into sublayers (Figure 4.10), so that the stability condition (Fourier number: $Fo < 0.5$) is fulfilled at every sublayer [46]:

$$\frac{\lambda_i \Delta t}{\rho_i c_{pi} \Delta x_i^2} < 0.5 \qquad (4.34)$$

If any subdivision is too thin ($<$ 0.02 m), then the time-step for the calculation of that sublayer is reduced as much as needed to fulfil the criteria keeping the differential thickness fixed in 0.02 m.

2. Boundary conditions:

The internal boundary conditions are the same for all three walls, while the external ones depend on the type.

[c]This condition is never fulfilled for WALLG as the ground already has a significant inertia.

Inside:

$$T_{conv} = T_{roomi} \tag{4.35}$$
$$\dot{q}_{radi} = \dot{q}_{rad\_swi} + \dot{q}_{rad\_lwi} + \dot{q}_{IGradi} \tag{4.36}$$

Outside:

WALL:

$$T_{conv} = T_{roomo} \tag{4.37}$$
$$\dot{q}_{rado} = \dot{q}_{rad\_swo} + \dot{q}_{rad\_lwo} + \dot{q}_{IGrado} \tag{4.38}$$

WALLX:

$$T_{conv} = T_{eq} \tag{4.39}$$
$$\dot{q}_{rado} = \dot{q}_{sol} \tag{4.40}$$

T_{conv} is the temperature for the convective exchange.

WALLG:

The ground wall is modelled following the ISO 13370-2007 [103]. It proposes to model the floor construction together with the ground below the building as a single component, consisting of each layer in the floor construction plus 0.5 m depth of ground plus a virtual layer. This last one is included so that the annual average heat flow is correct. It has thermal resistance, but a negligible thermal capacity and density ($\approx$ 1 J/kgK and 1 kg/m^3 respectively), and a thickness of 0.1 m (Figure 4.11). Finally, the boundary condition at the bottom of the virtual layer is a virtual temperature $T_{v,m}$, depending on the month.

$$T_{v,m} = T_{i,m} - \frac{\dot{q}_m}{U} \tag{4.41}$$

where $T_{i,m}$ is the monthly mean internal temperature for month m, and $\dot{q}_m$ is the average rate of heat flow through the ground surface in month m and depends on the internal temperature and the temperature of the ground, T_g. The calculation of $T_{i,m}$, U and $\dot{q}_m$ is explained in Appendix A of ISO 13370-2007. They are calculated during the weather and geometrical preprocessing (section 3.2).

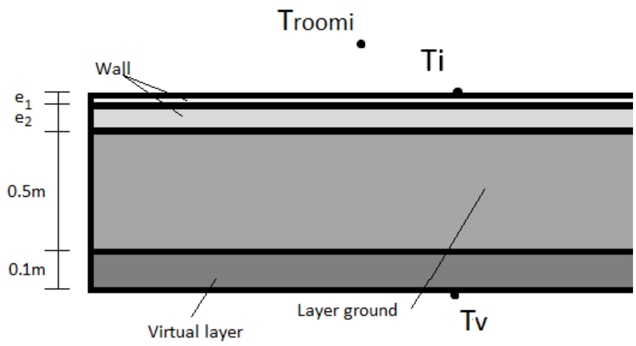

Figure 4.11: Definition of layers in ground wall.

The temperature profile inside the wall:

Internal surface temperature. In order to calculate the internal surface temperature, a surface energy balance is done for the boundary layer, using half of the first sublayer for surface heat capacity (Figure 4.12).

$$\frac{\Delta u_i}{\Delta t} = \dot{q}_{condi} + \dot{q}_{radi} + \dot{q}_{convi} \tag{4.42}$$

$$T_{(1,1)}(t) = T_i \tag{4.43}$$

$$\frac{\Delta x_1}{2}\rho_1 c_{p1}\frac{(T_{(1,1)}(t+\Delta t) - T_{(1,1)}(t))}{\Delta t} = \frac{\lambda_1}{\Delta x_1}(T_{(1,2)} - T_{(1,1)}) + h_{ci}(T_{roomi} - T_{(1,1)}) + \dot{q}_{radi} \tag{4.44}$$

Therefore, the temperature of the interior surface can be calculated as:

$$T_{(1,1)}(t+\Delta t) = T_{(1,1)}(t) + \frac{\Delta t}{\frac{\Delta x_1}{2}\rho_1 c_{p1}} \cdot [\dot{q}_{radi} + \dot{q}_{cond} + h_{ci}(T_{roomi} - T_{(1,1)}(t))] \tag{4.45}$$

$$\dot{q}_{cond} = \frac{\lambda_1}{\Delta x_1}(T_{(1,2)}(t) - T_{(1,1)}(t)) \tag{4.46}$$

External surface temperature depends on the type of wall.

[a]Rocío Monsalvete Álvarez-Uríbarri. Arquitectura e Interiorismo (`rociomonsalvete.com`).

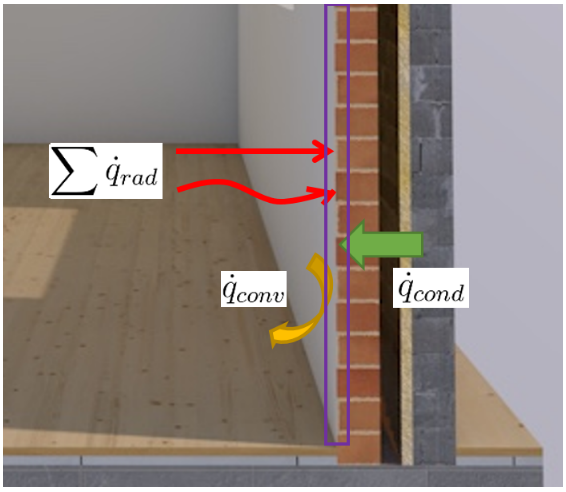

Figure 4.12: Energy balance in the internal surface of the wall (By R. Monsalvete[a]).

WALL: Following the same logic as before:

$$T_{(n+1,1)}(t+\Delta t) = T_{(n+1,1)}(t) + \frac{\Delta t}{\frac{\Delta x_n}{2}\rho_n c_{p\,n}} \cdot [\dot{q}_{rado} + \dot{q}_{cond} + h_{co}(T_{roomo} - T_{(n+1,1)}(t))] \tag{4.47}$$

$$\dot{q}_{cond} = \frac{\lambda_n}{\Delta x_n}(T_{(n,m)}(t) - T_{(n+1,1)}(t)) \tag{4.48}$$

where m is the number of divisions of the last layer.

WALLX:

$$T_{(n+1,1)}(t+\Delta t) = T_{(n+1,1)}(t) + \frac{\Delta t}{\frac{\Delta x_n}{2}\rho_n c_{p\,n}} \cdot \cdot[\dot{q}_{sol} + \dot{q}_{cond} + h_{co}(T_{roomo} - T_{(n+1,1)}(t)) + h_{ro}(T_{sky} - T_{(n+1,1)}(t))] \tag{4.49}$$

$$\dot{q}_{cond} = \frac{\lambda_n}{\Delta x_n}(T_{(n,m)}(t) - T_{(n+1,1)}(t)) \tag{4.50}$$

WALLG: The temperature of the layer touching the ground is not an output.

Every other sublayer temperature:.

$$T_{(i,j)}(t+\Delta t) = T_{(i,j)}(t) + \frac{\Delta t}{\frac{\Delta x_i}{2}\rho_i c_{p\,i}} \cdot [\dot{q}_{cond\_l} + \dot{q}_{cond\_r}] \tag{4.51}$$

where $\dot{q}_{cond\_l}$ and $\dot{q}_{cond\_r}$ are the conductive flows from previous and following sublayers to the objective one at time-step $= t$. Finally, the convective flows are calculated:

$$\dot{q}_{convi} = h_{ci}(T_{roomi} - T_{(1,1)}(t + \Delta t)) \tag{4.52}$$

$$\dot{q}_{convo} = h_{co}(T_{roomo} - T_{(n+1,1)}(t + \Delta t)) \tag{4.53}$$

4.5 WINDOW block

4.5.1 Model scope and objectives

The WINDOW block does a steady stage calculation of the behaviour of a window, including the effect of the internal blinds and curtains.

4.5.2 Physical model description

The window model is divided into two differentiated parts:

1. The conduction through the window is calculated under steady-state conditions:

$$\dot{q}_{cond} = U_c(T_i - T_o) \tag{4.54}$$

$$T_i = T_{roomi} + \frac{\dot{q}_{cond} - \dot{q}_{rad\_lwi}}{h_{ci}} \tag{4.55}$$

$$T_o = T_{eq} - \frac{\dot{q}_{cond}}{h_{cro}} \tag{4.56}$$

$$h_{cro} = h_{co} + h_{ro} \tag{4.57}$$

$$h_{co} = h_{co1} + h_{co2} \cdot ws \tag{4.58}$$

$$T_{eq} = \frac{h_{co}T_a + h_{ro}T_{sky}}{h_{co} + h_{ro}} \tag{4.59}$$

$$\dot{q}_{convi} = h_{ci}(T_{roomi} - T_i) \tag{4.60}$$

2. The transmitted solar radiation (Figure 4.13):

$$\dot{q}_d = (1 - f_b) \cdot g_w \cdot I_d \tag{4.61}$$

$$\dot{q}_b = (1 - f_b) \cdot g_w \cdot (I_g - I_d) \tag{4.62}$$

A door is defined as a WINDOW where $g_w = 0$.

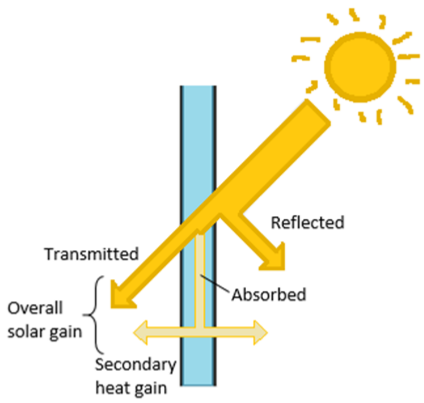

Figure 4.13: Transmitted solar radiation through windows.

4.6 RADI block

4.6.1 Model scope and objectives

The RADI block calculates the internal long-wave radiation between all enclosing surfaces.

4.6.2 Physical model description

The radiation flux emitted by a surface i in a given enclosure is calculated as:

$$\dot{q}_{rad\_lwi} = \epsilon_i \frac{\sum_{j=1}^{n} (A_j F_{ij}(E_j + (1-\epsilon_j)\overline{q_{rad}}))}{A_i} - E_i \tag{4.63}$$

where:

$$\overline{q_{rad}} = \frac{\sum_{i=1}^{n} E_i A_i}{\sum_{i=1}^{n} \epsilon_i A_i} \tag{4.64}$$

and:

$$E_i = \sigma \epsilon_i T_i^4 \tag{4.65}$$

4.7 IRADIA block

4.7.1 Model scope and objectives

It calculates the distribution of solar radiation on the surfaces of the internal walls, roofs and floors.

4.7.2 Physical model description

The IRADIA block distributes the solar radiation, entering in the room through all windows between the enclosing surfaces. The radiation corresponding to transparent surfaces is assumed to leave back the room:

$$\forall surface \quad i, \quad \dot{q}_{rad\_swi} = \dot{q}_g \frac{SF_i}{A_i} \tag{4.66}$$

where:

$$\dot{q}_g = \sum (\dot{q}_b + \dot{q}_d) \tag{4.67}$$

where $\dot{q}_b$ and $\dot{q}_d$ are the beam and diffuse solar radiation transmitted through every window calculated with the WINDOW block.

4.8 Building model verification: BESTEST

Very few real examples exist to allow developers to test building simulation tools and verify their results. Therefore, several norms and guidelines appeared to set the minimum requirements concerning the methods of calculation and check the simulation results. This section presents the BESTEST, which is widely used by building simulation software developers as part of the standard quality control. The model results are in this section compared not only with those of the BESTEST but also with `EnergyPlus`, as it is one of the most commonly used tools. The `EnergyPlus` results are provided by the developers for the version 8.0.0.008 [66].

4.8.1 BESTEST description

The BESTEST is a project conducted by the Model Evaluation and Improvement IEA Experts Group [111]. In this project, a method was developed for systematically testing whole-building energy simulation programs and diagnosing the sources of predictive disagreement. Based on this project, section 5.2 of ANSI/ASHRAE standard 140-2011, Standard Method of Test for the Evaluation of Building Energy Analysis Computer Programs [11] was developed. The test is based on the comparison between the results provided by the new model and several reference programs that represent the best state-of-the-art.

4.8.2 Test cases

Two qualification flow diagrams are presented in the BESTEST documentation, low-mass (series 600) and high-mass buildings (series 900), together with a list of diagnostic cases. These cases, from 195 to 320, were used for debugging the model before the qualification series were performed. Only the qualification cases are considered relevant and presented in this chapter.

The basic test building (Fig. 4.14) is a shoe-box (8 m wide x 6 m long x 2.7 m high) building with two windows (6 m^2 each) on the south wall and without interior partitions. This geometry is used for all cases except for 620, 920, which have the windows oriented east-west (Fig. 4.15), and the Sunspace case 960 (Fig. 4.16), which has an interior partition. The weather file is provided together with the BESTEST documentation. It corresponds to the city of Denver, Colorado (latitude 39.8°north, longitude 104.9°west, time zone 7) and is characterized as “cold clear winters/hot dry summers”. Tables from 4.3 to 4.15 present the parameters needed to build the cases, from construction characteristics to internal gains definitions or control strategies.

4.8.3 Cases description

All cases of series 600 are based on the Basic Test Building (case 600). From this, every change is used to test one specific field, specified in column “Test” of Table 4.14. Case 900 is also compared with the Basic Test Building and afterwards used as basic case for series 900. Cases 610, 630, 910 and 930 have not been performed because they test shading overhangs. The radiation on every external surface, wall or window, is not calculated within the building

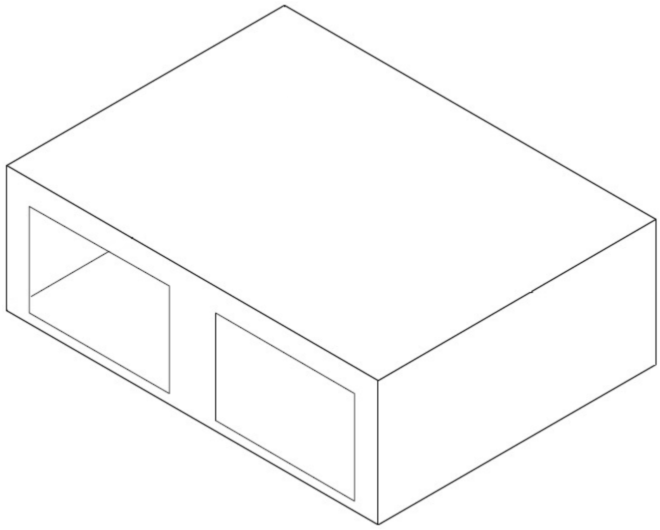

Figure 4.14: Basic test building. Windows oriented south.

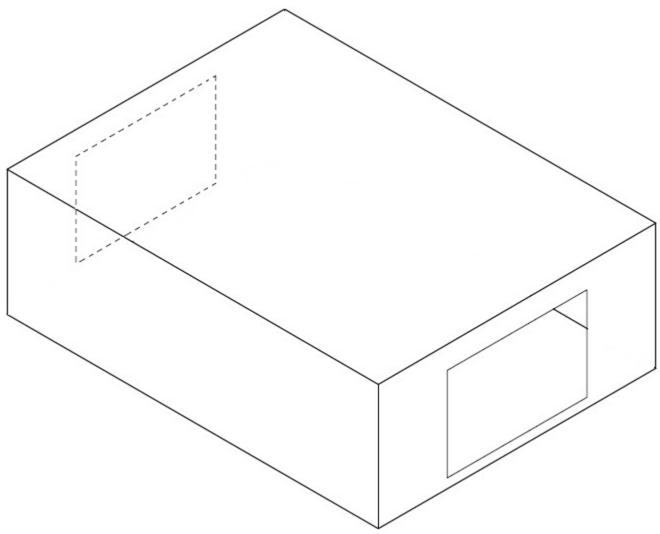

Figure 4.15: Tests 620 and 920. Windows oriented east-west.

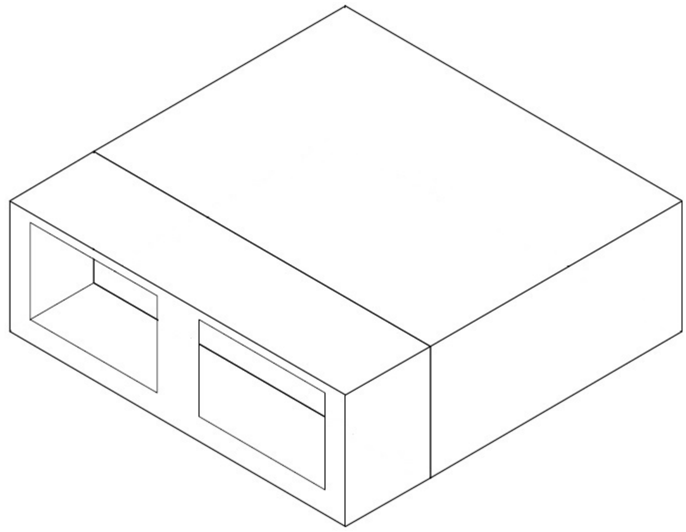

Figure 4.16: Sunspace building. Windows oriented south.

model but preprocessed from the data model as any other aspect of the geometry.That is the reason why these four cases were not considered in the evaluation of the building model (see chapter 4 for further explanations). Finally, cases 960 and 990 are exceptional cases. In case 960, the Basic Test Building is divided into two spaces by an internal wall (See Table 4.12). The cooling and ventilation systems are connected to the back room, leaving the front one in free-floating state. The temperatures of this free-floating space are also reported in the results. The purpose of case 990 is to study the coupling with the ground. Therefore, the characteristics of the floor as well as the temperature of the ground are special issues for this case.

Case 990 is the same as case 900, except that:

- The building has sunk 1.35 m into the ground.

- The non-masonry layers have been stripped from the floor and the sub-grade portion of the walls.

- The south window is reduced in area to 10.8 m^2 and completely fills the above-grade portion of the south wall.

- The ground temperature is not specified. It must be calculated as a function of the meteorological data, soil properties and heat exchange with the building.

4.8.4 Results and conclusions

All simulations were done with a time-step of 5 minutes, but the results are reported hourly or annually as required.

Figures 4.17, 4.18, 4.19 and 4.20 show the results of cases 600 to 990 and Figures 4.21, 4.22 and 4.23 those results of considering cases 600, 650, 900, and 950 in free-floating conditions, together with the front room of the Sunspace case. The results are compared to the minimum and maximum values of all programs, together with those of `EnergyPlus` (for the cases that have been performed with this program) [66].

The model has successfully past almost all cases. From the 51 results obtained (Tables 4.16 to 4.18), only three are out of the ranges, The peak heating of cases 640 and 940 and the maximum temperature in free-floating of case 950. The norm does not require the result to be in the range between the minimum and maximum to pass each test, but just to not have a significant disagreement with the reference programs. Therefore, cases 940 and 950 –whose errors are smaller than 1.6%– are considered passed. Only case 640 seems to produce a considerable error on the calculation of the peak heating (14% over the upper boundary of the range). That is a pervasive problem in building energy programs. The BESTEST documentation already warns about this case: *"However, disagreements were particularly large in the peak heating predictions for thermostat setback cases (640 and 940)..."*. In fact, one of the benchmark programs, `SERIRES UK-BRE` report also a value out of the range and even higher than the one obtained with the model (8.078 kW). Part of the problem may depend on the impact of the inertia in the calculation of the peak, and that is why this problem appears in case 640 (low mass) and not in 940 (high mass). Also, `EnergyPlus` reports this same problem from previous versions and specify the way they solved it, by modifying their algorithm for variable system time-step. Modifying the time-step only at certain moments in the simulation is not trivial to code, and the solution of this disagreement was left for further studies.

Surface	Specified infrared emissivity 0.9	Specified infrared emissivity 0.1
Walls and roofs	29.3 W/m^{2}K	25.2 W/m^{2}K
Windows and high-conductive walls	21.0 W/m^{2}K	16.9 W/m^{2}K

Table 4.1: Exterior combined surface coefficient.

Surface	
Vertical surfaces	3.16 W/m^{2}K
Horizontal ceiling	4.13 W/m^{2}K
Horizontal floor	1 W/m^{2}K

Table 4.2: Interior surface coefficient.

Ground reflectivity	0.2
Site	Flat, unobstructed, located exactly at the weather station
Ground temperature	10 °C
Infiltration rate adjustment factor	0.822
Internal generated heat	200 W (60% radiative, 40% convective; 100% sensible, 0% latent)
Ideal equipments for cooling and heating	P = 1000 kW and 100% efficiency
Mechanical system	100% convective air system. No latent loads
Ventilation	10.8 Air Changes per Hour (ACH)

Table 4.3: General data.

	20,27	Setback	Venting
Heating	If T<20 °C	23:00-07:00, if T<10 °C 07:00-23:00, if T<20 °C	Off
Cooling	If T>27 °C	If T>27 °C	18:00-07:00, off 07:00-18:00, if T>27 °C
Ventilation	Off	Off	18:00-07:00, on 07:00-18:00, off

Table 4.4: Control strategies.

Surface	South Window cases $\alpha = 0.6$	East/West Window cases $\alpha = 0.6$	South Window cases $\alpha = 0.9$	East/West Window cases $\alpha = 0.9$	South Window cases $\alpha = 0.1$	Sunspace case
Floor	0.642	0.642	0.651	0.651	0.244	0.6
Ceiling	0.168	0.168	0.177	0.177	0.191	0.06
East wall	0.038	0.025	0.041	0.027	0.057	0.02
West wall	0.038	0.025	0.041	0.027	0.057	0.02
North wall	0.053	0.0525	0.056	0.056	0.082	0.2
South wall	0.026	0.0525	0.028	0.056	0.065	0.03
Solar lost through windows (2x)	0.0175	0.0175	0.003	0.003	0.152	0.035

Table 4.5: Interior solar distribution (100% of the incoming radiation strikes the floor first and all reflections are diffuse).

Number of panes	2
Double-pane solar heat gain coefficient at normal incidence	0.787
U-value from interior pane to exterior pane	6.057 W/m^{2}K
Total thickness of window	19.35 mm
Double-pane solar heat gain coefficient at normal incidence	0.787

Table 4.6: Window properties.

Element	k (W/mK)	Thickness (m)	U (W/m^{2}K)	Density (kg/m^3)	Cp (J/kgK)
Int. Surface Coeff.			8.290		
Plasterboard	0.160	0.010	16.000	950	840
Fiberglass Quilt	0.040	0.1118	0.358	12	840
Roof Deck	0.140	0.019	7.368	530	900
Ext. Surface Coeff.			29.300		

Table 4.7: Roof construction (inside to outside).

Element L	k (W/mK)	Thickness (m)	U (W/m^2K)	Density (kg/m^3)	Cp (J/kgK)
Int. Surface Coeff.			8.290		
Plasterboard	0.160	0.012	13.333	950	840
Fiberglass Quilt	0.040	0.066	0.606	12	840
Wood Siding	0.140	0.009	15.556	530	900
Ext. Surface Coeff.			29.300		

Table 4.8: Low-mass. Exterior wall construction (inside to outside).

Element L	k (W/mK)	Thickness (m)	U (W/m^2K)	Density (kg/m^3)	Cp (J/kgK)
Int. Surface Coeff.			8.290		
Timber flooring	0.140	0.025	5.600	650	1200
Insulation	0.040	1.003	0.040		

Table 4.9: Low-mass. Floor construction (inside to outside).

Element H	k (W/mK)	Thickness (m)	U (W/m^2K)	Density (kg/m^3)	Cp (J/kgK)
Int. Surface Coeff.			8.290		
Concrete Block	0.510	0.10	0 5.100	1400	1000
Foam Insulation	0.040	0.0615	0.651	10	1400
Wood Siding	0.140	0.009	15.556	530	900
Ext. Surface Coeff.			29.300		

Table 4.10: High-mass. Exterior wall construction (inside to outside).

Element H	k (W/mK)	Thickness (m)	U (W/m^2K)	Density (kg/m^3)	Cp (J/kgK)
Int. Surface Coeff.			8.290		
Timber flooring	0.130	0.080	14.125	1400	1000
Insulation	0.040	1.007	0.040		

Table 4.11: High-mass. Floor construction (inside to outside).

k (W/mK)	Thickness (m)	U (W/m^2K)	Density (kg/m^3)	Cp (J/kgK)	Shortwave absorptance
0.510	0.20	2.55	1400	1000	0.6

Table 4.12: Internal wall construction.

Conductivity	1.3 W/mK
Density	1500 kg/m^3
Specific heat	800 J/kgK

Table 4.13: Soil characteristics for case 990.

Case	Setpoints H, C, V	Mass	IntGen	Infilt ACH	Int IR emissiv	Ext IR emissiv	Int SW absorpt	Ext SW absorpt	Glass (m^2)	Orient	Test
600	20,27	L	200	.5	.9	.9	.6	.6	12	S	South solar transmission
620	20,27	L	200	.5	.9	.9	.6	.6	6,6	E,W	East/west solar transmittance/incidence
640	Setback	L	200	.5	.9	.9	.6	.6	12	S	Night setback
650	Venting	L	200	.5	.9	.9	.6	.6	12	S	Venting

Table 4.14: Low-Mass diagnostics.

Case	Setpoints H, C, V	Mass	IntGen	Infilt ACH	Int IR emissiv	Ext IR emissiv	Int SW absorpt	Ext SW absorpt	Glass (m^2)	Orient	Test
900	20,27	H	200	.5	.9	.9	.6	.6	12	S	Thermal mass and solar interaction
920	20,27	H	200	.5	.9	.9	.6	.6	6,6	E,W	East/West transmittance/mass interaction
940	Setback	H	200	.5	.9	.9	.6	.6	12	S	Setback/mass interaction
950	Venting	H	200	.5	.9	.9	.6	.6	12	S	Venting/mass interaction
960	Venting*	H	200*	.5	.9	.9	.6	.6	12	S	(*In back room) Passive solar/interzone heat transfer
990	20,27	H	200	.5	.9	.9	.6	.6	12	S	Ground coupling

Table 4.15: High-Mass diagnostics.

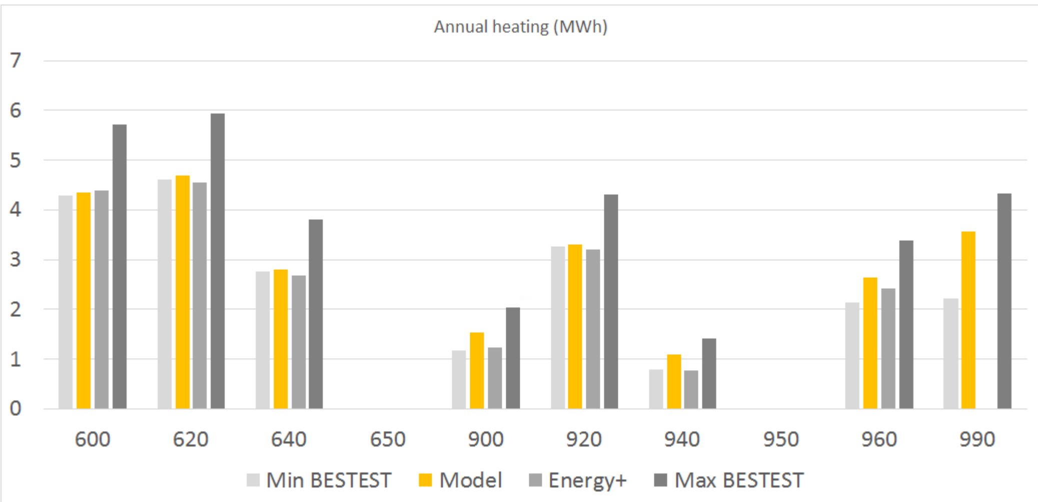

Figure 4.17: Annual heating.

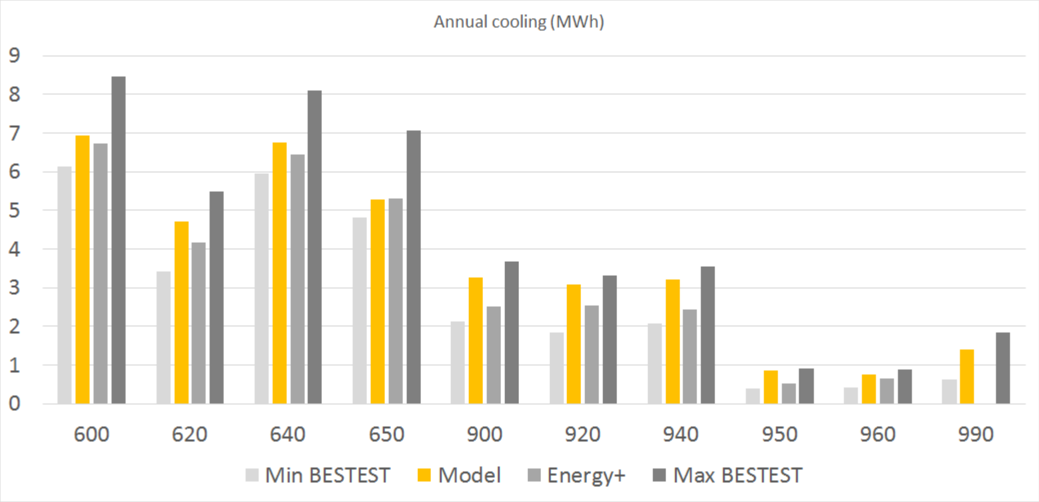

Figure 4.18: Annual cooling.

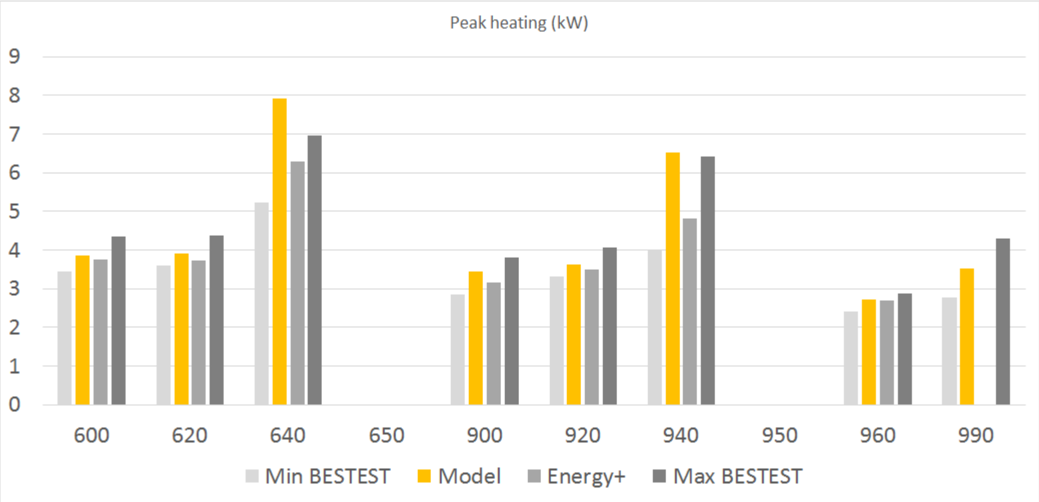

Figure 4.19: Peak heating.

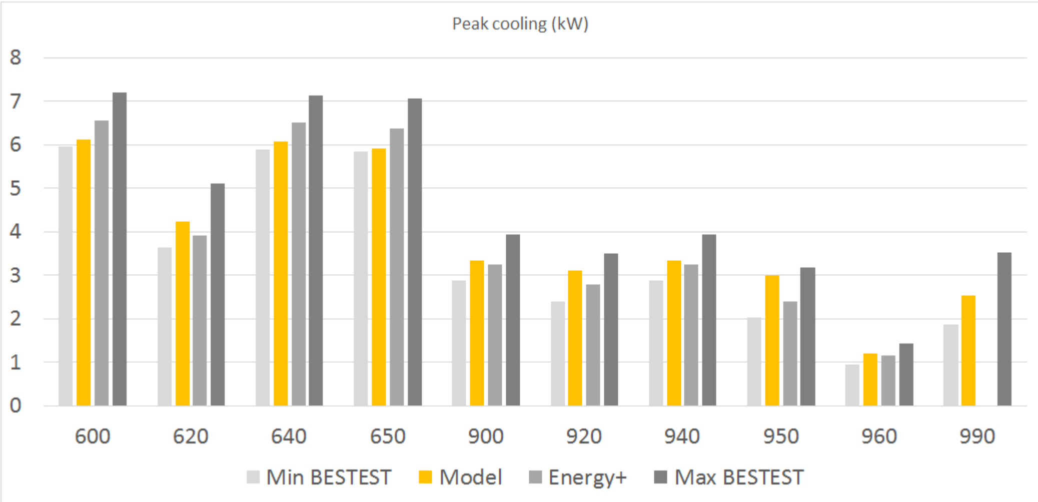

Figure 4.20: Peak cooling.

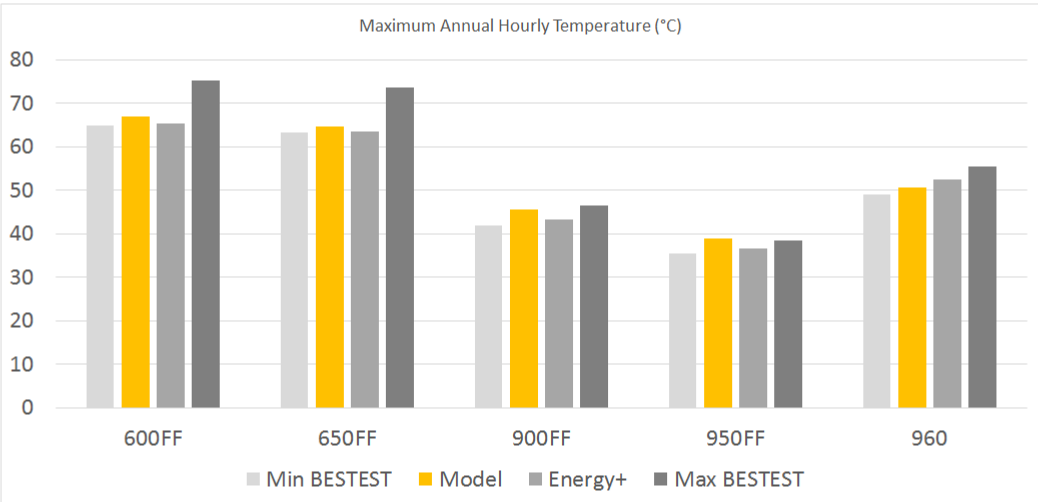

Figure 4.21: Maximum Annual Hourly Temperature.

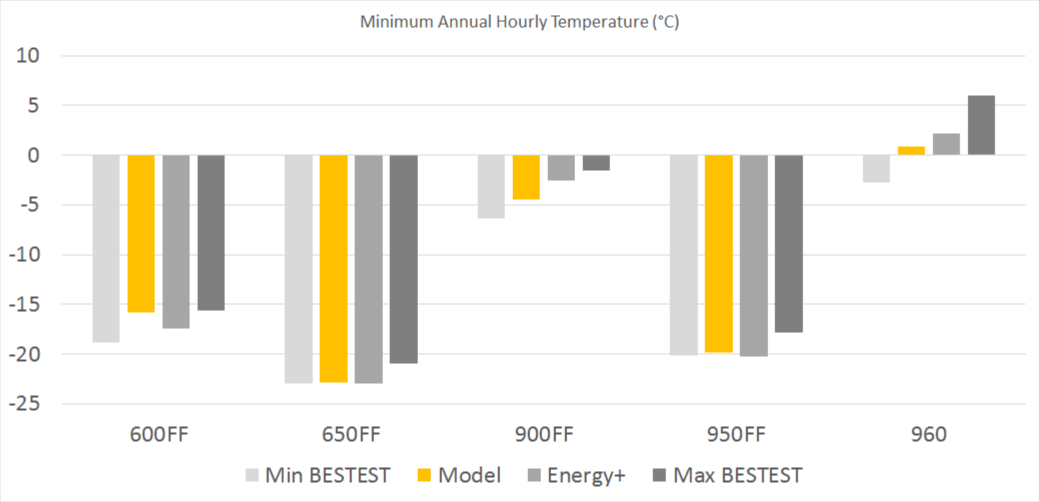

Figure 4.22: Minimum Annual Hourly Temperature.

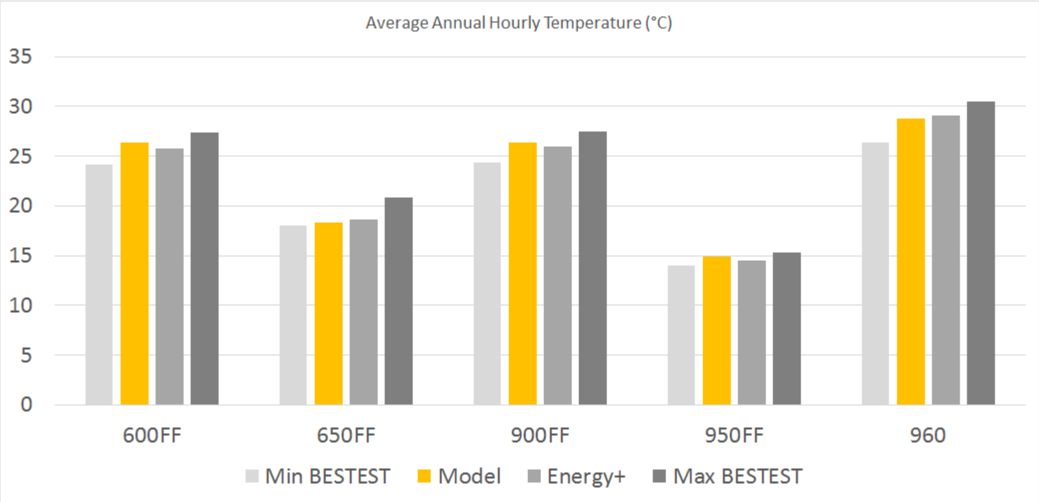

Figure 4.23: Average Annual Hourly Temperature.

Low Mass				
Annual heating (MWh)	600	620	640	650
Minimum	4.296	4.613	2.751	0
Maximum	5.709	5.944	3.803	0
Average	5.046	5.328	3.135	0
Model	4.355	4.680	2.795	0
EnergyPlus	4.378	4.550	2.684	0
Annual cooling (MWh)	600	620	640	650
Minimum	6.137	3.417	5.952	4.816
Maximum	8.448	5.482	8.097	7.064
Average	7.053	4.416	6.790	5.708
Model	6.945	4.709	6.762	5.290
EnergyPlus	6.740	4.168	6.454	5.304
Peaking heating (kW)	600	620	640	650
Minimum	3.437	3.591	5.232	0
Maximum	4.354	4.379	6.954	0
Average	3.952	3.998	5.903	0
Model	3.867	3.898	7.929	0
EnergyPlus	3.750	3.741	6.277	0
Peaking cooling (kW)	600	620	640	650
Minimum	5.965	3.634	5.884	5.831
Maximum	7.188	5.096	7.126	7.068
Average	6.535	4.393	6.478	6.404
Model	6.109	4.233	6.073	5.907
EnergyPlus	6.565	3.921	6.501	6.373

Table 4.16: Results Low Mass Series.

High Mass						
Annual heating (MWh)	900	920	940	950	960	990
Minimum	1.170	3.261	0.793	0	2.144	2.222
Maximum	2.041	4.300	1.411	0	3.373	4.324
Average	1.649	3.828	1.086	0	2.709	3.501
Model	1.530	3.295	1.094	0	2.638	3.571
EnergyPlus	1.224	3.193	0.768	0	2.408	-
Annual cooling (MWh)	900	920	940	950	960	990
Minimum	2.132	1.840	2.079	0.387	0.411	0.616
Maximum	3.669	3.313	3.546	0.921	0.895	1.841
Average	2.826	2.684	2.725	0.635	0.669	1.227
Model	3.264	3.086	3.205	0.848	0.756	1.393
EnergyPlus	2.508	2.548	2.433	0.530	0.640	-
Peaking heating (kW)	900	920	940	950	960	990
Minimum	2.850	3.308	3.980	0	2.410	2.769
Maximum	3.797	4.061	6.428	0	2.863	4.296
Average	3.452	3.738	5.414	0	2.686	3.525
Model	3.444	3.637	6.532	0	2.729	3.517
EnergyPlus	3.172	3.483	4.815	0	2.693	-
Peaking cooling (kW)	900	920	940	950	960	990
Minimum	2.888	2.385	2.888	2.033	0.953	1.859
Maximum	3.932	3.505	3.932	3.170	1.422	3.525
Average	3.460	3.123	3.460	2.724	1.210	2.829
Model	3.335	3.110	3.334	3.001	1.206	2.524
EnergyPlus	3.250	2.777	3.250	2.388	1.143	-

Table 4.17: Results High Mass Series.

Free floating temperatures					
Maximum annual hourly temperature (°C)	600FF	650FF	900FF	950FF	960
Minimum	64.9	63.2	41.8	35.5	48.9
Maximum	75.1	73.5	46.4	38.5	55.3
Average	67.7	66.1	43.7	36.6	50.5
Model	67.0	64.5	45.5	38.8	50.7
EnergyPlus	65.3	63.5	43.2	36.6	52.4
Minimum annual hourly temperature (°C)	600FF	650FF	900FF	950FF	960
Minimum	-18.8	-23.0	-6.4	-20.2	-2.8
Maximum	-15.6	-21.0	-1.6	-17.8	6.0
Average	-17.6	-22.4	-3.7	-19.3	2.3
Model	-15.8	-22.9	-4.4	-19.9	0.9
EnergyPlus	-17.4	-23.0	-2.6	-20.3	2.2
Average annual hourly temperature (°C)	600FF	650FF	900FF	950FF	960
Minimum	24.2	18.0	24.4	14.0	26.4
Maximum	27.4	20.8	27.5	15.3	30.5
Average	25.3	18.9	25.5	14.5	28.2
Model	26.4	18.3	26.4	14.9	28.7
EnergyPlus	25.8	18.6	26.0	14.5	29.1

Table 4.18: Results free-floating temperatures.

4.9 Conclusions of Building model

This chapter presented the physical description of the developed building model. The set of equations that describe the model have been clustered in blocks representing different phenomena, including the heat transfer through the transparent and opaque envelope surfaces, the internal short-wave and long-wave exchange between enclosing surfaces and the convective transfer to the internal air node. In this way, a very modular and flexible model is obtained, allowing the modification of the different parts independently. Finally, the model has been tested using BESTEST and compared with `EnergyPlus` obtaining excellent results.

Chapter 5

District Heating Network and Solar System Models

The previous chapter presented the model of the demand side of a DHS. In this chapter, both the network, and the solar supply system models are introduced. The blocks used to build the network and the solar system have not been developed by the author, unlike those of the dynamic building model. Instead, some standard INSEL blocks have been used to make up the solar system model. That includes the SCDYN block for the solar collectors, TANKST block for the storage tanks and the HXS block for the heat exchangers.
Also, the user-developed block[a] SpHeat, created by Ilyes Ben Hassine [93], has been selected and further improved within this thesis. The selection was supported on the following reasons:

- SpHeat is a pseudo-dynamic model, which is the most suitable model for thermodynamic studies of DHN (see section 2.1.2).
- It is based on the element method, that allows to model both, tree-shape and meshed networks.
- It is coded in INSEL, so there is no need for a new tool.
- It is fully accessible for modifications and updates.

[a] INSEL provides some standard blocks and allows the user to develop and share new ones, the so-called ‘User blocks’.

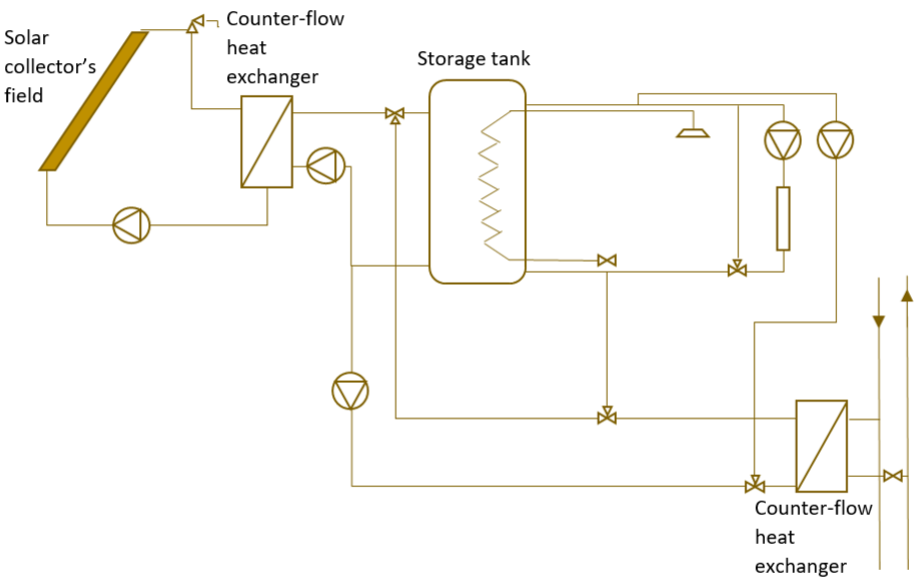

Figure 5.1: Solar system schema.

5.1 Solar System Model

As a first attempt, only one solar system schema has been developed and included in the platform. Figure 5.1 shows again the hydraulic schema (already presented in section 3.3). It is based on three main elements, including solar collectors' field (flat-plate or evacuated-tube), storage tank (stratified or fully mixed) and counter-flow heat exchangers. Their physical principles and computational models are presented in this section.

5.1.1 Solar collector: SCDYN block

Model scope and objectives

The SCDYN block simulates solar collectors under dynamic conditions based on the European Standard EN 12975-2:2006 [190]. It is a 1-node model that allows the discretization of the collector to increase the accuracy of the model and to avoid temperature oscillations.

Physical model description

The solar collectors are modelled under dynamic conditions. The outlet temperature is calculated depending on the solar heat absorbed by the collector and its thermal capacity. The heat absorbed Q_{abs} [W] depends on the efficiency of the collector:

$$\dot{Q}_{abs} = A_a I_g \eta \tag{5.1}$$

where A_a [m^2] is the aperture area of the collector, η is [-] its efficiency, and I_g [W/m^2] is the global radiation perpendicular to the collector surface. The global radiation is an input to the model. It is previously calculated in the *Geometrical preprocessing* workflow step (see section 3.2). The collector efficiency is defined in the standard as:

$$\eta = \eta_0 K_\theta - a_1 \frac{T_m - T_a}{I_g} - a_2 \frac{(T_m - T_a)^2}{I_g} \tag{5.2}$$

where η_0 [-], a_1 [W/m^{2}K] and a_2 [W/m^{2}K^2] are the zero-loss efficiency of the collector and the linear and quadratic heat loss coefficients, respectively. These coefficients are provided by the producers based on this same standard. T_a [°C] is the ambient air temperature, and the mean temperature T_m [°C] is defined as:

$$T_m = \frac{T_{in} + T_{out}}{2} \tag{5.3}$$

where T_{in} [°C] and T_{out} [°C] are the inlet and outlet temperatures of the collector. Finally, K_θ [-] is the Incidence Angle Modifier (IAM), which measures the influence of the incidence angle on the collector efficiency and is also provided by the producers for different incidence angles θ. Part of the heat absorbed by the collector is stored by increasing the temperature of the collector itself. The other part is transmitted to the thermal carrier:

$$\dot{Q}_{abs} = \dot{Q}_{coll} + \dot{m} c_p \Delta T \tag{5.4}$$

where $\dot{m}$ [kg/s] is the thermal carrier mass flow and c_p [J/kgK] its heat capacity. $\Delta T = T_{out} - T_{in}$ [°C] is the variation of temperature of the thermal fluid from inlet to outlet, and finally, $\dot{Q}_{coll} = C_{coll} A_a (T'_m - T_m)$ is the heat absorbed by the collector itself assuming that it has the same temperature as the thermal fluid inside. C_{coll} [J/m^{2}K] is the thermal capacity of the collector and T_m [°C] is the mean temperature of the thermal fluid, T at the beginning of the time-step and T' at the end.

By joining equations 5.1 and 5.4, the following equation is derived:

$$A_a I_g \eta = \dot{Q}_{coll} + \dot{m} c_p \Delta T \tag{5.5}$$

And so:

$$A_a I_g (\eta_0 K_\theta - a_1 \frac{T_m - T_a}{I_g} - a_2 \frac{(T_m - T_a)^2}{I_g}) - C_{coll} A_a (T'_m - T_m) = \dot{m} c_p (T_{out} - T_{in}) \tag{5.6}$$

Adding 5.3 and reorganising, the mean temperature at the end of the time-step is calculated as:

$$T'_m = \frac{\eta_0 K_\theta + a_1 T_a - a_2 (T_m - T_a)^2 + \frac{2\dot{m} c_p}{A_a} T_{in} + \frac{C_{coll}}{\Delta t} T_m}{a_1 + \frac{2\dot{m} c_p}{A_a} + \frac{C_{coll}}{\Delta t}} \tag{5.7}$$

And the outlet temperature at the end of the time-step using 5.3 again:

$$T'_{out} = 2T'_m - T_{in} \tag{5.8}$$

The model allows the simulation of several modules connected either in series or in parallel. Each module can also be divided into partition elements to represent the temperature changes along the collector better. The first time the simulation engine calls the block, the aperture area per collector A_a [m^2], the total aperture area A_{tot} [m^2] (the sum of all collectors' areas), and the mass flow per each parallel row $\dot{m}$ [kg/s], are calculated while the starting conditions are defined as:

$$A_a = \frac{A}{N_{seg}} \tag{5.9}$$
$$A_{tot} = A \cdot N_s \cdot N_p \tag{5.10}$$
$$\dot{m} = \frac{\dot{m}_{tot}}{N_p} \tag{5.11}$$
$$T'_{out} = T_{m,0} \tag{5.12}$$
$$T'_m = T_{m,0} \tag{5.13}$$
$$\dot{m} = 0 \Rightarrow \dot{Q}_u = 0 \tag{5.14}$$
$$\eta = \eta_0 K_\theta \tag{5.15}$$
$$t_0 = t \tag{5.16}$$

From the second time on, the time-step Δt [s] is calculated as $\Delta t = t - t_0$. The temperatures at the end of the time-step can then be calculated using equations 5.7 and 5.8 for each partition element. These equations use the outputs of the first partition element for the following one and these outputs as inputs to the next collector in series. The outputs of the block are finally calculated as:

$$T'_{out} = \frac{\sum_{i=1}^{N_p} T'_{out,i}}{N_p} \tag{5.17}$$

$$T'_{m} = \frac{\sum_{i=1}^{N_p \cdot N_s} T'_{out,i}}{N_p \cdot N_s} \tag{5.18}$$

$$\dot{Q}_u = \sum \dot{Q}_{abs} - \dot{Q}_{coll} \;\forall \text{ partition element} \tag{5.19}$$

$$\eta = \frac{\dot{Q}_u}{(I_b + I_d)A_{tot}} \tag{5.20}$$

5.1.2 Storage Tank: TANKST block

Model scope and objectives

The TANKST block simulates stratified storage tanks by dividing it vertically in N fully-mixed equal volumes. Then, a fully-mixed storage tank can also be simulated if only one node is defined.

Physical model description

The stratified storage tank model (Figure 5.2) has two flow inputs, one coming from the heat source field (Hot side) and the other from the cold source or consumption (Cold side). The hot mass flow enters at the top of the tank, and the same mass flow exits at the bottom to go back to the heat source. On the cold side, the flow mass enters at the bottom and the same amount of fluid exits at the top to consumption.

The simulation is based on a multi-node approach, in which the tank is divided vertically in N nodes with the same mass. Each node is a fully mixed fluid volume with a single temperature T_n [°C]. An energy balance on each node leads to a set of N differential equations:

$$m\, c_p \frac{dT_n}{dt} = \dot{Q}_{hot,n} + \dot{Q}_{cold,n} - \dot{Q}_{loss,n} \tag{5.21}$$

where $\dot{Q}_{hot,n}$ [W] and $\dot{Q}_{cold,n}$ [W] are the heat flows coming from neighbour nodes above (*hot*) and below (*cold*), respectively, and $\dot{Q}_{loss,n}$ [W] the heat

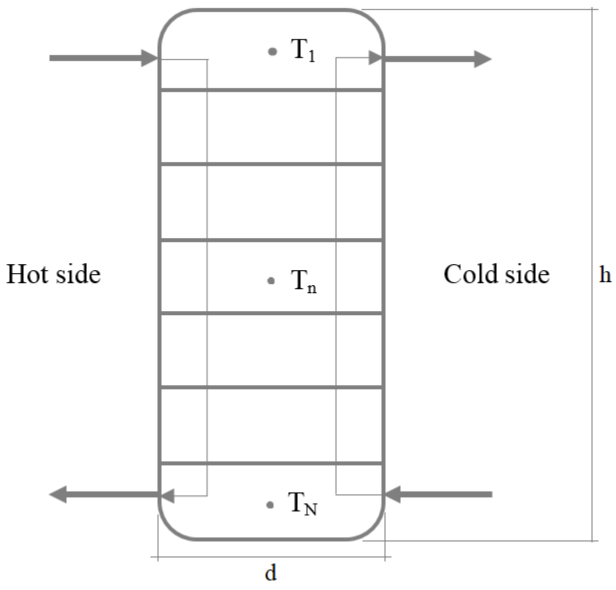

Figure 5.2: Stratified storage tank.

losses through the tank wall. Two types of nodes can be found: those at the extremes (1 and N) and those in between (the internal nodes). The heat balance can be written at each internal node n as:

$$m\,c_p \frac{dT_n}{dt} = \dot{m}_{hot} c_p (T_{n-1} - T_n) + \dot{m}_{cold} c_p (T_{n+1} - T_n) - UA_n (T_n - T_a) \tag{5.22}$$

At the top and the bottom of the tank, the energy balance becomes:

$$m\,c_p \frac{dT_1}{dt} = \dot{m}_{hot} c_p (T_{hot} - T_1) + \dot{m}_{cold} c_p (T_2 - T_1) - UA_1 (T_1 - T_a) \tag{5.23}$$

$$m\,c_p \frac{dT_N}{dt} = \dot{m}_{hot} c_p (T_{N-1} - T_N) + \dot{m}_{cold} c_p (T_{cold} - T_N) - UA_N (T_N - T_a) \tag{5.24}$$

where m [kg] are the fluid mass belonging to each node and c_p [J/kgK] the thermal capacity of the fluid, it is assumed the same fluid inside the tank than that from the two inlets. $\dot{m}$ [kg/s] are the mass flows at the hot and cold inlets. U [W/m^2] is the heat loss coefficient of the tank wall, including the isolation and A [m^2] the area of wall touching each fluid volume, being A_1 and A_N those at the top and bottom of the tank. These two areas include the top and bottom areas, respectively and the corresponding part of the vertical wall. A_n is the corresponding part of the vertical wall of every other node, which is the same for all:

$$A_1 = \pi\frac{d^2}{4} + \pi d\frac{h}{N} \tag{5.25}$$

$$A_N = A_1 \tag{5.26}$$

$$A_n = \pi d\frac{h}{N} \tag{5.27}$$

where d [m] and h [m] are the tank diameter and high, respectively. Finally, T [°C] are the nodes temperatures (1, n, N) and that of the hot (*hot*) and cold (*cold*) inlet flows (Figure 5.2).

The equation system is solved by using the Euler method, which leads to the following set of equations with which the temperatures at the end of the time-step can be directly calculated:

$$T_1' = T_1 + \frac{\Delta t}{mc_p}\left[\dot{m}_{hot}c_p(T_{hot} - T_1) + \dot{m}_{cold}c_p(T_2 - T_1) - UA_1(T_1 - T_a)\right] \tag{5.28}$$

$$T_n' = T_n + \frac{\Delta t}{mc_p}\left[\dot{m}_{hot}c_p(T_{n-1} - T_n) + \dot{m}_{cold}c_p(T_{n+1} - T_n) - UA_n(T_n - T_a)\right] \tag{5.29}$$

$$T_N' = T_N + \frac{\Delta t}{mc_p}\left[\dot{m}_{hot}c_p(T_{N-1} - T_N) + \dot{m}_{cold}c_p(T_{cold} - T_N) - UA_N(T_N - T_a)\right] \tag{5.30}$$

The first time the block is called by the simulation engine, the variables are initialised:

$$h = \frac{V}{\pi d^2/4} \tag{5.31}$$

$$m = \rho V \tag{5.32}$$

$$T'n = T_0 \tag{5.33}$$

$$t_0 = t \tag{5.34}$$

At the second call, the time-step Δt [s] is calculated as $\Delta t = t - t_0$ and from this call on, the temperatures at the end of the time-step can be calculated as presented in equations 5.28 to 5.30.

5.1.3 Heat exchanger: HXS block

Model scope and objectives

The HXS block simulates a sensible counter-flow heat exchanger based on a steady-state approach following the NTU method.

Physical model description

The exchanged heat is calculated assuming constant thermal capacity of both fluids and constant UA, which is provided by the heat exchanger manufacturers and considered not to be dependent on temperatures:

$$\dot{Q} = UA \cdot LMTD \tag{5.35}$$

where UA [W/K] is the overall heat transfer coefficient times the area of exchange and $LMTD$ [K] is the logarithmic mean temperature difference, which is defined as:

$$LMTD = \frac{\Delta T_{hot} - \Delta T_{cold}}{\ln \frac{\Delta T_{hot}}{\Delta T_{cold}}} \tag{5.36}$$

Furthermore, the heat exchanged affects both fluids modifying their temperatures:

$$\dot{Q} = -C_{hot}\Delta T_{hot} \tag{5.37}$$

$$\dot{Q} = C_{cold}\Delta T_{cold} \tag{5.38}$$

where $C = \dot{m}c_p$ [W/K] is the heat capacity of the fluid and $\Delta T = T_{out} - T_{in}$ [°C] the difference of temperatures for the hot (*hot*) and cold (*cold*) streams.

The NTU method solves the resulting equation system defining the efficiency of a heat exchanger and its relationship with two dimensionless parameters, NTU and R. The efficiency of a heat exchanger is defined as the transferred heat divided by the maximum transferred heat, which is that of an ideal heat exchanger with $UA = \infty$:

$$\varepsilon = \frac{\dot{Q}}{\dot{Q}_{max}} = \frac{\dot{Q}}{C_{min}(T_{hot,in} - T_{cold,in})} \tag{5.39}$$

$$NTU = \frac{-UA}{C_{min}} \tag{5.40}$$

$$R = \frac{C_{min}}{C_{max}} \tag{5.41}$$

where $C_{min} = \min(C_{hot}, C_{cold})$ and $C_{max} = \max(C_{hot}, C_{cold})$.
The relationship between the efficiency and the dimensionless numbers depend on the type of heat exchanger for a counter-flow heat exchanger is defined as follows:

$$\text{If } R = 0 \quad \Rightarrow \quad \varepsilon = \frac{NTU}{NTU + 1} \tag{5.42}$$

$$\text{Else} \quad \Rightarrow \quad \varepsilon = \frac{1 - \exp(-NTU(1 - R))}{1 - R\exp(-NTU(1 - R))} \tag{5.43}$$

Once the efficiency is obtained, the outlet temperatures are calculated using equations 5.37 and 5.38 together with 5.39:

$$T_{hot,out} = T_{hot,in} - \varepsilon \frac{C_{min}}{C_{hot}} (T_{hot,in} - T_{cold,in}) \tag{5.44}$$

$$T_{cold,out} = T_{cold,in} + \varepsilon \frac{C_{min}}{C_{cold}} (T_{hot,in} - T_{cold,in}) \tag{5.45}$$

5.2 District Heating Network

Along this section, first, the theoretical basis together with the corresponding `INSEL` block are presented, and some possible improvements are highlighted to describe the methodology used to solve one of the drawbacks of the model in the following section.

5.2.1 Physical description

SpHeat is divided into two parts, the hydraulic and the thermal models, in the so-called SpHydro and SpThermo subroutines, respectively, both embedded in the same block. The hydraulic model calculates the pressure and mass flows along the pipes under steady-state conditions. Then, the thermal model uses –per time-step– the calculated values as inputs to dynamically simulate the thermal behaviour of the net, making up both together a pseudo-dynamic model (see section 2.1.2).

SpHydro

The network is sketched as a *planar graph* (i.e. abstract graphs that can be drawn in a way that the edges meet only in common ends, so no other intersections are found [63]). It is represented by a set of nodes and oriented branches (edges) as illustrated in Figure 5.3, where each node is either a substation ('consumer' or 'producer')[b], or a pipe junction. The edges represent the pipes, including plumbing fittings like elbows or couplings. When the fittings connect more than two pipes, or the pipes have different characteristics (e.g. internal diameter, roughness), then they are represented as nodes,

[b]The information about the substations is updated every time-step, allowing the transformation of 'producers' into 'consumers' and vice-versa.

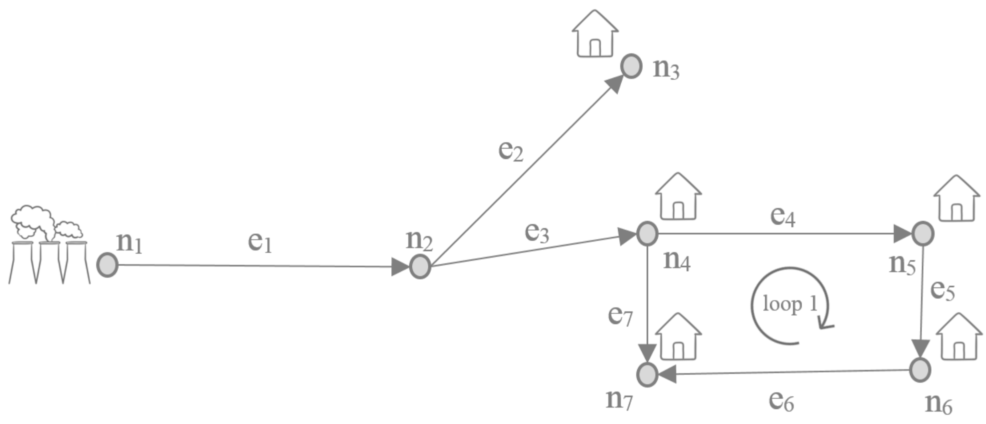

Figure 5.3: Example of network represented as a planar graph.

and the pipes as different edges. The orientation of the edges is set by the user and can be done arbitrarily as they ere used only to define the paths, not the direction of the flows. The flows are calculated depending on the distribution of pressures. The paths (finite sequence of edges) can be open or close, creating loops. These loops require at least one link, i.e. an edge which specifies the orientation of the loop where it belongs. For example, in Figure 5.3, either e_4 or e_7 could define the direction of the loop. If e_4 is selected, then the loop is oriented as in the figure.

The incidence matrices, $X_{E\times N}$ and $Y_{L\times E}$, store the network topology. X represents the edges-nodes interconnections and Y describes the orientation of the edges in a loop. E, N and L are the number of edges, nodes and loops, respectively. The matrices entries $x_{e,n}, y_{l,e} \in \{-1, 0, 1\}$
$x_{e,n} = 1$ when node n is the starting point of edge e, $x_{e,n} = -1$ when node n is the ending point of edge e, and $x_{e,n} = 0$ if there is no connection between node n and edge e.
$y_{l,e} = 1$ when edge e has the same orientation of loop l and $y_{l,e} = -1$ in the opposite case. Finally and $y_{l,e} = 0$ if edge e does not belong to loop l. In the example presented in Figure 5.3, e_4, e_5 and e_6 would give a 1 in the Y matrix while for e_7 would correspond a -1. The following matrices are the $X_{E\times N}$ and $Y_{L\times E}$ correspondent to the example:

$$X_{E\times N} = \begin{pmatrix} 1 & -1 & 0 & 0 & 0 & 0 & 0 \\ 0 & 1 & -1 & 0 & 0 & 0 & 0 \\ 0 & 1 & 0 & -1 & 0 & 0 & 0 \\ 0 & 0 & 0 & 1 & -1 & 0 & 0 \\ 0 & 0 & 0 & 0 & 1 & -1 & 0 \\ 0 & 0 & 0 & 0 & 0 & 1 & -1 \\ 0 & 0 & 0 & 1 & 0 & 0 & -1 \end{pmatrix}$$

$$Y_{L\times E} = \begin{pmatrix} 0 & 0 & 0 & 1 & 1 & 1 & -1 \end{pmatrix}$$

The network topology represents in one graph the two identical sub-networks, including supply and return. These two sub-networks are interconnected through the substations. Once the topography is defined, the pressures and flows are calculated using the electrical analogy to formulate both, the conservation of mass and the conservation of energy (equation 5.50) at each node. The first one is derived into the conservation of volume assuming, that the density is constant over the complete network (equation 5.46):

$$X\vec{\dot{V}} = \vec{0} \tag{5.46}$$

where $\vec{\dot{V}}$ [m^3/s] is the volumetric flow rates vector.

The friction losses through the edges are calculated with the Darcy-Weisbach formula, considering the edges straight conduits of constant cross-sections. For each edge is written as:

$$\frac{\Delta p}{L} = f_D \frac{\rho}{2} \frac{(\vec{\dot{v}}/A)^2}{D} \tag{5.47}$$

where $\dot{v}$ [m^3/s] is the volumetric flow rate along the edge and Δp [Pa] is the pressure losses between the initial and ending nodes. L [m] is the edge length, ρ [kg/m^3] the density of the fluid, A [m^2] is the cross-section, D [m] is the hydraulic diameter (which for circular cross areas is equal to the internal diameter), and f_D [-] is the Darcy friction factor. The Darcy friction factor depends on the flow characteristics. For laminar flows ($Re \leq 2100$) it is calculated as in equation 5.48 while the Colebrook-White equation is used

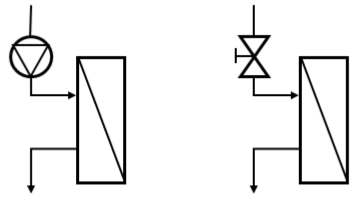

(a) Producer. (b) Consumer.

Figure 5.4: Substations connections.

for turbulent regimes ($Re \geq 4000$), which is valid for smooth and rough pipes (equation 5.49):

$$f_D = \frac{64}{Re} \tag{5.48}$$

$$\frac{1}{\sqrt{f_D}} = -2\log\left(\frac{\varepsilon}{3.7D} + \frac{2.51}{Re\sqrt{f_D}}\right) \tag{5.49}$$

where $Re = \frac{\dot{v}L}{\mu}$ [Pa/s] is the Reynolds number, μ is the dynamic viscosity of the fluid and ε [m] the roughness of the pipe. Both the Darcy-Weisbach and the Colebrook-White equations are accepted as the most accurate ones on its respective flow regimes. The transition regime ($2100 < Re < 4000$) is calculated as the linear interpolation between the two limits of both regimes: the corresponding friction factor for laminar regime at $Re = 2100$ and that of turbulent regime at $Re = 4000$.

If there are loops, the conservation of energy is formulated as:

$$Y\vec{\Delta P} = \vec{0} \tag{5.50}$$

where $\vec{\Delta P}$ [Pa] is the vector of pressure losses along the edges in the direction of the corresponding flows.

The connections through the substations between the supply and the return pipes provoke also pressure drops. The 'consumers' are assumed to have a valve to control the mass flow and a heat exchanger to transmit the heat to the secondary network connected, as shown in Figure 5.4(b). The pressure losses are calculated as:

$$\Delta p = \frac{100000\dot{v}^2}{(crl \cdot K_{vs}/3600)^2} + \gamma K_{hx}\dot{v}^2 \tag{5.51}$$

The first term represents the pressure losses through the valve based on the k_v method, where crl [-] is the control for the valve opening and K_{vs} [m^3/h] the coefficient of pressure losses through a valve when it is fully open, which is defined as:

$$K_{vs} = \frac{\dot{v}}{\sqrt{\Delta p}} \tag{5.52}$$

Δp should be in bar and $\dot{v}$ in m^3/h.

The second part of equation 5.51 represents the pressure losses due to the heat exchanger, where, K_{hx} $[m/(m^3/s)^2]$ is the localised pressure drop coefficient of the heat exchanger.

The 'producers' instead are composed of a pump and a heat exchanger connected as in Figure 5.4(a). The increment of pressure is calculated as:

$$\Delta p = \gamma \left(crl^2 \cdot p(\dot{v}) - K_{hx}\dot{v}^2 \right) \tag{5.53}$$

The first term of the right side of the equation is the increment of the pressure provided by the pump. The second part represents again the pressure losses due to the heat exchanger, and it is treated in the same way as for the 'consumer'. crl [-] is the control parameter defined as the ratio between the working point power and the nominal power of the pump, and $p(\dot{v})$ [Pa] is the pressure drop extracted from the characteristic curve of the pump at volume flow $\dot{v}$ $[m^3/s]$, which is expressed as:

$$p(\dot{v}) = A\,\dot{v}^2 + B\,\dot{v} + C \tag{5.54}$$

Both the characteristic curve and the control parameter and K_{hx} are inputs to the model.

A large resistance is assumed to prevent backflow at 'producer' substations, being the pressure losses at such substation calculated as:

$$\Delta p = \gamma \left((crl\ C)^2 + 1000 K_{hx}\dot{v}^2 \right) \tag{5.55}$$

Finally, the system of non-linear equations is solved by the Newton-Raphson method within a loop where the user sets the tolerance and the maximum number of iterations.

SpThermo

Once the flow rates are determined, SpThermo calculates the propagation of temperature through the pipes. An energy balance is established for the fluid at each pipe at every time-step (equation 5.57), assuming that the fluid is incompressible, and therefore:

$$\dot{m}_{out} = \dot{m}_{in} \tag{5.56}$$

where $\dot{m}$ [kg/s] are the mass flows entering (in) and leaving (out) the pipe.

$$M\frac{du}{dt} = \frac{m_{in}dh}{dt} - \dot{Q}_{loss} \tag{5.57}$$

where M [kg] is the total mass of the control volume, m_{in} [kg] is the mass that enters (and leaves) the control volume during the calculation time, du [J/kg] is the difference of internal energy of the fluid, dh [J/kg] is the difference of the fluids' enthalpy between the inlet and the outlet, $\dot{Q}_{loss}$ [W] are the losses to the surrounding ground, and Δt [s] is the time-step length. The formula is also based on a fully-mixed control volume.

Considering that the internal (fluid properties) and external (inlet and ground temperatures) conditions do not change over calculation time-step, the equation can be solved with an explicit 1^{st} order backward FDM as in equation 5.58:

$$Mc_p(T' - T_{out}) = m_{in}c_p(T_{in} - T_{out}) - UA\Delta t(T_{loss} - T_g) \tag{5.58}$$

where T_{loss} [°C] is the mean temperature used to simulate the losses to the ground and is calculated using the superposition principle as:

$$T_{loss} - T_g = \frac{(M - m_{in})(T_{out} - T_g)}{M} + \frac{m_{in}(T_{in} - T_g)}{M} \tag{5.59}$$

In the previous equations, c_p [J/kgK] is the fluid's heat capacity, UA [W/K] is the overall heat transfer coefficient through the pipe's wall, and T [°C] represent the temperatures. T_g is the temperature of the surroundings, T_{out} and T_{in} are the outlet and inlet temperatures at the beginning of the time-step, T' is the outlet temperature at the end of the time-step.
Both UA and T_g are inputs to the model. The user can decide whether providing the total UA coefficient, including not only the different layers of the pipe but also the ground, or only the pipe's UA coefficient. The first option implies the use of the undisturbed ground temperature. The second option, however, requires a coupling of the model with a ground model to calculate the new ground temperatures every time-step. The fluid properties instead are fixed internally, assuming water at 50°C.

5.2.2 Modifications in SpHeat block

Both the model itself and its implementation as an `INSEL` block leave some room for improvement. On the one side, some of the assumptions that are internally taken could be externally provided. Meaning, the fluid properties so other liquids rather than water could also be used as thermal carrier or the diameter of ground that should be taken into account in case that the ground is modelled externally with other assumptions. On the other side, the model has two major problems, including the way the matrices X and Y are solved and the way of solving the thermal energy balance, in equation 5.57.

The model does not include any logic to reduce the matrices before using them for the fluid dynamic calculation. Therefore, the processing time rises exponentially with the increase in the number of nodes and edges. For that reason, the model has a maximum number of nodes and edges of 100 each. If an increase of these numbers is required, the incorporation of a matrix reduction algorithm and a deep modification of the code structure must be done.

Finally, the explicit 1^{st} order backward FDM needs small control volumes to provide accurate results. Still, the model as it is coded takes the control volumes equal to the volume of water inside each pipe, no matter the relationship between the length of this one and the volume flow, as long as it is ensured that the inlet volume is lower or equal to the one inside the pipe, namely:

$$AL \geq A\,v\Delta t \tag{5.60}$$

where L [m] is the length of the pipe, A [m^2] is the cross-sectional area, v [m/s] is the linear velocity of the flow and Δt [s] is the time-step.
For those cases where the pipe is long and the volume flow low, the temperature front suffers of artificial diffusion inside the pipe. A careful selection of floating points (the number of divisions of the control volume) along the pipe must be made to avoid this situation. The following sections present an empirical calibration of the model and a methodology to determine the best number of floating points developed using the results of this calibration.

5.3 Empirical calibration of the DHN model

A methodology to determine the best number of floating points to avoid artificial diffusion and delay in the element model has been developed based on the results of an experiment carried out in Vilnius, Lithuania. A second set of measured values has been used, the Girasolstrasse branch to test the methodology resulting from the empirical calibration with the Vilnius experiment. Both datasets are first introduced in this section. Then the methodology is explained, and some conclusions extracted after testing it are presented at the end of the section.

5.3.1 Data sets

The Vilnius experiment

This experiment was carried out by Ciuprinskas and Narbutis in Vilnius, Lithuania, on May 19^{th}-24^{th}, 1997. They tested two types of pipes parallelly arranged between two heat chambers to determine the real heat losses in the pipelines. One of the pipelines was a pre-insulated pipe (from Chamber 1 to Chamber 3), and the other an insulated pipeline within impassable concrete canals (from Chamber 1 to Chamber 2) (Figure 5.5).

They provoked a temperature wave of around 5°C at the supply station of the network and measured the temperatures at both ends of the 470 m length pipes. As said, the experiment was conducted in May, when heat demand is low, and therefore, mass-flow is also very low and almost constant. More details can be found in [49] in Lithuanian (the original document), or in English in [79]. The pre-isolated pipe dataset has been used for the development of the methodology presented in section 5.3.2. It provides temperatures at both sides (Chamber 1 and Chamber 3) of both pipes (supply and return) with a precision of 0.5°C together with the mass flow (precision of 0.2 kg/s) every 10 minutes during 24 hours. No external or ground temperature are provided. The wave has been used to improve the dynamics of the network model while the rest of the day was used to calibrate the thermal transmittance in steady-state conditions. Figure 5.6 shows the wave progression. The wave is provoked at the supply station (Tin Supply) and moves along the supply pipe to arrive at its outlet after around three hours (Tout Supply), losing heat on its way (temperature difference between inlet and outlet temperatures during steady-state conditions) and changing its shape due to

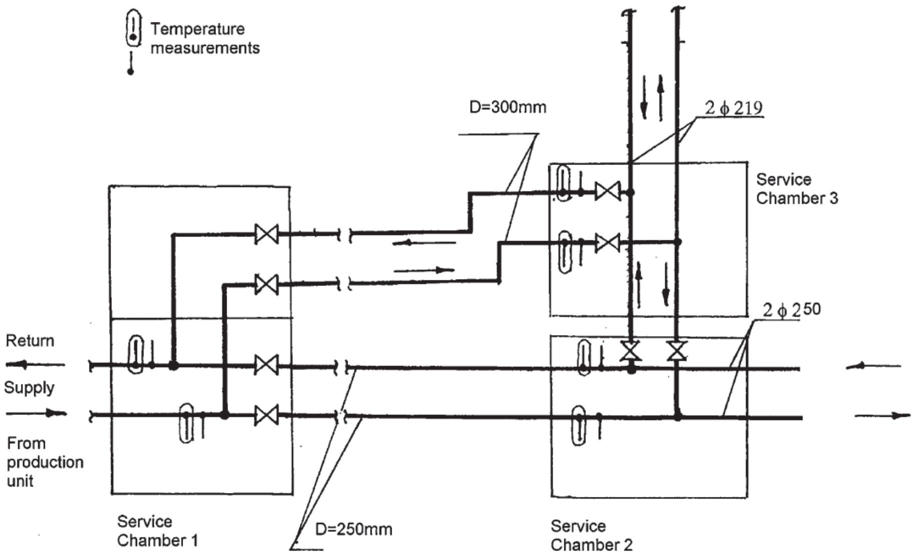

Figure 5.5: Schematic view of experimental site (Source: modified by [79] from [49]).

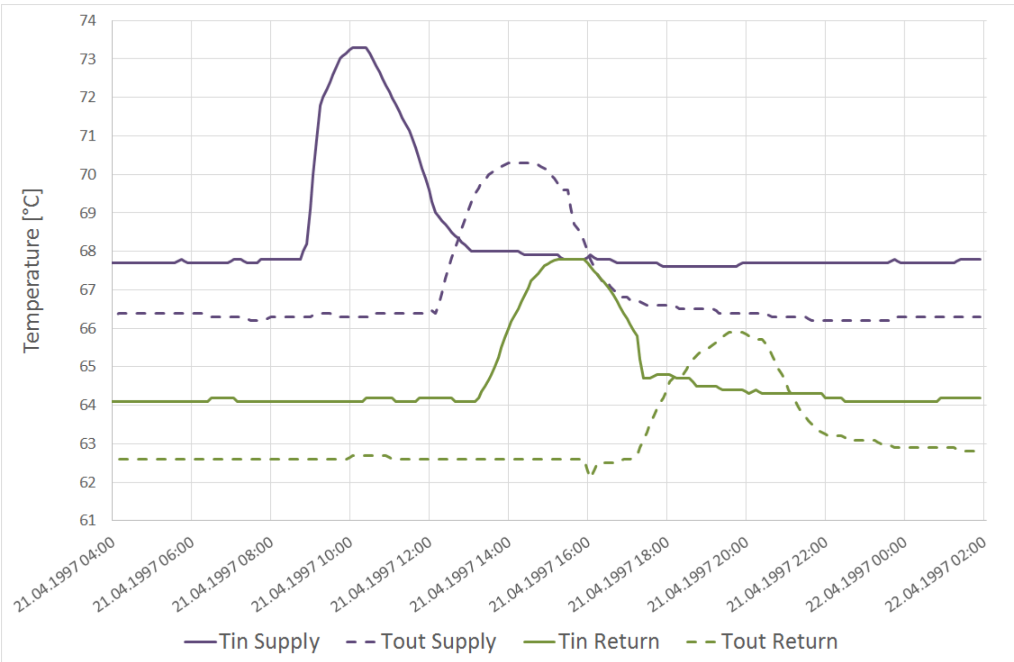

Figure 5.6: Temperatures at inlet and outlet of supply and return pipes (Source: data extracted from [49]).

diffusion. Then, the flow is sent to demand and returns to the supply pipe about one hour later (Tin Return) reaching the end of the return pipe after four hours (Tout Return). Same losses and diffusion are observed in the return pipe. This dataset has already been used by other researchers for comparison and validation of thermal networks models [79, 86].

The Girasolstrasse dataset

TU Wien, Institute for Energy Systems and Thermodynamics, provided the specifications of a branch of the Vienna DHN called Girasolstrasse for the present study. It is composed of 19 substations where one or more consumers are connected (G-A to G-N-2) and one supply substation (S-G) that connects the primary network of Vienna with the Girasolstrasse branch. Figure 5.8 shows the schema of the network.
The dataset holds inlet and outlet temperatures and volume flows at all consumer substations together with the ambient temperature and the temperatures and volume flow of the primary side (Vienna's primary network) at the supply substation registered every 15 minutes during four years (2012-2015). The values at the secondary side (Girasolstrasse branch) of the supply substation are not provided. The precision of this dataset, provided only within the Ci-Nergy project, is not as high in as the previous case. Not only the data is recovered every 15 minutes (for a much higher water velocity), but also the temperatures accuracy is 1°C. Nevertheless, no datasets with such complete information are freely accessible. This was the best available dataset for testing the methodology. The behaviour of the network is similar every day; at around 2:30 a.m. a temperature wave of about 10°C and 2 hours width, is generated and propagated along the complete network. This waves are used to check and calibrate the DHN's control system. As in the previous case, the wave has been used to analyse the dynamics of the network while the quasi-steady-state period was used to calibrate the thermal transmittance to the surroundings. One week in January 2015 has been selected for the study. Figure 5.7 shows the typical temperature profile at the last substation (G-A) during one day.

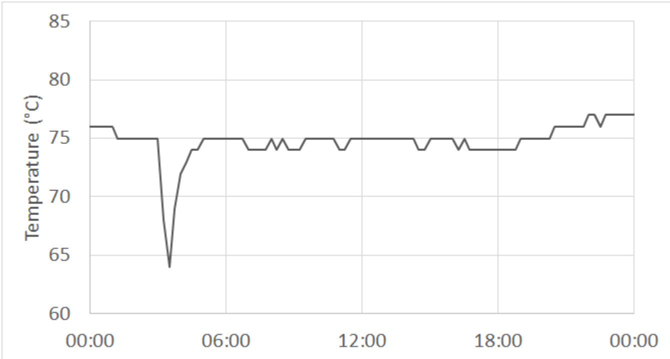

Figure 5.7: Supply temperature profile of one typical day.

5.3.2 Methodology to avoid artificial diffusion and wave delay in element method based models

SpHeat was used to reproduce the propagation of the wave along both pipes of the Vilnius experiment presented in the previous section, supply and return. The temperature waves are normalised to quantify the accuracy of the model, and three indicators are defined: (1) the instant the wave begins, t_s in seconds, (2) the wave width Δt_w also in seconds, and (3) the normalised wave amplitude A_w, dimensionless. The normalised temperature profile $T_{out,adim}$ is defined following the proposal of [79]:

$$T_{out,adim} = \frac{(T_{tr\_out} - T_{st\_out})}{(T_{tr\_max,meas} - T_{st,meas})_{inlet}} \tag{5.61}$$

The same definition is valid for the measured and the calculated temperatures. In the numerator, T_{tr_out} is the transient temperature and T_{st_out} the temperature at steady-state conditions at the outlet of the pipe for both, measured and calculated temperatures. The denominator represents the amplitude of the inlet temperature, which is the measured maximum temperature $T_{tr_max,meas}$ minus the steady-state measured temperature $T_{st,meas}$, both at the inlet. The normalised temperature $T_{out,adim}$ is equal to 1 when the wave peak reaches the pipe outlet if no heat loss or diffusion occur in between, and is equal to 0 during steady-state conditions.

Finally, the wave amplitude is defined as the maximum value of the dimensionless temperature wave. The amplitude and wave width are used to study

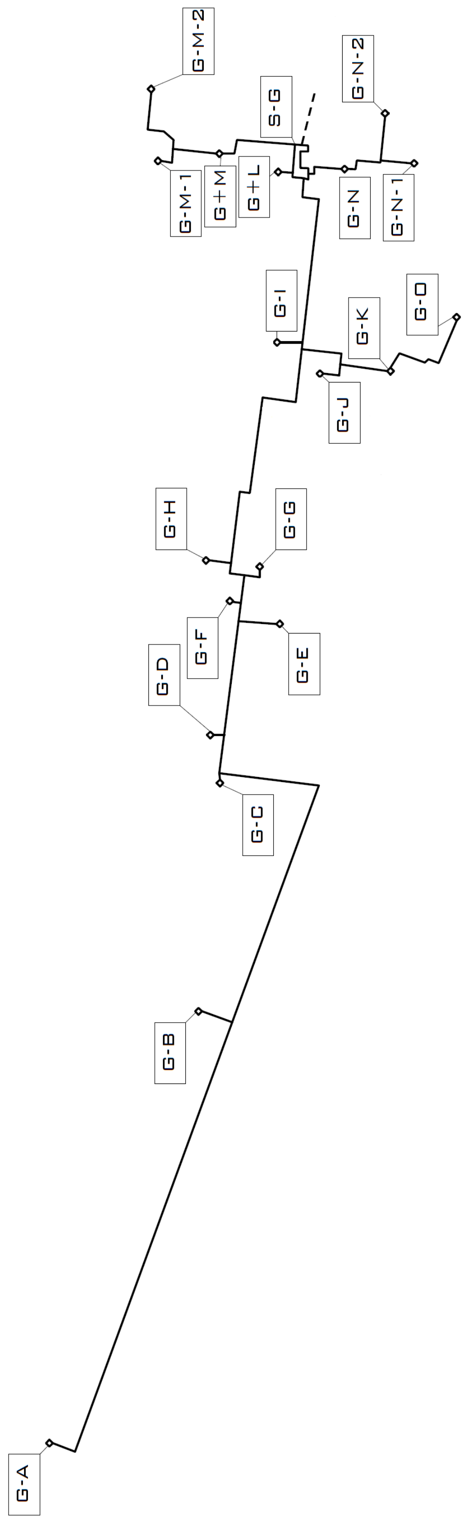

Figure 5.8: Schema of Girasolstrasse heating network.

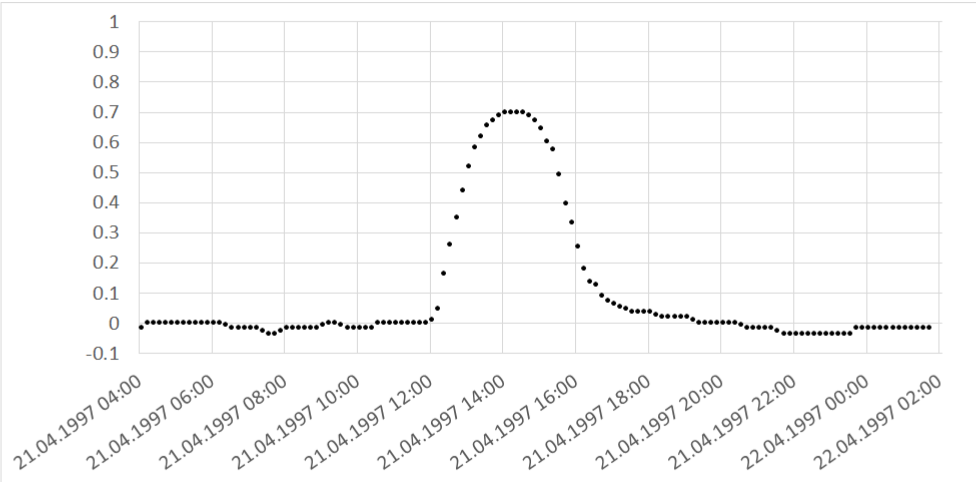

(a) Outlet temperature of the supply pipe of the Vilnius experiment.

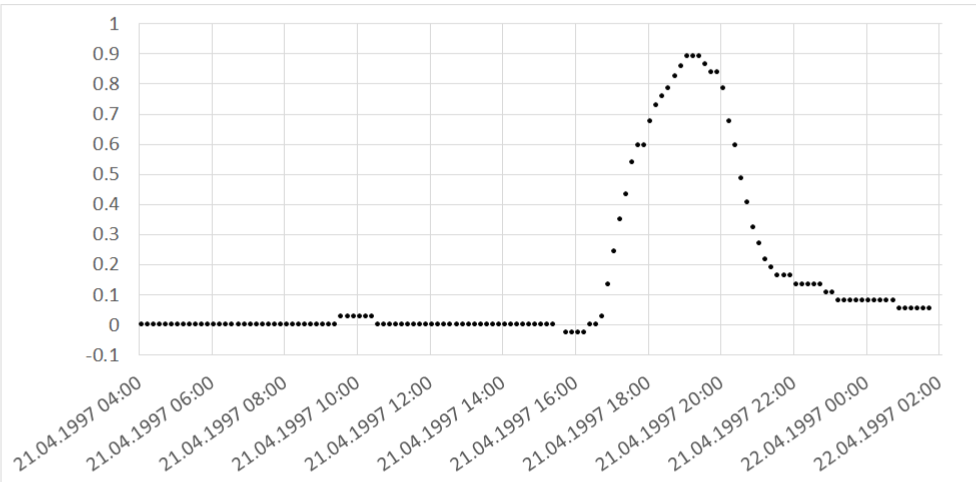

(b) Outlet temperature of the return pipe of the Vilnius experiment.

Figure 5.9: Dimensionless profiles of temperatures in supply and return pipes.

the artificial diffusion while with the time of wave start, the delay is analysed. With these indicators, three errors have been defined, including (1) error in the wave start e_s [%], (2) error in the wave width e_w [%] and (3) error in amplitude e_A [%]. These errors are determined as a function of the CFL number for a given time-step Δt used by the solver. The CFL is a dimensionless number that expresses the ratio between the physical velocity v (velocity of the water stream in each pipe element [m/s]) and the velocity of calculation, i.e. the ratio between the length of each element Δx [m] and the time-step Δt [s] used by the numerical method to update the temperature distribution.

$$CFL = \frac{v\Delta t}{\Delta x} \tag{5.62}$$

The CFL number indicates how fast the temperature information travels on the computational grid. It is considered as the most important parameter for the performance of numerical methods in DHN modelling [157]. In explicit numerical schemes, a necessary condition for stability is $CFL \leq 1$: the time step size must be smaller than the time required for the flow to cross the smallest distance between two adjacent points [56]. The three errors are defined then as:

$$e_s^{\Delta t}(CFL) = \frac{(t_{s,calc}^{\Delta t}(CFL) - t_{s,meas})_{outlet}}{t_{s,meas,outlet} - t_{s,meas,inlet}} \cdot 100\% \tag{5.63}$$

$$e_w^{\Delta t}(CFL) = \frac{\Delta t_{w,calc}^{\Delta t}(CFL) - \Delta t_{w,meas}}{\Delta t_{w,meas}} \cdot 100\% \tag{5.64}$$

$$e_A^{\Delta t}(CFL) = \frac{A_{w,calc}^{\Delta t}(CFL) - A_{w,meas}}{A_{w,meas}} \cdot 100\% \tag{5.65}$$

For the reproduction of the wave using SpHeat, the profile of inlet temperatures and the pump's load factor are given as inputs in two separated simulations, one to the supply and other to the return pipes. The mass flow and outlet temperatures are calculated and compared to the measured values. The pump's load factor is set in such a way that the calculated and measured mass flows match (reproducing exactly the 2.75 kg/s of the experiment), feeding the thermal model with the right hydraulic conditions. Table 5.1 present the parameters and boundary conditions of the simulation.

Due to the relationship between the error indicators and the CFL number, a parametrisation in two directions, time-step and number of floating points,

Parameter	Value
Pipe length, L [m]	470
Internal diameter of the pipe, d_i [mm]	312.7
Total thermal conductivity, including insulation and ground, λ $[W/mK]$	0.587
Temperature of the undisturbed ground, T_∞ [°C]	12.0
Initial temperature at inlet of supply pipe [°C]	67.7
Initial temperature at outlet for supply pipe [°C]	66.3
Initial temperature at inlet for return pipe [°C]	64.1
Initial temperature at outlet for return pipe [°C]	62.6
Mass flow rate (constant) [kg/s]	2.75

Table 5.1: Parameters and boundary conditions of the pre-insulated pipe.

has been done. Nine cases of floating points, ranging from 1 (no discretization) to 100 (maximum allowed by the tool, see section 5.2.2), and three time-step lengths (30 seconds, 1 minute and 5 minutes) have been selected, covering a wide range of CFL numbers from 0.0015 to over 1.

Figure 5.10 shows an example of the temperature profiles measured at pipe outlet in the experiment described in section 5.3.1 (dotted line) and some of those calculated with SpHeat for a Δt of 5 minutes. Values at times between two consecutive loggings were linearly interpolated. Not all results have been plotted for a more transparent exposition. When increasing the number of floating points (from 1 to 41 in the figure), a better match of the three indicators is expected up to a specific value when overshooting may occur [91]. However, it can be observed in figure 5.10 that the return pipe follows this tendency, but in the supply pipe, it seems that the overshooting appears too early. Giraud, L. [86] already discussed this phenomenon, concluding that the flat shape of the peak in the supply line profile may be caused by stratification effects that occurred during the experiment due to the very low velocity of the flow. These effects are not considered within the model, resulting in an overestimation of the peak. Therefore, the wave amplitude of the supply pipe is not considered as an indicator of the model's accuracy.

Figure 5.11 plots the errors in time start and wave width in function of the CFL number for $\Delta t = 30$ seconds. It can be observed how both errors tend to decrease in absolute value when increasing the CFL number until the best value when they start increasing again with what seems to be a logarithmic trend. The errors have been plotted in a logarithmic scale that gave a better view of the best points.

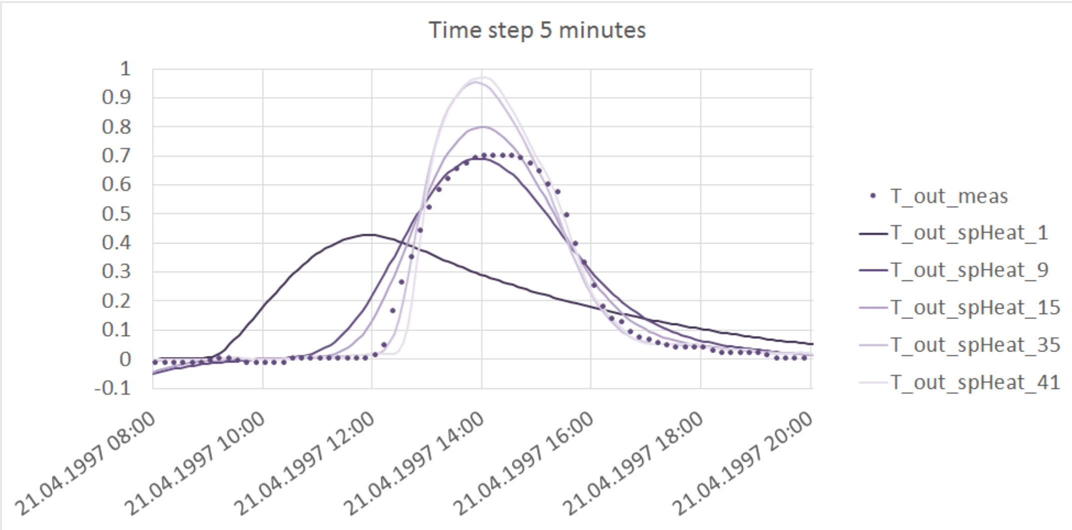

(a) Supply pipe.

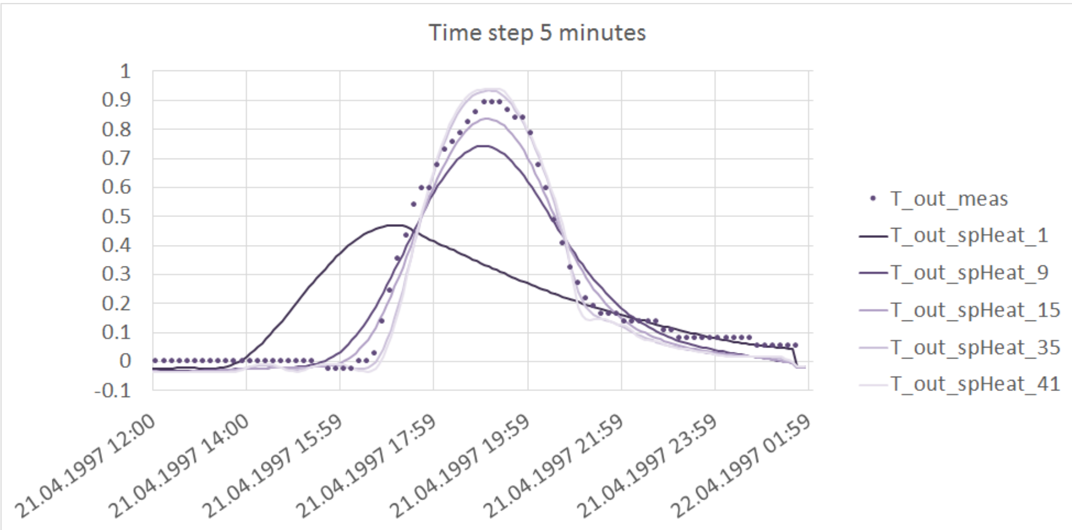

(b) Return pipe.

Figure 5.10: Dimensionless outlet temperature profiles, comparing calculated with measured for $\Delta t = 5$ minutes.

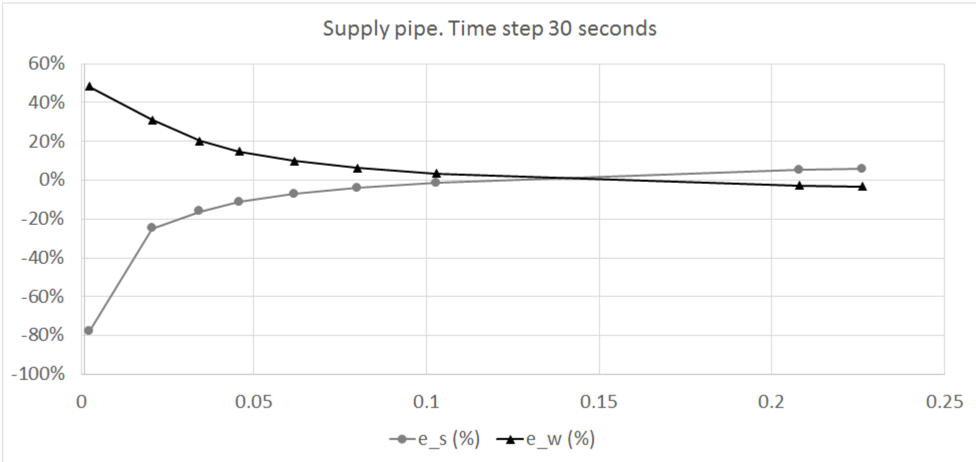

(a) Supply pipe.

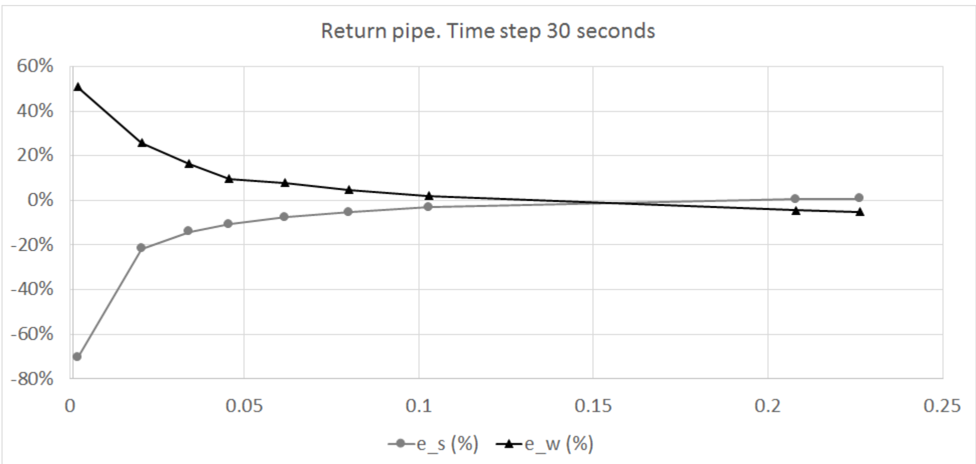

(b) Return pipe.

Figure 5.11: Errors in time start and wave width for 30 seconds time-step.

	$\Delta t = 30$ s	$\Delta t = 60$ s	$\Delta t = 300$ s
CFL min	0.1	0.25	0.55
CFL max	0.2	0.31	0.62

Table 5.2: Optimum range of CFL number for the Vilnius.

It can be observed an almost linear evolution of both, e_s and e_w when plotting them as a function of the CFL number in a logarithmic scale. Figure 5.12 shows that this tendency completely changes when exceeding CFL = 1, increasing the error rapidly. This behaviour was expected due to the stability condition for explicit solutions previously discussed in this section. Figures 5.13 and 5.14 do not reach CFL = 1 because of the upper limit of 100 floating points. For a $\Delta t = 60$ seconds, the highest reachable CFL is 0.45, and 0.23 for $\Delta t = 30$ seconds. When comparing the three sets of figures, the same tendency is observed in all three cases, but the CFL number when the best value is reached increases with the time-step length.

Finally, figure 5.15 present the evolution of the errors in amplitude with the CFL number in a logarithmic scale for the return pipe. Once more, the errors decrease in absolute values when approaching to the best CFL number to afterwards, increase again. One more time, this best value increases with the Δt. The precision of the dataset gives an uncertainty range that is different for each error. The 10 minutes time-step of the data acquisition transfers into a 5% error in the time start and 4% in width. The precision of 0.5°C in temperature means a 10% error in amplitude. Therefore, the values under those errors must also be defined as valid results because the precision in the data acquisition does not allow better accuracy. When combining the results with the uncertainty due to the acquisition precision, a range of best CFL numbers can be defined. Table 5.2 resume the range of CFL numbers by Δt where all errors are inside the limits set by the acquisition uncertainties.

Some conclusions have been extracted from the Vilnius experiment:

- Decreasing the error in the time when the wave starts, t_s, means a better delay forecast.
- Decreasing the errors in wave width, Δt_w, and amplitude, A_w, means less artificial diffusion.
- The three errors decrease in absolute terms when CFL increases, finding the best range after which they start increasing again. This conclusion fits with theoretical studies [157].
- The best ranges can be found at lower CFL when decreasing Δt.

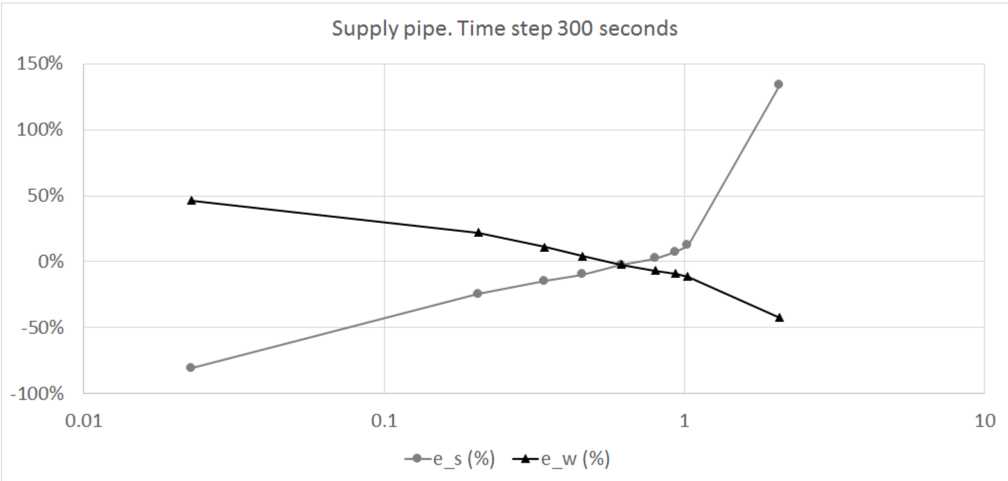

(a) Supply pipe.

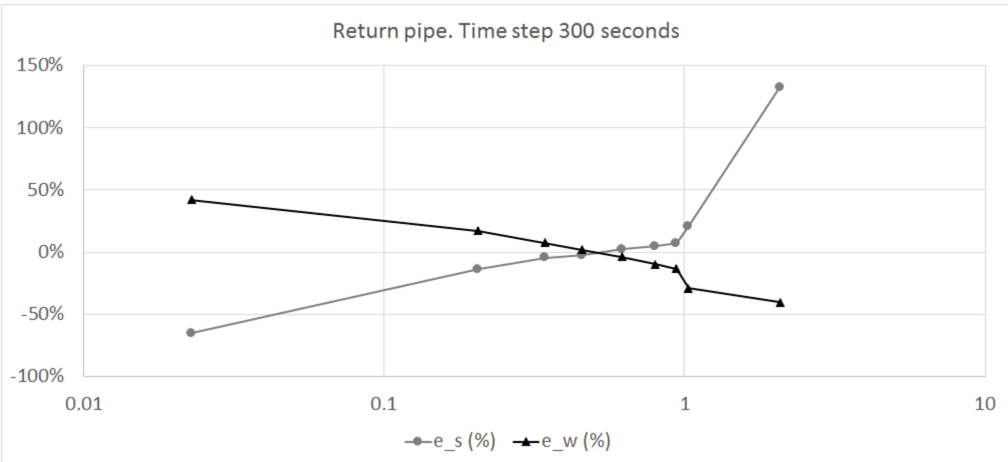

(b) Return pipe.

Figure 5.12: Errors in time start and wave width for 300 seconds time-step in logarithmic scale.

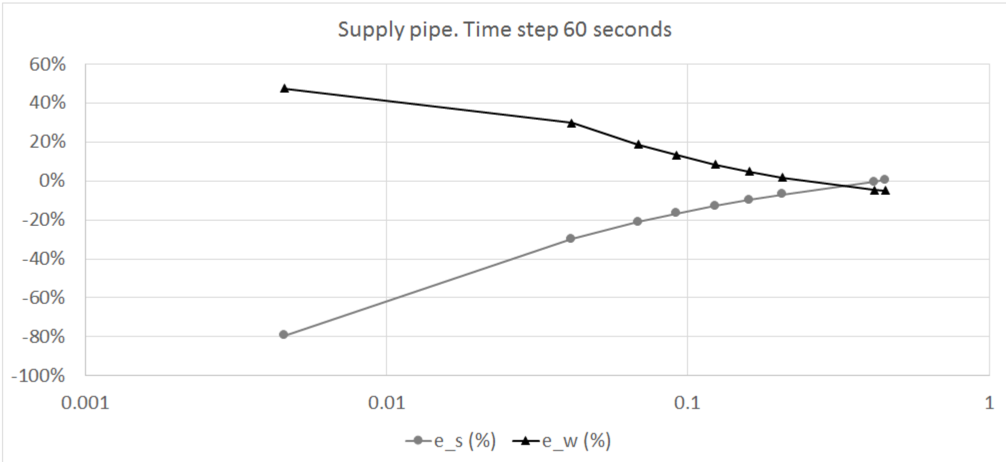

(a) Supply pipe.

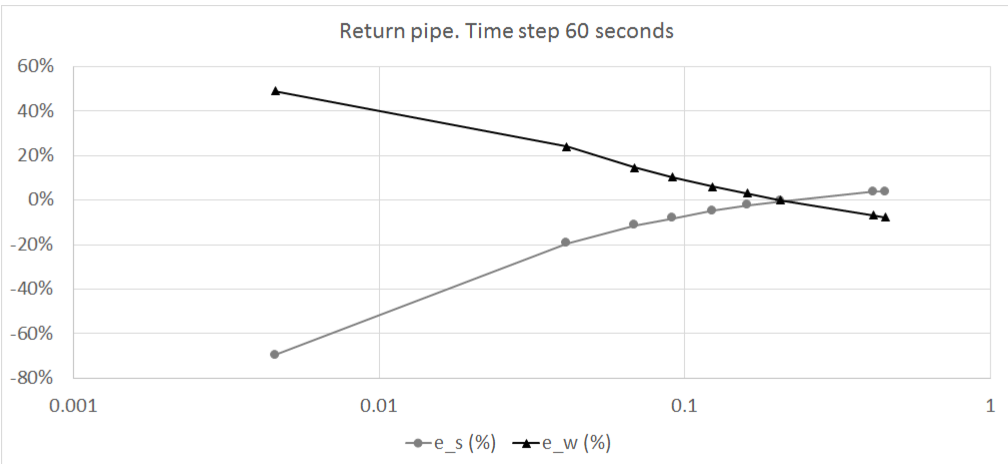

(b) Return pipe.

Figure 5.13: Errors in time start and wave width for 60 seconds time-step in logarithmic scale.

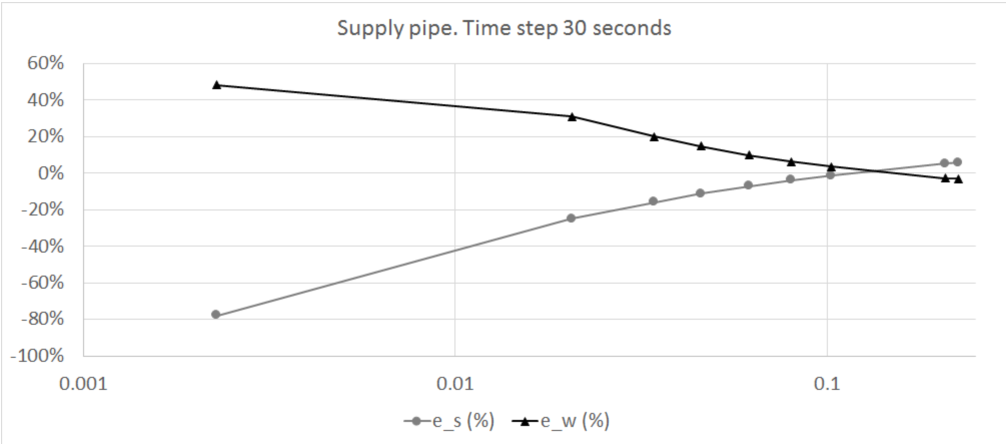

(a) Supply pipe.

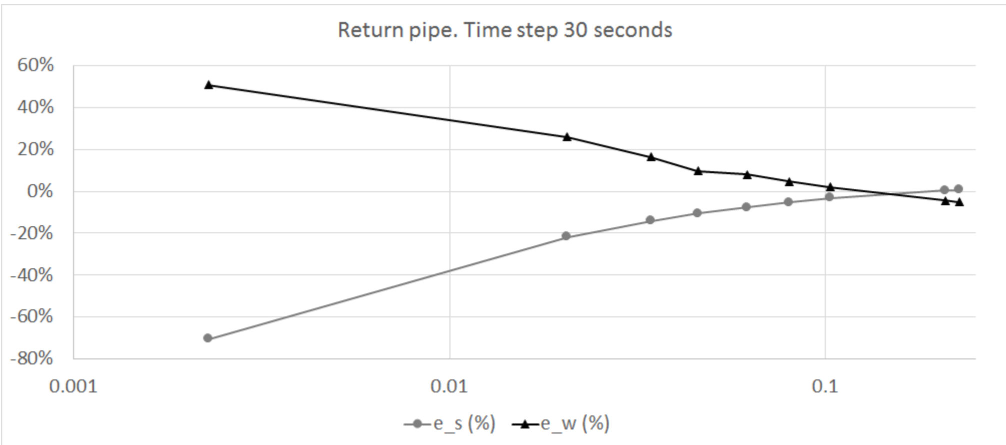

(b) Return pipe.

Figure 5.14: Errors in time start and wave width for 30 seconds time-step in logarithmic scale.

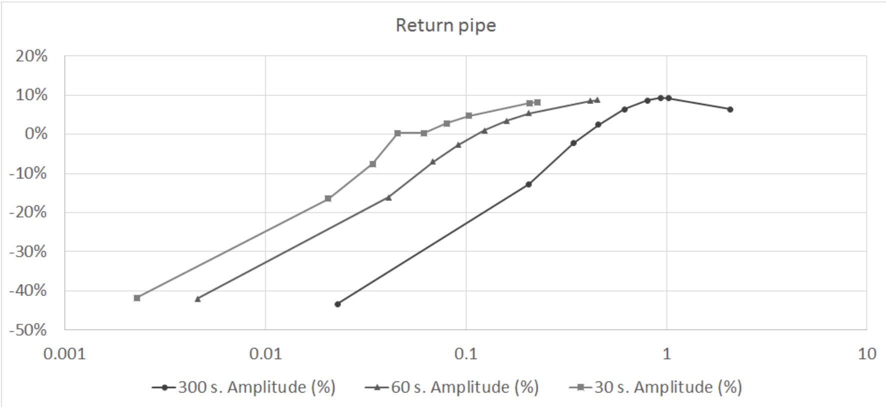

Figure 5.15: Errors in amplitude for the return pipe.

- Due to the logarithmic scale of the error's graphs, those increase much faster when decreasing the CFL number under the lower limit of the best range than when increasing it over the upper limit.

Methodology proposed

Based on the conclusions extracted from the study of the Vilnius network, the following methodology to avoid artificial diffusion and wave delay in DHN models based on the element method is proposed:

1. Find the maximum Δt for which all pipes comply $CFL_i = \frac{\Delta t \dot{v}_{i,max}}{L_i} \leq 1$. Any Δt lower than that would also work, but it slows down the computation.
2. For each pipe, find the minimum number of floating points that keep the CFL number within those limits defined for the calculated Δt (Table 5.2). If this is not possible, the upper limit can be exceeded, but never should be the lower one.

Note. It is impossible to ensure, for a defined Δt, it can be found a number of floating points for each pipe of a DHN that keep all CFL numbers between the limits.
Suppose n is the minimum number of floating points that comply that $CFL(\Delta t)^n \geq CFL(\Delta t)_{min}$: if $CFL(\Delta t)^n > CFL(\Delta t)_{max} \Rightarrow \nexists\ m \in \mathbb{N} \mid m > n\ \&\ CFL(\Delta t)^m = \frac{\dot{v}\Delta t}{L/m} \leq CFL(\Delta t)_{max}$.

	Length [m]	Internal diameter [mm]	Nominal volume flow [m^3/h]
1	63.56	100	9.2
2	34.68	100	6.36
3	20.62	80	1.98
4	21.57	125	11.1
5	28.05	100	5.59
6	14.83	65	2.91
7	104.84	250	88.02
8	30.3	80	12.2
9	28.28	80	9.76
10	32.35	80	9.76
11	153.24	250	63.82
12	21.79	250	60.17
13	13.74	250	57.7
14	9.05	250	47.1
15	65.36	200	44.9
16	25.06	200	23.9
17	198.22	150	22.1
18	269.62	125	17.9

Table 5.3: Pipes' parameters.

where $\dot{v}$ [m/s] is the nominal velocity of the flow through the pipe, and L [m] is its total length. A practical case of the use of this methodology is presented in the following section.

5.3.3 Testing the methodology with the Girasolstrasse network

The Girasolstrasse network is composed by 20 substations, including one supply (S-G) and nineteen consumers (G-A to G-N2) connected by 18 pipes whose lengths and diameters are resumed in Table 5.3 together with the nominal volume flow through each pipe.

The information provided within the dataset was introduced in section 5.3.3. An inlet temperature profile and the pump's load factor are given as inputs.

As the temperatures at the secondary side of the supply substation are not available, the supply temperature has been calculated as the mean inlet temperature between the three closer consumer substations (G-L: 14.83 m, G-M: 63.56 m and G-N: 21.57 m). The north branch of the network (see Figure 5.8) has been chosen to discuss the temperature's recorded values in the dataset.

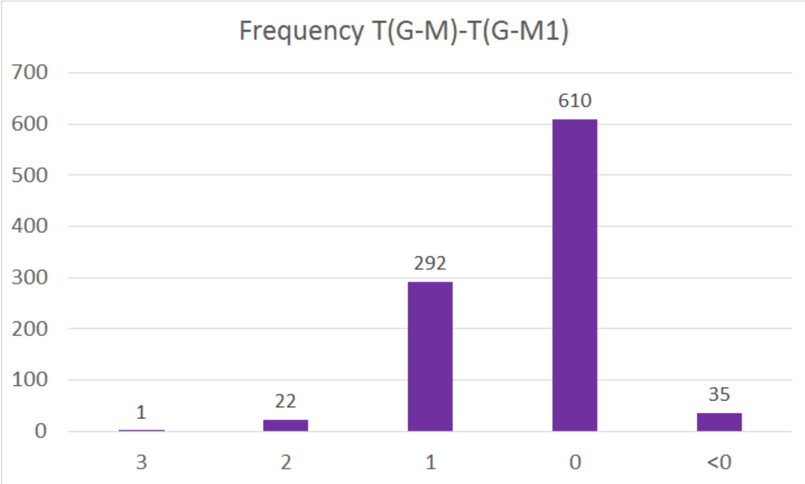

Figure 5.16: Frequency $T_{G-M} - T_{G-M1}$.

Figure 5.16 shows the frequency of the difference between the temperature at the beginning of the north branch (G-M) and one of the extremes (G-M1) equal to certain values. Due to the dataset's accuracy of 1°C, it was expected that the temperature at G-M1 was the same as the temperature at G-M or 1 or 2°C less. The first thing that can be observed is that 3.65% of the time, the difference of temperatures is negative, which means that the temperature at the end of the branch is bigger than at the beginning. That is thermodynamically not possible considering that there is no other supply source that S-G. This unexpected behaviour is also found in the other branches. This fact affects the reliability of the dataset. Nonetheless, considering the lack of better values, this has been used to perform the example.

The pump's load factor is adjusted to fit the measured flow at all substations, ensuring the required inputs to the thermal model. Figure 5.17 shows the calculated volume flow at four selected substations compared to the measured ones, together with the limits of ±10%. The normalised Root Mean Square Error (nRMSE) has been calculated for each of them obtaining satisfactory results presented in Table 5.4.

$$nRMSE = \frac{\sqrt{\overline{(\dot{v}_{calc} - \dot{v}_{meas})^2}}}{\overline{\dot{v}_{meas}}} 100\% \tag{5.66}$$

where $\dot{v}$ [m^3/s] is the volume flow calculated ($calc$) and measured ($meas$).

	G-A	G-H	G-K	G-M2
nRMSE (%)	1.4	4.2	3.6	3.9

Table 5.4: Normalized RMSE of the four selected substations.

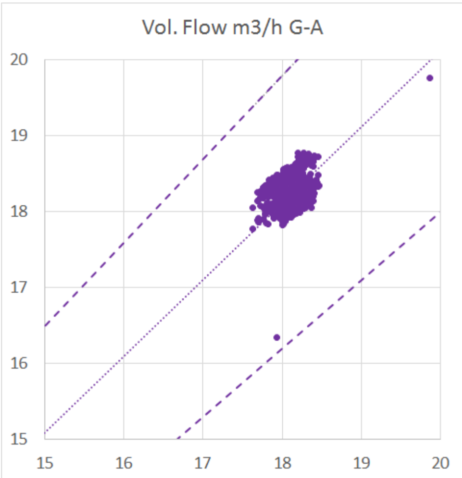

(a) Substation G-A

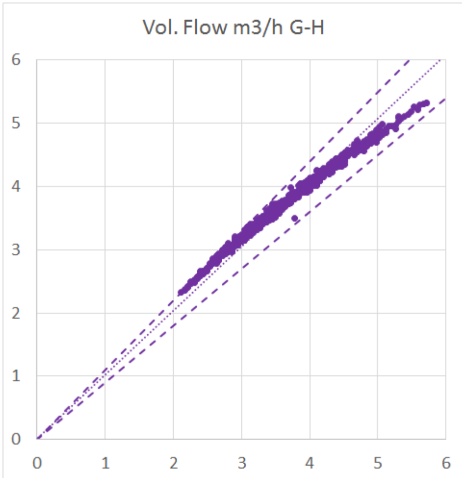

(b) Substation G-H

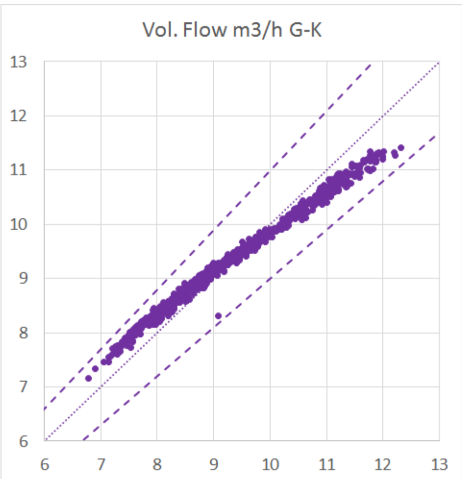

(c) Substation G-K

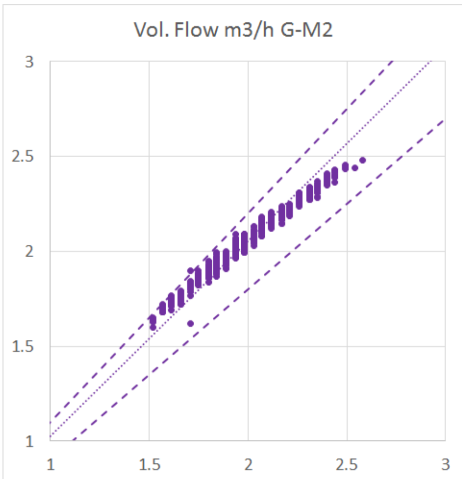

(d) Substation G-M2

Figure 5.17: Calculated (vertical axis) vs Measured (horizontal axis) volume flows [m^3/h] at four substations.

Pipe number	Floating points	CFL number
1	1	0.15
2	1	0.19
3	1	0.16
4	1	0.35
5	1	0.21
6	1	0.49
7	1	0.14
8	1	0.67
9	1	0.73
10	1	0.50
11	2	0.14
12	1	0.47
13	1	0.71
14	1	0.88
15	1	0.18
16	1	0.25
17	2	0.11
18	3	0.14

Table 5.5: Number of floating points of each pipe to keep CFL bigger than 0.1

How these errors affect the thermal model are later discussed in this section. The model of the network have been performed following the two steps defined in 5.3.2:

Step 1. Find the maximum Δt for which all pipes comply CFL < 1

Using the data from Table 5.3, the maximum Δt that ensures all CFL numbers to be under 1 is 39 seconds. A $\Delta t = 30$ seconds has been selected to perform the simulation. According to Table 5.2, the CFL number must be between 0.1 and 0.2.

Step 2. For each pipe, find the minimum number of floating points that keep the CFL number within those limits defined for the calculated Δt

As previously commented, the essential requirement is that the CFL number is higher than the lower limit of the best range, i.e. 0.1. Table 5.5 presents the minimum number of floating points that ensure a CFL number for each pipe bigger than 0.1, together with the corresponding CFL number calculated with the nominal velocity calculated from values in Table 5.3.

In light of the obtained results, it can be ensured that the margins of the errors in the velocity prediction would not affect the temperature simulation substantially. A difference of 10% in the calculation of the velocity means the same 10% in the calculation of the CFL, as this one linearly depends on the first one. Looking at Table 5.5, a decrease of 10% in the CFL numbers keeps the values always over the minimum, and an increase of 10% maintains them still under 1, so there should not be significant changes in the results. The pipes that need discretization are:

11: pipe connecting substations G-I and G-H.
17: pipe connecting substations G-C and G-B.
18: pipe connecting substations G-B and G-A.

The model based on the discretization extracted from Table 5.5 was performed and run for an entire week. The same simulation has also been performed without any discretization to test whether the methodology improves the results or not.

The same process to obtain dimensionless temperatures presented in section 5.3.2 has been followed with the Girasolstrasse data with an additional step that had to be done. The wave has been flipped upside-down, and the steady-state line has been pivoted to obtain a similar shape as in the Vilnius experiment, resulting in:

$$T_{out,adim} = \frac{(T^*_{st\_out} - T_{tr\_out})}{(T^*_{st,meas} - T_{tr\_min,meas})_{inlet}} \tag{5.67}$$

where $T^*_{st\_out}$ and $(T^*_{st,meas})_{inlet}$ are the tendency line of the steady-state part of the outlet and inlet temperature profiles, respectively (see Figure 5.18).

Figure 5.19 presents the resulting profile of one day at substation G-A as an example. The mean values of the errors for the seven days are presented in Table 5.6, comparing both cases with and without discretization of the three branches that require it.

On the one hand, it can be observed that the errors on substations G-K and G-M2 do not change, which was expected as there was no need of discretization of any pipe before them. On the other hand, the simulation results at substation G-H improve a bit with the discretization but, where the improvement is more evident at the last substation, G-A.

The low resolution of the dataset and the problems found in temperatures make it hard to extract conclusion in absolute values from the test. Still,

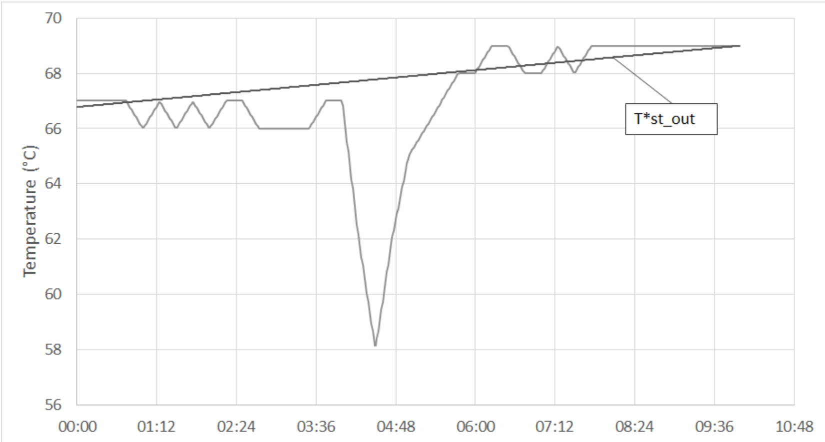

Figure 5.18: Temperature profile and tendency line in steady-state conditions.

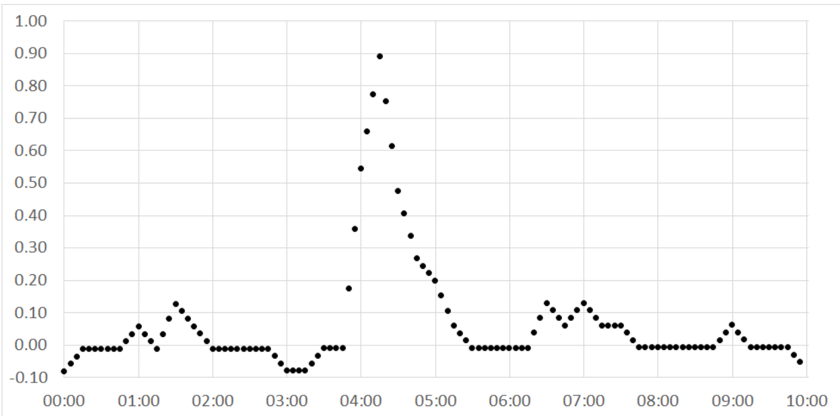

Figure 5.19: Inlet dimensionless temperature in the last substation (G-A) of the Girasolstrasse network.

	Not discretized				Discretized			
%	G-A	G-H	G-K	G-M2	G-A	G-H	G-K	G-M2
$\bar{e}_s$	10	4	10	4	7	3	10	4
$\bar{e}_w$	20	10	7	9	12	10	7	9
$\bar{e}_A$	43	29	20	23	25	22	20	23

Table 5.6: Compared results between discretized and no-discretized models.

a relative improvement was obtained when applying the methodology. Nevertheless, more datasets with better resolution are needed to validate the methodology, checking the limits of the best ranges of CFL and searching if a relationship exists, between the best range and the Δt.

5.4 Conclusions of District Heating Network and Solar System Models

This chapter presented the physical description of the elements that conform the supply solar system as well as the DHN. Furthermore, a methodology to calibrate DHN models, avoiding artificial diffusion and wave delay, have been developed and proved in a real DHN in Vienna. The experiment showed a significant improvement in the results when following the developed methodology, especially in long pipes, reducing errors by up to 60%. This methodology ensures the capability of the model to capture the dynamics of the system when it is connected to very intermittent renewable sources.

Chapter 6

Application 1. Dynamic simulation of heating demand at block scale

Two important aspects are addressed in this chapter. First, the developed workflow is presented, starting from the 3D data model and ending in the energy 'consumption' results. This part gives an overview of the modular tool developed, explaining step by step, the workflow used to calculate the thermal demand of a neighbourhood. It also shows the adaptability of the tool to the variety of a city's building stock, including residential, industrial buildings, offices, etc. The demand calculation is done for two different levels of detail of the geometrical input data. The differences in the results of these two levels are also analysed in the last section. And, the adaptability of the tool to different levels of detail of the input data is proved.

6.1 Description of the case study

Stöckach is a neighbourhood placed in Stuttgart, Germany. It used to be an industrialised area and nowadays it is composed of buildings with different usages that go from single-family houses to offices or industrial buildings. A DHN supplies almost 75% of the heating demand of the neighbourhood. This demand is mainly produced in the industrial buildings. The rest is covered almost at 50% between natural gas and gas-oil boilers, with only a few electrical heaters. In order to illustrate the functioning of the developed tool,

Figure 6.1: Stöckach neighbourhood marked in green.

a study to figure out the convenience of substituting the installed conditioning systems by a decentralised heating system was carried out. The new system is composed of air-water HP powered by PV panels distributed on roofs and supported by the grid if necessary. Figure 6.1 shows, in green, the neighbourhood area. The footprint of the buildings are also included. Those in yellow represent the ones connected to the network, while those that have any other heating devices are shown in purple. The red lines represent the main pipes of the heating network. The black perimeter groups two blocks that have been selected to carry out this study, where no building is connected to the network.

6.2 Demand calculation

6.2.1 Input data

Only one input, the list of building IDs, that is extracted from the gml file, is needed to run the simulation.

The gml file of the case under study contains a total of 166 buildings, 72 of those belong to the target blocks. The other 94 form the surroundings needed to simulate the short-wave radiation exchange. Two levels of detail of the 3D data have been compared (in section 6.4), LoD1 and LoD2. Figure

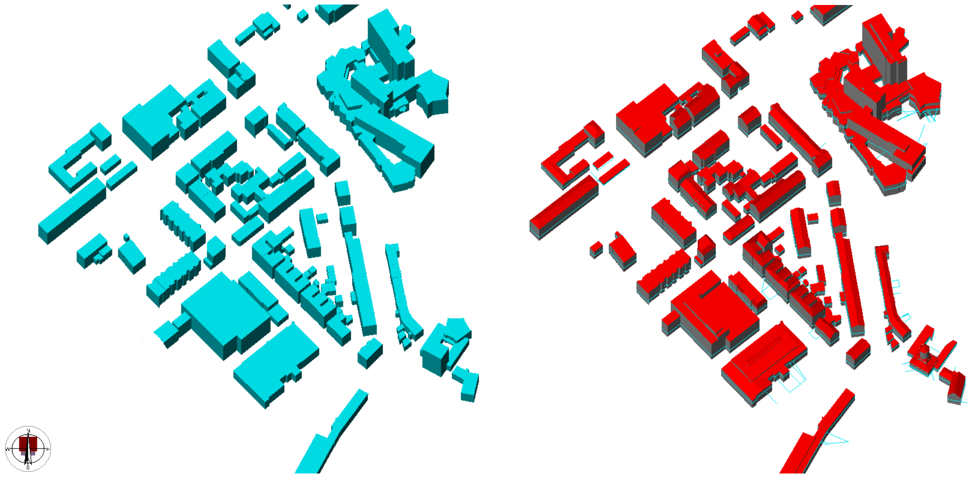

(a) LoD1. (b) LoD2.

Figure 6.2: 3D representation of the buildings of the area under study at two levels of detail.

6.2 shows the 3D representation of the area in both levels. On the left, the LoD1 is presented in light blue, which is the typical representation used by CityGML. On the right, the LoD2 model has the outer walls coloured in grey while the roofs are red and in light blue intersection with the terrain.

Together with the 3D model and the location, the gml file also includes two indispensable attributes, including usage and year of construction. Tables 6.1 and 6.2 summarise the attributes of the 72 target buildings. Figure 6.3 shows their distribution in the blocks.

Usage	Number
Residential	27
Office & administration	1
Industry	2
Mixed usage	15
Retail	2
Hall	2
Non-heated	23

Table 6.1: Number of buildings by usage.

Period of construction	Number
1949-1957	29
1958-1968	18
1969-1983	10
1984-1994	8
1995-2001	2
2002-2013	2
After 2014	3

Table 6.2: Number of buildings by period of construction.

This information is completed with a list of settings from those offered by the tool (for more details, see section 3.1) that define the source of the rest of the required data:

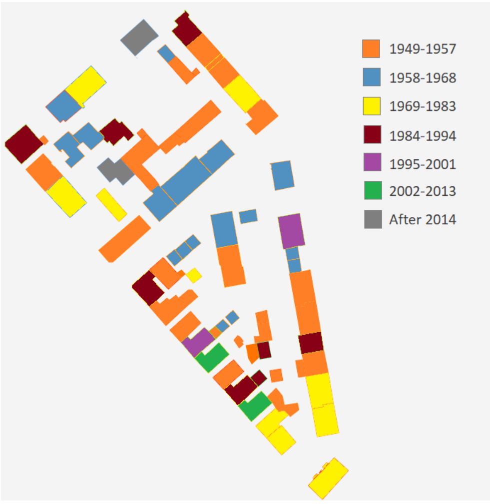

(a) Year of construction.

(b) Usage.

Figure 6.3: Distribution of attributes in the area.

1. Weather data. The TMY of Stuttgart was used. Figure 6.4 presents a summary of the weather with monthly resolution. Stuttgart has a slightly continental weather with comfortable summers and cold, but not freezing and windy winters, and is partly cloudy year-round.

2. Construction data. The *Construction library* containing the information extracted from the German standard *Deutsche Gebaeudetypologie, Institut Wohnen und Umwelt*[a] 2011 [105] was used. It is accessed by building type and year of construction. The building type is derived from the geometry of the building as it was explained in section 3.2.

3. Human behaviour and internal loads data. The *German Usage Library*, based on the standards *DIN 18599-10* [65] and *VDI 3807-2* [203], was chosen. This library is accessed by usage.

6.2.2 Workflow steps

Once the input and the settings are selected, the workflow runs following the schema presented in 6.5.

First, all buildings selected from the gml file are mapped to the corresponding input file for `SRA` (see section 2.2) declaring which of all are the target of cal-

[a]German Building Typologies, Institute for Housing and Environment

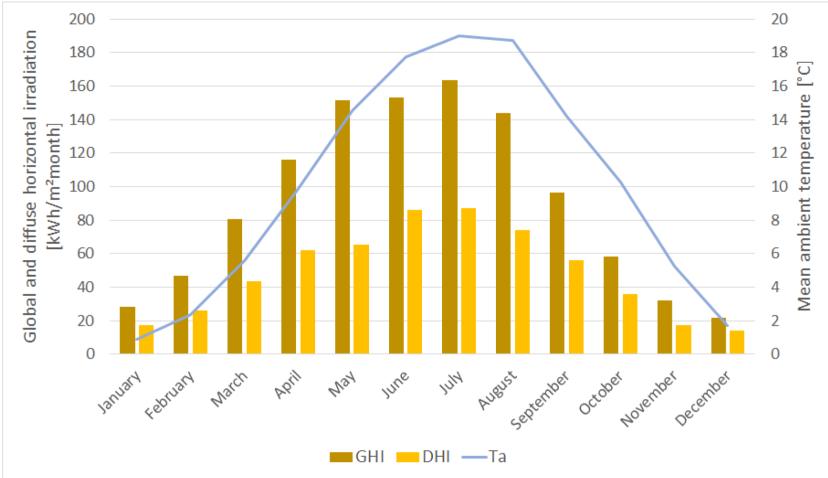

Figure 6.4: Monthly meteorological data of Stuttgart from the TMY (Source: METEONORM).

culation. Also, with the coordinates, the corresponding TMY file is selected to extract the direct normal and diffuse horizontal irradiance, also needed as inputs to `SRA`. Then, the tool is called obtaining the hourly irradiance on every wall and roof of the buildings under study. This information is used to calculate the heating demand as well as the PV production. From the TMY file, also the ambient temperature is extracted to, using the *Weather preprocessor*, calculate sky and ground temperatures. Once this is done, the following process starts for each building of the list. The process can be done in a loop or in parallel using different terminals thanks to the `Ci-NERGY` platform (see section 2.2).

1. Creation of weather file. The three temperatures, together with the irradiation on external surfaces, are written in a file. The insel model later uses this file during the simulation.

2. Creation of the INSEL file. The geometrical information is mapped from the gml file to the *Geometrical preprocessor* to define the type of building. With this parameter and the year of construction, the *Construction Library* is accessed. Finally, the geometrical and construction information is used to write the INSEL file, which is the main file used by the `INSEL` engine. It contains the definition of the building and the paths to read all files created during the process.

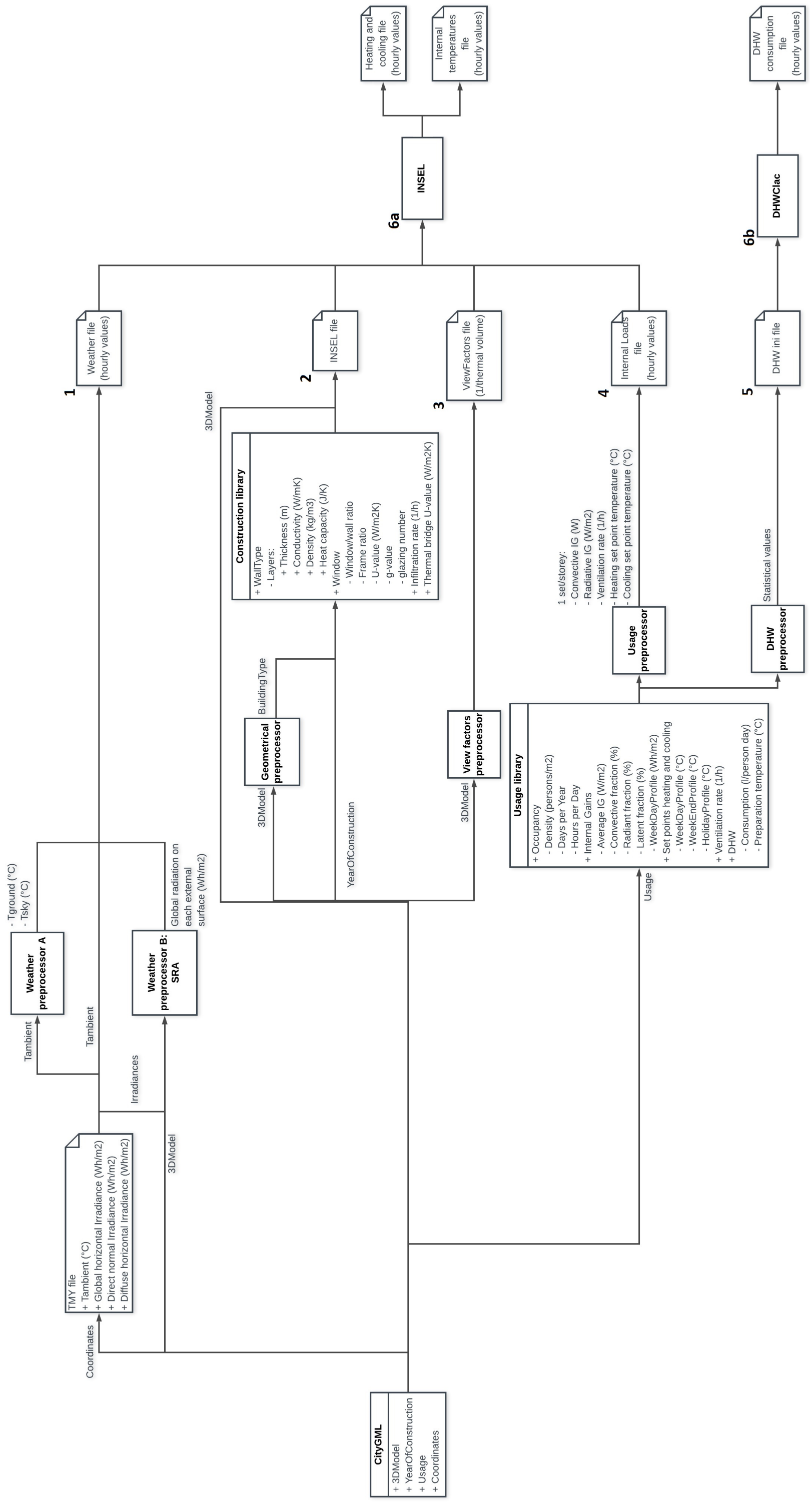

Figure 6.5: Workflow diagram.

3. Creation of the view factors files. Again with the geometrical information, the view factors of each thermal zone (one per storey) are calculated and then are written in separate ViewFactors files.

4. Creation of internal gains and setpoints file. The *Usage library* is called to extract the information needed according to the usage of the building. With this information, the InternalGains file is created.

5. Creation of the DHWCalc.ini file. The information related to the DHW consumption provided with the *Usage preprocessor* is used to generate the input file for `DHWCalc`.

6. Simulations. Finally, first `INSEL` is called, and two output files are generated. The ResulTemp file, containing the hourly distribution of temperatures over the year inside each defined thermal zone, and the ResulDem file, containing the hourly heating and cooling demands over the year again for each thermal zone. And secondly, `DHWCalc` is called to obtain the DHWout file with the hourly heat demand for DHW preparation for each defined thermal zone.

This whole process for all buildings is then repeated twice, once per level of detail. Figure 6.6 shows the comparison between the total monthly heating demand in both cases. At first glance, the demand in winter seems to be underestimated when modelled in LoD1 while in warmer seasons is overestimated. That is due to differences in solar penetration and window ratios between the two model's LoDs. A more detailed analysis is presented in section 6.4. After calculating it, the demand is used to analyse the energy 'consumption' of the correspondent supply system.

6.3 Supply system

To illustrate this second part of the workflow (steps 7 to 9), a supply system composed by decentralised sets of an air-water HP and a PV field have been selected as an example. Only those buildings with thermal demand have a supply system; thus, the roofs of those buildings without demand are not used to generate any extra PV electricity.
Two different prices are established in Germany for the electricity sold to the grid (12.5 cents/kWh), and that bought from the grid (26 cents/kWh). An economic analysis could be done to define whether it is economically interesting to include electrical storage in the system. Nevertheless, energetically

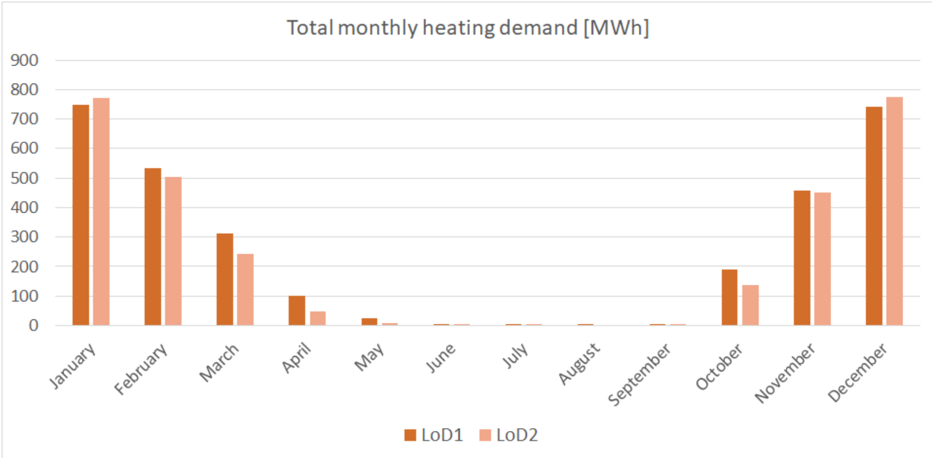

Figure 6.6: Comparison of the monthly heating demand [MWh] for two levels of detail.

is better to not having storage and therefore, avoiding the losses related to it (and the big environmental impact of the production and disposal). Besides, the economical analysis is out of the scope of this thesis. Thus, no electrical storage is assigned to the PV panels, assuming that the excess of electricity generated can be sent to the grid.

7. PV generation on roofs. Using the output of `SRA` on roofs (see Figure 6.7), the electricity generated hourly at each roof is calculated as:

$$P_{PV} = \sum_{i=1}^{roofs} (I_i \; A_i) \; C_{CON} \; C_{PROT} \; C_{GCR} \; \eta_{PV} \tag{6.1}$$

where I_i [W/m^2] is the hourly irradiance on roof i, A_i [m^2] is the area of the corresponding roof, and η_{PV} [-] is the efficiency of the PV system that includes the modules efficiency (assumed for the study 0.15) and the system performance ratio (0.85). Finally, the roof area reduction factors used are (see Solar System dimensioning in section 3.3):

- *Construction restrictions*: $C_{CON} = 0.8$ for flat roofs and $C_{CON} = 0.9$ for pitched roofs.

- *Protected buildings*: There are not protected buildings in the blocks, so $C_{PROT} = 1$.

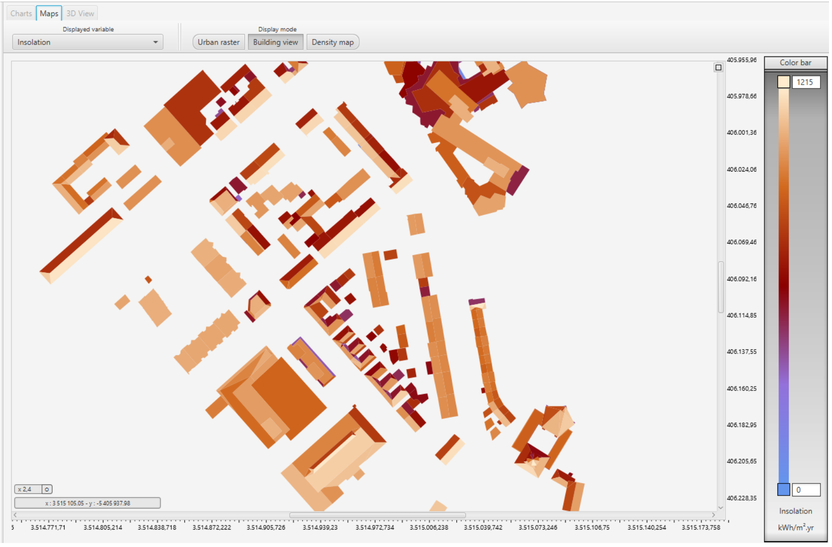

Figure 6.7: Yearly solar irradiance on roofs [kWh/m^2].

- *Separation of panels*: $C_{GCR} = 0.46$ for flat roofs and $C_{GCR} = 0.9$ for pitched roofs. This factor includes the reduction due to the service area.

8. Air-water heat pumps dimensioning. The dimensioning described in section 3.3 is followed. This dimensioning ensures a demand coverage by the HP bigger than 99.5% in all buildings.

9. Calculation of heat pumps consumption and contribution of PV. The output power (P_{HPout} [W]) is calculated at each hour as:

$$\text{If } P_{dem} < P_{HPnom} \;\Rightarrow\; P_{HPout} = P_{dem} \tag{6.2}$$

$$\text{Else} \;\Rightarrow\; P_{HPout} = P_{HPnom} \tag{6.3}$$

And, the required electricity (P_{HPelec} [W]) as:

$$P_{HPelec} = \frac{P_{HPout}}{COP} \tag{6.4}$$

where the COP is obtained as it was described in section 3.3.

Figure 6.8 shows the yearly electricity demand covered by both sources and the electricity fed into the grid, clustering the buildings by usage. All buildings reproduce the same behaviour, covering between 3% and a maximum of

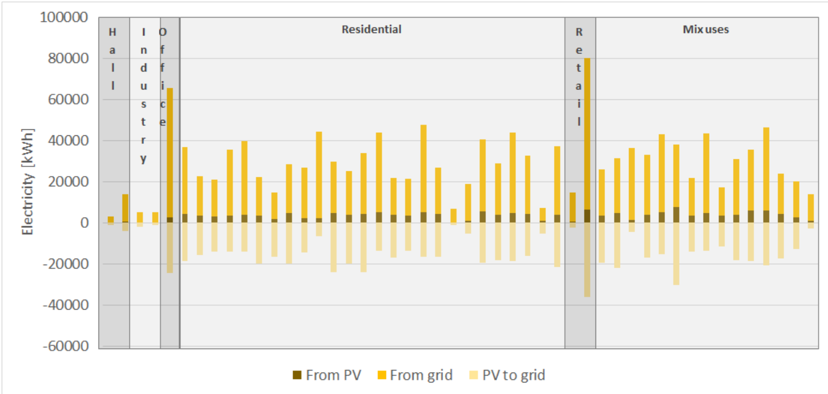

Figure 6.8: Yearly electricity use [kWh].

16.7% of the electricity demanded by the HP with the PV system (Figure 6.9). That is due to the mismatch between demand and supply not only during the day, but mainly over the year. An example is shown in Figure 6.11, where the monthly distribution is presented. It is clear how the mismatch between demand (mainly in winter) and supply (in summer) makes the PV production not directly usable by the system. The same behaviour occurs during a single day, when the bigger supply happens during the lowest demands (central hours of the day). That can be seen in Figure 6.13 (one week in winter) and Figure 6.14 (one week in summer) for three different usages (Figure 6.10 show the selected buildings: building A in dark blue, building B in red and building C in orange). If the grid could be considered a big electrical storage, a net balance between what is pumped in the grid and what is extracted could be done, increasing those percentages tremendously (Figure 6.12). Although this consideration is completely unreal, it is a way to somehow account on that extra renewable electricity that the small system contributes to the total electrical consumption.

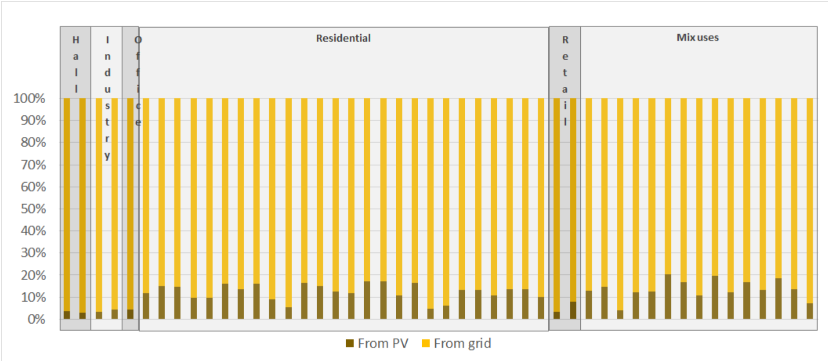

Figure 6.9: Percentage of annual electricity demand covered by PV and grid.

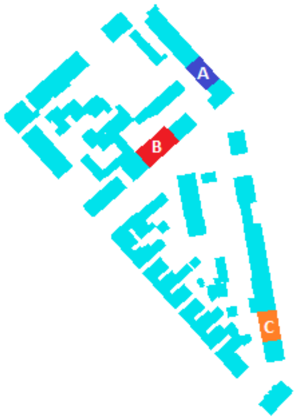

Figure 6.10: Selected buildings.

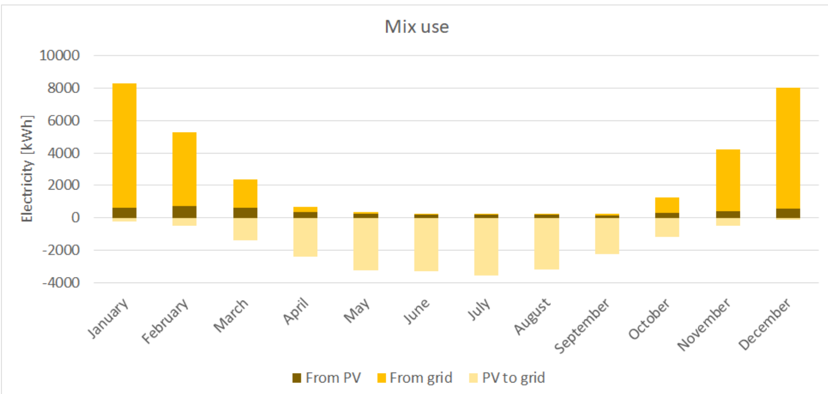

Figure 6.11: Monthly electricity use of one example building [kWh].

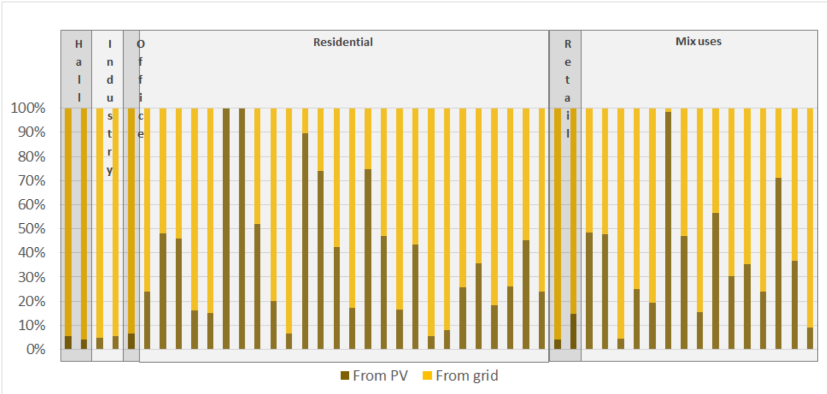

Figure 6.12: Percentage of annual electricity demand covered by PV and net grid.

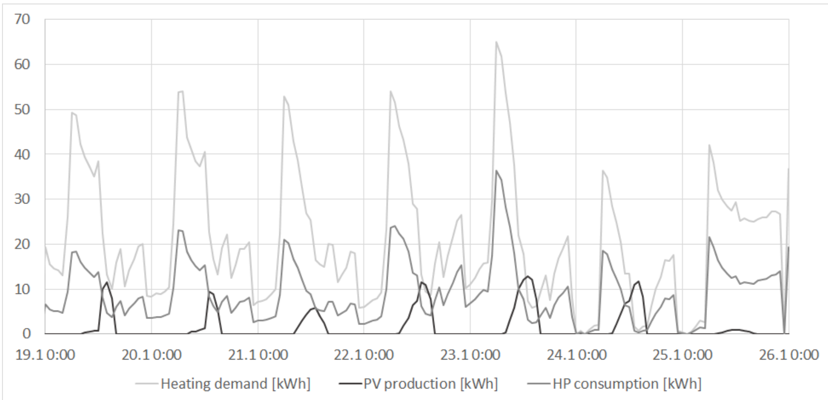

(a) Buildign A: Mixed, residential-office and administration.

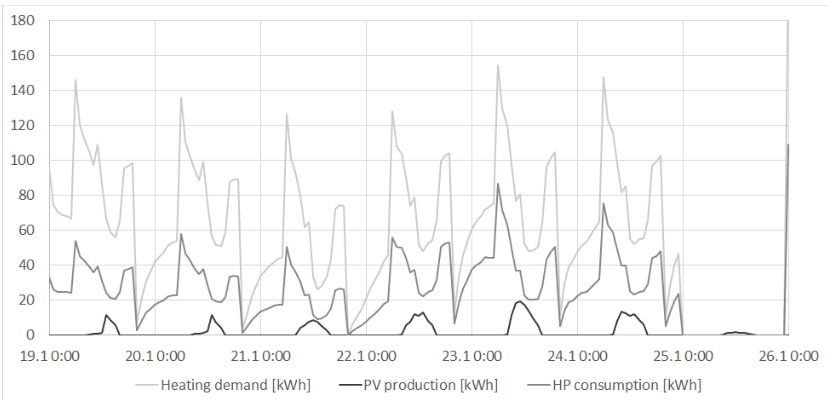

(b) Building B: Retail.

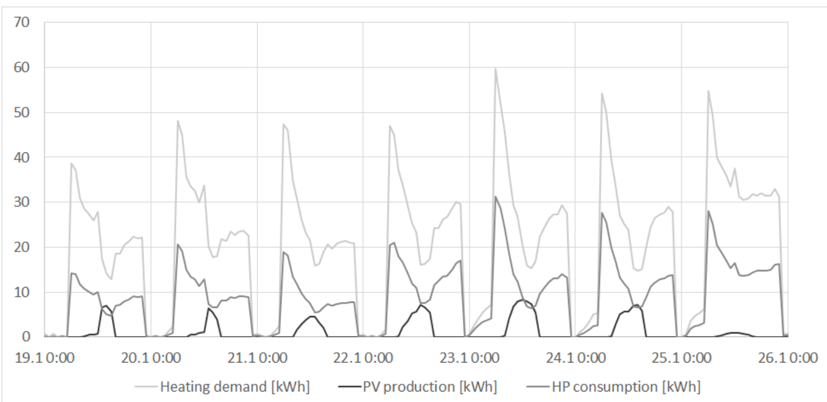

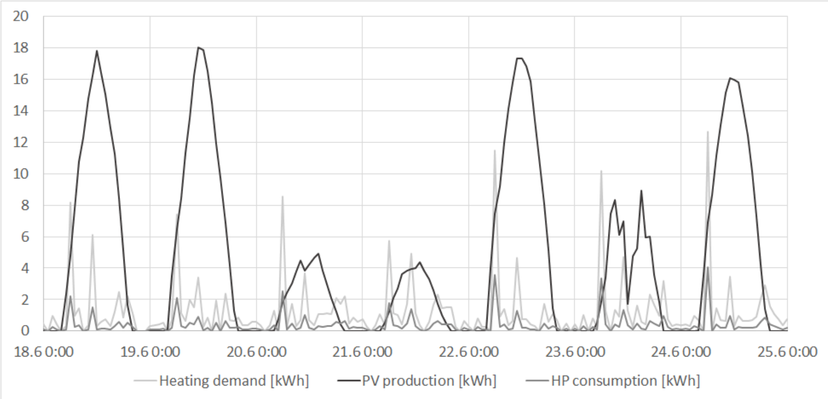

(a) Building A: Mixed, residential-office and administration.

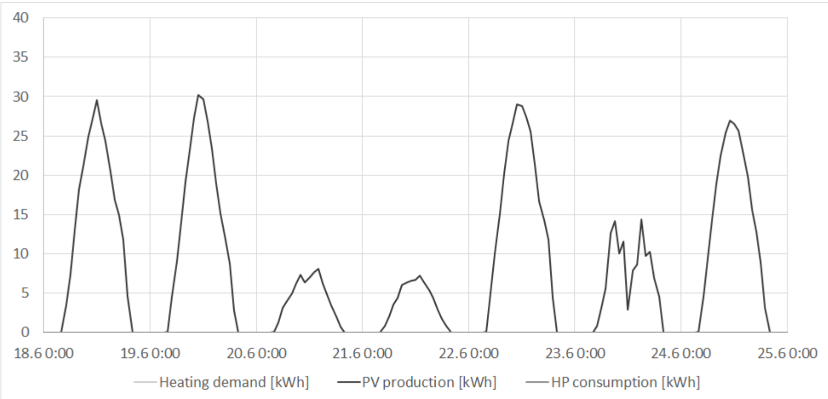

(b) Building B: Retail.

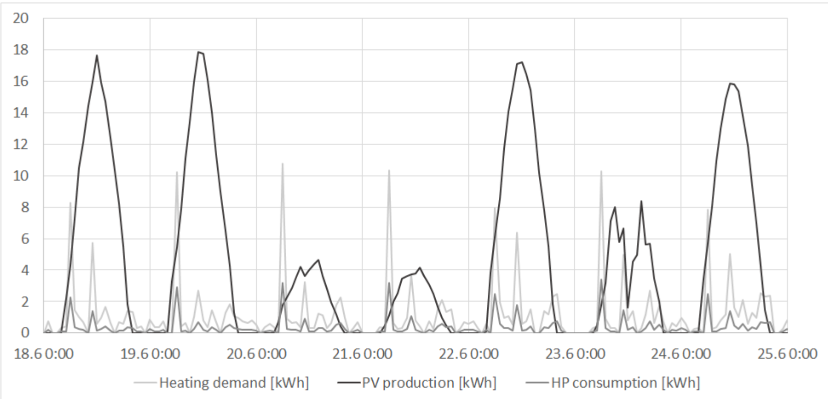

(c) Building C: Residential.

Figure 6.14: Behaviour of the system during one week in June.

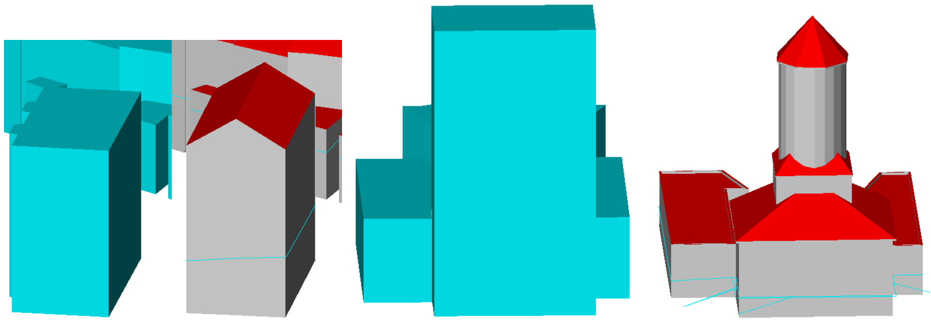

(a) LoD1 to roof eave. (b) LoD1 to roof ridge.

Figure 6.15: Definitions of LoD1.

6.4 Comparison between LoD1 and LoD2

In this section, an analysis of the results obtained during heat demand calculation in a group of buildings modelled in two different levels of detail of the 3D geometry is performed. Figure 6.2 shows the 3D representation of both levels of detail (LoD) again. The LoD1 model, as can be observed in the figure, is a vertical extrusion of the building's footprint to a defined height. This height depends on the modeller's criteria. It is usually defined to either the eave or the ridge of the roof, but also something in between. In the case of unheated roofs, isolated at ceiling level, the considered height should be, from a thermal perspective, up to the eave. While if heated, this should more correctly be approximated to the mid-height between the two (eave and ridge). This information is, however, very often unknown at the stage of the 3D model construction, so it is risky to assume that the modeller considered this concept. Figure 6.15 shows two buildings extracted from the case study that present both cases. On the left, a building modelled in LoD1 is defined to the eave height, while it is to the ridge height on the right. Before analysing the complete set, the results of some buildings have been extracted from the comparison exercise. That is due to some errors in their data models which were easy to detect (the buildings were simulated, but their results could not be compared). For example, building in Figure 6.16 was not represented in LoD1, so it could not be compared. That one in Figure 6.17 was modelled much taller than it should. It seems that the modeller has used the same height as the one of the adjacent building. That produces an overestimation of the thermal demand in LoD1.

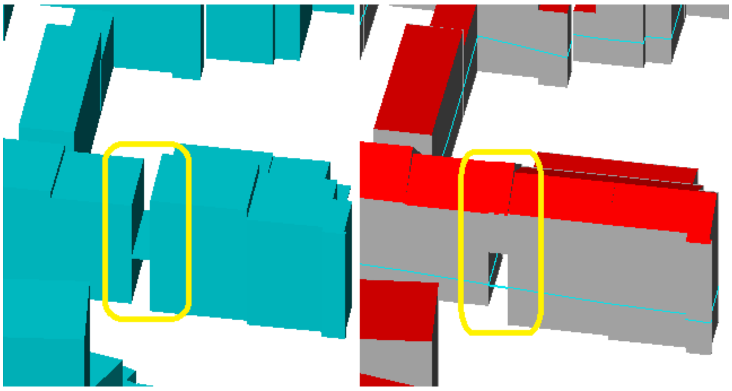

Figure 6.16: Error 1. A building missing in the LoD1 data model.

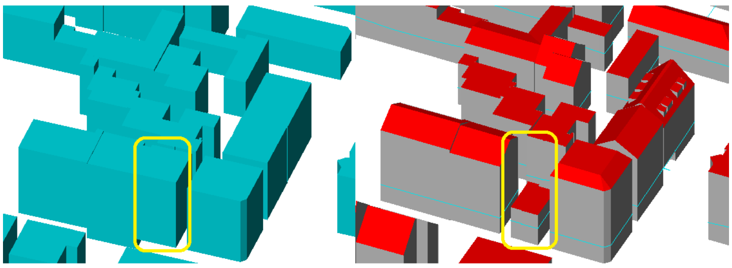

Figure 6.17: Error 2. Building much bigger in LoD1 model than in LoD2 model.

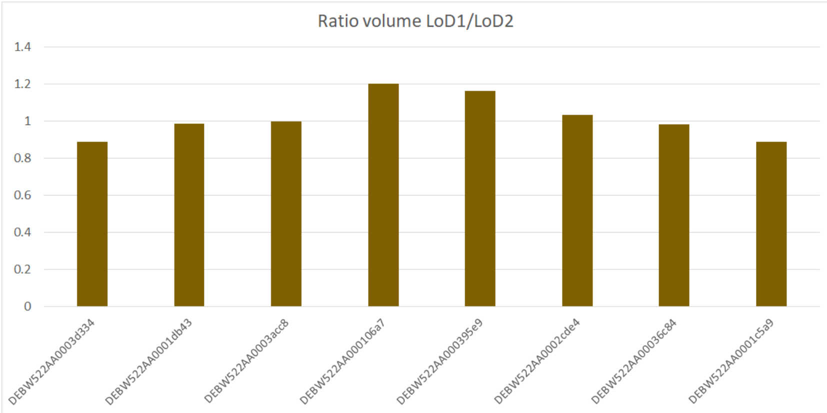

Figure 6.18: Ratio volume LoD1 vs LoD2.

The buildings contained in the two blocks under study are mainly modelled to the roof eave in LoD1, and therefore, this model represents the buildings in general smaller than in reality. The buildings can be divided into two groups; those with flat and those with tilted roofs. The first group has the advantage that their representation in both levels of detail is similar. In principle, there should be no difference between their representation in LoD1 or LoD2 and, therefore, the differences in simulated demand between the two details should only be due to the effect of the surroundings. That is not entirely true in the case under study. There are small differences in building's height –and therefore, volumes (the footprint areas are exactly the same in both details)– and shared-wall[b] areas between the flat-roof buildings represented in both levels of detail. Figure 6.18 presents the ratio between the volumes calculated in LoD1 and LoD2 of the flat-roof buildings with thermal demand, and Figure 6.19 compares their shared-wall ratios, understanding them as the shared-wall area divided by the sum of the areas of shared and no shared walls, windows and roofs.

These two geometrical parameters affect the buildings' area-volume ratio, and the lower this ratio, the lower the specific demand. Figure 6.20 shows the factor between the area-volume ratios in LoD1 and LoD2. In dark grey, the flat-roof buildings follow the expected behaviour, bigger volume or shared wall area implies lower area-volume ratio. The pitched-roofs case (light grey) also include other aspects as the geometry is not any more the same in both models. It can be observed how the area-volume ratio in LoD2 for tilted-

[b]Shared-walls are those that separate two adjacent buildings; they are thermally defined as adiabatic surfaces.

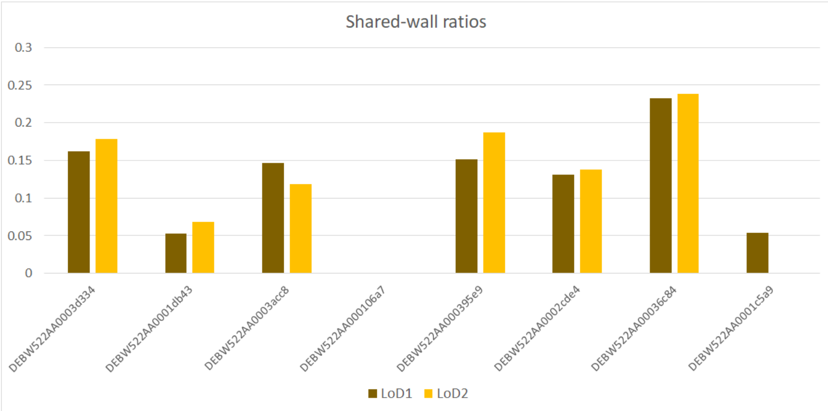

Figure 6.19: Shared-wall ratios LoD1 and LoD2.

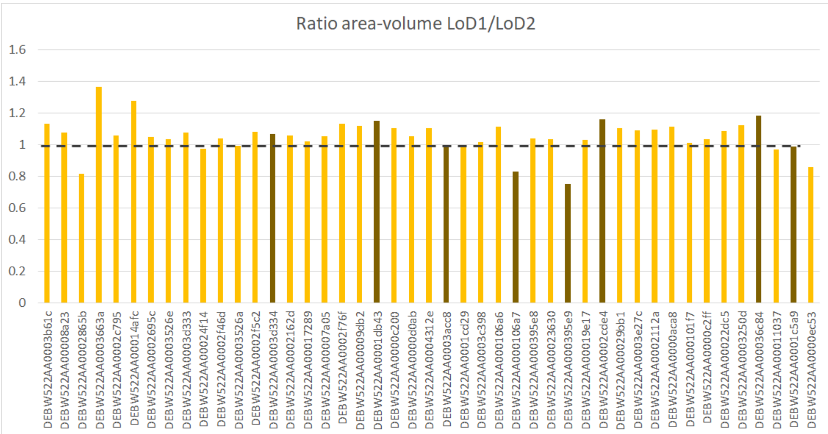

Figure 6.20: Factor area-volume ratios LoD1-LoD2.

roof buildings is in general smaller than in LoD1, which should imply lower specific demand.

But, a third phenomenon plays an essential role in the buildings' demands, the solar penetration. In the case of flat-roof buildings, it is expected that the solar penetration is higher in LoD1 than LoD2. That is because the tilted-roof buildings are taller in LoD2 and, as they surround the float-roof buildings, less solar irradiation can access their external surfaces. Figure 6.21 shows in dark grey those buildings with flat roofs. As expected, the ratio of the demands in LoD1 vs LoD2 is smaller than 1 for all buildings with flat roofs, as the effect of the solar penetration exceeds that of the compactness (inverse of area-volume ratio). The only exception is explained because of the error 2, as previously discuss (see Figure 6.17). Figure 6.22 shows the

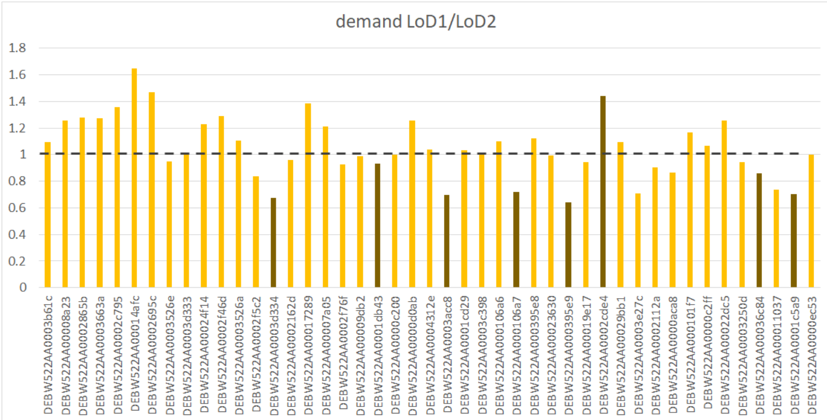

Figure 6.21: Ratio demand LoD1 vs LoD2.

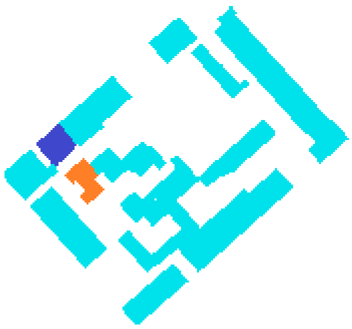

Figure 6.22: Footprint error 2. Location of the building described in error 2 (dark blue) and the building affected by the extra radiation received due to this error (orange).

footprint of the area where the buildings are placed. The building that causes the exception is highlighted in orange. The building in dark blue is that of error 2. Looking again at Figure 6.17, it can be observed that the building in orange has much higher solar penetration in LoD2 than in LoD1, causing the lower demand for the higher level of detail that is shown in Figure 6.21.

The solar penetration has an even higher effect on pitched-roof buildings due to the existence of extra windows. The German standard used for construction description defines a ratio of window area in tilted roofs (between 0.1 and 0.33, depending on the type of building and year of construction), while there are no windows assigned to flat roofs. As windows have higher U-value than walls, the losses increase in LoD2, and also do the solar gains through the transparent areas. Therefore, the building's total demand may increase or decrease in respect to the simulation in LoD1, depending on the relative importance of each phenomenon. Nevertheless, the effect on the hourly demand distribution is clear, during the central hours of the day when the radiation is higher, a faster decrease on demand in attics is expected in buildings represented in LoD2.

The same buildings presented in the previous section (Figure 6.10) have been used to visualise the results. Roofs of buildings A and B are oriented NE-SW and SE-NW respectively, while building C is oriented mainly E-W. Figure 6.23 shows the heating demand in the attics of two buildings during two days in January for comparing both levels of detail together with the radiation on the roofs in both cases. During the second day, with a clearer sky, the effect of the irradiation on roofs can be seen. The demand of building *A* decreases faster in LoD2 model than in LoD1 when the irradiation reaches the roofs, increasing this effect during the hours in the afternoon when the irradiation is more significant due to its orientation. The same effect, but more acute during the mornings, is observed for building *B*. In both cases, the demand increases, as expected, faster when modelled in LoD2 once the sun is gone. That is due to the effect of the losses to the ambient. This difference in the losses through the envelope is also observed in Figure 6.24. Figure 6.24(a) shows the thermal demands together with the solar irradiation on roofs in the same way as before. In contrast, Figure 6.24(b) presents the evolution of the temperature inside the thermal volume. The temperatures defined in the norm for residential buildings are 20°C as set point and 16°C as set back. When the room is left in free-floating conditions while passing from 20 to 16 °C, the temperature of the room modelled in LoD2 decreases faster than in the other case (see Figure 6.24(b)), confirming the effect of the losses already described.

6.5 Conclusions Application 1

This chapters has presented one application of the modular tool developed, focusing on the building demand calculation. It has been proved with this example that the tool can adapt to different levels of detail of the input data. And that it is able to model a variety of building types. Furthermore, the interaction building-urban context has been presented, highlighting the importance of including the surroundings of the area under study. Finally, a distributed supply system based on HP and PV panels has been analysed, showing that this solution is not optimal for cold-weather cities.

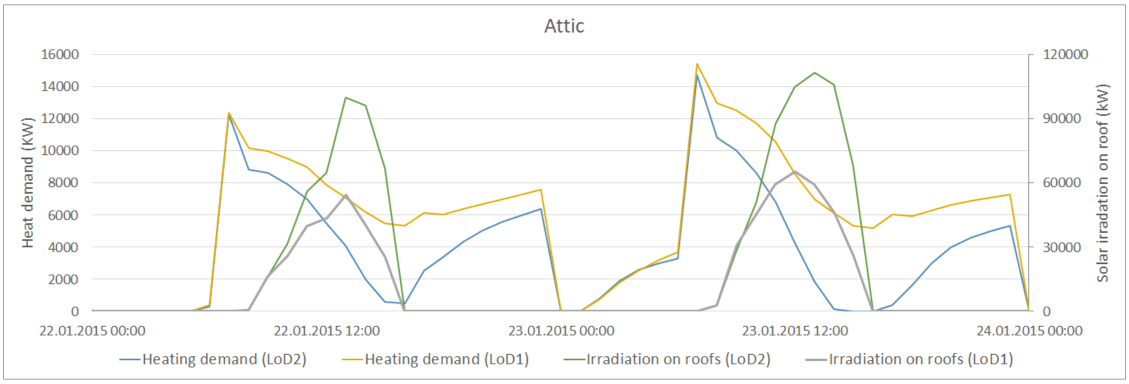

(a) Building A: Building oriented NE-SW.

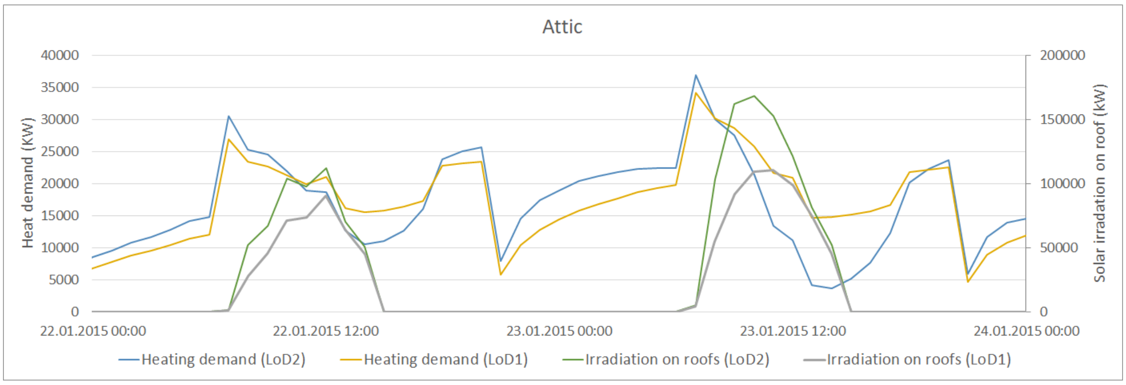

(b) Building B: Building oriented SE-NW.

Figure 6.23: Comparison between LoD1 and LoD2 in heating demand and solar irradiation on roofs.

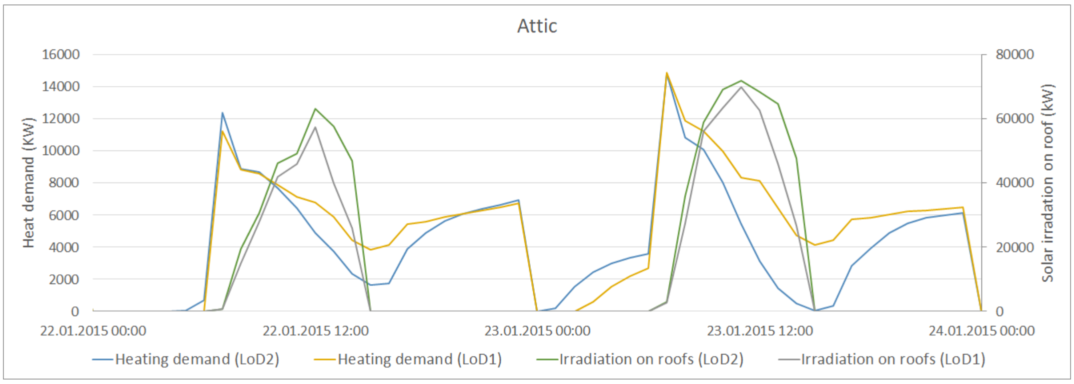

(a) Building C: Demand.

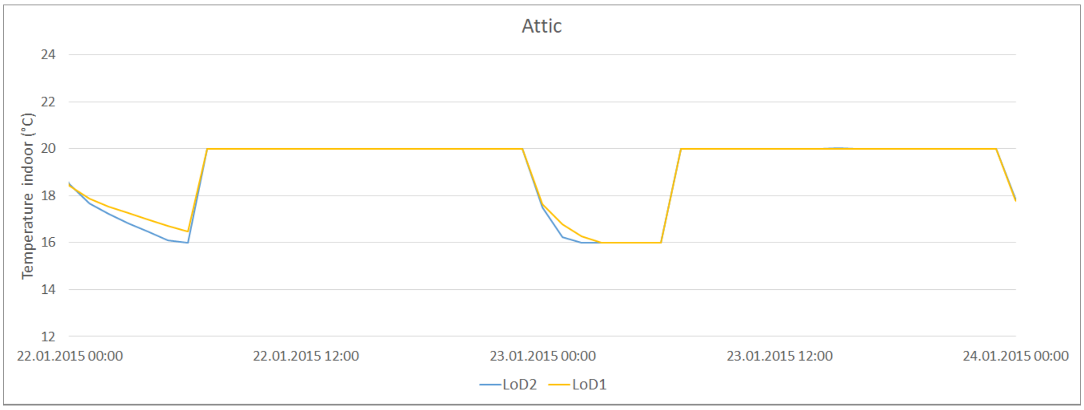

(b) Building C: Temperature.

Figure 6.24: Comparison between LoD1 and LoD2 in heating demand and internal temperature.

Chapter 7

Application 2. Energy performance of decentralised solar thermal, Vienna Case Study

This second application case focuses on the behaviour of a DHN. Given the heat demand as an input to the study (it has not been calculated), the impact of a distributed solar thermal system on the DHN has been analysed. Also, the potential of such a system on a real network in the city of Vienna was studied. Finally, a comparison of the solar thermal system with a system based on PV and heat pumps is discussed. The DHN model has been interconnected to several 'prosumers'. Therefore, the supply stations can change from heat 'consumers' to heat 'producers' at any calculation step, causing significant fluctuations. This context makes the dynamics of the network to play a crucial role.

This chapter was partially published in the book "Urban Energy Systems for Low Carbon Cities" under the title "Applying Modeling and Optimisation Tools to Existing City Quarters" [163].

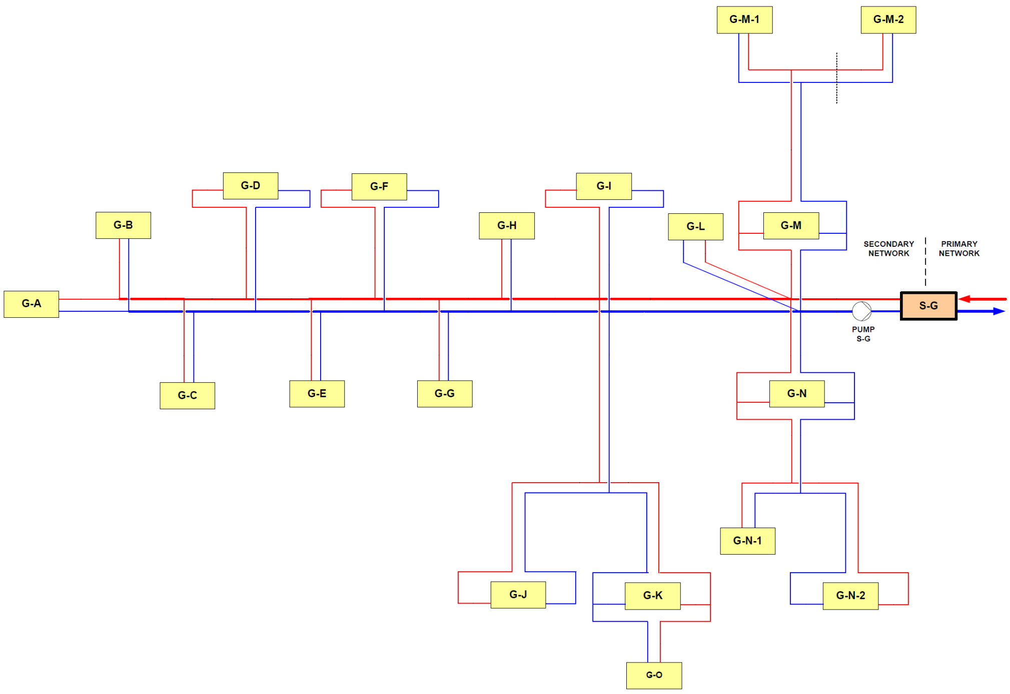

Figure 7.1: Schema of the Girasolstrasse branch (By: M. Potente).

7.1 Case study and Model description

7.1.1 Geographical area and heat demand

The network under study belongs to the DHN of the city of Vienna. It is a secondary branch connected through two heat-exchangers in the supply substation (S-G) to the main network. More than 25 buildings are connected in parallel to the Girasolstrasse branch through 19 substations (Figure 7.1).

All buildings connected to one substation have been aggregated and treated as a single entity, meaning, their demands have been added together. Also, the solar areas and the storage volumes, so they are seen from the primary side as just one consumer, and not separated buildings. The dataset containing the description of the network was very complete, providing the main parameters needed to define it, including length and diameters of pipes, together with four years with 15 minutes resolution of temperatures and flows at the substations of the secondary side, the temperatures and flow at the

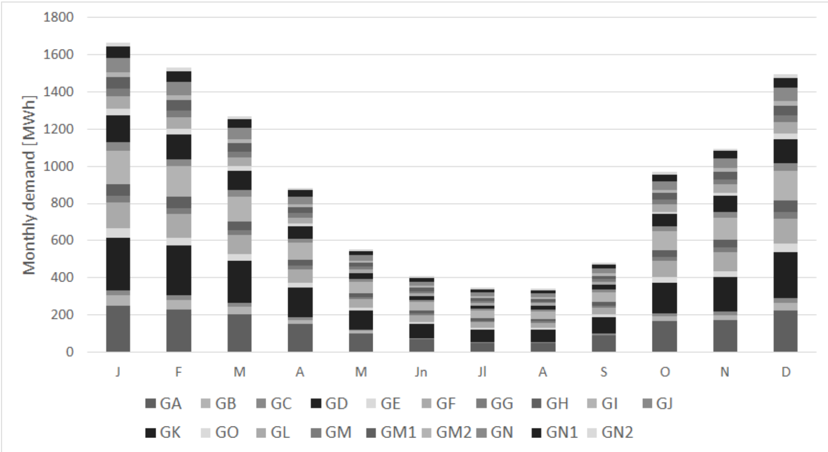

Figure 7.2: Monthly demand of the substations of Girasolstrasse.

S-G substation in the primary side and ambient temperature. Data of the year 2015 has been selected to develop the case study because it was the most complete one. Figure 7.2 shows the monthly demand of all substations over the year 2015. It can be seen how the total heat demand sharply decreases during summer season according to the decrease of heating demand, remaining only that due to the DHW preparation. This information was combined with solar radiation data provided by the Austrian Central Institution for Meteorology and Geodynamics (ZAMG by its German acronym). Figure 7.3 shows the monthly solar radiation on the city of Vienna during the year 2015.

No information about the buildings was available except for the total heated area and number of stories, but only for some of them. The footprint areas of the buildings range from around 200 m^2 to not much more than 2000 m^2 (the footprint areas were not available, but were estimated in section 7.1.3 as it is explained). This range, together with Figures 7.2 and 7.3 give a first impression of how difficult it may be to cover the complete demand of the network only with solar energy. Nevertheless, there is still the possibility of being an autonomous micro-grid during summer. The main idea of the study is to add solar installations to the system while keeping the rest untouched. Thus, no refurbishment on buildings was considered neither changes in the network like temperature levels or substations sizes. Knowing that, the buildings are not new, the heating systems in all buildings are assumed to be based on radiators. Therefore, the new solar systems installed must produce water at 60°C or more. Two months, January in winter and July in summer, have been selected to perform the study. These two months have the lowest and highest ratios of solar radiation to heat demand, respectively.

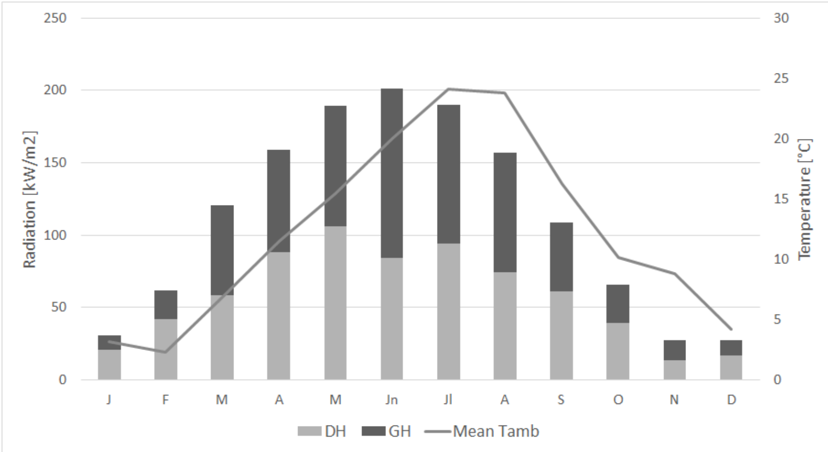

Figure 7.3: Monthly meteorological data of Vienna in 2015 (Source: self made with data from ZAMG).

7.1.2 The solar system models

The hydraulics of the solar system model are presented in Figure 7.4. The solar thermal system is mainly composed of solar panels connected to a storage tank through a heat exchanger. On the solar panels side, a standard water-glycol mixture is used to prevent freezing in winter. Through the rest of the pipes just water circulates. The system is thermally connected through a second heat exchanger to the DHN. The central component of the system is the storage tank. The solar input goes directly there as well as the input from the network. Both mass flows converge thanks to a mixing valve (V1), allowing the activation of pumps B2 and B3 in parallel. At the same time, the demand is always covered from the tank. This configuration is widely used in the sector to smooth the peaks in demand. The possible working modes are the following:

M 1. Solar heating mode: pumps B1 and B2 on.

M 2. Network heating mode: pump B3 on.

M 3. Solar surplus to net: pump B4 on.

M 4. Covering demand mode: pump B5 on.

Valves V3 and V4 separate modes 2 and 3, so they can not occur in parallel. There is no other hydraulic restriction; the activation-deactivation of other modes depend on the control system, which is based on tank temperatures and solar radiation. The control strategies are explained at the end of this section. The same components of the system were selected for all substations.

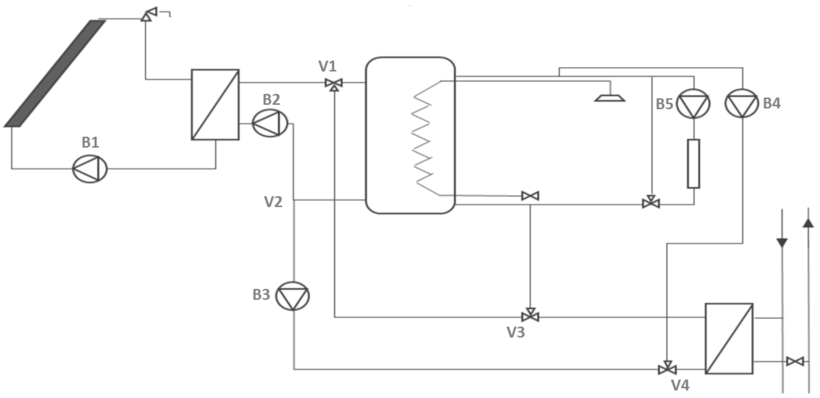

Figure 7.4: Schema of the solar thermal system.

Fluid [-]	Water-glycol mixture
Orientation [-]	South
Inclination of solar collector [°]	30.0
a_0 at normal incidence [-]	0.642
Linear heat loss coefficient [W/m^{2}K]	0.89
Quadratic heat loss coefficient [W/m^{2}K^2]	0.001
IAM [-]	0.9

Table 7.1: Solar thermal collector parameters.

Fluid [-]	Water
Overall heat loss coefficient [W/m^{2}K]	2.247
Ambient temperature around the tank [°C]	8

Table 7.2: Storage tank's parameters

Tables 7.1 and 7.2 present the simulation parameters of the solar thermal collectors and tanks. A very efficient evacuated tube collector from those found on the market has been chosen for the study. Two counterflow heat exchangers with an overall heat transfer coefficient of 3500 W/m^{2}K for the one on the solar side and 3000 W/m^{2}K for the one connecting with the DHN have been chosen. On the secondary side (the solar thermal systems), only the thermal behaviour is simulated. Still, the model of the network in the primary side takes into account both the thermal and the hydraulic behaviour. Therefore, a pressure loss of 200 kPa has been assumed on the primary side of the DHN heat exchanger. Finally, a control system for pumps and valves with the following strategy has been included:

- Whenever the radiation is high enough (threshold 150 W/m^2), the solar collector pumps start working to feed the tank.
- The solar field has a maximum working temperature of 99°C due to pressure restrictions. Whenever this temperature is reached, a security valve opens losing the energy.
- If the tank is "full" (the temperature at the top of the tank higher than 75°C), its energy is supplied to the net.
- If the tank is "empty" and the solar input is insufficient (temperature on top of the tank lower than 60°C), the deficit is supplied from the net.
- The pumps on the demand side work whenever there is a demand.

7.1.3 System dimensioning

The system dimensioning has been carried out considering the solar collector area as a limiting parameter. The rest of the components have been calculated according to this. The maximum solar collector area, as was presented in section 7.1.1, is not enough to cover the complete demand, so the systems are surely not oversized. The maximum collector area per building has been calculated based on the work developed by L. Romero et al. [178] where a systematic process to evaluate the usable roof area for PV and solar thermal depending on the available geometrical data of the building is defined. Due to data privacy reasons, the actual buildings connected to every substation were not known, but only some characteristics of them. Table 7.3 presents

	Floors	Heating surface [m²]	Annual demand [MWh]	Estimated footprint [m²]
GA	4	8320	1753	2080
GB	2	704	284	352
GC	6	1640	179	273
GD	6	19212	1930	3202
GE	9	2770	324	308
GF	5	11650	943	2330
GG	8	2408	244	301
GH	6	4036	429	673
GI	?	10835	1194	2709
GJ	?	2748	292	687
GK	8	4227	838	528
GO	?	?	169	321
GL	?	4662	446	1166
GM	?	2491	278	623
GM1	?	3351	406	838
GM2	5	2569	190	514
GN	3	5377	562	1792
GN1	5	3255	418	651
GN2	3	1766	163	589

Table 7.3: Substation parameters.

the known parameters per building, always aggregated by substation. The footprint has been estimated as follows:

- For those buildings with available information, the footprint has been calculated as the total heated surface divided by the number of floors.
- For those buildings where the number of floors was unknown, 4 floors were assumed. The footprint has been calculated as in the previous case.
- Finally, when the heated surface area was also unknown, then:
  1. The total specific demand of every other building was calculated as:
  $$q_h = \frac{Q_h}{A_h} \tag{7.1}$$
  2. The mean specific demand of the group $\bar{q_h}$ was then calculated.
  3. Finally, the heated surface of the unknown building was estimated as:
  $$A_{fp} = \frac{Q_h}{\bar{q_h} \cdot n_{floors}} \tag{7.2}$$

The roof was considered to be flat and with the same footprint area in the absence of further information. Then, according to the dimensioning process described in section 3.3, the reduction factor of the roof area used in the case study are:

- *Construction restrictions*: $C_{CON} = 0.8$ for flat roofs.
- *Protected buildings*: It was assumed that the district had not protected buildings, $C_{PROT} = 1$.
- *Separation of panels*: $C_{GCR} = 0.46$.
- *Service area*: This factor is already included in C_{GCR}.

For this specific case, where the roofs are flat and the shadows between solar panels have not been simulated, one more reduction factor must be added, also extracted from the study carried out by Romero, L. et al. in [178].

- *Shadow effects*: $C_{SH} = 0.7$ for flat roofs.

Finally, the total collector area (A_{coll}) is calculated using Equation 3.4.

A solar volume flow rate of 54 l/(m^{2}h) was set and, for the dimensioning of the tanks, two cases have been considered with a ratio of tank volume to solar area of 0.05 m^3/m^2 and 0.2 m^3/m^2. Table 7.4 summarises the size of the systems connected to each substation.

7.2 Results and discussion

Table 7.5 presents the results of cases 1 and 2 for both months, January and July. The solar energy used refers to the total amount of solar energy collected during the month and used either to cover demand or to feed the net. The solar energy lost accounts for the losses due to exceeding the maximum temperature in the collector field. The high amount of these losses are caused by the high tank temperatures required by the heating systems in the buildings. That leads, in turn, to high net temperatures, 65°C in summer and 70-85°C during winter. That leaves only a small margin for the solar collectors to operate. Heat imported refers to the total energy extracted from the net and the heat exported to that excess of solar energy released to the net. The losses to the ground are presented in total amount of energy and in percentage of the increase with respect to the initial value (original case without consumers). Finally, the energy consumed by the pumps has been

	Solar collector area[m^2]	Storage volume case 1 [m^3]	Storage volume case 2 [m^3]
GA	536	26.8	107.2
GB	91	4.5	18.2
GC	71	3.5	14.2
GD	825	41.2	165.0
GE	80	4.0	16.0
GF	600	30.0	120.0
GG	78	3.9	15.6
GH	173	8.7	34.6
GI	698	34.9	139.6
GJ	177	8.8	35.4
GK	136	6.8	27.2
GO	83	4.1	16.7
GL	300	15.0	60.0
GM	160	8.0	32.0
GM1	216	10.8	43.2
GM2	132	6.6	26.4
GN	462	23.1	92.4
GN1	168	8.4	33.6
GN2	152	7.6	30.4

Table 7.4: Solar systems of each substation.

	January		July	
	Case 1	Case 2	Case 1	Case 2
Total collector area [m^2]	5138	5138	5138	5138
Total tank volume [m^3]	1027.6	256.9	1027.6	256.9
Total demand [MWh]	1665.1	1665.1	345.8	345.8
Solar used [MWh]	68.71	62.65	403.21	396.25
Solar lost [MWh]	86.77	90.22	106.72	112.18
Heat imported [MWh]	1564.46	1596.36	26.04	18.24
Heat exported [MWh]	0.0	0.68	74.83	64.92
Losses to the ground [MWh]	65.86	65.74	51.24	53.83
Increase of losses to the ground [%]	2.12	1.93	40.18	47.29
Pumps consumption [MWh]	0.3	0.3	2.7	3.3

Table 7.5: Summary results solar thermal.

calculated assuming that the pumps operate with a constant efficiency as the hydraulics of the 'prosumer' are not simulated. A correlation of the power of the pumps E_p [Wh] as a function of the mass flow has been extracted from a water pumps catalogue:

$$E_p = \sum_i P_i \cdot h_i \tag{7.3}$$

where h_i [h] are the hours of operation of each pump and P_i [W] is its power calculated with the correlation as in 7.4.

$$P_i = 7.897 + 35.104 \cdot \dot{m}_i \tag{7.4}$$

Effects of the storage volume on the solar use. Increasing the storage volume has two opposite effects. On the one hand, the storage capacity ensures a bigger solar energy collection. But, on the other hand, it implies bigger thermal losses. These two effects may lead, as extracted from the results, to a low improvement or even worsening the system efficiency.

Restrictions to a bigger solar energy use:

- *Low solar area*: One of the main points, as predicted in the introduction, is the low solar area available, which is a common issue in cities. This fact can not even be compensated with the high efficiency of the evacuated tube collectors.

- *High net temperatures*: The setpoint net temperature is very high for an efficient solar energy use. That is more acute in winter when the net temperatures range between 70 and 85°C, but also when in summer they stay constant at 65°C. For example, a reduction of 10°C of the net temperature in winter could increase the solar use during January by 77 and 45 MWh for cases 1 and 2, respectively. This means more than double the energy for case 1 and an increase of almost 73% for case 2. Nevertheless, this reduction could only be made after a refurbishment of the buildings envelope and a modification of the heating systems inside them that would lead to a lower set-temperature for the heating systems in buildings.

- *Thresholds temperatures in the net*: This case study does not contemplate an upper threshold on net temperatures, so the maximum temperature is defined by the solar field (99°C). But, it is usual that the net does not allow temperatures above a limit to ensure the proper functioning of downstream substations. A limitation on the solar injection temperatures could highly decrease the harnessing of solar energy.

- *Increasing losses*: Finally, the increase of the temperatures of the net due to the solar injection increases, in turn, the thermal losses to the ground (between 40% and 47% in July in this study).

7.3 Comparison with a system based on PV and heat pumps

In this section, a new option is considered instead of the solar thermal system and the results are compared in terms of primary energy. The new system considered is a decentralised water-water heat pump (HP) installation. The condensers of the heat pumps are connected to the DHN, whose temperature is lowered to 40°C. The heat pumps are driven by photovoltaic electricity when possible. There is no storage for the PV, but if there is an electrical surplus, this can be fed back into the grid. These systems have two main advantages. First, the COP of the water-water heat pumps is very high, so the electrical consumption compared to, for example, air-water heat pumps is much lower. Second, the losses in the network are reduced with the temperature. Nevertheless, there is an extra electrical consumption from the HP that may not be covered entirely with PV. The calculation of this system has been done in a simplified way. Both the PV panels and the HP have been considered to have constant efficiency:

$$\eta_{PV} = 0.15$$

$$COP_{HP} = 4.5$$

Considering that the temperatures of condenser and evaporator of the HP remain almost constant over the year, the assumption is suitable. The electricity produced by the PV panels at each substation i, P_{PVi} $[W]$, has been calculated using Equation 3.7. Then, at every hour the needs of electricity have been compared with the PV production and two results per substation have been obtained:

$$If \quad \frac{\dot{Q}_i(t)}{COP_{HP}} > P_{PVi}(t), \quad P_{Gi}(t)[W] = \frac{\dot{Q}_i(t)}{COP_{HP}} - P_{PVi}(t) \tag{7.5}$$

$$Else, \quad P_{PV\_Gi}[W] = P_{PVi}(t) - \frac{\dot{Q}_i(t)}{COP_{HP}} \tag{7.6}$$

where $\dot{Q}_i$ [W] is the thermal demand for heating and DHW, P_{Gi} [W] is the electricity needed for driving the HP taken from the net and P_{PV_Gi} [W] is the extra electricity generated by the panels and sent back to the grid at each substation. Furthermore, the savings on the thermal side $\dot{Q}_{save}$ $[W]$ have been calculated as:

$$\dot{Q}_{save}(t) = \dot{Q}_i(t) \cdot \frac{1}{COP_{HP}} + \dot{Q_{lTs}} - \dot{Q_{l40}} \tag{7.7}$$

where $\dot{Q_{lTs}}$ [W] is the losses on the DHN at the original supply temperature and $\dot{Q_{l40}}$ [W] is the losses at 40°C. Both losses have been dynamically simulated for the complete network. Finally, the final energy has been converted to primary energy to be able to compare electricity with heat, using the following Primary Energy Factors assigned to Austria in [128]:

$$PEF_{elec} = 1.91$$

$$PEF_{heat} = 1.01$$

For the comparison between the two systems, only the best solar thermal case (Case 1) was chosen. Table 7.6 summarises the results from System 1 and System 2 for the comparison. System 1 is the combination of PV plus Heat Pump (PV + HP). System 2 is Case 1 of the solar thermal system (ST). The results are presented in Primary Energy by applying the corresponding Primary Energy Factors. Negative values refer to energy saved and positive values to extra energy demanded. The thermal savings achieved thanks to the system refers, in the case of System 1, to the savings in thermal energy due to the high COP of the heat pumps. In the case of System 2, the thermal savings are the solar energy used and exported minus the extra losses to the ground. System 1 has an extra amount of thermal energy demand saved due to the reduction of the network temperature to 40°C. Finally, the extra electricity consumption of System 1 is due to the electrical consumption of the heat pumps minus the electricity generated by the PV panels. When positive (January), it means that the system has consumed more electricity

	January		July	
	System 1 PV+HP	System 2 ST Case 1	System 1 PV+HP	System 2 ST Case 1
Demand covered by solar [%]	12.12	1.49	100	90.28
Thermal savings due to system [MWh]	-409.47	-68.02	-102.11	-467.99
Thermal savings for lowering Tsup [MWh]	-35.39	-	-24.25	-
Extra electricity consumption [MWh]	621.11	0.56	-137.96	5.15

Table 7.6: Comparison solar thermal vs PV plus Heat Pump

from the grid than generated. When negative (July), the opposite is true, i.e. the PV panels have generated more electricity, and this extra amount is sold to the grid. In the case of System 2, the extra electricity consumption is due to the pumps activity.

Figures 7.5 and 7.6 show how the savings in thermal energy in System 1 (PV + HP) come at the expense of high electrical energy consumption. Due to the limited solar area, a significant portion of this consumption comes from the grid. On the other hand, during summer the total demand can be covered with solar energy and some extra electricity can be sold to the grid. The energy mix in the grid plays a significant role in the selection of the best option, as it gives a clue to decide whether the thermal savings compensate the energy consumed from the grid or not. A better mix (with more renewable) can decrease the Primary Energy Factor significantly, and therefore, the 'Extra electricity consumption' bar. Figure 7.7 resumes the total primary energy consumption for both months and both systems. It can be clearly seen how System 1 consumes extra energy in winter, or it can save just a small amount of thermal energy in summer, depending on the relation between heat demand and solar supply. At the same time, system 1 exports electricity to the grid in summer. System 2 can save primary energy for heating and DHW in both months and that, apart from pumping electricity, has nearly no impact on the electrical grid. The selected months, January and July, are those that have the higher and lower relation of demand to solar supply. Therefore, it can be stated that the thermal savings over the year for System 2 would always be negative (i.e. always some energy saved), but not very high in absolute terms. As the savings of these two months amount to almost 26% of the total demand, it can be assumed that the

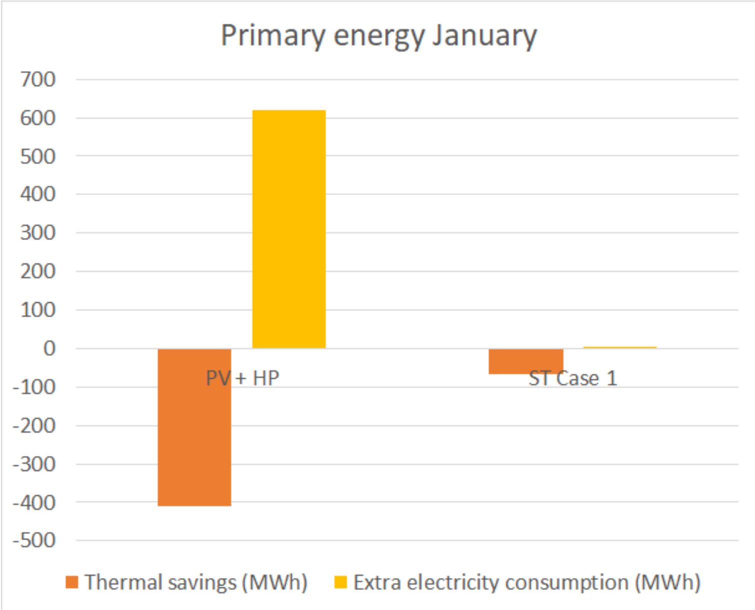

Figure 7.5: Comparative results in primary energy in January. It represents the total energy of all buildings together.

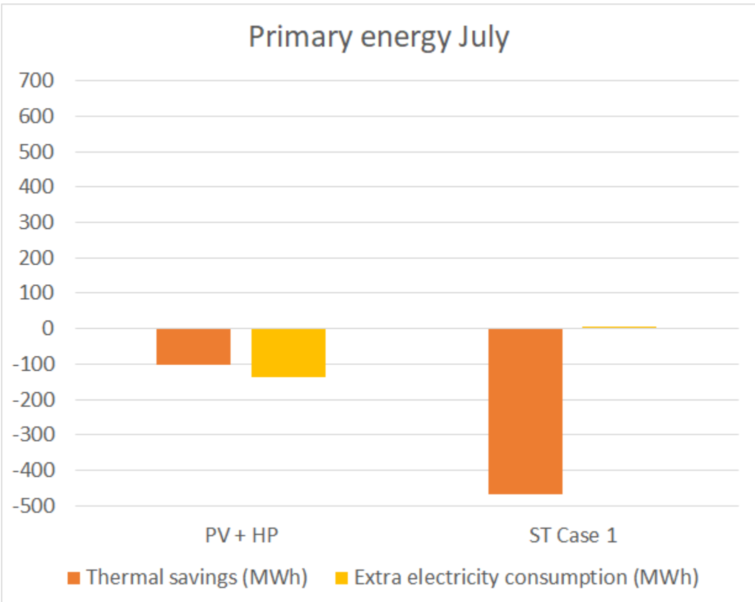

Figure 7.6: Comparative results in primary energy in July. It represents the total energy of all buildings together.

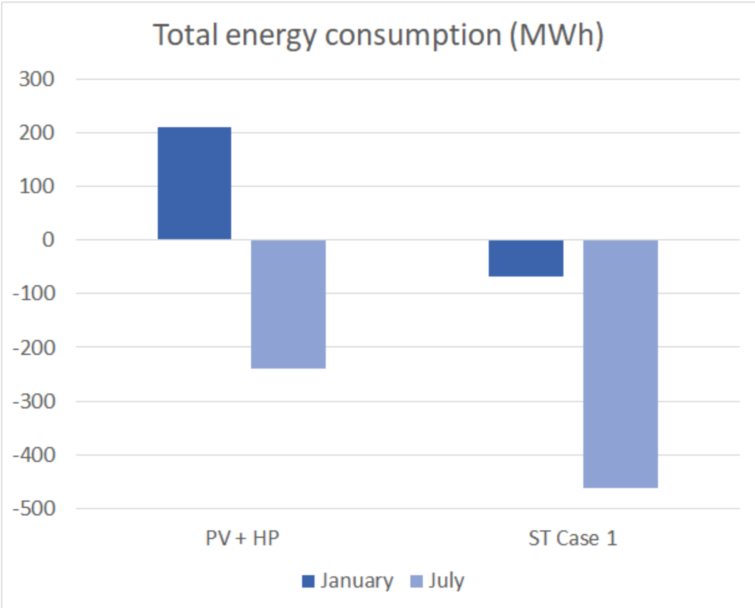

Figure 7.7: Resume in primary energy.

yearly percentage would be around that value. In terms of total primary energy savings, System 2 (Solar Thermal) performs better than the PV+Heat pump system. Nevertheless, none of them is an optimum solution. System 1 still needs a high amount of electricity consumed from the grid, and the high working temperatures of System 2 do not provide the best conditions for an efficient solar thermal system operation.

7.4 Conclusions Application 2

This chapter presented a second application of the developed tool. In this case, the focus was made on the DHN model and its interaction with the supply system. This example highlights the importance of being able to capture the dynamics of the network. It demonstrates that the temperature waves affect the behaviour of the system by reducing the capacity of the network to absorb all heat coming from the 'prosumers'. The application also shows the capacity of the tool to incorporate renewable sources, including solar thermal as well as PV systems. Finally, these two systems, including solar thermal and distributed HP + PV system, have been compared and their results discussed. None of them show important reductions in the energy 'consumption', being the thermal solution slightly better than the photovoltaic one.

Chapter 8

Conclusions and further research

8.1 Conclusions and summary of key findings

In section 1.2, the aim of this thesis was presented, which is to produce a useful and flexible tool by connecting data and system models in a coherent way to help in decision-making processes regarding the urban energy system with a particular focus on thermal energy performance and renewable energy potential in heating and cooling systems. To this end, a list of specific objectives was outlined.

1. To develop a flexible building model

In chapter 4, a new dynamic building model has been described. It is a white box model designed to be very modular in order to accommodate to diverse types of buildings in a city stock. It can also be automatically generated based on different details of the input data, allowing easy and fast multi-building simulation. The application presented in chapter 6 proves these characteristics. Finally, its modularity ensures the capability to integrate new modules for specific functions such as stochastic models of human behaviour profiles or more sophisticated and up-to-date construction alternatives.

2. To produce a DHN model

Chapter 5 presents a pseudo-dynamic DHN model and a methodology developed to ensure that the model captures the dynamics of the network. This property has been demonstrated to be crucial to understand the impact of distributed intermittent supply sources, very common in renewable systems (explained in section 5.2).

3. To validate models

Both models have been validated following different techniques, either an interprogram comparison or empirical validation when available. The results are exposed in their relevant chapters 4 and 5, proving their capability to model both elements accurately.

4. To integrate the models in a modular Urban Energy System simulation environment

A methodological approach has been developed and represented in a workflow, which was integrated into two different tools, including a desktop application (SimStadt) and an online server (Ci-NERGY). The workflow presents three main characteristics with which it can contribute to the area:

- It is very modular, allowing different studies with the same tool and being able to adjust the models to the level of detail of the input data available.
- It includes automation of data setting for dynamic simulation, which facilitates the simulation of large areas.
- It considers the interaction building-urban context as well as building-network.

Other aspects highlighted in the literature review as essential requirements have also been included in the tools. Section 8.1.1 reviews them.

5. To demonstrate the usefulness of the modular urban simulation tool for decision-making processes

Two applications, described in chapters 6 and 7, illustrate the usability of the developed tool. The first one studies the impact of a distributed HP+PV system in the electricity consumption of a neighbourhood. Instead, the second one focuses on the DHN, analysing the effect of connecting 'producers' to the network and its capacity to absorb the heat of a distributed solar system. It also reports the savings of the installation of such a system.

8.1.1 Achieving key requirements for Urban Energy System Model tools

R1. Automatic data mapping

The author has participated in the input data mapping related to the building geometry, its construction properties and the usage characteristics, as well as in the weather data mapping. Several classes were written in Java to automatize the input data mapping and preprocessing. This work has been presented in sections 3.1 and 3.2. Although some work was also done related to the definition of the DHN data models in the context of the development of the *Utility Network ADE*[a], the model structure is not fully defined, and the data mapping could not be developed yet.

R3. Model up to 4DH system

An extensive work has been done in this regard. First, a new dynamic building model (presented in chapter 4) has been developed and tested. Then, a methodology to improve a DHN model has been developed (described in section 5.3). After integrating it, the model is able to catch the dynamics of the network.

R4. Take into account the urban context

The author has worked on the integration of `SRA` in the workflow. Also, on the mapping of its outputs into the buildings and solar system models. `SRA` allows the urban model to rigorously account on the short-wave irradiation exchange in the urban context.

[a] `https://en.wiki.utilitynetworks.sig3d.org`

R6. Ability to accommodate to different levels of detail

Both the workflow structure and the models' composition has been developed, following a strategy of modularity and independence between parts. This modularity allows tailoring to different configurations and levels of detail of the input model. The application presented in chapter 6 makes use of this quality to perform a comparison between the outputs obtained with two LoD of the 3D input data, concluding that both LoD can be simulated although the results must be analysed. The differences in geometry due to errors or inaccuracies may provoke substantial differences in the outputs because of the building's geometry, but also due to the interactions with the surroundings. Three features that affect the demand were pointed out in the study: (1) the volume of the building, which differs from one level of detail to the other, affecting the total demand; (2) the solar penetration, which depends on the height of the buildings and their distribution, affecting the total gains in the buildings. Higher solar penetration results in lower total annual demand, but also has an impact on the distribution over the year (monthly demand) and the day. And finally, (3) the differences in the construction –in the case of study, the existence of windows on pitched roofs in LoD2–, that increase the total gains to the buildings mostly in central hours of the day. But also, the total losses during night hours. This behaviour affects mostly the attic where the windows are found.

R7. Ability to perform dynamic simulations

The dynamics of the system have been taken into account when developing the models considering that they play an essential role when renewable energies form part of it. Thus, the thermal behaviour of both the building and the network have been modelled according to that. That is reflected, for example, in the hourly outputs of the buildings studied in chapter 6. Also, in the capture of the temperature wave inside a network presented in section 5.3.

R8. Open to modifications, updates or improvements

Together with the modularity, the access to the model codes and the use of free tools is crucial to fulfilling this requirement. Therefore, the models have been developed in a tool (`INSEL`) that was entirely accessible to the author and that is freely available since 2018. The mapping and data preprocessing was coded in Java.

8.2 Further research

The research presented in this thesis can be seen as a stepping-stone towards the achievement of energy-efficient districts, providing models of building demand and DHN simulation to allow thermal energy analysis at district scale. However, the scope of the proposed tool is very wide, and the work in modelling urban energy systems is far from complete.

The models could be developed further to improve their scopes and increase their ability to provide insight into urban energy performance. Regarding building's demand simulation, models of special constructions such as green or Trombe walls could be added. The improvement of the building model by including air exchange between zones or latent flows is also an exciting path to follow. Even more, the interconnection with stochastic models of occupants presence or interaction with building envelope (for example in a similar way as Chapman et al. did coupling `No-MASS` with `EnergyPlus` using `FMI` [47]); or urban micro-climate, are also clear open tasks.

In the DHN model, the effect of the heat losses to the ground is neglected, considering that the ground temperature is not affected by the network; this could be another field of research.

The list of supply systems, either renewable or conventional is very short. An extensive work for incorporating distributed and centralised supply systems' models could be done. That would also require mechanisms to define how they should be coupled and controlled; prioritising more renewable systems over the non-renewable counterparts, for example, that would be engaged as a backup.

Furthermore, the databases accessible by the tool should increase with a particular focus on the CityGML ADEs.

Finally, the building physical model has been validated following several methodologies; a similar work should be done to test the complete work-flow, including hypothesis and weather interactions with particular interest also in cooling demand. A dedicated multi-building and system measurement campaign would be invaluable in this regard.

Bibliography

[1] Federal Office of Meteorology and Climatology MeteoSwiss. http://www.meteosuisse.admin.ch/home.html?tab=overview.

[2] KfW-Effizienzhaus. https://www.kfw.de/inlandsfoerderung/Privatpersonen/Bestandsimmobilie/Energieeffizient-Sanieren/Das-KfW-Effizienzhaus/.

[3] STANET. http://www.stafu.de/en/home.html.

[4] TABULA WebTool. http://webtool.building-typology.eu/.

[5] Project TABULA. http://episcope.eu/iee-project/tabula/, 2009-2012.

[6] CityGML wiki. http://www.citygmlwiki.org, 2015.

[7] Data | The World Bank. http://data.worldbank.org/, 2015.

[8] Our World in Data. http://ourworldindata.org/, 2015.

[9] TRNSYS FMU export utility. https://sourceforge.net/projects/trnsys-fmu/, 2015.

[10] Nottingham Multi Agent Stochastic Simulation. http://no-mass.io/en/, 2016.

[11] ANSI/ASHRAE 2011. Standard 140-2011, Standard Method of Test for the Evaluation of Building Energy Analysis Computer Programs. *American Society of Heating, Refrigerating and Air-Conditioning Engineers, Atlanta, GA.*, 2011.

[12] Thomas Afjei and Ralf Dott. Heat pump modelling for annual performance, design and new technologies. In *Proceedings of Building Simulation 2011: 12th Conference of International Building Performance*

Simulation Association, Sydney, 14-16 November, pages 2431–2438, 2011.

[13] G Agugiaro, J-L Robineau, and P Rodrigues. Project Ci-Nergy: Towards an integrated energy urban planning system from a data modelling and system architecture perspective. *ISPRS Annals of Photogrammetry, Remote Sensing & Spatial Information Sciences*, 4, 2017.

[14] Alaa Alaidroos and Moncef Krarti. Optimal design of residential building envelope systems in the Kingdom of Saudi Arabia. *Energy and Buildings*, 86:104 – 117, 2015.

[15] Abdelsalam Aldawoud. Thermal performance of courtyard buildings. *Energy and Buildings*, 40(5):906 – 910, 2008.

[16] Naief A. Aldossary, Yacine Rezgui, and Alan Kwan. Domestic energy consumption patterns in a hot and arid climate: A multiple-case study analysis. *Renewable Energy*, 62:369 – 378, 2014.

[17] Jonas Allegrini, Kristina Orehounig, Georgios Mavromatidis, Florian Ruesch, Viktor Dorer, and Ralph Evins. A review of modelling approaches and tools for the simulation of district-scale energy systems. *Renewable and Sustainable Energy Reviews*, 52:1391 – 1404, 2015.

[18] Abdulbasit Almhafdy, Norhati Ibrahim, Sabarinah Sh Ahmad, and Josmin Yahya. Courtyard Design Variants and Microclimate Performance. *Procedia - Social and Behavioral Sciences*, 101:170 – 180, 2013. AMER (ABRA malaysia) International Conference on Quality of Life, AicQoL2013Langkawi.

[19] Carolina A. Alves, Denise H.S. Duarte, and Fábio L.T. Gonçalves. Residential buildings - thermal performance and comfort for the elderly under climate changes context in the city of São Paulo, Brazil. *Energy and Buildings*, pages –, 2015.

[20] Maria A Ancona, Michele Bianchi, Lisa Branchini, and Francesco Melino. District heating network design and analysis. *Energy Procedia*, 45:1225–1234, 2014.

[21] IEAEBC Annex. 58, Reliable Building Energy Performance Characterisation Based on Full Scale Dynamic Measurements. In *Workshop in preparation of new IEA EBC Annex project–Brussels April*, volume 18, page 19, 2016.

[22] James Arvo and MA Chelmsford. Backward ray tracing. In *Developments in Ray Tracing, Computer Graphics, Proc. of ACM SIGGRAPH 86 Course Notes*, pages 259–263, 1986.

[23] Modelica Association. Functional Mock-up Interface (FMI). `https://fmi-standard.org/`.

[24] Modelica Association et al. Functional mock-up interface for model exchange and co-simulation. *Report Version*, 2, 2014.

[25] Fuad Baba. *Dynamic Effect of Thermal Bridges on the Energy Performance of Residential Buildings*. PhD thesis, Concordia University, 2015.

[26] Carliss Young Baldwin, Kim B Clark, Kim B Clark, et al. *Design rules: The power of modularity*, volume 1. MIT press, 2000.

[27] C.Y. Baldwin, K.B. Clark, and Harvard Business School. Division of Research. *Modularity in the Design of Complex Engineering Systems*. Working paper (Harvard Business School. Division of Research). Division of Research, Harvard Business School, 2004.

[28] D Bartholomew and D Robinson. Building energy and environmental modelling. *Application Manual AM11, CIBSE April*, 1998.

[29] Aleksandr A Basalaev, Tatyana A Barbasova, and Dmitry A Shnayder. Simulation study on supply temperature optimization of university campus heating system. *Procedia Engineering*, 129:587–594, 2015.

[30] Sam Behzadi and MM Farid. Energy efficient buildings: How to determine the most suitable pcm and interior environment to maximize energy saving in buildings. *Eurosun2010, 28th September to 1st October*, 2010.

[31] Atli Benonysson, Benny Bøhm, and Hans F Ravn. Operational optimization in a district heating system. *Energy conversion and management*, 36(5):297–314, 1995.

[32] Robert E Best, Forest Flager, and Michael D Lepech. Modeling and optimization of building mix and energy supply technology for urban districts. *Applied Energy*, 159:161–177, 2015.

[33] Filip Biljecki, Hugo Ledoux, and Jantien Stoter. An improved LOD specification for 3D building models. *Computers, Environment and Urban Systems*, 59:25–37, 2016.

[34] R.Gordon Bloomquist. Geothermal space heating. *Geothermics*, 32(4-6):513 – 526, 2003. Selected Papers from the European Geothermal Conference 2003.

[35] Benny Bøhm, T Koljonen, Helge V Larsen, M Lucht, Sipilä Yong-soon Park, M Wigbels, and M Wistbacka. Simple models for operational optimisation. Technical report, Netherlands Agency for Energy and the Environment, 2002.

[36] Christoph Böhringer and Thomas F Rutherford. Combining bottom-up and top-down. *Energy Economics*, 30(2):574–596, 2008.

[37] L Andrew Bollinger and Ralph Evins. Facilitating model reuse and integration in an urban energy simulation platform. *Procedia Computer Science*, 51:2127–2136, 2015. International Conference On Computational Science, ICCS 2015.

[38] Ranjan K Bose et al. *Energy efficient cities: assessment tools and benchmarking practices*. World Bank Publications, 2010.

[39] Julien Bouyer, Christian Inard, and Marjorie Musy. Microclimatic coupling as a solution to improve building energy simulation in an urban context. *Energy and Buildings*, 43(7):1549–1559, 2011.

[40] plc BP. BP Technology Outlook. 2018.

[41] L. Brand, P. Lauenburg, and J. Englund. District heating combined with decentralised heat supply in Hyllie, Malmö. *The 14th International Symposium on DH and Cooling*, 2014.

[42] Lisa Brand, Alexandra Calvén, Jessica Englund, Henrik Landersjö, and Patrick Lauenburg. Smart district heating networks–A simulation study of prosumers' impact on technical parameters in distribution networks. *Applied Energy*, 129:39–48, 2014.

[43] Lisa Brange, Jessica Englund, and Patrick Lauenburg. Prosumers in district heating networks - A Swedish case study. *Applied Energy*, 164:492 – 500, 2016.

[44] Bruno Bueno, Leslie Norford, Grégoire Pigeon, and Rex Britter. A resistance-capacitance network model for the analysis of the interactions between the energy performance of buildings and the urban climate. *Building and Environment*, 54:116 – 125, 2012.

[45] Alfonso Capozzoli, Alice Gorrino, and Vincenzo Corrado. A building thermal bridges sensitivity analysis. *Applied Energy*, 107:229–243, 07 2013.

[46] Yunus A Çengel and Afshin Jahanshahi Ghajar. *Transferencia de calor y masa: fundamentos y aplicaciones*. McGraw-Hill, 2011.

[47] Jacob Chapman, Peer-Olaf Siebers, and Darren Robinson. Multi-agent stochastic simulation of occupants for building simulation. 2017.

[48] J Chinchilla-Guarin and J Rosero. Evaluation of the Impact of Environmental Variables on Line Rating and Energy Dispatch. *Energy Procedia*, 100:405–411, 2016.

[49] K Ciuprinskas and B Narbutis. Experiments on heat losses from district heating pipelines. *Energetika*, 2:35–40, 1999.

[50] J.A. Clarke and P.A. Strachan. Climate change Energy and the environment Simulation of conventional and renewable building energy systems. *Renewable Energy*, 5(5):1178 – 1189, 1994.

[51] Joe A Clarke. *Energy simulation in building design*. Routledge, 2001.

[52] Wesley J. Cole, Kody M. Powell, Elaine T. Hale, and Thomas F. Edgar. Reduced-order residential home modeling for model predictive control. *Energy and Buildings*, 74:69 – 77, 2014.

[53] Ester Coma and Phil Jones. 'Buildings as Power Stations': An Energy Simulation Tool for Housing. *Procedia Engineering*, 118:58 – 71, 2015. Defining the future of sustainability and resilience in design, engineering and construction.

[54] E Commission. European Commission COM(2011) 109 final. Communication From The Commission To The European Parliament, The Council, The European Economic And Social Committee And The Committee Of The Regions. Energy Efficiency Plan 2011. 2011.

[55] European Commission. Europe 2020. A European strategy for smart, sustainable and inclusive growth, 2010.

[56] Richard Courant, Kurt Friedrichs, and Hans Lewy. On the partial difference equations of mathematical physics. *IBM journal of Research and Development*, 11(2):215–234, 1967.

[57] Drury B Crawley. Which weather data should you use for energy simulations of commercial buildings? *Transactions-American society of heating refrigerating and air conditioning engineers*, 104:498–515, 1998.

[58] Vinicio Curti, Michael R von Spakovsky, and Daniel Favrat. An environomic approach for the modeling and optimization of a district heating network based on centralized and decentralized heat pumps, cogeneration and/or gas furnace. Part I: Methodology. *International Journal of Thermal Sciences*, 39(7):721–730, 2000.

[59] Itai Danielski, Morgan Fröling, and Anna Joelsson. The impact of the shape factor on final energy demand in residential buildings in nordic climates. In *World Renewable Energy Forum, WREF 2012, Including World Renewable Energy Congress XII and Colorado Renewable Energy Society (CRES) Annual Conference; Denver, CO; 13 May 2012through17 May 2012; Code94564*, pages 4260–4264, 2012.

[60] Asociación Técnica Española de Climatización y Refrigeración (ATECYR). *Guía Técnica. Procedimientos y aspectos de la simulación de instalaciones térmicas en edificios*, 2008.

[61] Axelle Delangle, Romain SC Lambert, Nilay Shah, Salvador Acha, and Christos N Markides. Modelling and optimising the marginal expansion of an existing district heating network. *Energy*, 140:209–223, 2017.

[62] Michael Deru, R Judkoff, and P Torcellini. Sunrel technical reference manual. *NREL, Golden*, 13, 2002.

[63] Reinhard Diestel. *Graph theory.* Springer Publishing Company, Incorporated, 2018.

[64] Kristina Difs, Maria Danestig, and Louise Trygg. Increased use of district heating in industrial processes - Impacts on heat load duration. *Applied Energy*, 86(11):2327 – 2334, 2009.

[65] V DIN. 18599-10: 2007-02. *Energetische Bewertung von Gebäuden-Berechnung des Nutz-, Endund Primärenergiebedarfs für Heizung, Kühlung, Lüftung, Trinkwarmwasser und Beleuchtung-Teil*, 10.

[66] Energy Efficiency, Renewable Energy, Robert H Henninger, and Michael J Witte. EnergyPlus 8.3.0-b45b06b780 Testing with Building Thermal Envelope and Fabric Load Tests from ANSI/ASHRAE Standard 140-2011. 2015.

[67] María Eguaras-Martínez, Marina Vidaurre-Arbizu, and César Martín-Gómez. Simulation and evaluation of Building Information Modeling in a real pilot site. *Applied Energy*, 114:475 – 484, 2014.

[68] Paul R Ehrlich and John P Holdren. Impact of population growth. *Science*, 171(3977):1212–1217, 1971.

[69] Hilding Elmqvist, Dag Brück, and Martin Otter. Dymola-user's manual. *Dynasim AB, Research Park Ideon, Lund, Sweden*, 1996.

[70] Element Energy et al. The potential for recovering and using surplus heat from industry. *Department of Energy and Climate Change, London, UK*, 2014.

[71] EnEV. EnEV2014. *German Energy Saving Regulation*.

[72] Daryl G Erbs, WA Beckman, and SA Klein. Estimation of degree-days and ambient temperature bin data from monthly-average temperatures. *ASHRAE J.;(United States)*, 25(6), 1983.

[73] Gerhard Faninger. Combined solar-biomass district heating in Austria. *Solar Energy*, 69(6):425 – 435, 2000. Large Scale Solar Heating.

[74] Ingenieurbüro Fischer-Uhrig. Stanet netzberechnung. *Verfügbar unter: http://stafu. de/de/home. html (19.12. 18)*, 2018.

[75] AEE – Institute for Sustainable Technologies. Dimensioning and Design of Solar Thermal Systems. 2010.

[76] Aurélie Foucquier, Sylvain Robert, Frédéric Suard, Louis Stéphan, and Arnaud Jay. State of the art in building modelling and energy performances prediction: A review. *Renewable and Sustainable Energy Reviews*, 23:272–288, July 2013.

[77] Peter Fritzson and Vadim Engelson. Modelica—A unified object-oriented language for system modeling and simulation. In *European Conference on Object-Oriented Programming*, pages 67–90. Springer, 1998.

[78] Irena Gabrielaitiene. Numerical simulation of a district heating system with emphases on transient temperature behaviour. 2011.

[79] Irena Gabrielaitiene, Benny Bøhm, and Bengt Sunden. Evaluation of approaches for modeling temperature wave propagation in district heating pipelines. *Heat transfer engineering*, 29(1):45–56, 2008.

[80] Irena Gabrielaitiene, Rimantas Kačianauskas, and Bengt Sunden. Thermo-hydraulic finite element modelling of district heating network by the uncoupled approach. *Journal of Civil Engineering and Management*, 9(3):153–162, 2003.

[81] Irena Gabrielaitiene, Bengt Sundén, and R Kacianauskas. Analysis of Fluid flow and Heat transfer in District heating pipelines using the finite element method. *WIT Transactions on Engineering Sciences*, 35, 2002.

[82] Başak Güçyeter and H. Murat Günaydín. Optimization of an envelope retrofit strategy for an existing office building. *Energy and Buildings*, 55:647 – 659, 2012. Cool Roofs, Cool Pavements, Cool Cities, and Cool World.

[83] Alessandro Di Giorgio and Francesco Liberati. Near real time load shifting control for residential electricity prosumers under designed and market indexed pricing models. *Applied Energy*, 128:119 – 132, 2014.

[84] Loïc Giraud, Roland Bavière, and Cédric Paulus. Modeling of solar district heating: a comparison between TRNSYS and MODELICA. *Proc. of EuroSun 2014*, 2014.

[85] Loïc Giraud, Roland Bavière, Cédric Paulus, Mathieu Vallée, and Jean-François Robin. Dynamic Modelling, Experimental Validation and Simulation of a Virtual District Heating Network. In *Proc. of the 28th Int. Conf. on Efficiency, Cost, Optimization, Simulation and Environmental Impact of Energy Systems (ECOS)*, 2015.

[86] Loïc Giraud, Roland Bavière, Mathieu Vallée, and Cédric Paulus. Presentation, validation and application of the DistrictHeating Modelica library. In *Proceedings of the 11th International Modelica Conference, Versailles, France, September 21-23, 2015*, number 118, pages 79–88. Linköping University Electronic Press, 2015.

[87] Clara Stina Good, Gabriele Lobaccaro, and Siri Håklau. Optimization of Solar Energy Potential for Buildings in Urban Areas - A Norwegian Case Study. *Energy Procedia*, 58:166 – 171, 2014. Renewable Energy Research Conference, RERC 2014.

[88] JM Gordon and T Agami Reddy. Time series analysis of hourly global horizontal solar radiation. *Solar Energy*, 41(5):423–429, 1988.

[89] Stefan Gracik, Mohammad Heidarinejad, Jiying Liu, and Jelena Srebric. Effect of urban neighborhoods on the performance of building cooling systems. *Building and Environment*, 90:15 – 29, 2015.

[90] Gerhard Gröger, Thomas H Kolbe, Claus Nagel, and Karl-Heinz Häfele. OGC city geography markup language (CityGML) encoding standard. 2012.

[91] Stefan Grosswindhager, Andreas Voigt, and Martin Kozek. Linear finite-difference schemes for energy transport in district heating networks. In *Proceedings of the 2nd international conference on computer modelling and simulation*, pages 5–7, 2011.

[92] ASHRAE Handbook of Fundamentals 1975. American Society of Heating, Refrigerating and Air-Conditioning Engineers. *Inc., New York*, 1975.

[93] Ilyes Ben Hassine and Ursula Eicker. Impact of load structure variation and solar thermal energy integration on an existing district heating network. *Applied Thermal Engineering*, 50(2):1437–1446, 2013.

[94] D Henning. Energy scenarios for new buildings with district or solar heating. *The 14th International Symposium on District Heating and Cooling*, 2014.

[95] A Hepbasli and C Canakci. Geothermal district heating applications in Turkey: a case study of Izmir-Balcova. *Energy Conversion and Management*, 44(8):1285 – 1301, 2003.

[96] Morrison Hershfield. Building envelope thermal bridging guide, version 1.1, 2016.

[97] Kimmo Hilliaho, Jukka Lahdensivu, and Juha Vinha. Glazed space thermal simulation with IDA-ICE 4.61 software – Suitability analysis with case study. *Energy and Buildings*, 89:132 – 141, 2015.

[98] Kristina Holmgren. A system perspective on district heating and waste incineration. 2006.

[99] Tianzhen Hong, Mary Ann Piette, Yixing Chen, Sang Hoon Lee, Sarah C. Taylor-Lange, Rongpeng Zhang, Kaiyu Sun, and Phillip Price. Commercial Building Energy Saver: An energy retrofit analysis toolkit. *Applied Energy*, 159:298 – 309, 2015.

[100] Jörg Huber and Christoph Nytsch-Geusen. Development of modeling and simulation strategies for large-scale urban districts. In *Proceedings of Building Simulation*, pages 1753–1760, 2011.

[101] Jörgen Hurtig. Report-evaluation of a small scale district heating system in Ullared, Sweden, 2010.

[102] IBPSA. IBPSA Project 1. BIM/GIS and Modelica Framework for building and community energy system design and operation. `https://ibpsa.github.io/project1/`.

[103] EN ISO. 13370:(2007) Thermal performance of buildings, heat transfer via the ground, calculation methods. *Brussels: CEN*, 2007.

[104] Deutsche Gebäudetypologie IWU. Institut Wohnen und Umwelt. *Deutschland*, 2003.

[105] Deutsche Gebäudetypologie IWU. Institut Wohnen und Umwelt. *Deutschland*, 2011.

[106] William S Janna. *Engineering heat transfer*. CRC Press, 1999.

[107] D.P. Jenkins, V. Ingram, S.A. Simpson, and S. Patidar. Methods for assessing domestic overheating for future building regulation compliance. *Energy Policy*, 56:684 – 692, 2013.

[108] Phillip John Jones, Simon Charles Lannon, and Hendrik Rosenthal. Energy optimisation modelling for urban scale master planning. 2009.

[109] PJ Jones, S Lannon, and J Williams. Modelling building energy use at urban scale. In *7th International IBSPA conference, Rio de Janeiro, Brazil, August*, pages 1683–1697, 2001.

[110] U Jordan, K Vajen, and H Braas. Manual DHWcalc Tool for the Generation of Domestic Hot Water (DHW) Profiles on a Statistical Basis. Version 2.02b, 2017.

[111] R. Judkoff and J. Neymark. International Energy Agency Building Energy Simulation Test (BESTEST) and Diagnostic Method. 1995.

[112] Soteris A. Kalogirou. Generation of typical meteorological year (TMY-2) for Nicosia, Cyprus. *Renewable Energy*, 28(15):2317 – 2334, 2003.

[113] Calvin Kam and Martin Fischer. Capitalizing on early project decision-making opportunities to improve facility design, construction, and life-cycle performance – POP, PM4D, and decision dashboard approaches. *Automation in Construction*, 13(1):53 – 65, 2004. The best of ISARC 2002.

[114] Jérôme Henri Kämpf and Darren Robinson. A simplified thermal model to support analysis of urban resource flows. *Energy and buildings*, 39(4):445–453, 2007.

[115] V Karamarkovic, A Solujic, J Simovic, and B Ramic. Implementation program of energy development strategy in the field of industrial energy. In *The Society of Thermal Engineers of Serbia edition. Proceedings of the regional conference industrial energy and environmental protection in Southeast Europe, Zlatibor, Serbia*, pages 24–28, 2008.

[116] M. Kavgic, A. Mavrogianni, D. Mumovic, A. Summerfield, Z. Stevanovic, and M. Djurovic-Petrovic. A review of bottom-up building stock models for energy consumption in the residential sector. *Building and Environment*, 45(7):1683–1697, July 2010.

[117] M Kavgic, D Mumovic, A Summerfield, Z Stevanovic, and O Ecim-Djuric. Uncertainty and modeling energy consumption: Sensitivity analysis for a city-scale domestic energy model. *Energy and Buildings*, 60:1–11, 2013.

[118] Miroslava Kavgic. *A city scale physically disaggregated bottom-up energy model: technical options for decarbonising Belgrade residential stock*. PhD thesis, UCL (University College London), 2013.

[119] Ming-Tsun Ke, Chia-Hung Yeh, and Jhong-Ting Jian. Analysis of building energy consumption parameters and energy savings measurement and verification by applying eQUEST software. *Energy and Buildings*, 61:100 – 107, 2013.

[120] James Keirstead, Mark Jennings, and Aruna Sivakumar. A review of urban energy system models: Approaches, challenges and opportunities. *Renewable and Sustainable Energy Reviews*, 16(6):3847–3866, 2012.

[121] Jamal Khodakarami, Ian Knight, and Nazanin Nasrollahi. Reducing the demands of heating and cooling in Iranian hospitals. *Renewable Energy*, 34(4):1162 – 1168, 2009.

[122] Jérôme Henri Kämpf, Maryène Montavon, Josep Bunyesc, Raffaele Bolliger, and Darren Robinson. Optimisation of building's solar irradiation availability. *Solar Energy*, 84(4):596 – 603, 2010. International Conference CISBAT 2007.

[123] Leo Laakkonen. Predictive supply temperature optimization of district heating networks. 2016.

[124] Berkeley Lab. FMU Export of EnergyPlus. `http://simulationresearch.lbl.gov/fmu/EnergyPlus/export/index.html`, 2013.

[125] Chr. Lamnatou, J.D. Mondol, D. Chemisana, and C. Maurer. Modelling and simulation of Building-Integrated solar thermal systems: Behaviour of the coupled building/system configuration. *Renewable and Sustainable Energy Reviews*, 48:178 – 191, 2015.

[126] Helge V Larsen, Halldór Pálsson, Benny Bøhm, and Hans F Ravn. Aggregated dynamic simulation model of district heating networks. *Energy Conversion and Management*, 43(8):995–1019, 2002.

[127] P Lazzeroni, S Olivero, F Stirano, C Micono, P Montaldo, G Zanzottera, FU Calí, and Maurizio Repetto. Energy efficiency measures for buildings in hebron city and their expected impacts in the distribution grid. *Energy Procedia*, 134:121–130, 2017.

[128] L Leoncini. The Primary Energy Factors play a central role in European 2020 targets achievement. In *International Conference Portugal SB13-contribution of sustainable building to meet EU 20-20-20 targets*, pages 113–120. MULTICOMP-Artes Gráficas, Lda, 2013.

[129] P.T. Lewis and D.K. Alexander. HTB2: A flexible model for dynamic building simulation. *Building and Environment*, 25(1):7 – 16, 1990.

[130] Dapeng Li and Shengming Liao. An integrated approach to evaluate the performance of solar water heater in the urban environment. *Energy and Buildings*, 69:562 – 571, 2014.

[131] Mingzhe Liu, Kim Bjarne Wittchen, and Per Kvols Heiselberg. Development of a simplified method for intelligent glazed façade design under different control strategies and verified by building simulation tool BSim. *Building and Environment*, 74:31 – 38, 2014.

[132] Xuezhi Liu, Jianzhong Wu, Nick Jenkins, and Audrius Bagdanavicius. Combined analysis of electricity and heat networks. *Applied Energy*, 162:1238–1250, 2016.

[133] Tobias Loga, Britta Stein, and Nikolaus Diefenbach. TABULA building typologies in 20 European countries – Making energy-related features of residential building stocks comparable. *Energy and Buildings*, 132:4 – 12, 2016. Towards an energy efficient European housing stock: monitoring, mapping and modelling retrofitting processes.

[134] V Lottner, M.E Schulz, and E Hahne. Solar-Assisted District Heating Plants: Status of the German Programme Solarthermie-2000. *Solar Energy*, 69(6):449 – 459, 2000. Large Scale Solar Heating.

[135] Henrik Lund, Sven Werner, Robin Wiltshire, Svend Svendsen, Jan Eric Thorsen, Frede Hvelplund, and Brian Vad Mathiesen. 4th Generation District Heating (4GDH): Integrating smart thermal grids into future sustainable energy systems. *Energy*, 68(Supplement C):1 – 11, 2014.

[136] Mariya Marinova, Catherine Beaudry, Abdelaziz Taoussi, Martin Trépanier, and Jean Paris. Economic assessment of rural district heating by bio-steam supplied by a paper mill in Canada. *Bulletin of Science, Technology & Society*, 28(2):159–173, 2008.

[137] Michael Martin and Patricia Thornley. The potential for thermal storage to reduce the overall carbon emissions from district heating systems. Technical report, Tyndall Centre Working Paper 157, 2013.

[138] Miguel Martin, Afshin Afshari, Peter R. Armstrong, and Leslie K. Norford. Estimation of urban temperature and humidity using a lumped parameter model coupled with an EnergyPlus model. *Energy and Buildings*, 96:221 – 235, 2015.

[139] Helmut Mayer. Automatic object extraction from aerial imagery—a survey focusing on buildings. *Computer vision and image understanding*, 74(2):138–149, 1999.

[140] M Miara, D Günther, T Kramer, T Oltersdorf, and J Wapler. Heat pump efficiency: analysis and evaluation of heat pump efficiency in real-life conditions. *Fraunhofer ISE*, 2011.

[141] Parham A Mirzaei. Recent challenges in modeling of urban heat island. *Sustainable Cities and Society*, 19:200–206, 2015.

[142] Pilar Monsalvete Álvarez de Uribarri, Ursula Eicker, and Darren Robinson. Energy performance of decentralized solar thermal feed-in to district heating networks. *Energy Procedia*, 116:285–296, 2017.

[143] Lina Montuori, Manuel Alcázar-Ortega, Carlos Álvarez-Bel, and Alex Domijan. Integration of renewable energy in microgrids coordinated with demand response resources: Economic evaluation of a biomass gasification plant by homer simulator. *Applied Energy*, 132:15–22, 2014.

[144] Peter Moonen, Thijs Defraeye, Viktor Dorer, Bert Blocken, and Jan Carmeliet. Urban Physics: Effect of the micro-climate on comfort, health and energy demand. *Frontiers of Architectural Research*, 1(3):197 – 228, 2012.

[145] Benjamin Morille, Nicolas Lauzet, and Marjorie Musy. SOLENE-microclimate: A Tool to Evaluate Envelopes Efficiency on Energy Consumption at District Scale. *Energy Procedia*, 78:1165–1170, 2015.

[146] Steven Muegge and Roberto Milev. Measuring modularity in open source code bases. *Open Source Business Resource*, 04/2009 2009.

[147] Sukumar Natarajan and Geoffrey J. Levermore. Predicting future UK housing stock and carbon emissions. *Energy Policy*, 35(11):5719 – 5727, 2007.

[148] United Nations. World Urbanization Prospects: The 2014 Revision, Highlights. Department of Economic and Social Affairs. *Population Division, United Nations*, 2014.

[149] Romain Nouvel, Kai-Holger Brassel, Marcel Bruse, Eric Duminil, Volker Coors, Ursula Eicker, and Darren Robinson. SimStadt, a new workflow-driven urban energy simulation platform for CityGML city models. In *Proceedings of International Conference CISBAT 2015 Future Buildings and Districts Sustainability from Nano to Urban Scale*, number EPFL-CONF-213437, pages 889–894. LESO-PB, EPFL, 2015.

[150] Romain Nouvel, Alessio Mastrucci, Ulrich Leopold, Olivier Baume, Volker Coors, and Ursula Eicker. Combining GIS-based statistical and engineering urban heat consumption models: Towards a new framework for multi-scale policy support. *Energy and Buildings*, 107:204 – 212, 2015.

[151] IEA OECD. Linking Heat and Electricity Systems. co-generation and District Heating and Cooling Solutions for a Clean Energy Future. *International Energy Agency. Paris*, 2014.

[152] United Nations. Department of Economic. *The Millennium Development Goals Report 2008*. United Nations Publications, 2008.

[153] University of Wisconsin-Madison. Solar Energy Laboratory and Sanford A Klein. *TRNSYS, a transient system simulation program*. Solar Energy Laborataory, University of Wisconsin–Madison, 1979.

[154] U. Ottosson. Next generation district heating – Findings and lessons from the project. *The 14th International Symposium on DH and Cooling*, 2014.

[155] M Palme, L Inostroza, G Villacreses, Andrea Lobato-Cordero, and C Carrasco. From urban climate to energy consumption. Enhancing building performance simulation by including the urban heat island effect. *Energy and Buildings*, 145:107–120, 2017.

[156] H Palsson. Analysis of numerical methods for simulating temperature dynamics in district heating pipes. In *6th International Symposium on District Heating and Cooling Simulation*, pages 1–20. University of Iceland, Faculty of Engineering, 1997.

[157] Halldór Pálsson. *Methods for planning and operating decentralized combined heat and power plants*. Risø & DTU-Department of Energy Engineering (ET), 2000.

[158] Xiufeng Pang, Michael Wetter, Prajesh Bhattacharya, and Philip Haves. A framework for simulation-based real-time whole building performance assessment. *Building and Environment*, 54:100 – 108, 2012.

[159] E Parliament. Directive 2012/27/eu of the European Parliament and of the Council of 25 October 2012 on energy efficiency, amending directives 2009/125/EC and 2010/30/EU and repealing Directives 2004/8/ec and 2006/32/ec. 2012.

[160] Matija Pavičević, Tomislav Novosel, Tomislav Pukšec, and Neven Duić. Hourly optimization and sizing of district heating systems considering building refurbishment–Case study for the city of Zagreb. *Energy*, 137:1264–1276, 2017.

[161] Diane PEREZ. *A framework to model and simulate the disaggregated energy flows supplying buildings in urban areas.* PhD thesis, École Polytechnique Fédérale de Lausanne, 2014.

[162] B. Di Pietra, F. Zanghirella, and G. Puglisi. An Evaluation of Distributed Solar Thermal "Net Metering" in Small-scale District Heating Systems. *Energy Procedia*, 78:1859 – 1864, 2015. 6th International Building Physics Conference, IBPC 2015.

[163] Mario Potente Prieto, Pilar Monsalvete Álvarez de Uribarri, and Giovanni Tardioli. 10 - Applying modeling and optimization tools to existing city quarters. In Ursula Eicker, editor, *Urban Energy Systems for Low-Carbon Cities*, pages 333 – 414. Academic Press, 2019.

[164] Adeb Qaid, Hussanudin Bin Lamit, Dilshan Remaz Ossen, and Raja Nafida Raja Shahminan. Urban heat island and thermal comfort conditions at micro-climate scale in a tropical planned city. *Energy and Buildings*, 133:577–595, 2016.

[165] Steven Jige Quan, Qi Li, Godfried Augenbroe, Jason Brown, and Perry Pei-Ju Yang. A GIS-based energy balance modeling system for urban solar buildings. *Energy Procedia*, 75:2946–2952, 2015.

[166] Miika Rämä and S Mohammadi. Comparison of distributed and centralised integration of solar heat in a district heating system. *Energy*, 137:649–660, 2017.

[167] Anandakumar M. Ramiya, Rama Rao Nidamanuri, and Ramakrishan Krishnan. Segmentation based building detection approach from LiDAR point cloud. *The Egyptian Journal of Remote Sensing and Space Science*, 20(1):71 – 77, 2017.

[168] C. Reinhart, Timur Dogan, J. Alstan Jakubiec, Tarek Rakha, and Andrew Sang. UMI - An urban simulation environment for building energy use, daylighting and walkability. In *13th Conference of International Building Performance Simulation Association, Chambery, France*, 2013.

[169] Christoph F. Reinhart and Carlos Cerezo Davila. Urban building energy modeling–A review of a nascent field. *Building and Environment*, 97:196 – 202, 2016.

[170] Jan Remund and Stefan Kunz. *METEONORM: Global meteorological database for solar energy and applied climatology.* Meteotest, 1997.

[171] Behnaz Rezaie and Marc A. Rosen. District heating and cooling: Review of technology and potential enhancements. *Applied Energy*, 93:2 – 10, 2012.

[172] Melanie Riester and Andreas Geiger. Implementierung eines werkzeuges zur interpretation von versorgungsnetzen aus dem programmsystem stanet®. In *REAL CORP 2019–IS THIS THE REAL WORLD? Perfect Smart Cities vs. Real Emotional Cities. Proceedings of 24th International Conference on Urban Planning, Regional Development and Information Society*, pages 401–410. CORP–Compentence Center of Urban and Regional Planning, 2019.

[173] Miro Ristimäki, Antti Säynäjoki, Jukka Heinonen, and Seppo Junnila. Combining life cycle costing and life cycle assessment for an analysis of a new residential district energy system design. *Energy*, 63:168 – 179, 2013.

[174] D Robinson, S Stankovic, N Morel, F Deque, M Rylatt, K Kabele, E Manolakaki, and J Nieminen. Integrated resource flow modelling of urban neighbourhoods: Project SUNtool. In *Proc. Building Simulation*, 2003.

[175] Darren Robinson, N Campbell, W Gaiser, K Kabel, A Le-Mouel, Nicolas Morel, Jessen Page, S Stankovic, and A Stone. SUNtool–A new modelling paradigm for simulating and optimising urban sustainability. *Solar Energy*, 81(9):1196–1211, 2007. CISBAT 2005.

[176] Darren Robinson, Frédéric Haldi, J Kämpf, Philippe Leroux, Diane Perez, Adil Rasheed, and Urs Wilke. CitySim: Comprehensive microsimulation of resource flows for sustainable urban planning. 2009.

[177] Darren Robinson and Andrew Stone. Holistic radiation modelling with a fast simplified radiosity algorithm. In *Proc. Ninth Int. IBPSA Conf., Building Simulation*. Citeseer, 2005.

[178] Laura Romero Rodríguez, Eric Duminil, José Sánchez Ramos, and Ursula Eicker. Assessment of the photovoltaic potential at urban level based on 3D city models: A case study and new methodological approach. *Solar Energy*, 146:264–275, 2017.

[179] Amir Roth, David Goldwasser, and Andrew Parker. There's a measure for that! *Energy and Buildings*, pages –, 2015.

[180] Michael Rubin. Calculating heat transfer through windows. *International Journal of Energy Research*, 6(4):341–349, 1982.

[181] Philip H. Saleh. Thermal performance of glazed balconies within heavy weight/thermal mass buildings in Beirut, Lebanon's hot climate. *Energy and Buildings*, 108:291 – 303, 2015.

[182] Ruggero Schleicher-Tappeser. How renewables will change electricity markets in the next five years. *Energy Policy*, 48:64 – 75, 2012. Special Section: Frontiers of Sustainability.

[183] J Schuhmacher. INSEL–Interactive Simulation of Renewable Electrical Energy Supply Systems-, Reference Manual. *University of Oldenburg, Renewable Energy Group, Dept. of Physics, PO Box*, 2503, 1993.

[184] S Shaari and N Bowman. Photovoltaics in buildings: A case study for rural england and malaysia. *Renewable energy*, 15(1-4):558–561, 1998.

[185] Pervez Hameed Shaikh, Nursyarizal Bin Mohd Nor, Perumal Nallagownden, Irraivan Elamvazuthi, and Taib Ibrahim. A review on optimized control systems for building energy and comfort management of smart sustainable buildings. *Renewable and Sustainable Energy Reviews*, 34:409–429, June 2014.

[186] Bard Skagestad and Peter Mildenstein. *District heating and cooling connection handbook*. NOVEM, Netherlands Agency for Energy and the Environment, 2002.

[187] Jiafang Song, Xuelin Zhang, and Xiangquan Meng. Simulation and Analysis of a University Library Energy Consumption based on eQUEST. *Procedia Engineering*, 121:1382 – 1388, 2015. The 9th International Symposium on Heating, Ventilation and Air Conditioning (ISHVAC) joint with the 3rd International Conference on Building Energy and Environment (COBEE), 12-15 July 2015, Tianjin, China.

[188] Gustavo Sousa, Benjamin M Jones, Parham A Mirzaei, and Darren Robinson. A review and critique of uk housing stock energy models, modelling approaches and data sources. *Energy and Buildings*, 151:66–80, 2017.

[189] Gustavo Alfonso Sousa Ramírez. *Analysis of strategies to decarbonise the UK housing stock*. PhD thesis, University of Nottingham, 2017.

[190] BS Standard and BS EN. EN 12975-2: 2006, Thermal solar systems and components. Solar collectors, 2006.

[191] Vladimir D Stevanovic, Branislav Zivkovic, Sanja Prica, Blazenka Maslovaric, Vladan Karamarkovic, and Vojin Trkulja. Prediction of thermal transients in district heating systems. *Energy Conversion and Management*, 50(9):2167–2173, 2009.

[192] Aneta Strzalka, Nazmul Alam, Eric Duminil, Volker Coors, and Ursula Eicker. Large scale integration of photovoltaics in cities. *Applied Energy*, 93:413 – 421, 2012.

[193] SNR. Règle Suisse. SIA 2024:2015. Données d'utilisation des locaux pour l'énergie et les installations du bâtiment. *Société suisse des ingénieurs et des architectes*, 2015.

[194] Lukas G. Swan and V. Ismet Ugursal. Modeling of end-use energy consumption in the residential sector: A review of modeling techniques. *Renewable and Sustainable Energy Reviews*, 13(8):1819–1835, October 2009.

[195] W Swinbank. Long-wave radiation from clear skies. *Quarterly Journal of the Royal Meteorological Society*, 89(381):339–348, 1963.

[196] Dassault Systèmes. DYMOLA Systems Engineering. Multi-Engineering Modeling and Simulation based on Modelica and FMI. `https://www.3ds.com/products-services/catia/products/dymola`.

[197] Behrang Talebi, Parham A Mirzaei, Arash Bastani, and Fariborz Haghighat. A review of district heating systems: modeling and optimization. *Frontiers in Built Environment*, 2:22, 2016.

[198] Daren Thomas, Clayton Miller, Jérôme Kämpf, and Arno Schlueter. Multiscale co-simulation of EnergyPlus and CitySim models derived from a building information model. In *Bausim 2014: Fifth German-Austrian IBPSA Conference*, 2014.

[199] Nicole Van Beeck. *Classification of energy models*. Tilburg University, Faculty of Economics and Business Administration, 1999.

[200] Bram van der Heijde, Marcus Fuchs, C Ribas Tugores, Gerald Schweiger, Kevin Sartor, Daniele Basciotti, Dirk Müller, Christoph

Nytsch-Geusen, Michael Wetter, and Lieve Helsen. Dynamic equation-based thermo-hydraulic pipe model for district heating and cooling systems. *Energy Conversion and Management*, 151:158–169, 2017.

[201] Aristotelis Vartholomaios. The residential solar block envelope: A method for enabling the development of compact urban blocks with high passive solar potential. *Energy and Buildings*, 99:303 – 312, 2015.

[202] VDI. 2089-1: 2014. *Building Services in swimming baths. Indoor pools*, 1.

[203] VDI. 3807-2: 1998. *Characteristic values of energy consumption in buildings. Heating and electricity*, 2.

[204] VDI. German standard VDI 6020: 2001. *Beuth Verlag GmbH*, 2001.

[205] Vittorio Verda and Francesco Colella. Primary energy savings through thermal storage in district heating networks. *Energy*, 36(7):4278 – 4286, 2011.

[206] E. Vesaoja, H. Nikula, and S. Sierla. Hybrid modeling and co-simulation of district heating systems with distributed energy resources. *Workshop on Modeling and Simulation of Cyber-Physical Energy Systems (MSCPES)*, 2014.

[207] Mikko Wahlroos, Matti Pärssinen, Jukka Manner, and Sanna Syri. Utilizing data center waste heat in district heating–impacts on energy efficiency and prospects for low-temperature district heating networks. *Energy*, 140:1228–1238, 2017.

[208] Danhong Wang, Kristina Orehounig, and Jan Carmeliet. Investigating the potential for district heating networks with locally integrated solar thermal energy supply. *Energy Procedia*, 122:1057–1062, 2017.

[209] Yaran Wang, Shijun You, Huan Zhang, Xuejing Zheng, Wandong Zheng, Qingwei Miao, and Gang Lu. Thermal transient prediction of district heating pipeline: Optimal selection of the time and spatial steps for fast and accurate calculation. *Applied Energy*, 206:900–910, 2017.

[210] P Wate, P Rodrigues, E Duminil, and V Coors. Urban energy simulation based on 3d city models: a service-oriented approach. *ISPRS Annals of the Photogrammetry, Remote Sensing and Spatial Information Sciences*, 4:75, 2016.

[211] IEA WEO. World Energy Outlook 2008. *International Energy Agency. Paris*, 2008.

[212] IEA WEO. World Energy Outlook 2012. *International Energy Agency. Paris*, 2012.

[213] IEA WEO. World Energy Investment Outlook 2014 Special Report. *International Energy Agency. Paris*, 2014.

[214] Sven Werner. *The heat load in district heating systems*. PhD thesis, Chalmers University of Technology, 1984.

[215] Sven Werner. International review of district heating and cooling. *Energy*, 2017.

[216] Michael Wetter, Christoph van Treeck, and Jan Hensen. New generation computational tools for building and community energy systems. *Energy in Buildings and Communities Programme. IEA EBC Annex*, 60, 2013.

[217] Adam Wills, Cynthia A. Cruickshank, and Ian Beausoleil-Morrison. Application of the ESP-r/TRNSYS Co-Simulator to Study Solar Heating with a Single-House Scale Seasonal Storage. *Energy Procedia*, 30:715 – 722, 2012. 1st International Conference on Solar Heating and Coolingfor Buildings and Industry (SHC 2012).

[218] Carlo Winterscheid, Jan-Olof Dalenbäck, and Stefan Holler. Integration of solar thermal systems in existing district heating systems. *Energy*, 137:579–585, 2017.

[219] Janusz Wollerstrand. District Heating Substations. Performance, Operation and Design. 1997.

[220] E Benjamin Wylie and Victor Lyle Streeter. Fluid transients. *New York, McGraw-Hill International Book Co., 1978. 401 p.*, 1978.

[221] Jincheng Xing, Peng Ren, and Jihong Ling. Analysis of energy efficiency retrofit scheme for hotel buildings using eQUEST software: A case study from Tianjin, China. *Energy and Buildings*, 87:14 – 24, 2015.

[222] Zhao Xu and Volker Coors. Application of system dynamics, gis and 3d visualization in a study of residential sustainability. In *International Conference on Computational Science and Its Applications*, pages 300–314. Springer, 2011.

[223] Jan Zborník and Jan Andel. Transient Processes in LV Distribution Systems of Nuclear and Conventional Power Plants. *Journal of Energy and Power Engineering*, 7(2):404, 2013.

Appendix A

Brief glossary

Tool: Generic word referring to any application (simulation engine, software, platform or framework) susceptible to be used for simulation.

Simulation engine: Simulation tool without user interface.

Software: Stand-alone tool including simulation engine and user interfaces for data input and results.

Platform: Computational architecture that connects several software and/or simulation engines (each one modelling different components of the system) and feeds all of them with the needed data.

Some software are susceptible to be used also as simulation engines. In this case, the user interface is provided by the main tool where the simulation engine is embedded. These software may be found in the 'simulation engine' group or the 'software' group depending on the use made of it.

Although the three following terms are not thermodynamically accurate, they are widely used in the urban energy field and therefore, also in this thesis.

Consumer: An urban entity that is energy demander.

Producer: An urban entity that supplies energy to the urban system.

Prosumer: An urban entity that can behave as a 'consumer' or 'producer' depending on the circumstances.

Appendix B

Computational models

B.1 Building model

B.1.1 ROOM block

	Inputs		Parameters
1	t	1	V_{room}
2	$\dot{Q}_{sys\_conv}$	2	T_{i0}
3	$\dot{Q}_{IGconv}$	3	$Cooling$
4	T_a	4	P_c
5	n_{inf}	5	$Heating$
6	T_{max}	6	P_h
7	T_{min}	7	H_{TB}
8	n_{vent}	8	n
9	T_{vent}	9...	A_x
10	$\dot{Q}_{conv}$	10...	h_{cx}

	Outputs
1	T_{room}
2	$\dot{Q}_{cool}$
3	$\dot{Q}_{heat}$

INPUTS

1. t: second of the year when the calculation is being done [s]
2. $\dot{Q}_{sys\_conv}$: convective heating and cooling power from plants to air node [W]
3. $\dot{Q}_{IGconv}$: convective part of casual gains [W]
4. T_a: ambient temperature [°C]
5. n_{inf}: infiltration air change rate [1/h]

6. T_{max}: maximum air temperature set-point in the room [°C]
7. T_{min}: minimum air temperature set-point in the room [°C]
8. n_{vent}: ventilation air change rate [1/h]
9. T_{vent}: ventilation temperature [°C]
10. $\dot{Q}_{conv}$: internal convection flows from enclosing surfaces [W]

PARAMETERS

1. V_{room}: room air volume [m^3]
2. T_{i0}: initial temperature of air point node [°C]
3. $Cooling$: cooling system on/off
4. P_c: capacity of the cooling system [W]
5. $Heating$: heating system on/off
6. P_h: capacity of the heating system [W]
7. H_{TB}: total heat transmittance due to thermal bridges [W/K]
8. n: number of enclosing surfaces
9. A_x: area of enclosing surface x [m^2]
10. h_{cx}: convective heat transfer coefficient in enclosing surface x [W/m^2K]

OUTPUTS

1. T_{room}: temperature of the room air at the end of the time-step [°C]
2. $\dot{Q}_{cool}$: cooling load (negative values of $\dot{Q}_{dem}$) [W]
3. $\dot{Q}_{heat}$: heating load (positive values of $\dot{Q}_{dem}$) [W]

B.1.2 WALL blocks

WALL

	Inputs		Parameters
1	t	1	h_{ci}
2	$\dot{q}_{rad\_swi}$	2	h_{co}
3	$\dot{q}_{rad\_lwi}$	3	n
4	$\dot{q}_{IGradi}$	4...	e_x
5	$\dot{q}_{rad\_swo}$	5...	λ_x
6	$\dot{q}_{rad\_lwo}$	6...	ρ_x
7	$\dot{q}_{IGrado}$	7...	$c_{p\,x}$
8	T_{roomi}		
9	T_{roomo}		

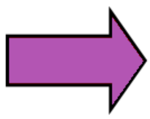

	Outputs
1	T_i
2	T_o
3	$\dot{q}_{convi}$
4	$\dot{q}_{convo}$

WALLX

	Inputs		Parameters
1	t	1	h_{ci}
2	$\dot{q}_{rad\_swi}$	2	h_{co1}
3	$\dot{q}_{rad\_lwi}$	3	h_{co2}
4	$\dot{q}_{IGradi}$	4	h_{ro}
5	$\dot{q}_{sol}$	5	$F_{wall-sky}$
6	T_a	6	n
7	T_{sky}	7...	e_x
8	ws	8...	λ_x
9	T_{roomi}	9...	ρ_x
		10...	$c_{p\ x}$

	Outputs
1	T_i
2	T_o
3	$\dot{q}_{convi}$

WALLG

	Inputs		Parameters
1	t	1	h_{ci}
2	$\dot{q}_{rad\_swi}$	2	n
3	$\dot{q}_{rad\_lwi}$	3...	e_x
4	$\dot{q}_{IGradi}$	4...	λ_x
5	T_v	5...	ρ_x
6	T_{roomi}	6...	$c_{p\ x}$
		$4n$+3	e_g
		$4n$+4	λ_g
		$4n$+5	ρ_g
		$4n$+6	$c_{p\ g}$
		$4n$+7	e_v
		$4n$+8	λ_v
		$4n$+9	ρ_v
		$4n$+0	$c_{p\ v}$

	Outputs
1	T_i
2	
3	q_{ci}

INPUTS

Common for all three walls:

1. t: second of the year when the calculation is being done [s]
2. $\dot{q}_{rad\_swi}$: specific short-wave radiation on internal surface [W/m^2]
3. $\dot{q}_{rad\_lwi}$: specific long-wave radiation on internal surface [W/m^2]
4. $\dot{q}_{IGradi}$: specific radiative part of casual gains inside [W/m^2]

Inputs dependent on the block:

For WALL:

5. $\dot{q}_{rad\_swo}$: specific short-wave radiation on external surface [W/m^2]
6. $\dot{q}_{rad\_lwo}$: specific long-wave radiation on external surface [W/m^2]
7. $\dot{q}_{IGrado}$: specific radiative part of casual gains outside [W/m^2]
8. T_{roomi}: temperature of room air node [°C]
9. T_{roomo}: temperature of adjacent room air node [°C]

For WALLX:

5. q_{sol}: specific solar gains on external surface [W/m^2]
6. T_a: ambient temperature [°C]
7. T_{sky}: sky temperature [°C]
8. ws: wind speed [m/s]
9. T_{roomi}: temperature of room air node [°C]

For WALLG:

5. T_v: virtual temperature at the end of the virtual layer [°C]
6. T_{roomi}: temperature of room air node [°C]

PARAMETERS

For WALL:

1. h_{ci}: convective heat transfer coefficient on internal surface [W/m^{2}K]
2. h_{co}: convective heat transfer coefficient on external surface [W/m^{2}K]
3. n: number of layers conforming the wall
4. e_x: thickness of layer x [m]
5. λ_x: thermal conductivity of layer x [W/mK]
6. ρ_x: density of layer x [kg/m^3]
7. $c_{p\,x}$: heat capacity of layer x [J/kgK]

For WALLX:

1. h_{ci}: convective heat transfer coefficient on internal surface [W/m^{2}K]
2. h_{co1}: parameter 1 of convective heat transfer coefficient on external surface [W/m^{2}K]
3. h_{co2}: parameter 2 of convective heat transfer coefficient on external surface [Ws/m^{3}K]

4. h_{ro}: radiative heat transfer coefficient on external surface [W/m^{2}K]
5. $F_{wall-sky}$: View factor from wall to sky
6. n: number of layers conforming the wall
7. e_x: thickness of layer x [m]
8. λ_x: thermal conductivity of layer x [W/mK]
9. ρ_x: density of layer x [kg/m^3]
10. $c_{p\,x}$: heat capacity of layer x [J/kgK]

For WALLG:

1. h_{ci}: convective heat transfer coefficient on internal surface [W/m^{2}K]
2. n: number of layers conforming the wall
3. e_x: thickness of layer x [m]
4. λ_x: thermal conductivity of layer x [W/mK]
5. ρ_x: density of layer x [kg/m^3]
6. $c_{p\,x}$: heat capacity of layer x [J/kgK]
7. e_g: thickness of the ground [m]
8. λ_g: thermal conductivity of the ground [W/mK]
9. ρ_g: density of the ground [kg/m^3]
10. $c_{p\,g}$: heat capacity of the ground [J/kgK]
11. e_v: thickness of the virtual layer [m]
12. λ_v: thermal conductivity of the virtual layer [W/mK]
13. ρ_v: density of the virtual layer [kg/m^3]
14. $c_{p\,v}$: heat capacity of the virtual layer [J/kgK]

OUTPUTS

1. T_i: temperature of internal surface at the end of the time-step [°C]
2. T_o: temperature of external surface at the end of the time-step [°C]
3. $\dot{q}_{convi}$: convective heat flow from room air node to the internal surface [W/m^2]
4. $\dot{q}_{convo}$: convective heat flow from adjacent room air node to the external surface [W/m^2]

B.1.3 WINDOW block

	Inputs		Parameters
1	T_{roomi}	1	U
2	T_a	2	h_{ci}
3	T_{sky}	3	h_{co1}
4	I_g	4	h_{co2}
5	I_d	5	h_{ro}
6	g_w		
7	f_b		
8	$\dot{q}_{rad\_lwi}$		
9	w_s		

	Outputs
1	$\dot{q}_{cond}$
2	$\dot{q}_b$
3	$\dot{q}_d$
4	T_i
5	T_o
6	$\dot{q}_{convi}$

INPUTS

1. T_{roomi}: room air node temperature [°C]
2. T_a: external temperature [°C]
3. T_{sky}: sky temperature [°C]
4. I_g: global solar radiation on the window plane [W/m^2]
5. I_d: diffuse solar radiation on the window plane [W/m^2]
6. g_w: solar factor of the window at that time-step [-]
7. f_b: darkness factor of blinds and curtains at that time-step (0=transparent, 1=opaque) [-]
8. $\dot{q}_{rad\_lwi}$: specific long-wave radiation on internal window pane [W/m^2]
9. w_s: wind speed perpendicular to surface's normal [m/s]

PARAMETERS

1. U: heat transfer coefficient [W/m^{2}K]
2. h_{ci}: convective heat transfer coefficient on internal surface [W/m^{2}K]
3. h_{co1}: parameter 1 of convective heat transfer coefficient on external surface [W/m^{2}K]
4. h_{co2}: parameter 2 of convective heat transfer coefficient on external surface [Ws/m^{3}K]
5. h_{ro}: radiative heat transfer coefficient on external surface [W/m^{2}K]

OUTPUTS

1. $\dot{q}_{cond}$: heat flux through the window [W/m^2]

2. $\dot{q}_b$: beam radiation transmitted through the window [W/m^2]
3. $\dot{q}_d$: diffuse radiation transmitted through the window [W/m^2]
4. T_1: Temperature of internal surface at the end of the time-step [°C]
5. T_2: Temperature of external surface at the end of the time-step [°C]
6. $\dot{q}_{convi}$: convective heat flow from room air node to the internal window pane [W/m^2]

B.1.4 RADI block

Inputs		Parameters	
1...	T_x	1	n
		2...	A_x
		3...	ϵ_x
		2n+2	Fij file

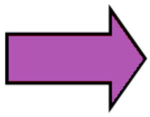

Outputs	
1...	$\dot{q}_{rad\_lwx}$

INPUTS

1. T_x: temperature of enclosing surface x [°C]

PARAMETERS

1. n: number of enclosing surfaces [-]
2. A_x: area of surface x [m^2]
3. ϵ_x: emission coefficient of surface x [-]
4. F_{ij} file: file with the view factors matrix

OUTPUTS

1. $\dot{q}_{rad\_lwx}$: specific long-wave radiation to wall x [W/m^2]

B.1.5 IRADIA block

Inputs		Parameters	
1	$\dot{q}_b$	1	n
2	$\dot{q}_d$	2...	A_x
		3...	SF_x

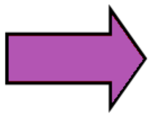

Outputs	
1...	$\dot{q}_{rad\_swx}$

INPUTS

1. $\dot{q}_b$: sum of transmitted direct solar radiation through all windows [W]
2. $\dot{q}_d$: sum of transmitted diffuse solar radiation through all windows [W]

PARAMETERS

1. n: number of surfaces that conform the room [-]
2. A_x: area of surface x [m^2]
3. SF_x: fraction of the solar radiation that arrives to surface x [-]

OUTPUTS

1. $\dot{q}_{rad\_swx}$: specific short-wave radiation to surface x [W/m^2]

B.2 DHN model

	Inputs		Parameters
1	t	1	N
2	T_g	2	E
3	Δt	3	T_{ini}
4...	$CorP_x$	4	$max_{iterations}$
5...	T_{inx}	5	$tol_{iterations}$
6...	crl_x	6	$nodesData$
		7	$edgesData$
		8	$substationsData$

	Outputs
1	$\dot{Q}_{loss}$
2	p_{critic}
3	Δt_{intern}
4...	T_{outx}
5...	$\dot{v}_x$
6...	p_x

INPUTS

1. t: second of the year when the calculation is being done [s]
2. T_g: temperature of the undisturbed surrounding soil [°C]
3. Δt: defined time-step of calculation [s]
4. $CorP_x$: Consumer or Producer for node x [-]
5. T_{inx}: supply temperature at node x [°C]
6. crl_x: control at node x [-]

For each node, a set of three inputs is defined, including $CorP_x$, T_{inx} and crl_x. $CorP_x$ informs about the nature of the node at every calculation call. It is an input because the substations connected to the nodes can see modified their status, passing from 'consumer' to 'producer' depending on external conditions. If the substations is a 'consumer', the control parameter defines the opening fraction of the substation's valve, while when the substation is a 'producer', it controls the pumping flow.

PARAMETERS

1. N: total number of nodes [-]
2. E: total number of edges [-]
3. $max_{iterations}$: maximum number of iterations allowed for solving the non-linear equations system [-]
4. $tol_{iterations}$: tolerance allowed for solving the non-linear equations system [-]
5. $nodesData$: file with the required information about the nodes
6. $edgesData$: file with the required information about the edges
7. $substationsData$: file with the required information about the substations

The *nodesData* file contains the coordinates of the nodes. The *edgesData* file defines which nodes are connected through each pipe, together with hydraulic and thermal parameters such as diameter [m], roughness [m], and heat transfer coefficient [W/mK]. Finally, the *substationsData* file defines the parameters of the substations when they perform as a 'consumer' (the flow coefficient of the valve [m^3/h], the pressure losses in the heat exchanger [$m/(m^3/s)^2$]) or as a 'producer' (parameters to define the pump's performance curve and pressure losses in the heat exchanger [$m/(m^3/s)^2$]). In appendix D the format of the three input files of SpHeat can be found.

OUTPUTS

1. $\dot{Q}$: total heat losses to the surrounding soil [Wh]
2. p_{critic}: critical pressure difference in the network (minimum pressure of all models) [Pa]
3. Δt_{intern}: time-step of calculation internally assigned [s]
4. T_{outx}: return temperature at node x [°C]
5. $\dot{v}_x$: flow at node x [m^3/s]
6. p_x: pressure difference at node x [Pa]

The model offers two possibilities to obtain the time-step length (Δt_{intern}), either it is externally provided by the user through input 3. Or if this input is negative or zero, then the model calculates internally the minimum Δt that ensures the convergence of the equations system, accounting on the velocity and the length of all pipes:

$$\Delta t_{intern} = \min \left(\frac{L_{pipe}}{\dot{v}_{pipe}} \right) \tag{B.1}$$

B.3 Solar system model

B.3.1 SCDYN block

Computational model

	Inputs		Parameters
1	T_{in}	1	A_a
2	$\dot{m}$	2	η_0
3	I_b	3	a_1
4	I_d	4	a_2
5	T_a	5	k_θ
6	θ	6	C_{coll}
7	t	7	c_p
		8	N_s
		9	N_p
		10	$T_{m,0}$
		11	N_{seg}

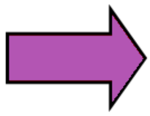

	Outputs
1	T'_{out}
2	T'_m
3	$\dot{Q}_u$
4	η

INPUTS

1. T_{in}: temperature at inlet [°C]
2. $\dot{m}_{tot}$: total mass flow [kg/s]
3. I_b: beam radiation on collector area [W/m^2]
4. I_d: diffuse radiation on collector area [W/m^2]
5. T_a: ambient temperature [°C]
6. θ: incidence angle of beam radiation [°]
7. t: second of the year when the calculation is being done [s]

PARAMETERS

1. A: aperture area per collector [m^2]

2. η_0: optical efficiency [-]
3. a_1: linear heat loss coefficient [W/m^{2}K]
4. a_2: quadratic heat loss coefficient [W/m^{2}K^2]
5. k_θ incidence angle modifier [-]
6. C_{coll}: thermal capacity of the collector [J/m^{2}K]
7. c_p: heat capacity of the thermal carrier [J/kgK]
8. N_s: number of collectors in series [-]
9. N_p: number of collectors in parallel [-]
10. $T_{m,0}$: initial mean temperature of the collector [°C]
11. N_{seg}:: number of partition elements per collector [-]

OUTPUTS

1. T'_{out}: outlet temperature at the end off the time-step [°C]
2. T'_m: mean temperature at the end off the time-step [°C]
3. $\dot{Q}_u$: heat absorbed by the thermal carrier [W]
4. η: global collector efficiency [-]

B.3.2 Storage Tank: TANKST block

Computational model

	Inputs		Parameters
1	T_{hot}	1	V
2	$\dot{m}_{hot}$	2	N
3	T_{cold}	3	d
4	$\dot{m}_{cold}$	4	c_p
5	T_a	5	ρ
6	t	6	U
		8	T_0

	Outputs
1	T'_1
2...	T'_2
N	T'_N

INPUTS

1. T_{hot}: temperature at top of the tank (hot) inlet [°C]
2. $\dot{m}_{hot}$: mass flow at top of the tank (hot) inlet [kg/s]
3. T_{cold}: temperature at bottom of the tank (cold) inlet [°C]
4. $\dot{m}_{cold}$: mass flow at bottom of the tank (cold) inlet [kg/s]

5. T_a: ambient temperature [°C]
6. t: second of the year when the calculation is being done [s]

PARAMETERS

1. V: tank volume [m^3]
2. N: number of nodes [-]
3. d: tank diameter [m]
4. c_p: heat capacity of the fluid [J/kgK]
5. ρ: density of the fluid [kg/m^3]
6. U: overall heat loss coefficient of the wall [W/m^2K]
7. T_0: initial tank temperature [°C]

OUTPUTS

1. T'_n: outlet temperature at node n [°C]

B.3.3 HXS block

Computational model

	Inputs		Parameters
1	$T_{hot,in}$	1	UA
2	$\dot{m}_{hot}$	2	$c_{p,hot}$
3	$T_{cold,in}$	3	$c_{p,cold}$
4	$\dot{m}_{cold}$		

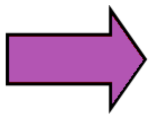

	Outputs
1	$T_{hot,out}$
2	$T_{cold,out}$
3	ε
3	$\dot{Q}$

INPUTS

1. $T_{hot,in}$: temperature at the hot inlet [°C]
2. $\dot{m}_{hot}$: mass flow at the hot inlet [kg/s]
3. $T_{cold,in}$: temperature at the cold inlet [°C]
4. $\dot{m}_{cold}$: mass flow at the cold inlet [kg/s]

PARAMETERS

1. UA: overall heat loss coefficient times the area of exchange [W/K]
2. $c_{p,hot}$: heat capacity of the hot fluid [J/kgK]
3. $c_{p,cold}$: heat capacity of the cold fluid [J/kgK]

OUTPUTS

1. $T_{hot,out}$: temperature at the hot outlet [°C]
2. $T_{cold,out}$: temperature at the cold outlet [°C]
3. ε: efficiency [-]
4. $\dot{Q}$: heat exchanged [W]

Appendix C

Building model tests

This Appendix present two other datasets used to validate the building model. The results are also provided and discussed.

C.1 VDI 6020 German Standard

The VDI 6020 German standard [204] defines a path to validate building energy models following small steps in a way that the thermal parameters and the boundary conditions for the building model tests are varied within a clearly defined sequence of tests. It also provides the results of some benchmark programs to compare with the proposed model in a similar way as in the BESTEST is done.

As presented in the standard, the following actions and reactions were tested in test examples 1 to 7:

1. Calculation of the reaction of the room air temperature to a convective internal loading.
2. Calculation of the reaction of the room air temperature to a radiant internal loading.
3. Calculation of the reaction of the heat load on the basis of a radiant internal loading and specified set value change in room air temperature.
4. Calculation of the reactions of the room air temperature at a specified internal loading and limited plant output.

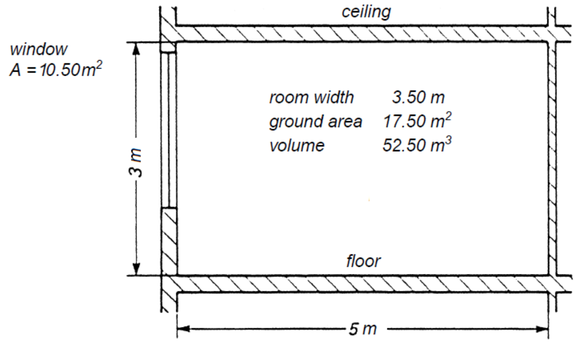

Figure C.1: Geometry of room.

C.1.1 Cases description

The 7 experiments are based on the same room geometry (Figure C.1). The physical structure and boundary conditions of each experiment are defined in Tables C.1 to C.9. The internal walls are considered adiabatic. All experiments run during sixty days (1440 hours) and their outputs in terms of internal temperatures or heat power are compared to the results of other benchmark programs in section C.1.2.

The test examples are defined as:

- Example 1: Room type S, convective internal load of 1000 W.
- Example 2: Room type S, radiant internal load of 1000 W.
- Example 3: Room type L, convective internal load of 1000 W.
- Example 4: Room type L, radiant internal load of 1000 W.
- Example 5: Room type S, mixed internal and external loads.
- Example 6: Load calculation with compliance of set values.
- Example 7: Calculation of temperature in the same conditions as in example 6, but with limited plant output.

Examples 1 to 5 have no air conditioning, the temperature is left in free-floating conditions.

C.1.2 Results and conclusions

The standard provides a collection of graphs with the results of seven tools for the days 1, 10 and 60 of the examples 1 to 5 plus one day of examples 6

	Construction	Thick. (m)	λ (W/mK)	ρ (kg/m^3)	c_p (J/kgK)
Ceiling and floor	Screed	0.03	1.4	2200	1050
	Rock wool	0.02	0.047	75	840
	Concrete	0.12	2.035	2100	920
	Air layer	-	R=0.13 m^{2}K/W	-	-
	Rock wool	0.2	0.047	75	840
	Metal ceiling	0.001	58.0	1800	480
Internal walls	Aerated concrete	0.12	0.4	1200	1050
Internal door	Aerated concrete	0.04	0.14	500	2520
External wall	Board formwork	0.01	0.14	500	2520
	Insulation	0.064	0.047	75	840
	Board formwork	0.01	0.14	500	2520

Table C.1: Opaque building components: Layer data of Room type L.

	Construction	Thick. (m)	λ (W/mK)	ρ (kg/m^3)	c_p (J/kgK)
Ceiling and floor	PVC covering	0.002	0.21	1300	1470
	Screed	0.045	1.4	2200	1050
	Rock wool	0.012	0.06	50	840
	Concrete	0.15	2.035	2400	1050
Internal walls	Cavity blocks	0.24	0.56	1300	1050
Internal door	Beech, solid	0.04	0.21	700	2520
External wall	Concrete	0.24	2.035	2100	920
	Insulation	0.062	0.047	75	840
	Façade slab	0.025	0.45	1300	1050

Table C.2: Opaque building components: Layer data of Room type S.

	Internal (W/m^{2}K)	External (W/m^{2}K)
External wall	2.7	20
Internal wall	2.7	2.7
Floor	1.67	1.67
Ceiling	1.67	1.67

Table C.3: Opaque building components: convective heat transfer coefficients.

Convective heat transfer coeff.		Glazing type	Window data			
Internal (W/m^{2}K)	External (W/m^{2}K)	%	k-value (W/m^{2}K)	g-value (%)	Frame proportion (%)	Light transmission (%)
2.7	20	6/12/6 (clear glass/air/clear glass)	2.1	75	0	81.7

Table C.4: Transparent building components.

Time (h)	Temperature (°C)	Total radiation (W/m²)	Diffuse radiation (W/m²)
1	17.3	0	0
2	16.9	0	0
3	16.1	0	0
4	16.1	0	0
5	16.8	17	17
6	18.7	38	38
7	21.8	59	59
8	23.8	98	80
9	25.8	186	99
10	27.5	287	115
11	28.6	359	125
12	29.4	385	129
13	30.0	359	125
14	30.7	287	115
15	31.0	186	99
16	31.0	98	80
17	30.5	59	59
18	29.6	38	38
19	28.1	17	17
20	25.9	0	0
21	23.5	0	0
22	22.3	0	0
23	21.4	0	0
24	20.3	0	0

Table C.5: Outside temperature and radiation data behind double glazing for example 5.

	Unit	Example 1	Example 2	Example 3	Example 4	Example 5	Example 6	Example 7
Outside temperature	°C	22	22	22	22	22	22	22
Short-wave horizontal solar radiation	W/m²	none	none	none	none	Table C.5	none	none
Long-wave ambient radiation	W/m²K	none	none	none	none		none	none
Room type		S	S	L	L	S	S	S

Table C.6: Boundary conditions.

	Unit	Example 1	Example 2	Example 3	Example 4	Example 5	Example 6	Example 7
Radiation for sun shading = close	W/m²	-	-	-	-	100	-	-
b-value	-	-	-	-	-	0.15	-	-

Table C.7: Sun shading.

	Unit	Example 1	Example 2	Example 3	Example 4	Example 5	Example 6	Example 7
Machines, convective	W	1000	-	1000	-	200	-	-
Machines, radiant	W	-	1000	-	1000	-	1000	1000
Machine operating time		6-18 h	6-18 h	6-18 h	6-18 h	8-17 h	0-24 h	0-24 h
People, convective	W	-	-	-	-	800	-	-
People, radiant	W	-	-	-	-	800	-	-
Occupation time		-	-	-	-	8-17 h	-	-

Table C.8: Internal heat sources.

	Unit	Example 6	Example 7
Plant operating time		0-24 h	0-24 h
Plant output	W	unlimited	500
Set point during office hours	°C	27	27
Set point outside office hours	°C	22	22
Office hours		6-18 h	6-18 h

Table C.9: Climatisation (purely convective air heating).

and 7 in order to compare them with those of the new model. Figures C.2 to C.8 show in yellow the results of the new model compared to those provided by the standard (in other colours).

The figures show a very good match between the model and the benchmark tool's results, kept always between the maximum and minimum values of all other results. Only experiment 5 starts slightly over the benchmark values at the central hours of the day. This deviation is not very significant, being in the same range as the differences between the results of the benchmark programs, and the temperature goes back to the mean values in days 10 and 60.
Therefore it has been considered that the results are admissible and that the building model has satisfactorily passed the example tests.

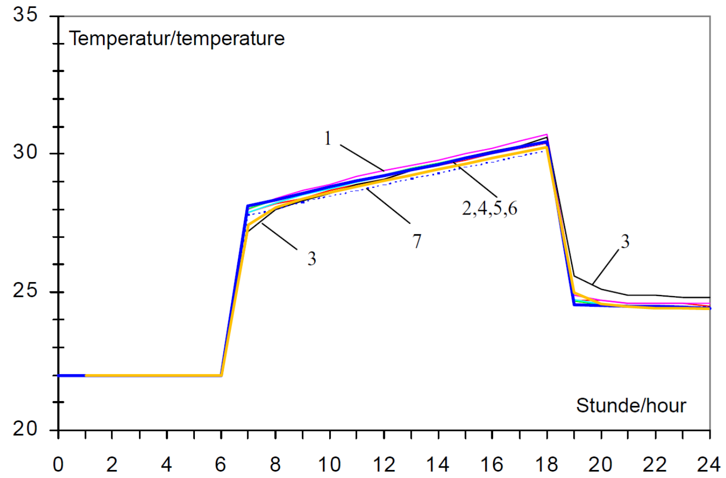

(a) Day 1

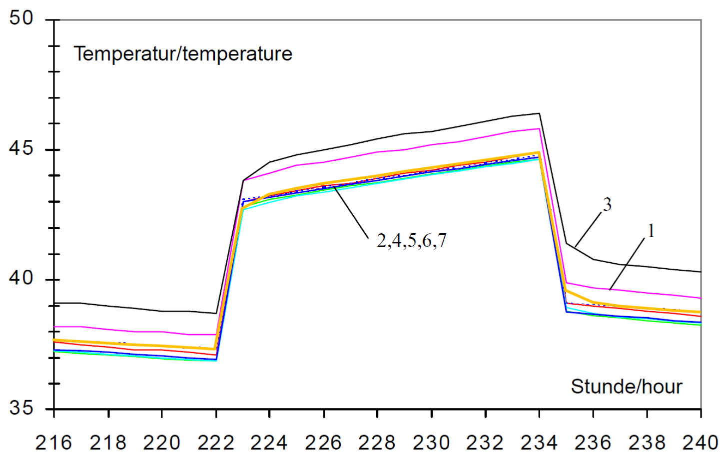

(b) Day 10

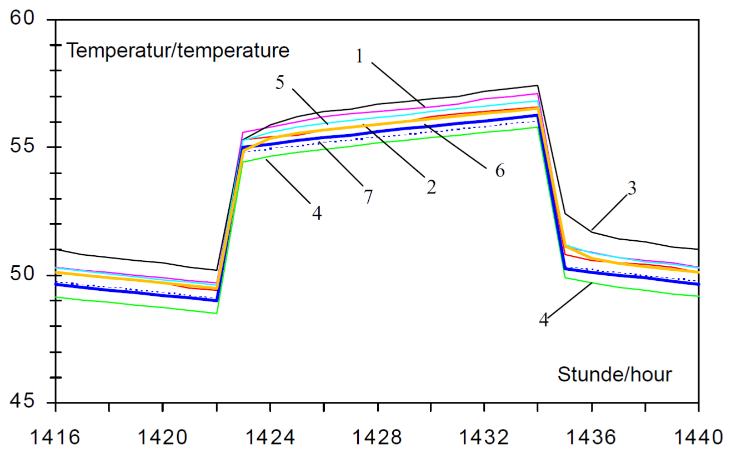

(c) Day 60

Figure C.2: Example 1. Room type S, convective internal load of 1000 W

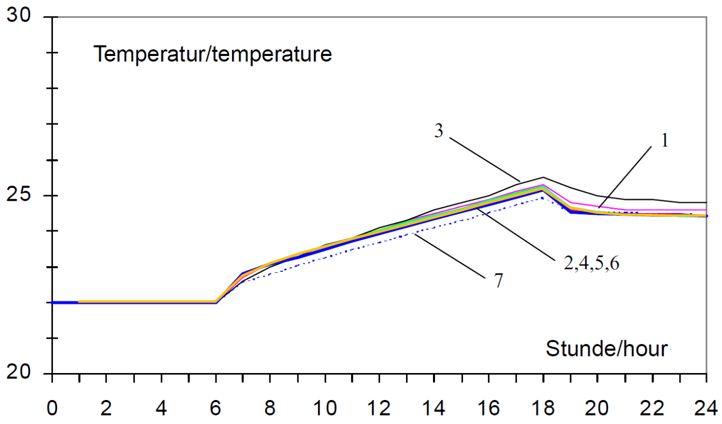

(a) Day 1

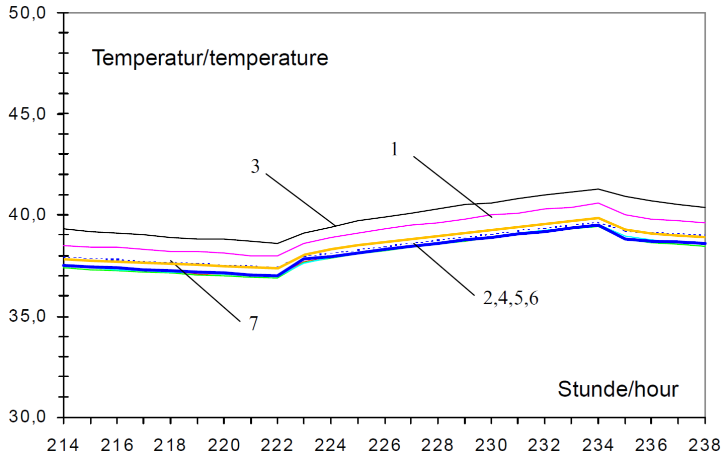

(b) Day 10

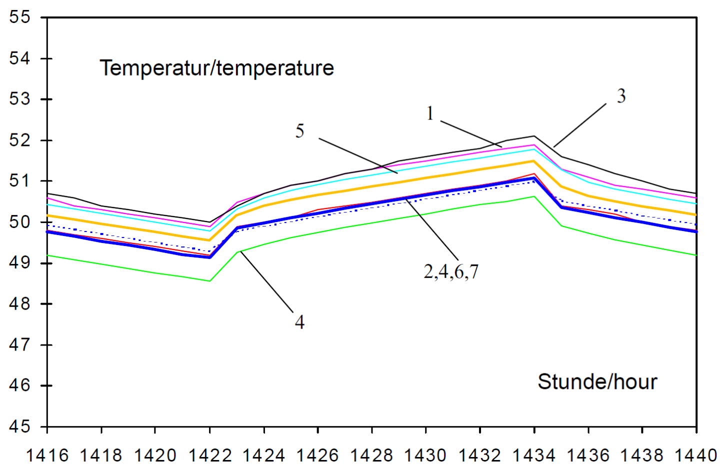

(c) Day 60

Figure C.3: Example 2. Room type S, radiant internal load of 1000 W

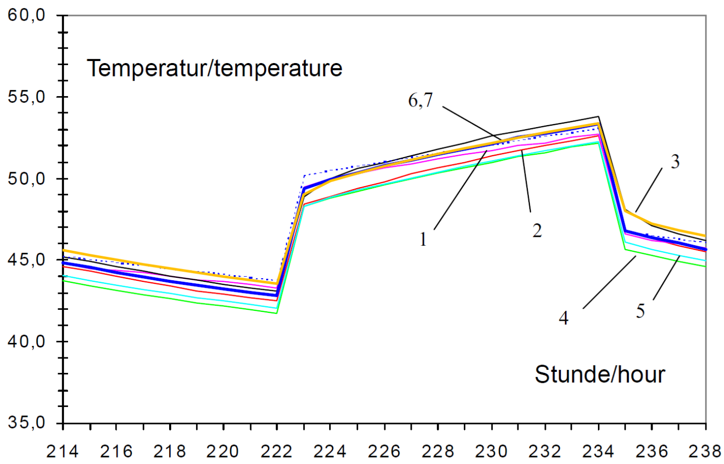

(a) Day 1

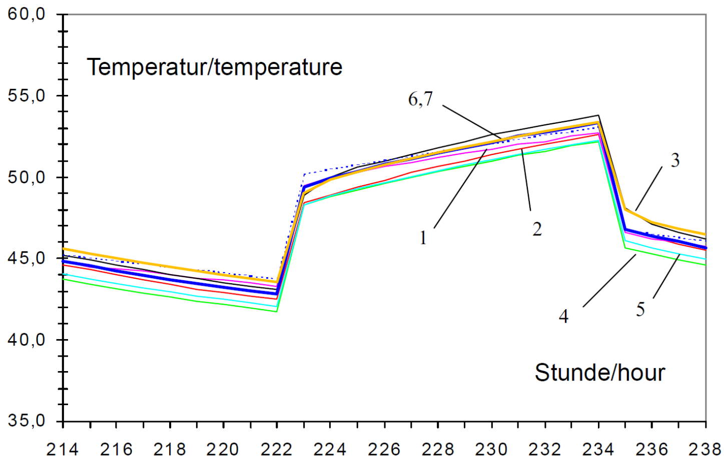

(b) Day 10

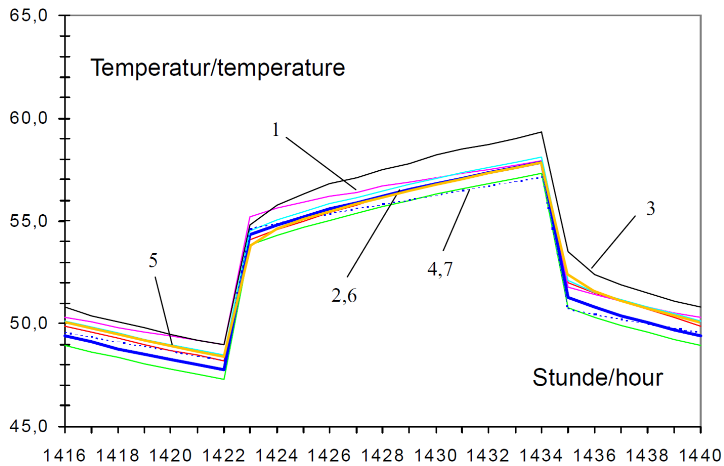

(c) Day 60

Figure C.4: Example 3. Room type L, convective internal load of 1000 W

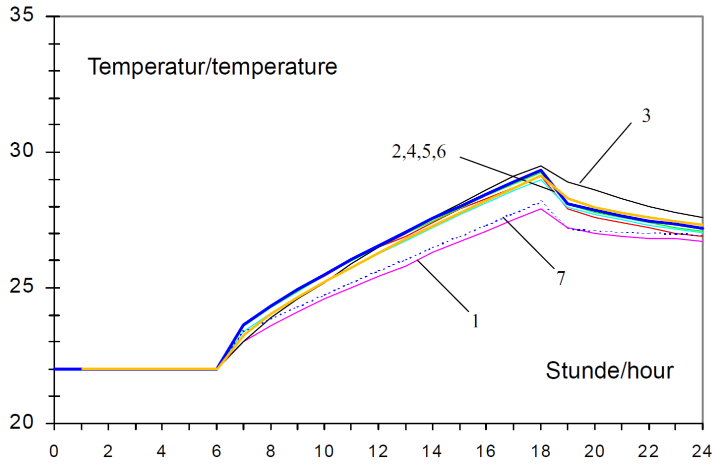

(a) Day 1

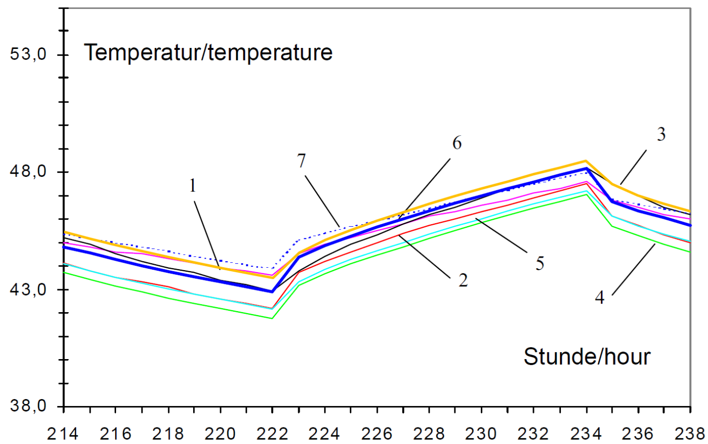

(b) Day 10

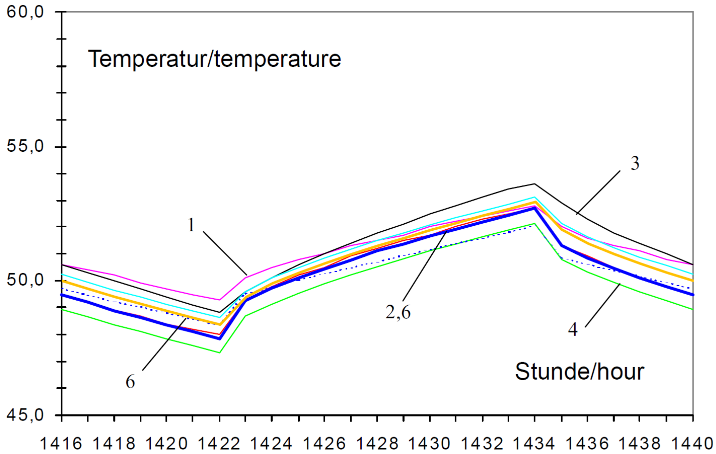

(c) Day 60

Figure C.5: Example 4. Room type L, radiant internal load of 1000 W

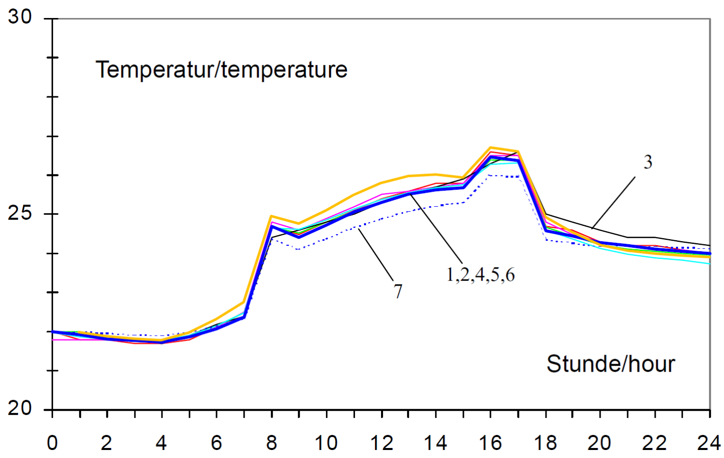

(a) Day 1

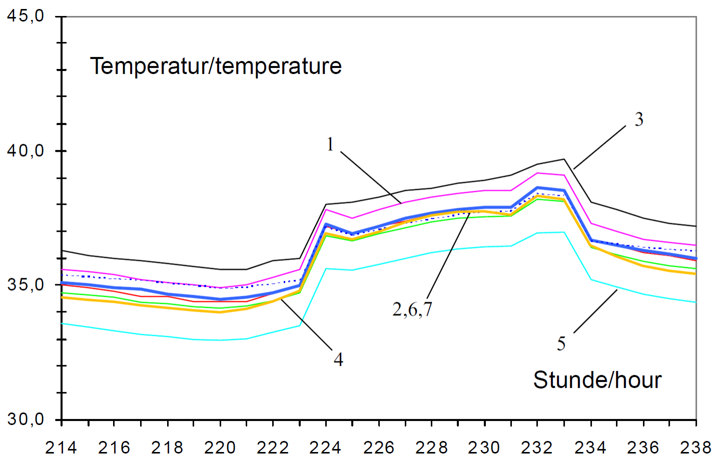

(b) Day 10

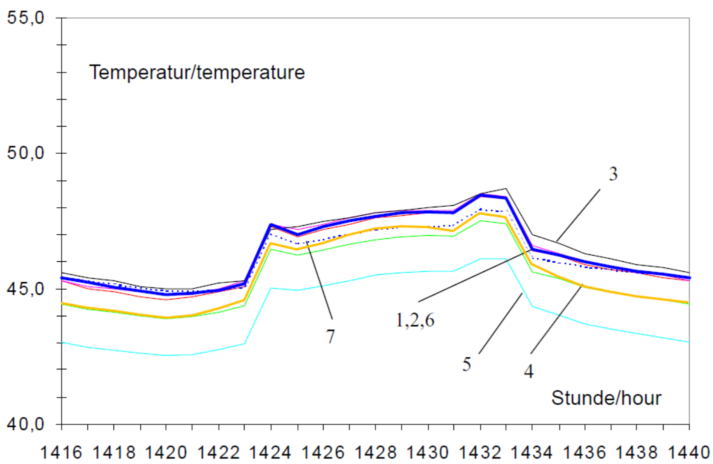

(c) Day 60

Figure C.6: Example 5. Room type S, mixed internal and external loads

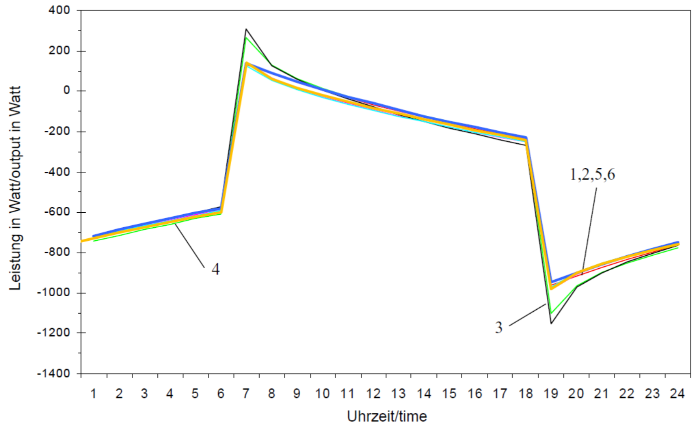

Figure C.7: Example 6. Load calculation with compliance of set values. Day 10.

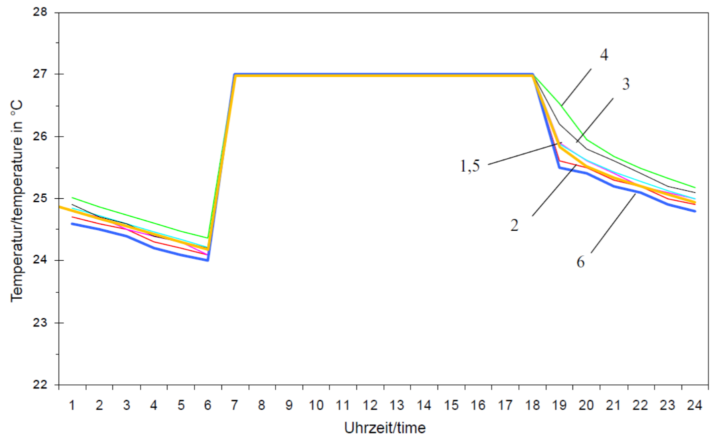

Figure C.8: Example 7. Same conditions as in example 6, but with limited plant output. Day 10

C.2 Twin Houses Experiments

Two empirical validation experiments were undertaken, based on experiments conducted on the Twin Houses at Fraunhofer IBP, Holzkirchen and involving over 20 modelling teams, including the author of this thesis. The dynamic building model was one of the models tested with the first experiment. A detailed definition of the experiments and all data required can be found in the Report of Subtask 4a of the IEA, EBC Annex 58 [21].

The first experiment was undertaken in summer 2013. It was divided into five different periods:
Period 1: Initialization phase (7 days) in which both buildings were heated to a constant temperature of 30°C to obtain identical and well-defined start conditions.
Period 2: Room air temperatures were kept constant at 30°C for 7 days with a required heating power controlled by the building management system.
Period 3: A Randomly Ordered Logarithmic Binary Sequence (ROLBS) for heat inputs into the living room was implemented, with heat injections of 0 and 500 W. This test sequence lasted for 2 weeks. All other rooms were without heating power in this period to increase the interaction between the rooms.
Period 4: A constant temperature period of 7 days was kept to re-initialize the two houses to the same state. The controlled temperature level was set at 25°C.
Period 5: In this 7-days period, there were no artificial heat injections.

Figure C.9 shows the planned schedule schematically.

The Twin Houses have seven rooms. The three facing north (Küche –room 2–, Flur –room 1– and Schlafen –room 6–) are completely isolated from the others by sealing the doors. The southern rooms (Wohnen –room 3–, Flur –room 7–, Bad WC –room 5– and Schlafen –room 4–) are fully connected. There are no doors between them and a mechanical ventilation system was installed with a supply point in the north-west corner of room 3 (red dot) and two extract points in the north-east and south-east corners of room 5 of room 4 respectively (blue dots). As the building model does not consider air exchange between thermal zones and the ventilation rate demonstrated to be very high, the last four rooms were grouped together in a single thermal zone. Therefore, a four thermal zones building model was defined.
Figure C.10(a) shows the cross section of the Twin Houses and the simplifica-

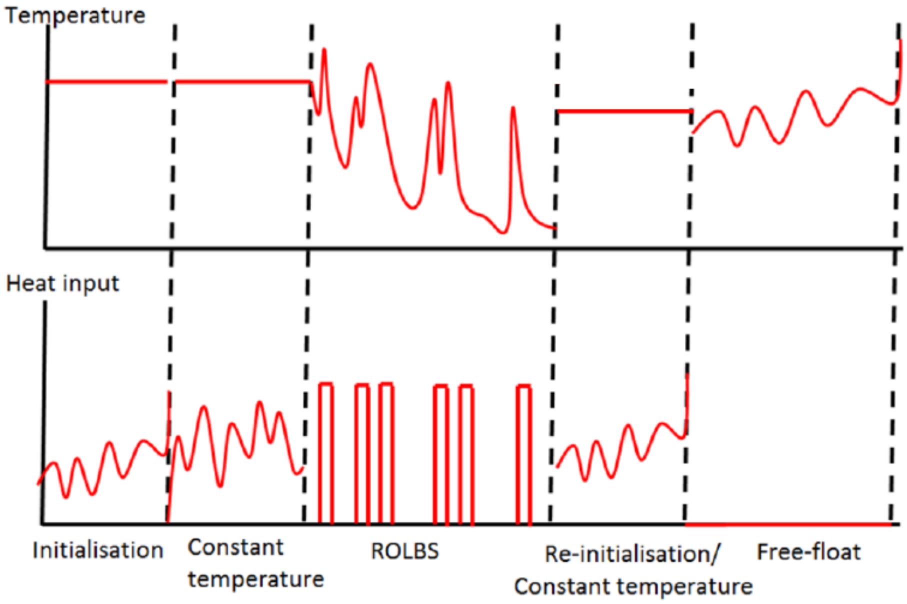

Figure C.9: Schematic of test schedule. Source [21]

tion carried out in the model. In Figure C.10(b) a front view from south-west can be observed.

To compare the results of the jointed southern room, the mean temperature of rooms 3, 4, 5 and 7 has been used.

[21] also describes how the temperature sensors placed in room 3 at three different heights show an stratification of the temperatures inside the rooms from floor (67 cm height) to ceiling (187 cm height) of about 1.5°C at steady-state and around 2.5°C during some minutes after turning on the heating system. Therefore, an uncertainty band of 1°C at steady-state has been

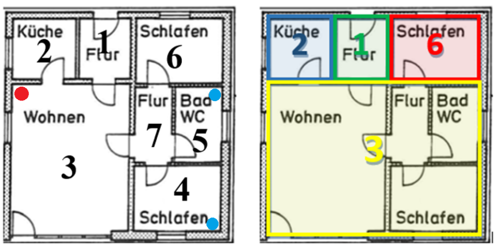

(a) Cross section of Twin house.

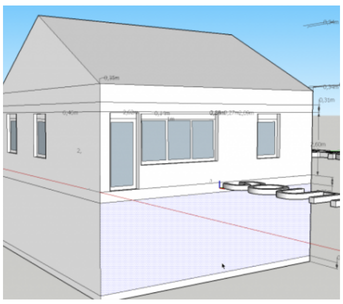

(b) 3D view of Twin house.

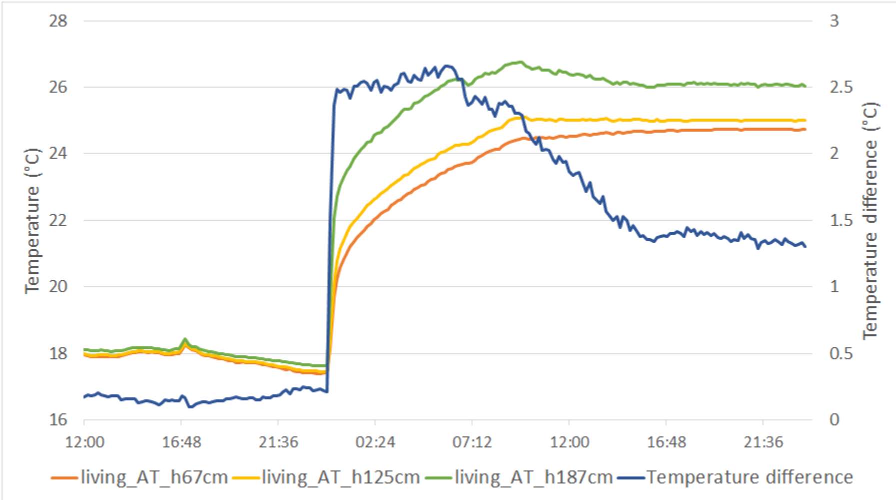

Figure C.10: Temperatures at different heights in the leaving room.

considered a good estimation of the mean temperatures, while the band just after the ignition of the heater increases to 2°C (see Figure C.10).

The temperature and temperature errors measured in °C can be seen in Figures C.11, C.12, C.13 and C.14, presenting a good agreement most of the time. A special moment must be commented, when around hour 580 the heaters turn on after a free-floating period, where the errors become much higher than expected.

Nevertheless, when comparing the results with the other simulation model results provided in the cited report [21], the model presented in this paper (Sim 24 in the report) seems to be amongst the best in temperature magnitude and total heat, while the temperature shape suggests deeper studies (see Figure C.15).

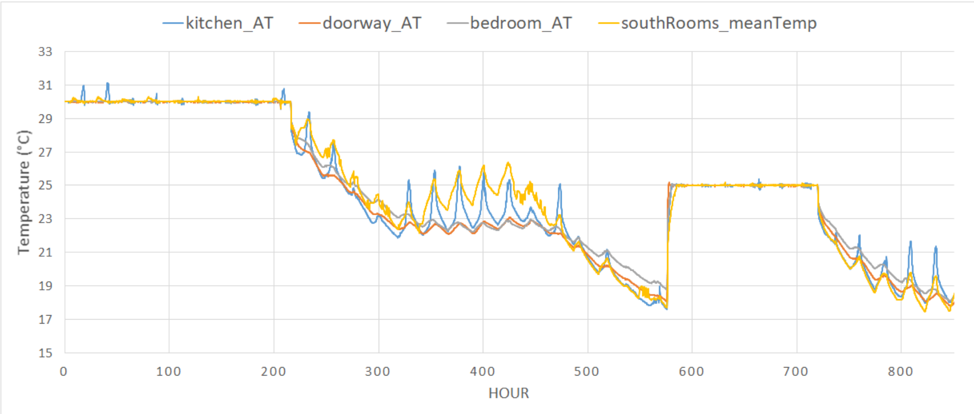

Figure C.11: Temperature blinds down.

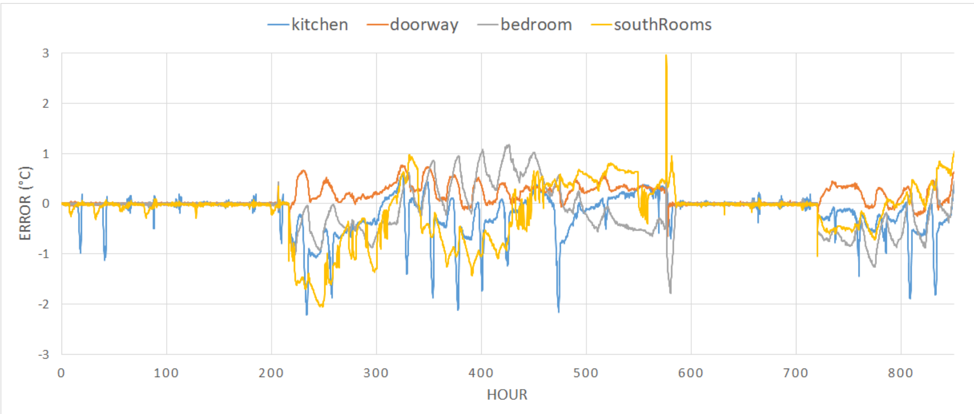

Figure C.12: Temperature errors blinds down.

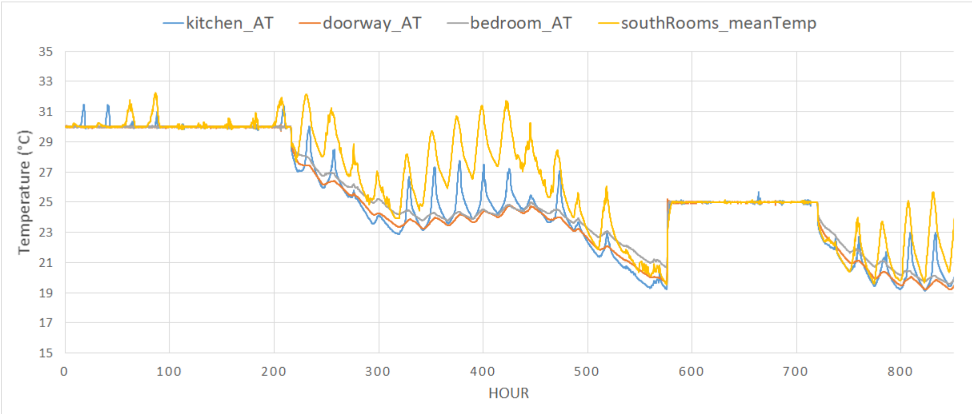

Figure C.13: Temperature blinds up.

Figure C.14: Temperature errors blinds up.

Rank	Temperature Magnitude	Temperature Shape	Total heat
1	Sim 23	Sim 23	Sim 2
2	Sim 11	Sim 11	Sim 11
3	Sim 2	Sim 2	Sim 22
4	Sim 7	Sim 10	Sim 3
5	Sim 10	Sim 19	Sim 24
6	Sim 16	Sim 7	Sim 6
7	Sim 24	Sim 22	Sim 5
8	Sim 5	Sim 4	Sim 8
9	Sim 20	Sim 1	Sim 4
10	Sim 21	Sim 3	Sim 19
11	Sim 18	Sim 20	Sim 7
12	Sim 3	Sim 21	Sim 16
13	Sim 1	Sim 6	Sim 10
14	Sim 4	Sim 24	Sim 21
15	Sim 6	Sim 16	Sim 23
16	Sim 22	Sim 5	Sim 18
17	Sim 19	Sim 18	Sim 1
18	Sim 8	Sim 8	Sim 20

Figure C.15: Rank order of simulation predictions against measured data for various metrics. Source [21]

Appendix D

Format files for SpHeat parameters

The SpHeat model needs three different sets of parameters that define the network and its connections:

1. nodes.txt
2. edges.txt
3. stations.txt

D.1 nodes.txt

It defines the geometrical position of the nodes that conform the model. The reference node can be placed anywhere and each other node must be defined by the 3 coordinates measured in meters. The order of the nodes is also irrelevant.

For example, the distribution of nodes in graph D.1 should be saved as a .txt file to be loaded from the SpHeat block following the format showed in Figure D.2.

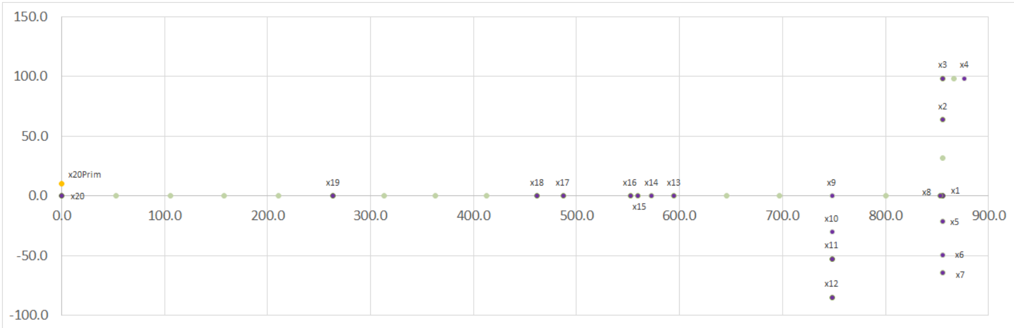

Figure D.1: Nodes distribution.

Nodes

NodeID	relative coordinates [m] X	Y	Z
1	855.8	0.0	0.0
2	0.0	0.0	0.0
3	263.6	0.0	0.0
4	461.8	0.0	0.0
5	486.9	0.0	0.0
6	552.3	0.0	0.0
7	559.2	0.0	0.0
8	572.9	0.0	0.0
9	594.7	0.0	0.0
10	747.9	0.0	0.0
11	747.9	-30.3	0.0
12	747.9	-52.6	0.0
13	747.9	-84.9	0.0
14	852.8	0.0	0.0
15	855.8	63.6	0.0
16	855.8	98.2	0.0
17	876.4	98.2	0.0
18	855.8	-21.6	0.0
19	855.8	-64.5	0.0
20	855.8	-49.6	0.0
21	0.0	10.0	0.0
22	52.724	0.0	0.0
23	105.448	0.0	0.0
24	158.172	0.0	0.0
25	210.896	0.0	0.0
26	313.175	0.0	0.0
27	362.73	0.0	0.0
28	412.285	0.0	0.0
29	645.77	0.0	0.0
30	696.85	0.0	0.0
31	800.35	0.0	0.0
32	866.1	98.2	0.0
33	855.8	31.8	0.0

Figure D.2: Example of nodes.txt.

Pipes	Network main pipes		hydraulic		thermal	
			mountings etc.	thermal	resistance (alternativ)	
PipeID	SourceNode	TargetNode	diameter [m]	roughness [m]	Kadd [m/(m³/s)²]	heat transfer coef UA[W/m²K]
1	1	33	0.1022	0.0000015	0	0.5
2	15	16	0.1022	0.0000015	0	0.5
3	16	32	0.0736	0.0000015	0	0.5
4	1	18	0.1308	0.0000015	0	0.5
5	18	20	0.1022	0.0000015	0	0.5
6	20	19	0.0614	0.0000015	0	0.5
7	1	14	0.2578	0.0000015	0	0.5
8	14	31	0.2578	0.0000015	0	0.5
9	10	11	0.0736	0.0000015	0	0.5
10	11	12	0.0736	0.0000015	0	0.5
11	12	13	0.0736	0.0000015	0	0.5
12	10	30	0.2578	0.0000015	0	0.5
13	9	8	0.2578	0.0000015	0	0.5
14	8	7	0.2578	0.0000015	0	0.5
15	7	6	0.2578	0.0000015	0	0.5
16	6	5	0.2046	0.0000015	0	0.5
17	5	4	0.2046	0.0000015	0	0.5
18	4	28	0.1636	0.0000015	0	0.5
19	3	25	0.1308	0.0000015	0	0.5
20	2	21	0.2578	0.0000015	0	0.5
21	28	27	0.1636	0.0000015	0	0.5
22	27	26	0.1636	0.0000015	0	0.5
23	26	3	0.1636	0.0000015	0	0.5
24	25	24	0.1308	0.0000015	0	0.5
25	24	23	0.1308	0.0000015	0	0.5
26	23	22	0.1308	0.0000015	0	0.5
27	22	2	0.1308	0.0000015	0	0.5
28	30	29	0.2578	0.0000015	0	0.5
29	29	9	0.2578	0.0000015	0	0.5
30	31	10	0.2578	0.0000015	0	0.5
31	32	17	0.0736	0.0000015	0	0.5
32	33	15	0.1022	0.0000015	0	0.5

Figure D.3: Example of edges.txt.

D.2 edges.txt

The file edges.txt defines the pipes as connexion between two of the nodes defined in nodes.txt and with some physical parameters as presented in Figure D.3.

The first three columns of the file must be: the number of the pipe and the numbers of the two nodes that the pipe connects. Then, in this order, the internal diameter [m], the internal roughness [m], the coefficient of pressure losses $[m/(m^2s)^2]$ of any component that may be found along the pipe (e.g. valves), and finally the linear heat losses [W/mK].

D.3 stations.txt

The file stations.txt provides the block with the required parameters of the substations. The file is divided in three parts, the number of the station and the node where it is connected (the first two columns), the parameters needed if the substations operates as a 'consumer' (next 5 columns) and those required if it operates as a ‘producer’ (the rest). An example is presented in Figure D.4.

The parameters related to the ‘consumer’ are, in this order, the coefficient of pressure losses $[\mathrm{m}/(\mathrm{m}^2/\mathrm{s})^2]$ of the valve, the internal diameter [m], internal roughness [m] and length [m] of the service pipe and the coefficient of pressure losses $[\mathrm{m}/(\mathrm{m}^2/\mathrm{s})^2]$ of the heat exchanger.

Those related to the ‘producer’ are, instead, the six parameters (a set of three points that relate head losses [m] with volume flow $[\mathrm{m}^3/\mathrm{s}]$) that define the pump curve and finally, the coefficient of pressure losses $[\mathrm{m}/(\mathrm{m}^2/\mathrm{s})^2]$ of the heat exchanger.

		consumer data				producer data								
		control valve	consumer pipe			HX	pump					HX	thermal	
Station	ID	Node ID Kvs [m^3/h]		diam [m]	rough [m]		length [m]	Khx [m/(m^3/s)^2]		hp1 [m] Q1 [m^3/s]		hp2 [m] Q2 [m^3/s]		hp3 [m] Q3 [m^3/s] Khx [m/(m^3/s)^2]
1	2	14.6152888	0.5	0.0000015	6	8.09E+04	21	0	20	0.000273333	15	0.000546666	8.09E+04	
2	3	3.42928564	0.5	0.0000015	28.37	1.47E+06	21	0	20	0.000273333	15	0.000546666	1.47E+06	
3	4	1.469693846	0.5	0.0000015	4.77	8.00E+06	21	0	20	0.000273333	15	0.000546666	8.00E+06	
4	5	17.1464282	0.5	0.0000015	6.95	5.88E+04	21	0	20	0.000273333	15	0.000546666	5.88E+04	
5	6	1.796292478	0.5	0.0000015	24.54	5.36E+06	21	0	20	0.000273333	15	0.000546666	5.36E+06	
6	7	8.654863758	0.5	0.0000015	7.58	2.31E+05	21	0	20	0.000273333	15	0.000546666	2.31E+05	
7	8	2.016746555	0.5	0.0000015	13.74	4.25E+06	21	0	20	0.000273333	15	0.000546666	4.25E+06	
8	9	2.98021252	0.5	0.0000015	16.02	1.95E+06	21	0	20	0.000273333	15	0.000546666	1.95E+06	
9	10	9.797958971	0.5	0.0000015	17.82	1.80E+05	21	0	20	0.000273333	15	0.000546666	1.80E+05	
10	11	1.992251657	0.5	0.0000015	18.49	4.35E+06	21	0	20	0.000273333	15	0.000546666	4.35E+06	
11	12	7.96900663	0.5	0.0000015	6	2.72E+05	21	0	20	0.000273333	15	0.000546666	2.72E+05	
12	13	5.307227776	0.5	0.0000015	32.35	6.13E+05	21	0	20	0.000273333	15	0.000546666	6.13E+05	
13	14	4.588710785	0.5	0.0000015	6.18	8.21E+05	21	0	20	0.000273333	15	0.000546666	8.21E+05	
14	15	2.31885029	0.5	0.0000015	6	3.21E+06	21	0	20	0.000273333	15	0.000546666	3.21E+06	
15	16	3.576255024	0.5	0.0000015	15.75	1.35E+06	21	0	20	0.000273333	15	0.000546666	1.35E+06	
16	17	1.61666323	0.5	0.0000015	24.44	6.61E+06	21	0	20	0.000273333	15	0.000546666	6.61E+06	
17	18	4.498896161	0.5	0.0000015	1	8.54E+05	21	0	20	0.000273333	15	0.000546666	8.54E+05	
18	19	2.37600505	0.5	0.0000015	6	3.06E+06	21	0	20	0.000273333	15	0.000546666	3.06E+06	
19	20	2.188210837	0.5	0.0000015	27	3.61E+06	21	0	20	0.000273333	15	0.000546666	3.61E+06	
20	1	98.33884821	0.5	0.0000015	1	1.79E+03	21	0	20	0.041	15	0.082	1.79E+03	
21	21	9.797958971	0.5	0.0000015	1	1.79E+05	0	0	0	0	0	0	1.79E+05	
22	22	7.071067812	0.5	0.0000015	1	0.00E+00	0	0	0	0	0	0	0.00E+00	
23	23	7.071067812	0.5	0.0000015	1	0.00E+00	0	0	0	0	0	0	0.00E+00	
24	24	7.071067812	0.5	0.0000015	1	0.00E+00	0	0	0	0	0	0	0.00E+00	
25	25	7.071067812	0.5	0.0000015	1	0.00E+00	0	0	0	0	0	0	0.00E+00	
26	26	7.071067812	0.5	0.0000015	1	0.00E+00	0	0	0	0	0	0	0.00E+00	
27	27	7.071067812	0.5	0.0000015	1	0.00E+00	0	0	0	0	0	0	0.00E+00	
28	28	7.071067812	0.5	0.0000015	1	0.00E+00	0	0	0	0	0	0	0.00E+00	
29	29	7.071067812	0.5	0.0000015	1	0.00E+00	0	0	0	0	0	0	0.00E+00	
30	30	7.071067812	0.5	0.0000015	1	0.00E+00	0	0	0	0	0	0	0.00E+00	
31	31	7.071067812	0.5	0.0000015	1	0.00E+00	0	0	0	0	0	0	0.00E+00	
32	32	7.071067812	0.5	0.0000015	1	0.00E+00	0	0	0	0	0	0	0.00E+00	
33	33	7.071067812	0.5	0.0000015	1	0.00E+00	0	0	0	0	0	0	0.00E+00	

Figure D.4: Example of stations.txt.

Appendix E

Published papers

E.1 Dynamic simulation methodologies for urban energy demand

Peer-review under responsibility of the CENTRO CONGRESSI INTERNAZIONALE SRL

E.2 Energy performance of decentralized solar thermal feed-in to district heating networks

Peer-review under responsibility of the Scientific Committee of The 15th International Symposium on District Heating and Cooling

E.3 The effect of discretization on the accuracy of two district heating network models based on finite-difference methods

Peer-review under responsibility of the Scientific Committee of The 16th International Symposium on District Heating and Cooling.

Available online at www.sciencedirect.com

ScienceDirect

Energy Procedia 78 (2015) 3360 – 3365

Energy Procedia

6th International Building Physics Conference, IBPC 2015

Dynamic simulation methodologies for urban energy demand

Pilar Monsalvete[a]*, Darren Robinson[b], Ursula Eicker[a]

[a]HfT-Stuttgart, Centre of Applied Research Sustainable Energy Technologies, zafh.net, Schellingstr.24, 70174 Stuttgart, Germany
[b]University of Nottingham, University Park, Nottingham, NG7 2RD, United Kingdom

Abstract

This paper presents a new dynamic physical energy model of building for simulating the energy demand of cities. Firstly, a justification it is given regarding the necessity of a new building model and the advantages of using modular building simulation when dealing with large numbers of buildings in an urban context. The main motivation was a flexible and very modular interaction of 3D urban geometry description with the CityGML data format and energy related attributes for building parts.
The paper then presents the modular dynamic building model and its validation with a real case of study for single buildings.
The model integration into an urban modeling platform named SimStadt is explained with the necessary input data for a city heat demand calculation.

Peer-review under responsibility of the CENTRO CONGRESSI INTERNAZIONALE SRL

Keywords: Building modelling; dynamic simulation; cityGML; modular building simulation

1. Introduction

The energy consumption in the building sector for heating and cooling worldwide amounts to more than one third of the total [1], where the building stock certainly plays the most important role.

Many people are therefore working on how to improve building energy systems' efficiency and how to reduce the use of conventional energy resources and CO_2 emissions. One trend is increase network based energy distribution systems instead of individual supply for each building.

* Corresponding author. Tel.: +49-711-8926-2339.
E-mail address: pilar.monsalvete@hft-stuttgart.de

Peer-review under responsibility of the CENTRO CONGRESSI INTERNAZIONALE SRL
doi:10.1016/j.egypro.2015.11.751

Understanding urban energy consumption is vital to address energy issues and climate change. The simulation of urban energy consumption linked with the energy supply systems is an appropriate way of improving this understanding. The calculus of each individual building´s demand inside the urban zone can strongly support this analysis.

Many different models have been developed and implemented in software tools to estimate the energy consumption in buildings using either statistical or physical methods [2]. The nodal method, a physical method used to determinate the total energy consumption or the average indoor temperature and the cooling or heating load, has some interesting advantages as it is capable to calculate multiple zone buildings in a reasonable computation time with an easy implementation; the big drawback is that it is really difficult to study large volume systems [3]. In fact, a common problem found for most of the software is the limited data availability and how tedious is to set the parameters in the model, which in most cases means the highest time consumption [4,5,6]. This gets even worse when trying to calculate the urban energy demand that comprises several hundreds of buildings. Therefore, a new method to easy calculate urban energy demand is required.

In this paper, a modular physical building model is presented. The modularity of the physical model makes it very easy to connect it with urban geometry data models in the CityGML standard [7]. The urban simulation platform SimStadt developed by the authors [8] now allows the automation of the definition and parameter setting of the building model. Thus, a significant amount of time and effort is saved. Moreover, automation reduces errors and mismatches in the whole process. The definition of a large amount of buildings is then much easier to do.

2. The modular physical building model

2.1. Methodology

The building physical model has been developed in INSEL8 [9] using different blocks to define the thermal behavior of the building components in the most modular way. The main features of the building simulation blocks are the following:

- Room air block: calculates a one node air temperature in the room or the cooling and heating demand, taking into account all internal gains, the air exchange rate and the convective exchange with the surfaces using the energy balance and an explicit numerical solution.
- Internal and external walls: the Finite-Difference Approximation Method [10] is used to calculate the temperature profiles throughout the walls as well as the surface temperature of both sides of the wall on each time step as function of the energy fluxes from convection and short and longwave radiation.
  The temperature within the material is calculated in the boundary nodes separating layers with the stability criterium adjusting the time step for given layer thicknesses. Finally, the convective heat exchange with the room air temperature node is calculated following the Newton's law of cooling.
- Windows: are treated as the walls for the calculus of the heat transfer, and includes the calculus of the short wave radiation that passes through it using the angle dependent total energy transmission 'g-factor.
- Internal long wave radiant heat exchange between walls: calculates the radiant heat exchange between the surfaces depending on their temperature and the form factors. The form factors are numerically calculated in the block dividing the surfaces in small pieces.
- Internal distribution of solar radiation through the windows: assigns a fraction of the radiation that enters the room to each surface.
- The effect of the urban shape on the radiation that reaches the building is not calculated in the building physical model but obtained from the 3D city model geometry pre-processing. Shading time series and other climatic data (temperature, wind speed or wind direction) are as well inputs to the building physical model.
- The internal gains are also considered as inputs for the physical model, provided by the Building Physics and Usage Preprocessor.

By dividing the building physical model in this separate elements (blocks), the connection with the cityGML data model can be done quasi-directly. Thus, the assignment of the parameters and inputs of each block can be done automatically.

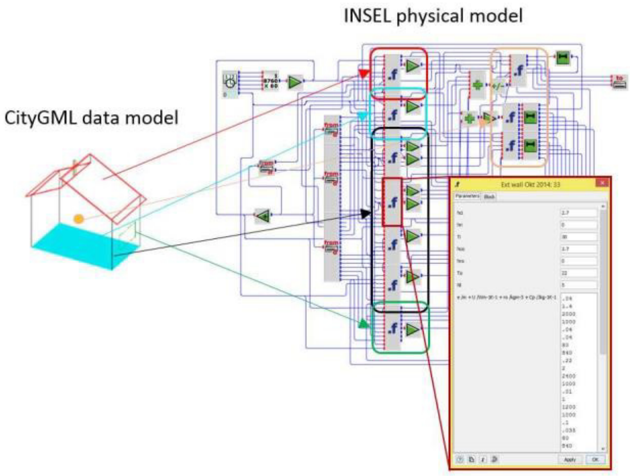

Fig. 1. Example of parameters in a one-zone building model

The next table shows the correspondence of the elements of both, the data model and the physical model.

Table 1. Correspondence from objects of the Data model to elements of the Physical model

Physical model	Data model
Room air	ThermalZone + UsageZone
Internal long wave radiant heat exchange between walls	ThermalZone
Internal distribution of solar radiation through the windows	ThermalZone
Wall	ThermalBoundarySurface
Window	ThermalBoundarySurface

2.2. Validation of the physical model

To ensure the good results provided by the physical model, a comprehensive full-scale building experiment carried out within the scope of IEA Annex 58 subtask 4, at the Fraunhofer test site (Holzkirchen, Germany) was used to test it. This experiment was undertaken on two buildings with identical constructions, the so called Twin Houses N2 and O5 in Holzkirchen, Germany.

The experiment, conducted in August and September 2013 was a side-by-side experiment, with external roller blinds down on the south facing windows of one building (N2) and fully up on the other (O5). A high mechanical ventilation rate was used. For the heating system, just electric convector heaters were used.

The twin houses have seven rooms. The three facing North [Küche (room 2), Flur (room 1) and Schlafen (room 6)] are completely isolated from the others by sealing the doors. The Southern rooms [Wohnen (room 3), Flur (room 7), Bad WC (room 5) and Schlafen (room 4)] are fully connected. There are no doors between them and a mechanical ventilation was installed with a supply point in the north-west corner of room 3 and two extract points in the south-east corners of the rooms 4 and 5 respectively. Therefore, a four room building model was defined.

Figure 1 shows the cross section of Twin houses and the simplification carried out in the model:

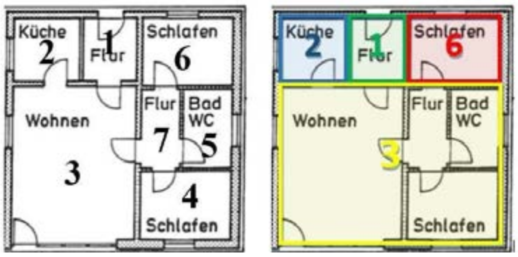

Fig. 2. Cross section of Twin house

The temperature of each room inside each house has been calculated with the building model. They have been compared with the measurements over the complete period using the same weather data and internal gains profiles provided by the authors of the experiment.

The temperature errors measured in °C for the forty days of the experiment can be seen in the following figures for both cases. To compare the results of room 3 of the model, the mean temperature of rooms 3, 4, 5 and 7 have been used.

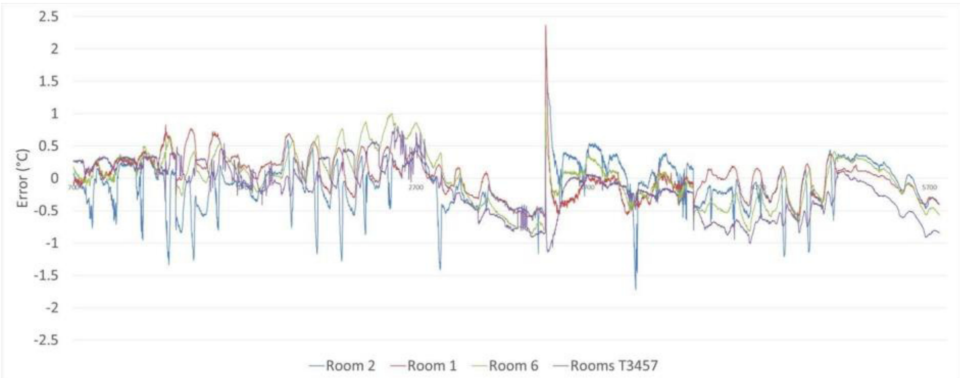

Fig. 3. Temperature errors blinds down (°C)

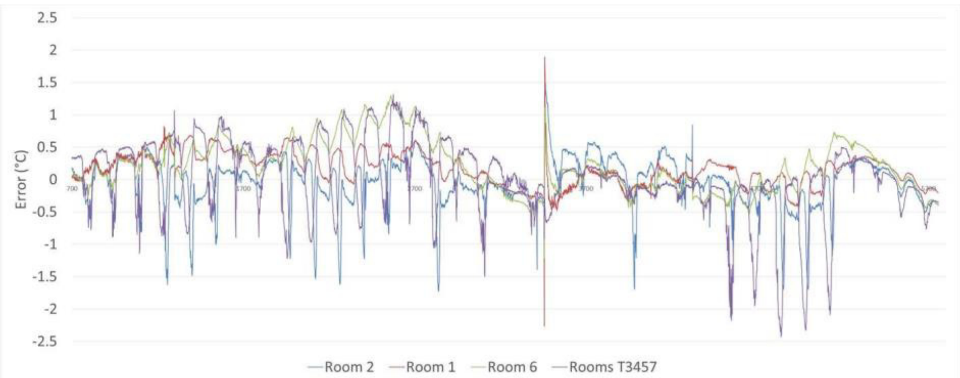

Fig. 4. Temperature errors blinds up (°C)

3. Integration in the urban simulation platform SimStadt

Once the model has been tested, it is ready to be integrated into the new urban energy simulation platform SimStadt in order to automatize the calculus of the thermal energy demand. This automation allows massive calculus of buildings.

SimStadt is being developed in the framework of a project funded by the German minister BMWi. The open format CityGML is the basis of design of SimStadt, which integrates the concept of Level of Details (LoD) of CityGML [11] and give the users the possibility to enhance the analysed virtual 3D city model, based on local building libraries and pre-processing functions. For the purpose of urban energy simulation, CityGML has been extended with an Energy Application Domain Extension (Energy ADE), developed within an international consortium of urban energy simulation and modelling experts.

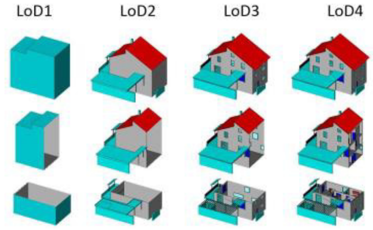

Fig. 5. Four levels of detail of CityGML (Groeger et al., 2012, page 72, Source: Karlsruhe Institute of Technology (KIT))

Another main design characteristic of SimStadt is its modular workflow-driven structure. Each workflow is built as a suite of unitary modules called workflow step, whose hypotheses, parameters and intermediary results are made explicit in the Graphical User Interface (GUI). Thus, the dynamic building model has been integrated inside a workflow as a workflow step:

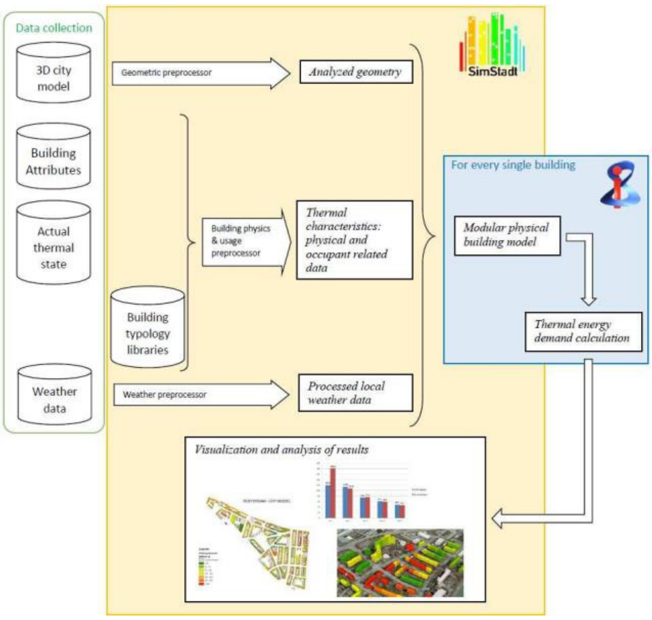

Fig. 6. Workflow schema

The dynamic energy calculation workflow starts with the pre-processing of the input data. This pre-processing is done for every single building available in the 3D city model:

- the Geometric Preprocessor, extracts the relevant geometrical information from the CityGML files, such as the volume and type of each zone, area and orientation of the boundary surfaces etc.,
- the Building Physics and Usage Preprocessor, enhances the model with physical parameters and with occupant-related parameters as occupancy schedule, set-point temperatures, air change rate etc., stored in a Building Typology Library,
- finally the Weather Preprocessor, supplies the model with weather-related values for every hour of the year, as ambient temperature, irradiation hitting each external wall (taking into account shadows), wind speed…

The second step in the workflow is the generation of a dynamic physical model for every single building. Depending on the quality of the data available, the physical model produced is also LoD2, LoD3 or LoD4. This physical model cannot be used if the LoD of the data model is lower than 2.

Then, the models are sent to INSEL, one by one, to do the calculus. Currently, the results provided by the calculus are internal temperature and thermal demand in every zone.

Finally, these results are displayed in different ways to facilitate their analysis.

4. Conclusions

A new highly modular and extremely flexible dynamic building simulation model has been developed and validated with experimental results. The main goal of the model development was to enable direct parameter transfer between 3D CityGML urban geometry data models and energy related parameters required for building simulation. This direct transfer has been successfully achieved allowing the automation of the definition of physical building models.

The physical building model adjusts to the data available in each case and automatizes the parameters setting, reducing strongly the time consumption.

The validation reported really good results, being in both cases of the IEA 58 experiment, the errors in the calculus of the internal temperature lower than 1.5°C almost always.

Acknowledgements

The authors gratefully acknowledge European Commission for providing financial support during conduct of research under FP7-PEOPLE-2013 Marie Curie Initial Training Network “CI-NERGY” project with Grant Agreement Number 606851. Pilar Monsalvete, would also like to thank Jürgen Schumacher and Romain Nouvel for their discussions and suggestions during the work. And of course, many thanks to Matthias Kersken and Ingo Heusler of Fraunhofer-Institut für Bauphysik IBP, and Paul Strachan of ESRU, University of Strathclyde for providing the experimental specification and data from the IEA Annex 58 experiments.

References

[1] Lucon O., D. Urge-Vorsatz, A. Zain Ahmed, H. Akbari, P. Bertoldi, L. F. Cabeza, N. Eyre, A. Gadgil, L. D. D. Harvey, Y. Jiang, E. Liphoto, S. Mirasgedis, S. Murakami, J. Parikh, C. Pyke, and M. V. Vilarino, 2014: Buildings. In: Climate Change 2014: Mitigation of Climate Change. Contribution of Working Group III to the Fifth Assessment Report of the Intergovernmental Panel on Climate Change [Edenhofer, O., R. Pichs-Madruga, Y. Sokona, E. Farahani, S. Kadner, K. Seyboth, A. Adler, I. Baum, S. Brunner, P. Eickemeier, B. Kriemann, J. Savolainen, S. Schlomer, C. von Stechow, T. Zwickel and J.C. Minx (eds.)]. Cambridge University Press, Cambridge, United Kingdom and New York, NY, USA.

[2] Lukas G. Swan, V. Ismet Ugursal, Modeling of end-use energy consumption in the residential sector: A review of modeling techniques, Renewable and Sustainable Energy Reviews, Volume 13, Issue 8, October 2009, Pages 1819-1835, ISSN 1364-0321.

[3] Aurélie Foucquier, Sylvain Robert, Frédéric Suard, Louis Stéphan, Arnaud Jay, State of the art in building modelling and energy performances prediction: A review, Renewable and Sustainable Energy Reviews, Volume 23, July 2013, Pages 272-288

[4] M. Kavgic, A. Mavrogianni, D. Mumovic, A. Summerfield, Z. Stevanovic, M. Djurovic-Petrovic, A review of bottom-up building stock models for energy consumption in the residential sector, Building and Environment, Volume 45, Issue 7, July 2010, Pages 1683-1697

[5] James Keirstead, Mark Jennings, Aruna Sivakumar, A review of urban energy system models: Approaches, challenges and opportunities, Renewable and Sustainable Energy Reviews, Volume 16, Issue 6, August 2012, Pages 3847-3866

[6] Pervez Hameed Shaikh, Nursyarizal Bin Mohd Nor, Perumal Nallagownden, Irraivan Elamvazuthi, Taib Ibrahim, A review on optimized control systems for building energy and comfort management of smart sustainable buildings, Renewable and Sustainable Energy Reviews, Volume 34, June 2014, Pages 409-429

[7] Gerhard Gröger, Lutz Plümer, CityGML – Interoperable semantic 3D city models, ISPRS Journal of Photogrammetry and Remote Sensing, Volume 71, July 2012, Pages 12-33, ISSN 0924-2716.

[8] SimStadt website: *http://www.simstadt.eu/en/index.html*

[9] INSEL website: *http://www.insel.eu/*

[10] Janna, William S. Engineering Heat Transfer, Second Edition. CRC Press. December 1999.

[11] Nouvel R., Schulte C., Eicker U., Pietruschka D., Coors V. CityGML-based 3D City Model for energy diagnostics and urban energy policy support. Proceedings IBPSA World. August 2013.

Available online at www.sciencedirect.com

ScienceDirect

Energy Procedia 00 (2017) 000–000

Energy Procedia

www.elsevier.com/locate/procedia

The 15th International Symposium on District Heating and Cooling

Energy performance of decentralized solar thermal feed-in to district heating networks

P. Monsalvete Álvarez de Uribarri[a]*, Ursula Eicker[a], Darren Robinson[b]

[a]University of Applied Sciences, Schellingstrasse 24, Stuttgart, 70174, Germany
[b]University of Nottingham, University Park, Nottingham, NG7 2RD, United Kingdom

Abstract

Many papers have been written over the last years addressing the potential of decentralized solar thermal systems in District Heating Networks (DHN), assuming that the network can be used as a virtual storage so that prosumers can release excess solar energy into the network and use it later when it is needed.
When looking at the district heating systems in detail, many questions still remain unanswered. Is it possible to feed in all the surplus solar energy into the net? How does the solar input affect the network and the other prosumers? Is it sensible from the energy balance perspective? We have studied an existing DHN in an attempt to answer these questions.
A simulation model of the DHN in the Southern German city quarter Ludwigsburg-Sonnenberg was developed and extended to include decentralized feed-in of heat from solar thermal collectors to evaluate their potential contribution to network demands. It could be shown that prosumers supply during summer period significantly more heat than they demand, so that the thermal network could operate as an autonomous micro-grid.
By comparing the amount of electrical pumping energy that is needed to feed heat to the DHN with usable solar thermal energy, the benefit ratio of feeding heat into the DHN can be quantified.

Peer-review under responsibility of the Scientific Committee of The 15th International Symposium on District Heating and Cooling.

Keywords: District heating; distributed solar generation; solar thermal; prosumer; excess heat

* Corresponding author. Tel.: +49-017682673226.
E-mail address: pilar.monsalvete@hft-stuttgart.de

1876-6102 © 2017 The Authors. Published by Elsevier Ltd.
Peer-review under responsibility of the Scientific Committee of The 15th International Symposium on District Heating and Cooling.

1. Introduction

The present paper forms part of a larger research project investigating the intelligent management of an existing heating network.

The main objective of this project is the simulation of the integration of distributed renewable heat sources in the existing district heating network of Ludwigsburg-Sonnenberg and its extensions.

Among other possibilities contemplated within the project, this paper studies the integration of distributed solar heat generation and local storage in the new branch of the DHN, which will be built to feed a planned extension of the district (shaded area in Fig. 1).

The new buildings to be constructed will become prosumers as they will be able to "consume" energy from the net as well as "produce" renewable energy for self-consumption or feeding into the net thanks to a solar thermal system.

Fig. 1. Urban structure planning Grünbühl/ Sonnenberg with a city extension to the South West (Source: City of Ludwigsburg)

The term "prosumer" is already used in the power sector [1],[12], and in recent years, starts to be also used in the thermal energy sector [2],[3],[9],[10],[11],[16], although we do acknowledge that this terminology is incompatible with the first law of thermodynamics.

2. Background

Some papers have been written over the last years addressing the potential of decentralized energy systems in DHN as well as some of the possible technical problems that this connection could provoke.

Excess energy has first been discussed for the industrial sector in terms of the thermal energy contribution to DHN [13],[17].

More recently the concept has been extended to the residential sector.

An interesting overview of the state of the art includes distributed solar energy in DHN in combination with seasonal storage or using heat pumps [9]. The influence of excess heat production with seasonal storage has also been analysed [14].

Others investigate the benefits of local thermal storage for direct utilisation of heat from solar collectors in a dwelling connected to a DHN, but with no injection into the net [7]; or connected and using the net as a virtual storage system [2].

The impacts of feed-in to the net have also been studied, in particular how the temperatures, pressure or flow rates and velocities can be affected by the introduction of small scale prosumers into the DHN [9].

But these past studies tend to treat the network as an ideal storage facility without constrains on capacity or dynamics, so that prosumers can release excess solar energy into the network and use it later when it is needed [2],[3],[7],[14]. This idealisation may lead to optimistic results especially for the warm seasons.

Thus, this study takes into account the possible thermal saturation of the net by simulating it together with the prosumers.

The simulation software INSEL8.2 [8] has been used to dynamically model the net thermodynamics [4], as well as the thermal (but not hydraulic) behaviour of the prosumers. The weather and the heat demand of the prosumers are considered as inputs to the model.

3. Case study and model description

Geographical area and heat demand

Ludwigsburg is a city located in Baden-Wurttemberg in the South-west of Germany. Annually, this temperate region receives around 1.2 MWh/m2 solar irradiation (Fig. 2).

The city quarter Ludwigsburg-Sonnenberg, where the new residential area extension will be built, is mainly composed of dwellings that are connected to a 1.1 km long DHN that operates between 40°C and 70°C, supplied by a cogeneration engine (235 kW thermal) and a heat pump (200 kW thermal) with vertical geothermal heat exchangers.

An existing heating network branch in Sonnenberg, close to the new area has been selected to be modelled so that the obtained solar thermal potential can be extrapolated to the new area.

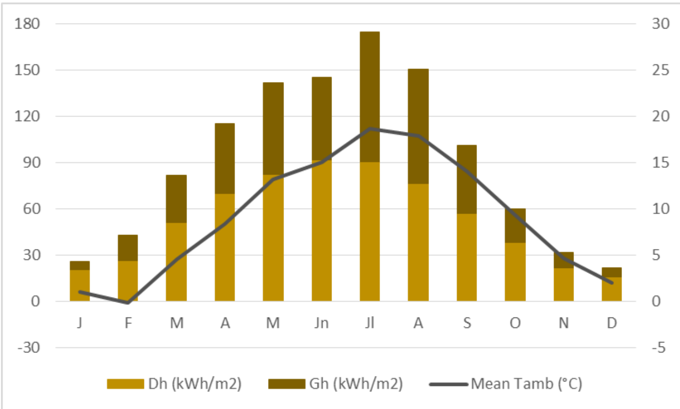

Fig. 2. Monthly meteorological data extracted from the TRY of Ludwigsburg

The selected branch has two different kinds of dwellings, five single-family and two multi-family houses (SFH and MFH respectively). Most are constructed according to the current energy saving standards, here denominated class 100 of the German financing institution KfW, but SFH1 is a passive house and SFH4 is class 55. This means that these buildings have a lower heating demand, around 20% and 55% of the upper permissible limit.

The dwellings have been numbered in the same order as they are connected to the DHN, first the five SFH and last the two MFH. Upstream of the SFH1 can be found the central heat source SFH1 can be found, which can deliver heat to the other nodes.

The space heating demands of the dwellings has been simulated using EnergyPlus [6] and the DHW demand with DHWcalc [15] using local Test Reference Year [5] weather data. Both demands together have been compared with the annual consumption during two different years measured and provided by the energy supply company of Ludwigsburg, from which a good match has been confirmed (Fig. 3).

The only exception is SFH1. Taking into account that in passive houses the inhabitants' behaviour plays a much bigger role, the mismatching may be induced by this fact. Nevertheless, this paper does not go deep into the demand simulation, so the obtained results have been considered good enough for the study especially when considering that in absolute terms the demand of SFH1 is only about 3% of the total demand.

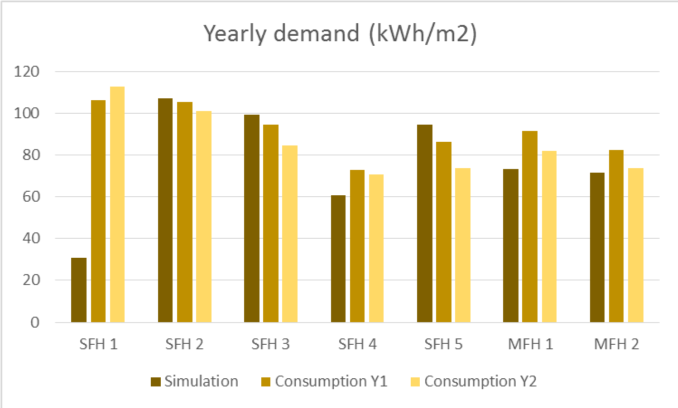

Fig. 3. Simulated vs. observed heating demand for two different years

These demands, together with the weather file are the main inputs of the model.

Fig. 4 shows the daily resolved annual demand for both DHW of 22 kWh/m2 annual and space heating of a multi-family house (MFH).

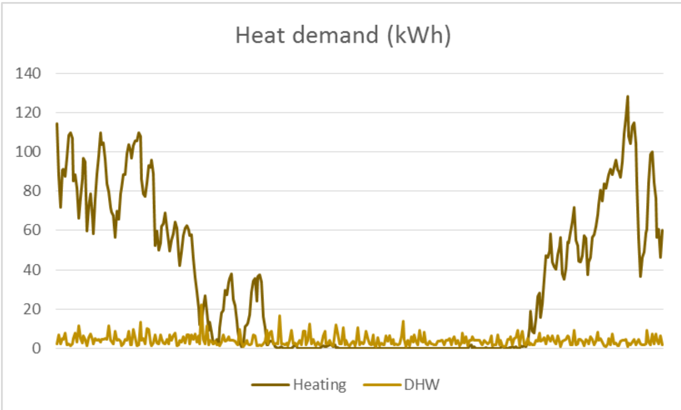

Fig. 4. Simulated heat demand of MFH2

During the winter, the space heating demand dominates, while in summer there is only DHW demand.

The solar systems

In these buildings a solar thermal system was simulated with two different configurations, one for SFH and another for MFH (Fig. 5 (a) and (b) respectively).

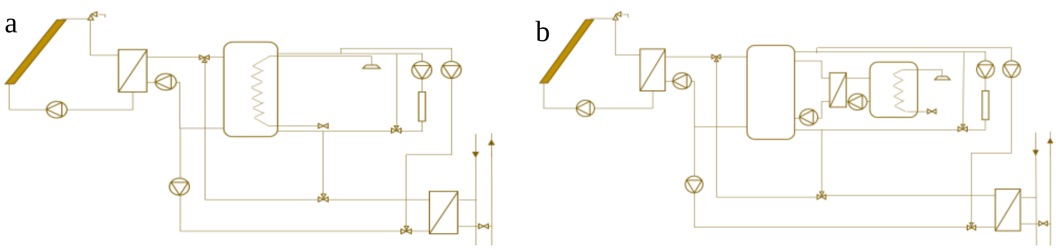

Fig. 5. (a) Solar thermal system for SFH; (b) Solar thermal system for MFH.

The main difference between them lies in the presence of a second storage tank with an intermediate heat exchanger in the case of MFH.

The same components of the system were selected for all dwellings. Table 1 and Table 2 show the simulation parameters of the collectors and tanks.

Table 1. Solar thermal collector data.

Latitude (UTM)	Degree	48.77
Inclination of solar collector	Degree	30
a0 at normal incidence	-	0.644
Linear heat loss coefficient	W/(m2K)	2.247
Quadratic heat loss coefficient	W/(m2K2)	0.015
IAM	-	0.9

Table 2. Storage tank data.

Fluid	-	water
Overall eat loss coefficient	W/(m2K)	0.5
Ambient temp. around tank	°C	8

The primary storage tank volumes depend on the case, but the secondary tank ones are always 0.5 m3.

The heat exchangers used in the solar systems as well as those connecting to the network are counterflow, with an overall heat transfer coefficient of 3 kW/K.

Those connected to the network have a pressure loss of 200kPa on the primary side.

Finally, a control system for pumps and valves with the following strategy has been included:

- Whenever the radiation is high enough, the solar collector pumps start working to feed the tank.
- If the tank is full (of energy), its energy is supplied to the net.
- If the tank is empty and the solar input is insufficient, the deficit is supplied from the net.
- The pumps or valves on the demand side work whenever there is a corresponding demand.

The scenarios

Our modelling scenarios are based on the characteristics presented in Table 3. Apart from the reduction factor (Rf), which indicates the energy standard as a percentage of the legal requirements (KfW value or the passive house standard), two other criteria have been defined: the reference heated area ratio (RAR) and the maximum solar area.

Table 3. Dwelling characteristics.

	Heated area (m2)	Rf (%)	Roof area (m2)	RAR (-)	Max solar area (m2)
SFH1	115.2	100	72	1	30
SFH2	130.4	100	85	1	30
SFH3	147.6	100	76.9	1	30
SFH4	127.7	20	79.8	1	30
SFH5	205.7	55	115.1	1.4	42
MFH1	2077.6	100	506.2	2	250
MFH2	1070.1	100	288	1	125

System dimension are similar for all dwellings of the same type, but take into account the reference heated area ratio as well as the construction type. So, the solar area for each dwelling *i* is calculated as in (1):

$$A_{coll}^{i} = A_{coll}^{ref} \cdot \frac{R_f}{100} \cdot RAR \tag{1}$$

Moreover, we assume that no more than half of the roof area is available for installation of solar collectors.
In all cases we considered a solar volume flow rate of 54 l/(hm2), and the following control constraints:

- Maximum solar collector temperature: 100 °C
- Maximum tank temperature: 97 °C
- Temperature to feed the net: 83 °C
- Minimum irradiance for starting solar pumps: 150 W/m2

Different scenarios have been proposed to study the impact of the solar systems as shown in Table 4.
Case 1 is considered the base case, to which several modifications have been tested.
The effect of increasing the solar collector area is shown comparing cases 1, 2 and 7. Comparing cases 3 and 4 with case 1, the effect of modifying the storage tank volume is studied.
Cases 5 and 6 show the importance of modelling the district heating net together with the prosumers, so the effect of the saturation of the network can be taken into account. Case 5, is normally connected to the network and case 6 is connected to a network with infinite virtual storage.
The saturation of the network is one of the main issues found in the literature, where in most cases the network behaves as an infinite virtual thermal storage system. This idealisation normally leads to optimistic results.

Table 4. Scenarios

Simulation case	Dwelling type	Reference solar area (m2)	Tank volume (m3/m2)
Case 1	SFH	10	0.05
	MFH	100	0.05
Case 2	SFH	30	0.05
	MFH	125	0.05
Case 3	SFH	10	0.2
	MFH	100	0.2
Case 4	SFH	10	0.05
	MFH	100	0.02
Case 5	SFH	Max solar area in all buildings	0.05
	MFH	Max solar area in all buildings	0.02
Case 6	SFH	Max solar area in all buildings	0.05
	MFH	Max solar area in all buildings	0.02
Case 7	SFH	Max solar area in all buildings	0.05
	MFH	Max solar area in all buildings	0.05

4. Results

The first interesting output from the study is that, even though the solar energy collected increases with the solar area and also with the tank volume this does not necessary lead to bigger savings.
Fig. 6 compares cases 1, 2 and 7, increasing the collector area but conserving the volume ratio.

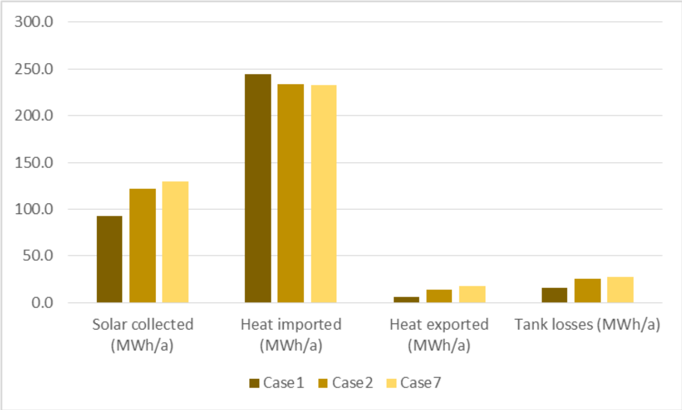

Fig. 6. Effect of increasing collector area.

It can be seen how the collected solar energy increases with the collector area, but from case 2 to 7 there isn't substantial reduction in the imported energy. This is due to asynchronicity in periods with higher demand and higher solar energy conversion. (Fig. 7).

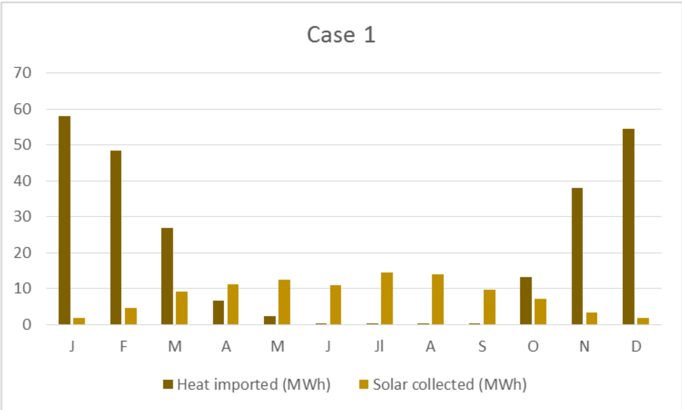

Fig. 7. Monthly mismatch.

A similar situation occurs when increasing the tank volume. Up to a certain point increasing the volume leads to an increase in the solar energy collected and a reduction of the imported energy. But if the volume is too big, the extra solar energy collected is mainly used to reach the operation temperatures. Also a higher volume means higher tank losses (Fig. 8).

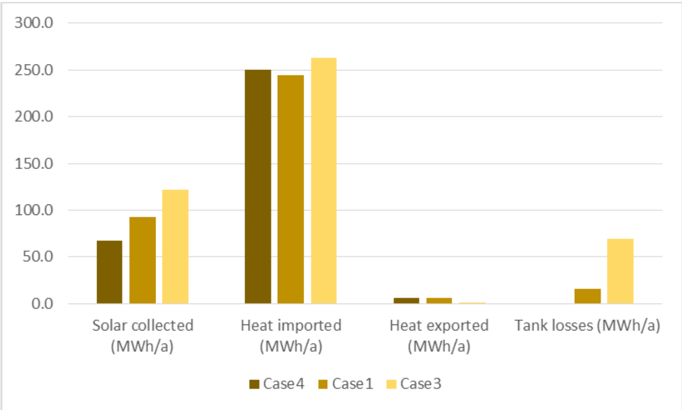

Fig. 8. Effect of modifying tank volume.

Furthermore, a bigger tank implies bigger losses and, therefore, more imported energy during winter time (Fig. 9).

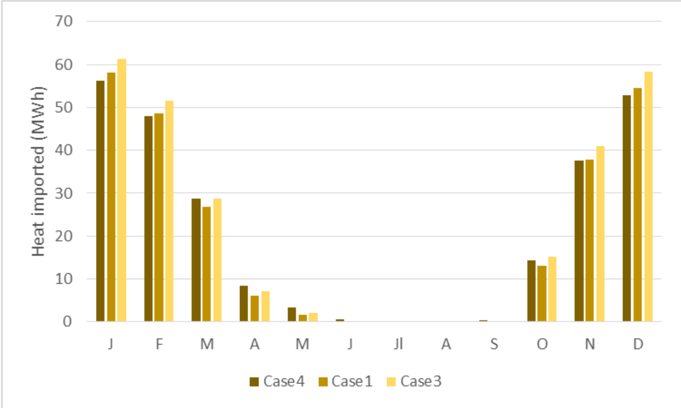

Fig. 9. Monthly disaggregation.

Fig. 10 shows the difference between imported and exported energy to the network, called here "net imported".

As expected, this net imported energy is negative during the summer season, the magnitude depending upon the solar system capacity (the figure shows the results for the smaller and bigger systems considered in this study). The negative values mean that during those months the dwellings export more energy that they import from the net. This energy, as there is no storage considered in the network branch, is transformed into net losses or exported out of the branch to the main network. Nevertheless, this suggests that isolation of the branch is feasible.

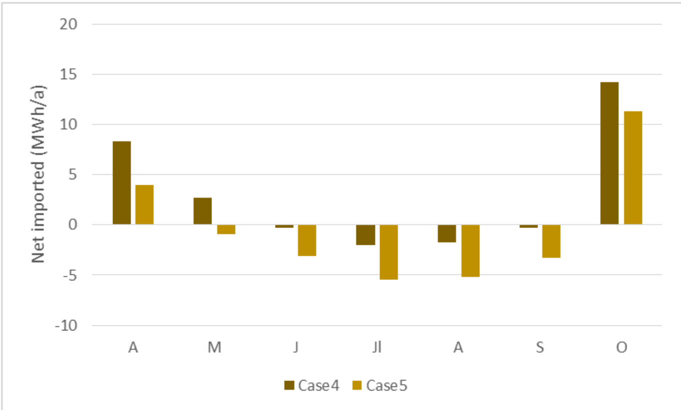

Fig. 10. Net energy imported from network during warm period.

Looking more closely, it can be observed that a storage facility in the branch is needed to actually carry out this disconnection. That is true especially at the extremes of the period (Case 4 in Fig. 11.a) and not that pronounced for intermediate months (Fig. 11.b). An increase of the total storage volume of the prosumers is another option but can increase demand for imported energy during winter as discussed before. Furthermore, seasonal storage in the branch could extend the period of disconnection.

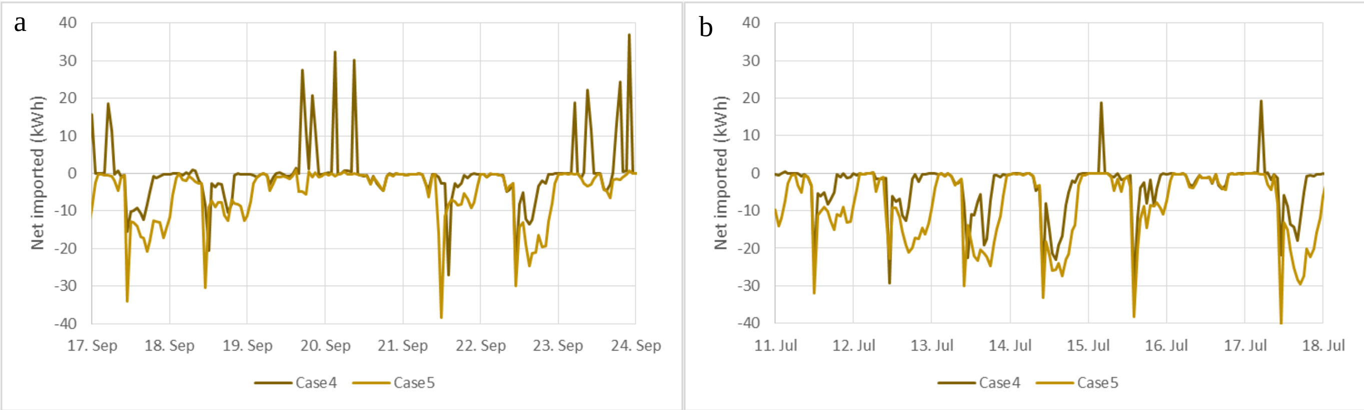

Fig. 11. Hourly net exported energy in a week in (a) September; (b) July.

Fig. 12 show the behaviour of the system with or without the idealisation of the network.

Fig. 12.a shows how including the thermodynamics of the net in the simulation (Case 5) results in a decrease of heat exported compared to the ideal case (Case 6). This leads to a reduction of the total solar energy that the system is able to collect, which is more prominent during the summer season (Fig. 12.b and Fig. 12.c).

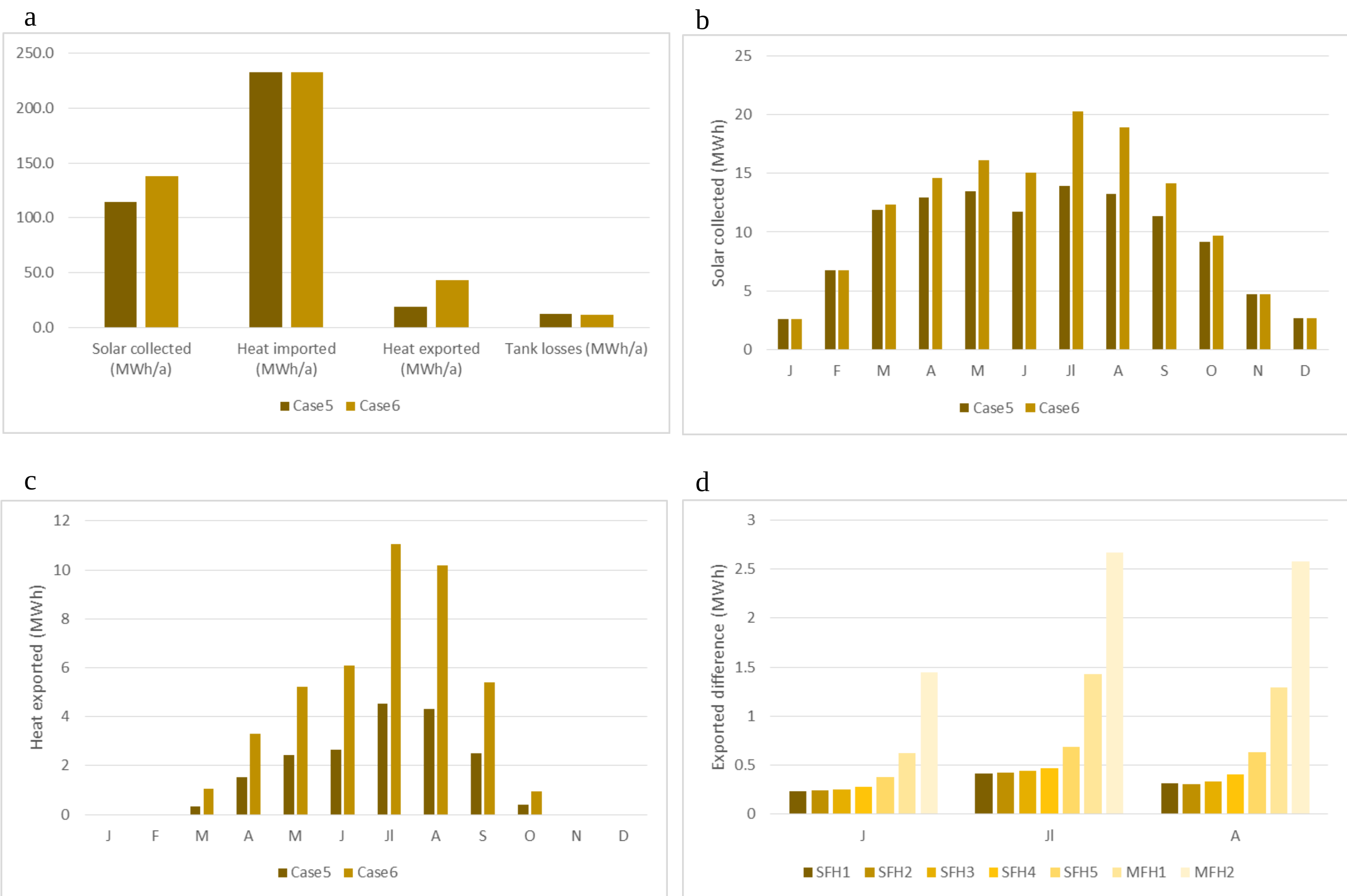

Fig. 12. Ideal -case 6- vs. non-ideal cases: (a) energy balances; (b) solar energy collected; (c) heat exported; (d) impact of saturation in downstream neighbours

Finally, Fig. 12.d how saturation of the net impacts on downstream neighbours. The more remote the dwelling from the starting point of the branch, the difference between the ideal exported energy of case 6 and the exported in case 5 grows. A bigger difference means the more difficult it is to export the energy into the net. This is due to the rise of the temperature of the return line. Every subsequent dwelling experiences a reduced temperature drop; reducing the capacity to export heat.

Table 5 and Table 6 summaries the main results from this study. The annual demand for all the cases is 311.1 MWh.

Table 5. Results summary 1.

Case	Collector area (m^2)	Tank volume (m^3)	Solar collected (MWh/a)	Heat imported (MWh/a)	Heat exported (MWh/a)	Net imported (MWh/a)	Pump for exporting heat (MWh/a)	All pumps consump. (MWh/a)
1	341.5	18.1	92.6	244.5	5.6	238.9	0.183	2.9
2	499.5	26.0	121.7	233.9	14.0	219.9	0.292	3.7
3	341.5	69.3	121.7	262.5	1.0	261.5	0.017	2.8
4	341.5	9.1	67.7	250.0	5.5	244.5	0.131	2.8
5	537.0	16.6	114.5	233.1	18.7	214.4	0.292	3.7
6 (ideal)	537.0	16.6	137.9	233.1	43.3	189.8	0.077	3.6
7	537.0	27.9	129.7	232.6	7.9	224.7	0.321	3.8

The energy consumed by the pumps has been calculated assuming that the pumps operate with a constant efficiency always, as the dynamics of the prosumer are not simulated. A correlation of the power of the pumps as a function of the mass flow has been extracted from a water pumps catalogue.

$$E_p = \sum_i P_i \cdot h_i \tag{2}$$

Where hi are the hours of operation of each pump and Pi its power calculated with the correlation as in (3).

$$P_i(W) = 7.897 + 35.104 \cdot \dot{m}_i(kg/s) \tag{3}$$

The first column in Table 6 presents the energy savings that are calculated as the total demand minus the imported energy (it is assumed that the reference case is a consumer dwelling which has no internal system and takes all the needed energy from the net). Between 20 and 25% of the total demand can be saved by the solar thermal systems. As discussed before, the larger energy savings result from the larger solar area but with an adequate storage volume ratio. For example, case 3 has smaller savings because the volume ratio is too big.

The second column compares the specific solar energy collected. The values are in in general rather low, but they could be increased if the network had a storage facility to store the exported energy (compare cases 5 and 6).

Finally, two ratios are calculated and presented in the table. The first one is the specific energy used by pumps which gives an idea of how much electrical energy is needed for every kWh saved. The ratios are very low, which is very positive from an energy saving perspective.

The second ratio is the specific energy used only for the pump used to export the heat into the net. This ratio can be useful for the energy supply company of Ludwigsburg, which operates the network and has to calculate the costs for selling or buying energy from the prosumers.

Table 6. Results summary 2.

Case	Energy savings (MWh/a)	Specific solar energy (kWh/m2a)	FEp /FEs %	FEp / FEe %
1	66.6	271.1	3.8	8.3
2	77.2	243.7	6.1	5.3
3	48.7	356.2	5.0	4.5
4	61.1	198.4	4.0	6.1
5	78.0	213.1	6.6	4.0
6 (ideal)	78.1	256.8	6.3	0.5
7	78.6	241.5	6.6	4.6

Cases 2 and 5 are the most promising of those studied, in terms of both savings and exported heat. The choice between these two may however lie in other considerations, such as available room for storage tanks or the difference in price between solar collectors and storage tanks (Case 5 involves a larger collector area and case 2 a larger storage volume); factors that are not taken into direct account in this study.

5. Conclusion

An existing heating network branch in Sonnenberg has been modelled and used in this paper to evaluate the questions exposed in the abstract.

The potential contribution of the solar systems is between 20% and 25% of the total demand, with specific auxiliary energy requirements lower than 7%. During the summer season, this contribution is high enough to enable the branch to be isolated for about three months (depending on the size of the solar thermal system). The period can be increased if a seasonal storage facility is added to the branch.

Furthermore, the study indicates that bigger solar systems do not necessarily imply higher savings, mostly because of the asynchronicity in periods with higher demand and higher solar energy conversion. Again, seasonal storage in the net could help to increase the total savings for bigger systems.

Finally, the thermodynamics of the network must to be taken into account. When the network is not idealised, the influence of the first prosumers to the others is considered, as well as the total thermal capacity of the net, resulting in lower but more realistic values of exported energy.

Acknowledgements

The authors gratefully acknowledge the European Commission for providing financial support during conduct of research under FP7-PEOPLE-2013 Marie Curie Initial Training Network "CI-NERGY" project with Grant Agreement Number 606851.

The authors would also like to thank the leaders of the project *"Simulationsbasierte Optimierung energieeffizienter Wärmenetze mit Umsetzung in EnEff:Stadt Ludwigsburg"*, included in the EnEff:Stadt research initiatives promoted by the Federal Ministry of Economics and Energy in Germany for providing data for this study.

And finally, Ruben Pesch and Ilyes Ben Hassine for their suggestions and discussions during the work.

References

[1] Di Giorgio and F. Liberati, "Near real time load shifting control for residential electricity prosumers under designed and market indexed pricing models", Applied Energy, Volume 128, 1 September 2014, Pages 119-132.

[2] B. Di Pietra, F. Zanghirella and G. Puglisi, "An Evaluation of Distributed Solar Thermal "Net Metering" in Small-scale District Heating Systems", Energy Procedia, Volume 78, November 2015, Pages 1859-1864.

[3] E. Vesaoja, H. Nikula, S. Sierla, T. Karhela, P. Flikkema and C-W. Yang, "Hybrid modeling and co-simulation of district heating systems with distributed energy resources", In Workshop on Modeling and Simulation of Cyber-Physical Energy Systems (MSCPES), (April, 2014), pp. 1-6.

[4] I.B. Hassine and U. Eicker, "Control Aspects of Decentralized Solar Thermal Integration into District Heating Networks", Energy Procedia, Volume 48, 2014, Pages 1055-1064

[5] I.J. Hall, R.R. Prairie, H.E. Anderson and E. Boes, 1978. "Generation of Typical Reference Years for 26 SOLMET stations". Sandia Laboratories Report SAND 78-1601, Albuquerque, NM, USA.

[6] J. Feng., Y. Ding and H.W. Wu, EnergyPlus energy simulation software [Software], (2012). Website: https://energyplus.net/

[7] J. Heikkinen, M. Rämä, K. Klobut and A. Laitinen, "Solar Thermal Integration Into A District Heated Small House", Submitted to the 14th International Symposium on District Heating and Cooling, 2014 Stockholm.

[8] J. Luther and J. Schumacher-Gröhn, INSEL- A Simulation System for Renewable Energy Supply Systems [Software]. Version 8.2. Website: http://www.insel.eu/

[9] L. Brand, A. Calvén, J. Englund, H. Landersjö and P. Lauenburg, "Smart district heating networks – A simulation study of prosumers' impact on technical parameters in distribution networks", Applied Energy, Volume 129, 15 September 2014, Pages 39-48.

[10] L. Brand, P. Lauenburg and J. Englund, "District Heating Combined With Decentralised Heat Supply In Hyllie, Malmö", Submitted to the 14th International Symposium on District Heating and Cooling, 2014 Stockholm.

[11] L. Brange, J. Englund and P. Lauenburg, "Prosumers in district heating networks – A Swedish case study", Applied Energy, Volume 164, 15 February 2016, Pages 492-500.

[12] R. Schleicher-Tappeser, "How renewables will change electricity markets in the next five years", Energy Policy, Volume 48, September 2012, Pages 64-75.

[13] S. Broberg, S. Backlund, M. Karlsson and P. Thollander, "Industrial excess heat deliveries to Swedish district heating networks: Drop it like it's hot", Energy Policy, Volume 51, December 2012, Pages 332-339.

[14] S. Nielsen and B. Möller, "Excess heat production of future net zero energy buildings within district heating areas in Denmark", Energy, Volume 48, Issue 1, December 2012, Pages 23-31.

[15] U. Jordan and K. Vajen, 2000. DHW-calc. [Software] Version 1.10: Universitat Kassel.

[16] U. Ottosson, "Next generation district heating – Findings and lessons from the project", Submitted to the 14th International Symposium on District Heating and Cooling, 2014 Stockholm.

[17] U. Persson, B. Möller and S. Werner, "Heat Roadmap Europe: Identifying strategic heat synergy regions", Energy Policy, Volume 74, November 2014, Pages 663-681.

Available online at www.sciencedirect.com

ScienceDirect

Energy Procedia 00 (2018) 000–000

Energy Procedia

www.elsevier.com/locate/procedia

16th International Symposium on District Heating and Cooling, DHC2018, 9–12 September 2018, Hamburg, Germany

The effect of discretization on the accuracy of two district heating network models based on finite-difference methods

J. Vivian[a,*], P. Monsalvete Álvarez de Uribarri[b], U. Eicker[b], A. Zarrella[a]

[a]*University of Padova, Dept. of Industrial Engineering, Via Venezia 1, Padova, 35131, Italy*
[b]*University of Applied Sciences Stuttgart, Center for Sustainable Energy Technology (zafh.net), Schellingstrasse 24, Stuttgart, 70174, Germany*

Abstract

District heating and cooling (DHC) networks play a fundamental role in the transition towards a sustainable supply of heating and cooling, due to their ability to integrate any available source of thermal energy and to distribute it to the buildings. However, the use of renewable non-constant sources together with the variable heat demand of the buildings creates instable and pronounced transient operating conditions. In order to analyse the hydraulic and thermal behaviour and the dynamics occurring within these networks, several physical models based on different methods were proposed by previous researchers. Numerical thermal models based on finite difference methods (FDM) were pointed out to suffer from artificial diffusion when simulating the propagation of heat through the network. However, due to a wide and well-known literature on these methods, they are still used by many researchers and are therefore worth being investigated. The present paper analyses the effects of artificial diffusion using two models based on two different first-order approximation schemes. An ideal temperature wave and a dataset from a real DH network were used to evaluate the accuracy of the models using different discretization levels in time and space. As a result, the paper provides a framework to set a proper discretization when simulating a DHC network with FDM-based models considering both the expected accuracy and the computation time as criteria.

Keywords: District heating and cooling; models; finite-difference; accuracy

* Corresponding author. Tel.: +39 049 827 6879. E-mail address: jacopo.vivian@unipd.it

1. Introduction

District heating systems are characterized by temperature and velocity fluctuations, especially when unstable heat sources such as waste or solar heat are connected. Furthermore, in many DH systems, a temperature wave is deliberately produced to reduce the flow during peak consumption periods.

In literature two types of models for the simulation of the transient thermal behaviour in district heating systems can be found, namely the element-method and the node-method [1]. The element method finds an explicit solution to the transient heat balance equation by means of different possible finite difference schemes. It was shown that low-order schemes suffer of artificial numerical diffusion, thus resulting in abnormal smoothing of sharp temperature profiles [2] and that higher order schemes may instead bring to overshooting [3]. In the element method, the temperature at each time–step is determined only from the time–step before. The node method, instead, uses temperature values at different time–steps to determine the current temperature situation [2]. Pálsson et al. [1] implemented and tested two models based on the different two methods. The comparison revealed that, unless higher order schemes are used, the node method is superior to the element method at low Courant numbers, which corresponds to a situation with long district heating pipes and sharp temperature gradients which in turn require small time-steps. Furthermore, the computational effort seems to be also lower for the node-method. The application of the node method is however limited to tree-shaped networks [4].

Later on, another experiment was carried out to measure the temperature in a district heating pipeline under transient conditions [5]; both models were used to simulate the propagation of the temperature front and then compared against measured data. The comparison showed that the element-method predicts better the amplitude of the wave when the temperature changes rapidly, whereas the node-method predicts better the delay of the temperature front.

Nevertheless, to obtain acceptable results with the element-method, an adequate discretization in time and space must be done in the pre-processing phase [6].

In this paper we aim at investigating to which extent the performance of the models can be improved by a correct discretization of the network in relationship with the Courant number, and the impact that this discretization has on the accuracy of the results and the computational time.

Nomenclature

c_p	Specific heat capacity (J/(kg K))
Co	Courant number
e	Error
f	Performance indicator
G	Mass flow rate (kg/s)
K	Stiffness matrix
L	Length (m)
M	Mass matrix
q	Vector of known terms
T	Temperature (°C)
T_{CPU}	CPU time (s)
U	radial heat transmission coefficient (W/(m^2 K))
v	Velocity (m/s)
V	Volume (m^3)
z	Depth (m)

Abbreviations

FDM	Finite difference method(s)
ODE	Ordinary differential equation

Subscripts

adim	dimensionless
i	i-th node
j	j-th node
g	Undisturbed ground
in	Inlet
min	Minimum
n	Number of nodes
out	Outlet
s	Wave start
st	Steady state
Tr	Transient
w	Wave width

Greek symbols

τ	Time (s)
Ω	Pipe section perimeter (m)
ρ	Density of the heat carrier fluid (kg/m^3)
λ	Thermal conductivity (W/(m K))

2. Models

Both models describe the topology of the network using graph theory. The network is represented by a set of nodes and oriented branches and an adjacency matrix determines their mutual connections. Once the geometry is established, the pressure and temperature profiles are calculated.

When forced convection occurs, the velocity of the heat carrier fluid does not depend on the temperature distribution. Therefore, the hydraulic and thermal sub-models can be uncoupled. This allows the calculation of the mass flow rates and the pressures across the network in a first step; then, given the mass flow rates, the energy balance is performed to find out the temperature distribution.

Both models rely on the following assumptions:

- A slug flow is assumed, which implies that the velocity of the heat carrier fluid is uniform in the radial direction (one dimensional model)
- The heat conduction through the wall pipe along the axial direction is neglected
- The heat transfer in the radial direction considers the convection between the heat carrier fluid and the inner pipe surface, the thermal insulation of the pipe and the thermal resistance of the surrounding ground
- The heat capacity of the surrounding ground is neglected

2.1. NeMo

Due to the uncompressible nature of the heat carrier fluid, the hydraulic problem can be described using only two equations: the continuity and the momentum equations. NeMo solves these equations using the SIMPLE method proposed by Patankar and Spalding [7]. The heat propagation in the network is then described by the energy balance performed on the volume of heat carrier fluid around the nodes of the network. The control volume of the *i-th* node corresponds to half of the heat carrier fluid volume of all the branches connected to it.

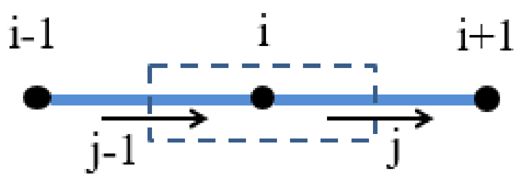

Fig. 1. Control volume of the *i-th* node.

Applying the energy balance to the node shown in Figure 1 leads to Equation (1):

$$\rho V_i c_p \frac{\partial T_i}{\partial \tau} = G_{j-1} c_p T_{j-1} - G_j c_p T_j - \frac{1}{2} (L_j \Omega_j U_j + L_{j-1} \Omega_{j-1} U_{j-1})(T_i - T_\infty) \tag{1}$$

Where G are the mass flow rates, V is the volume of heat carrier fluid enclosed in the control volume, Ω is the perimeter of the pipe section, U is the radial heat transmission coefficient from fluid to the ground and T_∞ is the undisturbed ground temperature. The temperature of the branches is then associated to the temperature of the corresponding upwind nodes, according to the well-known *upwind scheme*. Therefore, Equation (1) becomes:

$$\rho V_i c_p \frac{T_i^{(\tau)} - T_i^{(\tau-\Delta\tau)}}{\Delta\tau} = G_{j-1} c_p T_{i-1}^{(\tau)} - G_j c_p T_i^{(\tau)} - \frac{1}{2} (L_j \Omega_j U_j + L_{j-1} \Omega_{j-1} U_{j-1}) \left(T_i^{(\tau)} - T_g\right) \tag{2}$$

Equation (2) can be represented in matrix form as:

$$M \dot{T} = q - K T \tag{3}$$

Where ***M*** and ***K*** are the so-called *mass matrix* and *stiffness matrix*, respectively. The temperature at the inlet node is fixed (*Dirichlet condition*). The first-order ordinary differential equation (ODE) (3) is solved by the ODE solver *ode15s* of Matlab, that implements the Numerical Differentiation Formulas (NDF) [8]. The mass matrix is singular as the inlet node is massless according to the Dirichlet condition. The missing mass is attributed to the adjacent node.

2.2. spHeat

Also in spHeat model the hydraulic balance is solved before calculating the temperature distribution. Pressures at the nodes and mass flows along the edges are calculated assuming steady-state conditions using the electrical analogy to formulate the conservation of mass and the conservation of momentum. The pressure losses are calculated using the Darcy-Weisbach equation and the system of non-linear equations is solved by means of the Newton-Raphson method. The energy balance accounts for the transient behaviour of the heat carrier fluid using a finite difference method. Each pipe is discretized into a set of elements of length L. Equation (1) is applied to each of these elements. Then, the temperature at the node is calculated using an explicit formulation, as in Equation (4).

$$\rho \mathrm{V_i} \mathrm{c_p} \frac{T_i^{(\tau)} - T_i^{(\tau-\Delta\tau)}}{\Delta\tau} = G_{j-1} c_p T_{j-1}^{(\tau-\Delta\tau)} - G_{j1} c_p T_j^{(\tau-\Delta\tau)} - L_i \Omega_i U_i \left(T_i^{(\tau-\Delta\tau)} - \mathrm{T_g}\right) \quad (4)$$

While in NeMo the time step of the calculation is decided by MATLAB, in spHeat the time step is externally set by the user. Further explanations for the spHeat model can be found in [9].

3. Cases of study

This Paragraph describes the two cases of study (Section 3.1 and 3.2) used to test the accuracy of the models presented above.

3.1. Ideal square temperature wave

The first case study consists of an ideal square wave that propagates through a single pipe. The inlet temperature is 30°C in the first 40 minutes, then it is 50°C for the next 40 minutes and finally drops to 30°C and remains constant for the last 80 minutes. The characteristics of the case study are summarized in Table 1.

Table 1. Parameters and boundary conditions of the pre-insulated pipe.

Parameter	Units	Value
Pipe length, L	M	500
Internal diameter of the pipe, d_i	mm	80.0
External diameter of the pipe, d_e	mm	83.0
Diameter of casing, D	mm	150.0
Thermal conductivity of insulation, λ	W/(m K)	0.033
Thermal conductivity of the ground, λ_g	W/(m K)	2.0
Depth, z	m	1.0
Temperature of the undisturbed ground, T_g	°C	8.0
Initial temperature at inlet node	°C	30.0
Initial temperature at outlet node	°C	30.0
Mass flow rate (constant)	kg/s	2.74

3.2. Real case study: measured data

In the second case study the propagation of the temperature front in a 470 m long pre-insulated pipe, as logged during an experiment that was carried out by Ciuprinskas et al. [10] in the district heating system of Vilnius (Lithuania) during May 1997. This dataset was already used by other researchers for comparing and validating thermal networks models [5,11]. A schematic view of the experimental site is depicted in Figure 2.

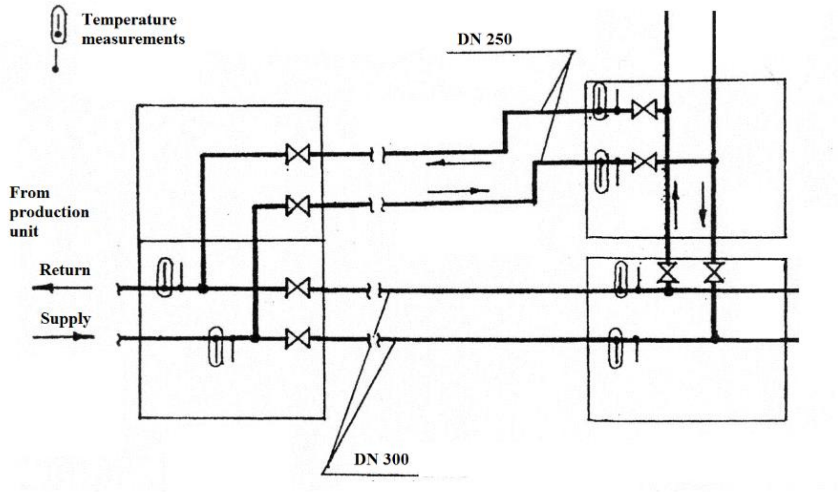

Fig. 2. Schematics of the experimental site (taken from [10]).

The inlet temperature and the mass flow rate of the supply pipe are set as boundary conditions and the resulting outlet temperature profile is compared with the measured values. Due to the very low fluid velocity in the considered period (about 0.036 m/s), it takes hours for the temperature front to reach the outlet of the pipe. This unusual condition affects the accuracy of the models as discussed in Gabrielaitiene [5]. The parameters and the boundary conditions used in the simulations are reported in Table 2. The time-step of simulation is 5 minutes and the sample-time of the dataset is 10 minutes. Values at times between two consecutive loggings were linearly interpolated.

Table 2. Parameters and boundary conditions of the pre-insulated pipe.

Parameter	Units	Value
Pipe length, L	m	470
Internal diameter of the pipe, d_i	mm	312.7
External diameter of the pipe, d_e	mm	323.9
Diameter of casing, D	mm	450.0
Thermal conductivity of insulation, λ	W/(m K)	0.033
Thermal conductivity of the ground, λ_g	W/(m K)	2.0
Depth, z	M	1.0
Temperature of the undisturbed ground, T_∞	°C	8.0
Initial temperature at inlet node	°C	67.7
Initial temperature at outlet node	°C	66.3
Mass flow rate (constant)	kg/s	2.65

4. Methods

The temperature profiles at pipe outlet obtained from the simulations were compared to the theoretical ones (see 3.1) and then to the measured ones (3.2). In order to facilitate the analysis, the dimensionless temperature suggested by [5] was used:

$$T_{out,adim} = \frac{(T_{tr} - T_{st})_{out}}{\left(T_{tr,max} - T_{st}\right)_{in}} \tag{5}$$

where T_{tr} is the temperature output given by the model and T_{st} is the temperature during steady-state conditions. The normalized temperature T_{adim} is equal to 1 when the wave peak reaches the pipe outlet if no heat loss occurs in between, and is equal to 0 during steady state conditions –i.e. before and after the temperature wave arrives at pipe outlet.

The Courant number is a dimensionless number that expresses the ratio between the physical velocity v (velocity of the water stream in each pipe element) and the "velocity of calculation", i.e. the ratio between the length of each element Δx and the time step $\Delta\tau$ used by the numerical method to update the temperature distribution.

$$Co = \frac{v\,\Delta\tau}{\Delta x} \tag{6}$$

The Courant number indicates how fast the temperature information travels on the computational grid; the latter is regarded as the most important parameter as far as the performance of numerical methods for convective flow is concerned [1]. In explicit numerical schemes, a necessary condition for stability is $Co < 1$: the step size must be smaller than the time interval it takes for the flow to cross the smallest distance between two adjacent points [12].

Two indicators are used to measure the difference between simulated and actual temperature wave: the time of wave start t_s and the wave width Δt_w. As explained in Sections 3.1 and 3.2, a temperature profile was set at the inlet of a pipe and the resulting temperature profile at pipe outlet was then compared to a reference profile in order to assess the accuracy of the models. The reference temperature wave was represented in the first case study by the ideal temperature profile and in the second case study by the measured temperature profile.

The time of wave start was determined as the moment when the increment of temperature $T_{out,adim}$ between two consecutive steps was bigger than a certain value, set to 0 in the ideal case and to 0.0015 in the single-pipe case.

The wave width was instead determined as the time interval with the outlet temperature $T_{out,adim}$ above a certain value, that was set to 0.05 in the ideal case study and to 0.20 in the second one.

The error in the wave start e_s is the difference between the times at which the temperature front arrives at the pipe outlet with the model and in ideal/measured conditions. Here, for a given time step $\Delta\tau$ used by the solver the error is expressed as a function of the number of nodes n

$$e_s^{(n)} = t_s^{(n)} - t_s^{id} \tag{7}$$

An analogous definition holds true for the error in the wave width, that is the difference between the length (duration) of the wave between modelled and ideal/measured conditions

$$e_w^{(n)} = \Delta t_w^{(n)} - \Delta t_w^{id} \tag{8}$$

In order to evaluate the improvement in accuracy brought by a higher spatial discretization of the pipe, the accuracy improvement Δe was defined as the percent error between the model using n nodes and the error of the model using the minimum number of nodes considered (n_{min}). This indicator was used for both errors (e_s and e_w) as follows:

$$\Delta e_s^{(n)} = \frac{\left|e_s^{(n)} - e_s^{(n_{min})}\right|}{\left|e_s^{(n_{min})}\right|} \tag{9}$$

$$\Delta e_w^{(n)} = \frac{\left|e_w^{(n)} - e_w^{(n_{min})}\right|}{\left|e_w^{(n_{min})}\right|} \tag{10}$$

Finally, the indicator f was defined as the ratio between the accuracy improvement and the logarithm of the computational time T_{CPU} needed by the processor to find the solution. This indicator represents the efficiency of the model for each discretization level considered.

$$f_w^{(n)} = \frac{\Delta e_w^{(n)}}{\log_{10} T_{CPU}{}^{(n)}} \tag{11}$$

$$f_s^{(n)} = \frac{\Delta e_s^{(n)}}{\log_{10} T_{CPU}{}^{(n)}} \tag{12}$$

5. Results and discussion

5.1. Accuracy of the models: evaluation using an ideal square temperature wave

Figure 3 shows the outlet temperature of the step wave for both models, NeMo and spHeat. In both cases it can be seen that increasing the number of nodes reduces the artificial diffusion and leads to a better approximations of the theoretical wave. By comparing Figure 4(a) and 4(b), it seems that spHeat obtains a better fit on the amplitude of the wave.

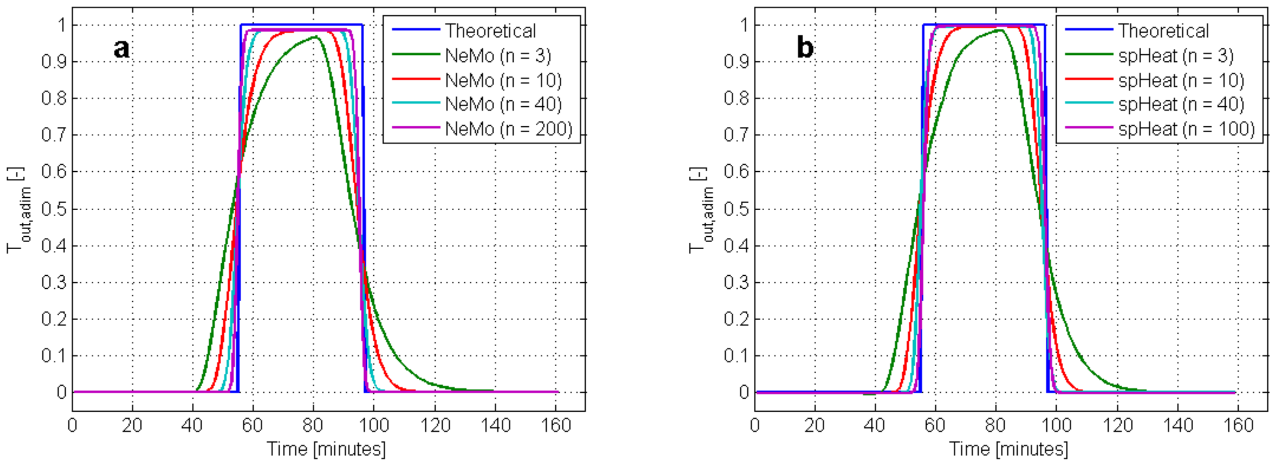

Fig. 3. Normalized temperature profiles with different discretization levels obtained with (a) NeMo and (b) spHeat.

Figure 4 plots the two errors (wave start and wave width) against the mean Courant number. Note that the MATLAB ODE Suite does not allow the user to set the time-step of the solver, but only to set an upper threshold. The solver used by NeMo is *ode15s*, that uses a variable step size. Therefore, the upper step size was fixed to the nominal values of $\Delta\tau = 3$ s and $\Delta\tau = 30$ s, and then after the simulation the average time-step $\Delta\tau$ was printed and used to calculate the mean Co *a posteriori*. In turn, spHeat does allow externally fixing the timestep, keeping it constant (and the Co number with it) during the complete period. On the flip side, spHeat does not support models with more than 100 nodes. Figure 4(a) confirms that, since NeMo is based on an implicit differentiation method, using Co > 1 does not imply convergence problems, and both errors decrease asymptotically with increasing Co, i.e. with increasing number of nodes. Figure 4(b) show the results obtained with spHeat. Co > 1 is not allowed on this model due to the explicit solution methodology. Nevertheless, the tendencies in the errors are similar to those of NeMo but with the maximum limit. For a given Courant number, the temperature profiles obtained with $\Delta\tau = 3$ s give a lower error than those obtained with $\Delta\tau = 30$ s. This is reasonable because the same Co number with a 10-times lower time-step implies solving the equation 10 times more, i.e. having a finer mesh in space and time.

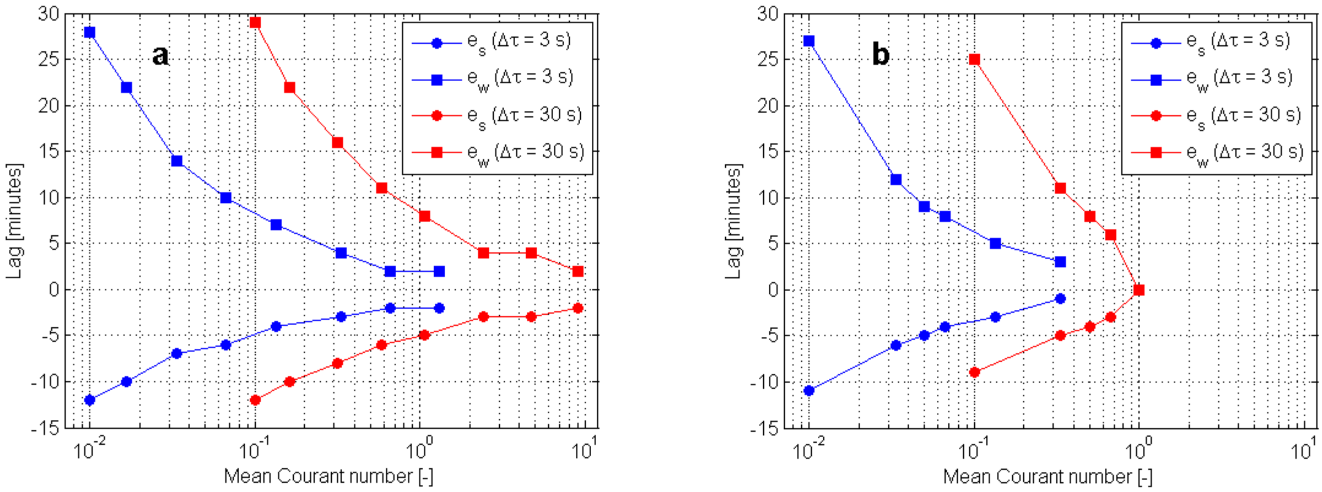

Fig. 4. Errors in wave start (es) and wave width (ew) for (a) NeMo and (b) spHeat.

It must be noticed that spHeat provides a perfect match with the theoretical solution for Co = 1. This is specific for this case and is due to the fact that the output temperature in the theoretical solution is very similar to the input temperature. In spHeat when Co = 1, the same shape of the wave is propagated along the pipe, i.e. there is absence of diffusion. This is due to the fact that there is no mass or heat exchange between pipe elements. So, the only phenomena considered is the heat loss to the ground.

It is interesting to calculate the accuracy improvement Δe defined in Equations (9-10) and to relate it to the computational time needed by the processor to find the solution. Figure 5 shows that, while the accuracy improvements Δes and Δew tend to 1, the CPU time grows exponentially. Therefore, choosing a discretization level that gives an acceptable accuracy at a reasonable computational cost seems to be an efficient criterion to determine the discretization level in the pre-processing phase. To which extent the accuracy is “acceptable” and the simulation time is “reasonable” depends on the scope of the simulation and on the time constraints of the user, and can not be generalized here. However, the performance indicator *f* plotted in Figure 5 demonstrates that a “region” of high efficiency arises from the compromise between accuracy and CPU time.

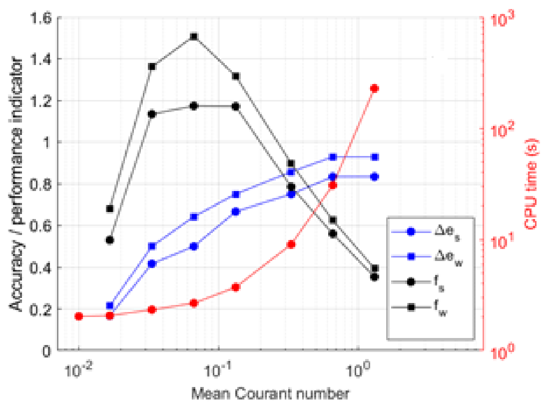

Fig. 5. Performance indicators of the first case study for NeMo simulations.

5.2. Accuracy of the models: evaluation using measured data

Figure 6 shows the temperature profiles measured at pipe outlet in the experiment described in Section 3.2 (dashed line) and those obtained by modelling the same pipe with the finite difference models. The effect of artificial diffusion, that is typical of FDM models based on first-order approximation, seems to drop significantly when a sufficiently high number of nodes is adopted. This consideration holds true for the wave start and for the wave width, whereas overshoots seem to occur when the mesh gets too fine. In fact, NeMo seems to best approximate the amplitude of the wave with only 21 nodes, and to overestimate the peak for higher number of nodes. This result does not agree neither with the observations of the first case study nor with the theory, as overshoots are expected from models of higher order [3]. However, this overestimation of the peak might be caused by stratification effects that occurred during the experiment due to very low velocity of the flow, as discussed in a previous paper [11] and that are not considered within the models. Therefore, the wave amplitude cannot be used as an indicator of the models accuracy.

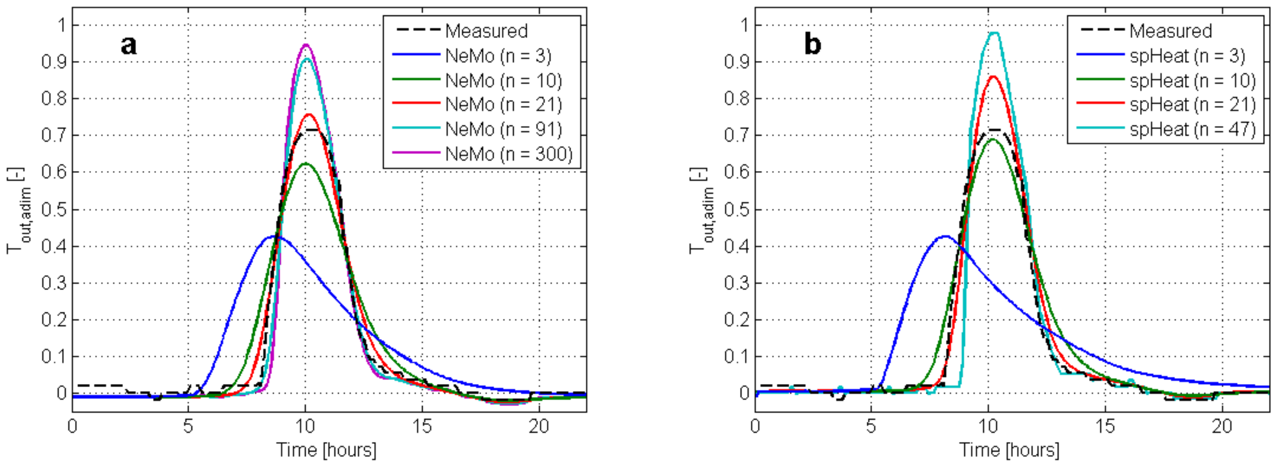

Fig. 6. Normalized temperature profiles obtained by (a) NeMo and (b) spHeat using different discretization of the pipe.

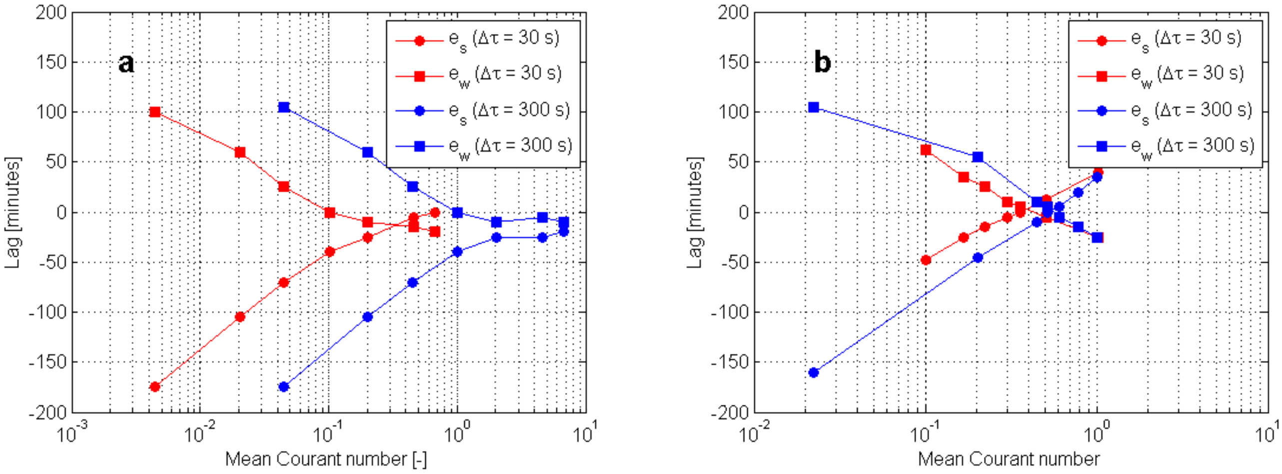

Fig. 7. Errors in wave start and wave width of (a) NeMo and (b) spHeat.

Figure 7(a) shows that the accuracy of NeMo has a similar trend compared to that discussed above for the ideal case study. In particular, the error in wave start shows the same tendency: it drops with increasing Courant number, with the approximation error asymptotically reaching 0 for very dense meshes. For a given Courant number, the lag decreases with increasing number of time steps. The errors in wave width have a similar trend, but above a certain Co the width becomes smaller than the measured one. Accordingly, an optimal accuracy arises at Co = 0.1 when the solver uses a 30 s time-step, and at Co = 1 when the time-step is 300 s. The explicit solution, Figure 7(b), follows a similar tendency, the error is reduced when the Co number increases but finding an optimum after which the errors start increasing again. In this sense, the implicit solution has the advantage that the best solutions can be found in a range, so the model is more adaptable to changes in the water velocity. This optimum of the explicit solution seems to be dependent also on the time step. As well as in the case of the implicit solution, the smaller the time-step, the smaller the optimum Co number. Nevertheless, the deviations from the "ideal" behaviour shown in Figures 6(a) and 6(b) suggest that either some errors in the experiment might have occurred, or that the models don't consider some physical effects that are occurring during the experiments. In fact, the tendency of the error in wave width seems to be in line with the one highlighted for the ideal temperature wave, but shifted downwards.

6. Conclusions

In the present work the effects of numerical diffusion obtained by two district heating network models based on two different first-order approximation schemes were analysed. The main difference between the models is that one (spHeat) uses an explicit method and the other (NeMo) is based on an implicit method. From the analysis of the results, the following conclusions can be drawn:

- Both models show good agreement with the outputs of a theoretical square temperature wave that propagates along a pipe, if the right Courant number is chosen for pipe discretization.
- When comparing the models with measurements of a real district heating pipe, some uncertainties appear and make the comparison less reliable. Nonetheless, both models show again good agreement with the experimental data in crucial zones such us the moment when the temperature starts to rise and when it ends its drop.
- The comparison with the experimental data suggests that there is an optimum range of Courant number and the relationship between this and the calculation time step must be further studied.
- While the accuracy of the models increases linearly/asymptotically with the number of elements/nodes set by the user, the computational time has an exponential increase.

A performance indicator such as the one shown in the paper could be used in the pre-processing phase to determine the best trade-off between expected accuracy and computational cost.

References

[1] Pálsson H, Bøhm B. Methods for planning and operating decentralized combined heat and power plants. PhD Thesis. Risø & DTU - Department of Energy Engineering (ET), 2000.
[2] Benonysson A, Bøhm B, Ravn HF. Operational optimization in a district heating system. Energy Conversion and Management 1995;36:297–314. doi:https://doi.org/10.1016/0196-8904(95)98895-T.
[3] Grosswindhager S., Voigt A., Kozek M. Linear Finite-Difference Schemes for Energy Transport in District Heating Networks, Brno, Czech Republic: 2011.
[4] Gabrielaitiene I, Sundén B, Kacianauskas R, Bohm B. Dynamic modeling of the thermal performance of district heating pipelines. Advances in Heat Transfer Engineering, Proceedings, Begell House; 2003, p. 185–192.
[5] Gabrielaitiene I, Bøhm B, Sunden B. Evaluation of Approaches for Modeling Temperature Wave Propagation in District Heating Pipelines. Heat Transfer Engineering 2008;29:45–56. doi:10.1080/01457630701677130.
[6] Wang Y, You S, Zhang H, Zheng X, Zheng W, Miao Q, et al. Thermal transient prediction of district heating pipeline: Optimal selection of the time and spatial steps for fast and accurate calculation. Applied Energy 2017;206:900–10. doi:10.1016/j.apenergy.2017.08.061.
[7] Patankar, S. V., Spalding, D.B. A calculation procedure for heat, mass and momentum transfer in three-dimensional parabolic flows. Int Journal of Heat and Mass Transfer 1972;15:1787–806.
[8] Shampine LF, Reichelt MW. The MATLAB ODE Suite. SIAM Journal on Scientific Computing 1997;18:1–22. doi:10.1137/S1064827594276424.
[9] Hassine IB, Eicker U. Impact of load structure variation and solar thermal energy integration on an existing district heating network. Applied Thermal Engineering 2013;50:1437–46. doi:https://doi.org/10.1016/j.applthermaleng.2011.12.037.
[10] Ciuprinskas, K., Narbutis, B. Experiments on Heat Losses from District Heating Pipelines. Energetika 1999;2:35–40.
[11] Giraud L, Baviere R, Vallée M, Paulus C. Presentation, Validation and Application of the DistrictHeating Modelica Library, 2015, p. 79–88. doi:10.3384/ecp1511879.
[12] Courant R, Friedrichs K, Lewy H. On the Partial Difference Equations of Mathematical Physics. IBM Journal of Research and Development 1967;11:215–34. doi:10.1147/rd.112.0215.